Role of TMED2 in Murine Labyrinth Layer Development and Non-Alcoholic Fatty Liver Disease

Wenyang Hou

A thesis submitted to McGill University in partial fulfillment of the requirements of the degree of Doctor of Philosophy

Department of Human Genetics
McGill University, Montreal, Canada
December 2017

Abstract

TMED2 belongs to the transmembrane emp24 domain (TMED) protein family, which is the key protein in the early transport of transmembrane and secretory proteins between the Endoplasmic Reticulum (ER) and the Golgi apparatus. *Tmed2* was expressed in the allantois and the chorion, two pre-placental tissues, and homozygous mutation of *Tmed2* (a 99J mouse line) resulted in abnormal chorioallantoic fusion and failure of placental labyrinth formation. Expression of genes associated with spongiotrophoblast, *Tpbp*α, and syncytiotrophoblast, *Gcm1,* differentiation was reduced in *Tmed2* null ($Tmed2^{99J/99J}$) placenta, and all $Tmed2^{99J/99J}$ embryos died by mid-gestation. *In situ hybridization* using a *Tmed2* probe revealed a tissue and temporal specific pattern of *Tmed2* expression in the embryo. Furthermore, *Tmed2* was highly expressed in the liver bud at embryonic day (E)9.5. Thus, we hypothesized that *Tmed2* exhibits a tissue-specific role in the chorion for normal chorioallantoic fusion and that disrupted TMED2 levels could result in perturbed function in the liver. We established a novel *ex vivo* culture model of pre-placental tissues of chorion and allantois, which recapitulated events associated with early placental labyrinth layer development. Then, we investigated the tissue-specific requirement for *Tmed2* using this *ex vivo* model. Recombinants of $Tmed2^{99J/99J}$ and wildtype pre-placental tissues suggested that *Tmed2* is required in the chorion for mixing of allantoic and chorionic cells. *Tmed2* mutant allantoic cells could mix with wild type chorionic cells, but *Tmed2* was found to be required in the allantois for proliferation. Although homozygous mutation in *Tmed2* led to embryonic lethality, *Tmed2* heterozygous mice ($Tmed2^{99J/+}$) were viable and fertile. Histological and molecular analysis using livers from $Tmed2^{99J/+}$ mice revealed a requirement for TMED2

in liver health. We showed that *Tmed2*$^{99J/+}$mice had decreased levels of TMED2 and TMED10, dilated endoplasmic reticulum membrane, and increased phosphorylation of an ER stress marker, eIF2α, and activation of the Unfolded Protein Response (UPR). Increased expression of sterol regulatory element binding protein (*Srebp) 1a* and *2* at the newborn stage and increased incidence of non-alcoholic fatty liver disease (NAFLD) were also found in *Tmed2*$^{99J/+}$ mice. Our data established *Tmed2*$^{99J/+}$ mice as a novel mouse model for NAFLD and suggests a novel role for TMED2 in liver health.

Résumé

TMED2 fait partie de la famille de protéines TMED (transmembrane emp24 domain). Celles-ci jouent un rôle dans le transport membranaire ainsi que dans la sécrétion des protéines entre le réticulum endoplasmique (RE) et l'appareil de Golgi. Le gène *Tmed2* est exprimé dans les tissus pré-placentaires de la souris, soit l'allantoïde et le chorion. De plus, une mutation homozygote de *Tmed2* (la lignée murine *99J*), provoque une fusion anormale de ces deux tissus, empêchant la formation de la région du labyrinthe du placenta. L'expression des gènes associés à la différenciation des spongiotrophoblastes, *Tpbp*α, et des syncytiotrophoblastes, *Gcm1,* est diminuée dans les placenta $Tmed2^{99J/99J}$. De plus, les embryons mutants $Tmed2^{99J/99J}$ meurent à la mi-gestation. Des données provenant d'hybridation *in situ* montrent un patron d'expression de *Tmed2* tissu et temps spécifique chez l'embryon murin. De manière intéressante, une forte expression de *Tmed2* a été observée dans le bourgeon hépatique.

Notre hypothèse est que 1) *Tmed2* joue un rôle spécifique dans le chorion, crucial à la fusion chorio-allantoïde et que 2) son inhibition partielle perturbe la fonction hépatique.

Pour tester notre première hypothèse, nous avons mis au point un système de culture *ex vivo* du chorion et de l'allantoïde murin, qui récapitule la formation de la couche placentaire du labyrinthe. En utilisant des tissus pré-placentaires de la souris mutante $Tmed2^{99J/99J}$ ou de type sauvage dans ce système *ex vivo*, nous avons pu évaluer le rôle de *Tmed2* exprimé exclusivement dans le chorion ou l'allantoïde dans la formation de la région du labyrinthe. Ainsi, nous avons déterminé que *Tmed2* est requis dans le chorion pour qu'il y ait un mélange des deux types de tissus. D'un autre côté, les cellules

allantoïdes *Tmed2*$^{99J/99J}$ pouvaient se mélanger aux cellules du chorion de type sauvage mais une diminution de leur prolifération a été observée.

Malgré la mort au stade embryonnaire des souris *Tmed2*$^{99J/99J}$, les souris hétérozygotes quant à elles sont viables et fertiles. Des analyses histologiques et moléculaires des foies de souris *Tmed2*$^{99J/+}$ ont révélées une augmentation de l'incidence de NAFLD (Non-Alcoholic Fatty Liver Disease). De plus, nous avons démontré une diminution significative de l'expression génique et protéique de TMED2 et TMED10, une dilatation de la membrane du réticulum endoplasmique (RE), une augmentation de la phosphorylation d'un marqueur de stress du RE, eIF2α, l'activation du UPR (unfolded protein response) et finalement, une augmentation des facteurs de transcription *Srebp 1a* et *2* (Sterol regulatory element binding protein). Pris dans leur ensemble, nos travaux mettent de l'avant un nouveau modèle murin pour étudier NAFLD et suggèrent un nouveau rôle de TMED2 dans le fonctionnement hépatique.

TABLE OF CONTENTS

List of Figures

List of Tables

List of Abbreviations

AD	Alzheimer's disease
AFLD	Alcoholic fatty liver disease
Ap. I	Apoptotic Index
APP	Amyloid precursor protein
ASK1	Apoptosis signal-regulating kinase 1
ATF 6	Actin transcription factor-6
BF	Bright field
bZIP	Basic leucine zipper protein
CDA	Dyserythropoietic anemia type
CHOP	C/EBP homologous protein
CLSD	Cranio lenticulo sutural dysplasia
COP	Coat protein complex
DAF	Decay-accelerating factor
DTT	Dithiothreitol
DNA	Deoxyribonucleic acid
EC	Ectoplacental cavity
ECM	Extracellular matrix
EGFP	Enhanced Green Fluorescent Protein
ELS	Endosomal/lysosomal system
ENU	N-Ethyl-N-Nitrosourea
EPC	Ectoplacental cone
ER	Endoplasmic reticulum
ERAD	ER-associated degradation
ERES	ER exit site
ERGIC	ER-Golgi Intermediate Compartment
FAS	Fatty acid synthase
GC	Giant cell
GDP	Guanosine diphosphate
GEF	Guanine nucleotide exchange factor
GPCR	G-protein-coupled receptor
GPI-AP	Glycosylphosphatidylinositol-anchored protein
GRP	Glucose regulated protein
GTP	Guanosine-5'-triphosphate
HCC	Hepatocellular carcinoma
ICM	Inner cell mass
IF	Immunofluorescence
IHC	Immunohistochemistry
IRE1	Inositol-requiring transmembrane kinase/endoribonuclease 1
ISH	*in situ* hybridization

MI	Mitotic index
NAFLD	Non-alcoholic fatty liver disease
NAS	Non-alcoholic Activity Score
NASH	Non-alcoholic steatohepatitis
PAR-2	Protease-activated receptor-2
PECAM	Platelet endothelial cell adhesion molecule
PERK	Double-stranded RNA-dependent protein kinase-like eukaryotic initiation factor 2α kinase
PF	Portal fibrosis
PFA	Paraformaldehyde
PUMA	P53 upregulated modulator of apoptosis
RESET	Rapid ER stress-induced export
RFA	Percutaneous Radiofrequency Ablation
RFP	Red fluorescent protein
RNA	Ribonucleic acid
RT-PCR	Real time-PCR
S1P	Site-1 protease
S2P	Site-2 protease
SEM	Standard error of mean
SREBP	Sterol regulatory element-binding protein
SynA	*Syncytin A*
SynB	*Syncytin B*
SynT	Syncytiotrophoblast
TEM	Transmission Electron Microscopy
TLR	Toll-like receptors
TMED	Transmembrane emp24 domain
TNF	Tumour necrosis factor
TRAF2	Tumor necrosis factor receptor associated factor 2
UPR	Unfolded Protein Response
VLDL	Very-low-density lipoprotein
VSVG	Vesicular stomatitis virus G protein
WES	Whole exome sequencing
WGS	Whole genome study
WT	Wildtype
XBP 1	X box protein 1
µm	Micrometre
µl	Microliter
µM	Micromolar (10^{-6} mol/L)
mg	Milligram
kg	Kilogram

Acknowledgements

This section is the hardest part in my thesis. There are countless help and advices that I received over years from so many intelligent and heart-warming people during my PhD study. Without them, this thesis would not exist. I am forever grateful to my supervisor, Dr. Loydie A. Jerome-Majewska. She accepted my application and brought me into her laboratory when I had just competed my undergraduate study in Vancouver. At the time, all I had was an interest in Biology, but because of her unbelievable patience, encouragement, guidance, and enthusiasm towards Science, this PhD thesis was possible. Seven years felt so short but it has left me with so many memories: I did not just obtain skills towards experiments, or interpret the data, but I became a better person who is more willing to share my knowledge and support others, as what Loydie did. I could not think of that one day I will leave her lab because I felt like family here. How could I not mention all members of Majewska's talking about family: Felix Boivin who taught me how to cast my first agarose gel. Timothée Revil, the coolest and funniest Post-Doc fellow in the lab, who always had answers for my questions. Libin Yuan and I spent so much time together discussing the hot science topics, and exploring all the bike tracks in Montreal over the weekend, those are priceless moments in my life. Dr. Swati Gupta, my little sister in the lab, for all these years we spent together in the lab. You are forever my friend. Most of all, Marie-Claude Beauchamp, no words can express my gratefulness to you. It is my greatest pleasure to work with you!

I would like to sincerely thank all members of my supervisory committee Dr. John Bergeron, Dr. Yojiro Yamanaka, and Dr. Heidi Mcbride for your time and great advice through committee meetings. Special thanks to Dr. Yojiro Yamanaka, for your generous gifts of reagents, and mice to help my research. I would like to also thank Dr. Aimee Ryan and Dr. Indra Gupta for their helpful feedbacks in the weekly lab meeting. I learned so much from you and became a better presenter in Science.

I would also like to express my dearest dedications to all surrounding friends and colleagues from Place Toulon and Glen: Brian Meehan, to whom I can talk everything: life stories, research problems; he is the ideal scientist and co-worker. Joanna Kalomiris, who encouraged and helped me over these years, I am forever grateful. Wei Cui, my big brother who is always cracking jokes, discussing politics, and sharing wisdoms with me, thank you! And, Amanda Baumholtz, we were admitted to Human Genetics Department together. I am so lucky to have a friend like you around and I am grateful of our priceless friendship.

Lastly, I must thank my dad, Liqun Hou, and my mum, Luqin Wang for their support over the years. I hope they are proud of me. I would like to specially thank my wife, Lei Zhang, who is always there to inspire and support me. I recall the time when we were just started dating, she would come to the lab with me and help me label Eppendorf tubes while I was dissecting the mouse embryos at the midnight.

Contribution of authors

Chapter II: Wenyang Hou performed all experiments, analyzed and interpreted all data and results. Didem pelin Sarikaya contributed to the experimental design, and manuscript editing, Loydie A. Jerome-Majewska designed the project and supervised all aspects of the project.

Chapter III: Wenyang Hou performed all experiments, analyzed and interpreted all data and results, Loydie A. Jerome-Majewska designed the project and supervised all aspects of the project.

Chapter IV: Wenyang Hou and Swati Gupta performed the qRT-PCR experiment, the histological analysis, and collected plasma samples for biochemical analysis. Marie-Claude Beauchamp and Wenyang Hou performed Tunicamycin injection experiment. Swati Gupta and Marie-Claude Beauchamp performed and interpreted western blot experiments. Libin Yuan performed and analyzed TEM results. Loydie A. Jerome-Majewska designed the project and supervised all aspects of the project.

Chapter I: Introduction

1.1 Early secretory pathway

1.1.1 Overview and function of early secretory pathway

In eukaryotic cells, transmembrane and secretory proteins function at the plasma membrane and extracellular space. These proteins are made inside of a cell and transported through the secretory pathway before reaching their destined sites for proper function. The synthesis of those proteins is initiated in the endoplasmic reticulum (ER), where proteins undergo post-translational modification such as protein glycosylation and folding. Properly modified proteins are sorted at the ER exit sites (ERESs) where ER-derived transport vesicles consisting of coat protein complex (COP) II are formed (Bannykh et al., 1996; Orci et al., 1991) (Figure 1.1). Transmembrane proteins at the ERESs can directly interact with COP proteins and be sorted into COPII vesicles, whereas luminal proteins are packaged into COPII vesicles via interaction with receptor proteins, which are ER-resident transmembrane proteins. The COPII vesicles which are associated with transmembrane proteins and receptor protein-coupled luminal proteins as "cargos" bud off from the ERES and traffic along microtubules towards the ER-Golgi Intermediate Compartment (ERGIC) (Sato, 2004). ERGIC functions as a quality control site where cargo proteins are scrutinized for proper folding and modification. Properly folded proteins are carried forward to the Golgi complex for further modifications and sorting to their destined sites such as the endosomal/lysosomal system (ELS) or the plasma membrane. This flow of trafficking is termed anterograde transport (Lee et al., 2004) (Figure 1.1). Improperly folded proteins can be either sent back to ER for re-folding through COPI vesicles-mediated retrograde transport or degraded via activation

of the ER-associated degradation (ERAD) pathway (Grootjans et al., 2016; Smith et al., 2011). The early secretory pathway involves three main compartments: ER, ERGIC, and Golgi complex, which work together for proper protein modification and transport.

1.1.2 COPII vesicles

COPII vesicles are key components of anterograde transport in the early secretory pathway; and they are conserved in all eukaryotes (Kaiser and Schekman, 1990; Orci et al., 1986). *In vitro* experiments in yeast have identified three main cytosolic components of the COPII coat, including the small GTPase SAR1, and two hetero-dimeric protein complexes, SEC23/24 and SEC13/31(Barlowe et al., 1994; Schekman and Rothman, 2002) (Figure1.2). COPII coating protein complexes are highly expressed at the ERESs (Horton and Ehlers, 2003). Formation of COPII vesicles occur in a stepwise fashion: 1. the GTPase SAR1 is recruited by an ER-resident guanine nucleotide exchange factor (GEF), SEC12 (Barlowe and Schekman, 1993). 2. The recruited SAR1 (GDP bound) is activated by SEC12 and changes to GTP-bound form (SAR1-GTP), then, the active SAR1-GTP recruits the SEC23/24 protein complex through direct binding to SEC23 (Barlowe et al., 1994; Bi et al., 2002) (Figure1.2). SEC24 interacts with SEC23 in a hetero-dimeric protein complex and serves as the major cargo-binding adaptor in COPII vesicles. SEC24 can interact with cargo proteins or cargo receptor proteins such as transmembrane emp24 domain (TMED)/P24 proteins during COPII vesicle formation and trafficking (Miller et al., 2002; Mossessova et al., 2003; Mark A Stamnes et al., 1995). 3. SEC23/24 recruits SEC13/31 hetero-dimeric protein complex through direct interaction between SEC23 and SEC31 (Bi et al., 2007). This association between SEC23 and SEC31 promotes GTP hydrolysis of SAR1 in the COPII coat and deformation of the

ER membrane, which result in the release of COPII vesicles from the ER (Bielli et al., 2005; Lee et al., 2005). Released COPII vesicles then transport cargo proteins to the ERGIC for quality check and further sorting in the secretion process. COPII vesicles containing properly folded cargo proteins reach the cis Golgi and release cargo proteins to the Golgi apparatus through tethering and fusion machineries. COPII vesicle-mediated trafficking is a very active process between ER and Golgi.

1.1.2.1 SEC12

SEC12 was originally identified in *S. cerevisiae* and is essential for the survival of yeast (Nakano et al., 1988). Later work has shown that SEC12 is conserved from yeast to human and functions as the GEF for SAR1 activation in both yeast and mammalian cells (Barlowe and Schekman, 1993; Rossanese et al., 1999; Weissman et al., 2001). These results suggest an evolutionary conserved role of SEC12 in the early secretory pathway. The localization of SEC12 inside of the cell, however, varies across different species: in the yeast strain *S. cerevisiae* and in human, SEC12 is dispersed throughout the ER; whereas in another yeast strain *Pichia pastoris*, SEC12 is only localized to the ERES (Rossanese et al., 1999; Weissman et al., 2001). It remains unclear whether this difference in localization has any implications for distinct functions of SEC12.

1.1.2.2 SAR1

SAR1 is a key small GTPase regulating COPII vesicle formation. When GDP-bound SAR1 is activated and switched to GTP-bound form via interaction with SEC12, SAR1 protein undergoes conformational changes and embeds an N-terminal α-helix into the lipid bilayer via interactions of hydrophobic residues with phospholipid groups in the membrane (Bi et al., 2002; Huang et al., 2001; Lee et al., 2005). This insertion is crucial

for both the initial phase and the end phase of the COPII vesicle formation. In the initial phase, the GTP-bound SAR1 interacts with both ER membrane phospholipids and SEC23 for recruiting the SEC23/24 protein complex to the synthetic liposomes (Bi et al., 2002; Huang et al., 2001). In addition, the electrostatic interactions between the basic residues at SEC23/24 protein complex and acidic phospholipids in the ER may provide additional affinity to the membrane (Bi et al., 2002; Matsuoka et al., 1998). The hydrolysis of SAR1-GTP rapidly changes cargo concentration and promotes COPII vesicle budding from the ER membrane (Sato and Nakano, 2005; Tabata et al., 2009). In the end phase, the insertion of the SAR1 α-helix also causes curvature on the membrane, together with hydrolysis of SAR1-GTP, are postulated to mediate the vesicle scission step of COPII vesicle budding (Bacia et al., 2011; Bielli et al., 2005; Lee et al., 2005; Long et al., 2010). The release of COPII vesicles can be interrupted when GTP hydrolysis on SAR1 is prevented (Bacia et al., 2011; Bielli et al., 2005).

1.1.2.3 SEC23/24

The heterodimeric SEC23/24 complex forms the inner layer of COPII vesicles. Following SAR1 activation, the SEC23/24 complex is recruited by SAR1 through interaction between an arginine residue from SEC23 and the catalytic pocket of SAR1 (Bi et al., 2002). In addition to this physical interaction, the arginine residue is also known to enhance the SAR1 GTPase activity via stabilization of its GTP phosphate groups (Bi et al., 2002). SEC23 is also suggested to help orientate SEC24 for optimized cargo binding through alternate conformational changes in binding sites on SEC31 in the outer layer coat (Bhattacharya et al., 2012). The orientation of SEC23/24 complex and its interaction with SEC13/31 complex also changes to allow binding of cargos of different

sizes as well as shapes, and even some significantly larger-sized vesicles to enable the transport of large cargos (Bhattacharya et al., 2012).

While SEC23 does not directly interact with cargo proteins, SEC24 functions as the major cargo-binding protein in COPII vesicles (Miller et al., 2002). SEC24 can directly bind to cargos or through its interactions via cargo receptor proteins such as TMED (Transmembrane emp24 domain)/P24 proteins (Mossessova et al., 2003; Mark A Stamnes et al., 1995). In the direct binding process, SEC24 interacts with cargo proteins at the cargo-borne export signals and cargo-binding sites at the surface of SEC24 (Mossessova et al., 2003). On the other hand, proteins such as soluble secretory proteins can not directly bind to SEC24, they require receptor proteins, such as linkers to SEC24 in COPII vesicles in order to be transported (Appenzeller et al., 1999; Belden and Barlowe, 2001). For example, most TMED proteins contain a dibasic motif that allows interaction with SEC24 in COPII vesicles and a disulfide bridge of two cysteine residues to mediate cargo recognition (Anantharaman and Aravind, 2002; Barlowe, 2003; Belden and Barlowe, 2001; Dominguez et al., 1998).

1.1.2.4 SEC13/31

Following the formation of the pre-budding complex, the SEC13/31 complex is recruited by SEC23 to form the cage-like outer layer of the COPII coat (Matsuoka et al., 2001). The architecture of the SEC13/31 complex is composed of a heterotetramer of two SEC31 and two SEC13 proteins. To form this cage-shaped outer layer, two SEC31 proteins dimerize tail-to-tail to form a rod structure (shown in green, Figure 1.3b) with two SEC13 proteins underneath (shown in blue, Figure 1.3b). Four rods of heterotetramer form the vertex of the COPII cage (Figure 1.3a, b). The angle of SEC31 hinge varies

from 135-165º and the angle of the β-vertex varies from 108-120º; whereas the angle for α-vertex is fixed at 60º (Stagg et al., 2008). The angle for both SEC31 hinge and the β-vertex changes according to interactions with SEC23/24 complex as well as to the size of COPII vesicles (Bhattacharya et al., 2012; Stagg et al., 2008). This flexibility of the COPII structure adds versatility to compensate for the different size and structure of cargo proteins during transport. For example, COPII export machinery can adapt to transport large secretory cargos up to ~300-400 nm in size, such as procollagen fibres while the typical size of COPII vesicles being 60-90nm (Bannykh et al., 1996; Barlowe et al., 1994; Bonfanti et al., 1998). Mutations in the SEC23A, one of four SEC23 members, cause developmental defects due to lack of collagen secretion (Boyadjiev et al., 2006; Fromme et al., 2008; Gupta et al., 2016; Lang et al., 2006). Several studies in yeast also show that assembly of SEC31 proteins is the driving force for outer layer formation, with SEC13 providing structural rigidity as SEC13 is not required for cage formation under certain conditions (Copic et al., 2012).

1.1.2.5 SEC16

In addition to core components of COPII vesicles such as SEC12, SAR1, SEC23/24, and SEC13/31 protein complexes, a large multidomain protein, SEC16, is found at ERES sites. Little is known about the mechanistic role of SEC16 during COPII vesicle formation *in vivo*, however, *in vitro* studies suggest that SEC16 regulates COPII vesicle formation via regulating SAR1 activity (Kung et al., 2012). SEC16 also interacts with SEC23/24 complex, as well as SEC31 protein, suggesting SEC16 may play a role in the assembly process of the core coating proteins (Espenshade et al., 1995; Gimeno et al., 1996; Supek et al., 2002; Whittle and Schwartz, 2010). In addition, via interactions with

other SEC core proteins, SEC16 is suggested to organize the ERES in the ER (Miller and Barlowe, 2010).

1.1.2.6 Cargo receptor proteins

Cargo receptor proteins serve as the linker to help transport soluble luminal proteins to COPII vesicles, since those cargos cannot interact with SEC24 directly. The two main types of cargo receptors that facilitate this process are transmembrane receptors and multispanning membrane receptors (Dancourt and Barlowe, 2010). Examples of transmembrane receptors include mammalian protein ERGIC53, a lectin-like receptor that facilitates glycoprotein transport; as well as the TMED/p24 family of proteins, which are implicated as receptors for glycosylphosphitdylinositol-anchored proteins (GPI-APs), WNT proteins, G-protein-coupled receptors (GPCRs), and Toll-like receptor (TLR) proteins (Buechling et al., 2011; Castillon et al., 2011; Liao et al., 2015; Liaunardy-Jopeace et al., 2014; Luo et al., 2011, 2007; Port et al., 2011a; Takida et al., 2008). ERGIC53 is a single transmembrane protein with a large N-terminus and a short cytoplasmic C-terminus (Itin et al., 1995). The C-terminus contains a diphenylalanine motif for COPII vesicle recognition, and a dilysine signal for COPI vesicle recognition (Itin et al., 1995; Kappeler et al., 1997). As a major cargo receptor protein, ERGIC53 is responsible for transporting fully folded glycoproteins (Itin et al., 1996) such as the nascent cathepsin Z and C (Christian Appenzeller-Herzog and Hauri, 2005; Dancourt and Barlowe, 2010), coagulation factor V and VIII (Nichols et al., 1998), and soluble glycoprotein, α1-antitrypsin (Nyfeler et al., 2008). Structurally similar to ERGIC53, members of TMED protein family are also single-transmembrane proteins, which have a large N-terminal luminal domain, a short cytoplasmic C-terminal domain containing

binding-motifs to both COPII and COPI vesicles (Strating and Martens, 2009a). The structure, function, localization, and expression of TMED family proteins will be further described in Section 1.2. Besides single-transmembrane receptor proteins, some non-canonical multispanning membrane receptors such as Erv proteins also exist. Erv proteins are conserved in yeast and human which function in cargo sorting and transport. In yeast, mutations in Erv proteins Erv29p, Erv14p, and Erv26p are associated with sorting defects in export of many integral membrane cargos (Belden, 2001; Bue et al., 2006; Bue and Barlowe, 2009; Powers and Barlowe, 2002).

1.1.3 COPI vesicles

Following uncoating of COPII vesicles and releasing of cargos at the cis- Golgi complex, cargo receptor proteins such as ERGIC53 and TMED proteins, as well as machinery proteins such as SNAREs can be transported back to ER via COPI vesicles in the retrograde transport. COPI sorts TMED proteins by recognizing their diphenylalanine motifs (FFxx) (Fiedler et al., 1996), or proteins like ERGIC 53, and OST48 (Fiedler et al., 1996; Letourneur et al., 1994) with their dilysine-based motifs (KKxx or KXKXX). In addition, COPI vesicles can mediate the trafficking of properly folded cargos in the intra-Golgi traffic (Beck et al., 2009) and possibly maintain the structure of normal mammalian Golgi complex (Duden, 2003). Similar to COPII vesicles, formation of COPI vesicles requires a small GTPase, ARF1, a B-subcomplex (α/β'/ε) and a heterotetrametric protein complex, F-subcomplex (β/δ/γ/ζ) (Jackson, 2014). In the presence of a potential cargo, ARF1-GDP is activated by a GEF to become ARF1-GTP, and the active GTP bound ARF1 recruits both B and F subcomplexes to initiate polymerization (Bremser et al., 1999; Serafini et al., 1991). Upon recruiting of all seven members of F-subcomplex

and B-subcomplex, the coatomer subunits α-COP, β'-COP, γ-COP, and δ-COP recognize the binding motif located at the cytoplasmic domain of cargo proteins and mediate cargos to be included into the COPI vesicles (Brandizzi and Barlowe, 2013). This results in conformational changes of the coat complex and membrane deformation, which lead to formation of the COPI vesicles (Langer et al., 2008; Reinhard et al., 1999). The hydrolysis of active ARF1-GTP by ARF-directed GTPase-activating proteins (ARFGAPS) is required for coat dissociation and release of cargos to the destination membranes (Brandizzi and Barlowe, 2013; Tanigawa et al., 1993).

1.1.3.1 ARF1

The initiation of COPI vesicle formation is via activation of the small GTPase protein ARF1. The inactive ARF1-GDP is a membrane bound protein, once activated by SEC7 family of GEFs (D'Souza-Schorey and Chavrier, 2006), ARF1 can recruit F-subcomplex proteins such as β-COP and γ-COP subunits (Zhao et al., 1999, 1997), or β-COP and ζ-COP subunits (Eugster et al., 2000) to initiate COPI vesicle formation. In addition, inactive ARF1-GFP interact with the cytoplasmic tail of dimeric TMED10/P23 (Contreras et al., 2004; Ishikawa et al., 2013). Upon activation via GEFs, ARF1-GTP dissociates from TMED10, suggesting a role for TMED proteins in early recruitment of ARF1 for COPI vesicle formation.

1.1.3.2 F-subcomplex

The F-subcomplex belongs to a family of heterotetrametric adaptor protein complexes of five members: AP1-5, which localizes to a specific cellular compartment for its function (Kelly and Owen, 2011; Traub, 2009). For instance, AP1, AP3, and AP4 function in the Golgi membrane whereas AP2 predominantly functions in the plasma

membrane (Boehm et al., 2001; Stamnes and Rothman, 1993; Yu et al., 2012). The F-subcomplex proteins are recruited by ARF1-GFP to form the inner layer core of COPI vesicles, and they have been shown to interact with B-subcomplex proteins, cargos with arginine based retrieval signals (Michelsen 2007) and the cytoplasmic tail of TMED proteins (Fiedler et al., 1996).

1.1.3.3 B-subcomplex

The B-subcomplex forms the outer layer of COPI vesicles (Hsia and Hoelz, 2010) and is implicated in cargo binding (Béthune et al., 2006a; Fiedler et al., 1996; Lowe and Kreis, 1995; Schröder-Köhne et al., 1998; Tritarelli et al., 2004). B-subcomplex proteins recognize and bind cargo proteins through their binding motifs: proteins containing dilysine-based motif (KKxx, or KxKxx) such as OST48, ERGIC53, and glycoproteins (Goepfert et al., 1997; Hsia and Hoelz, 2010; Lontok et al., 2004); diphenylalanine motifs (FFxx) such as TMED proteins (Fiedler et al., 1996); and KDEL/HDEL receptors (Lewis and Pelham, 1990; Tanigawa et al., 1993).

1.1.4 ER stress, UPR, and ERAD

The ER is the central organelle for folding and sorting newly synthesized transmembrane and secretory proteins. When proteins are misfolded, ER retains such proteins and prevents their release for transport. However, when cells experience stimuli of stress such as inhibition of glycosylation, increased ER protein synthesis, impaired ERAD, or mutations in ER resident proteins, misfolded proteins could accumulate in the ER. As a result, ER stress is induced. To cope with ER stress, eukaryotic cells can activate an adapted signalling pathway named unfolded protein response (UPR). The UPR pathway consists of three arms of action: 1. activating transcription factors to

increase expression of proteins involved in ER protein folding and degradation (Gething and Sambrook, 1992), 2. attenuating protein translation to reduce trafficking load (Harding et al., 1999), 3. activating lipogenesis and ER-associated degradation (ERAD) to relocate misfolded proteins into the cytosol via ubiquitin-proteasome mechanism (Mori, 2000). However, if the amount of misfolded proteins is overloaded or the UPR failed to function properly in cells, apoptosis and inflammation pathways could be activated to terminate such cells. As such, normal function of UPR is essential to maintain the cell homeostasis and normal function, and dysfunction of the UPR process may lead to severe diseases such as metabolic disease, inflammatory disease and cancer (Kadowaki and Nishitoh, 2013).

1.1.4.1 ER stress

ER stress is caused by the accumulation of misfolded proteins in the ER. Several stimuli are known to induce ER accumulation of unfolded/misfolded proteins: 1. glucose deprivation as it is involved in N-linked protein glycosylation, 2. disruption in calcium balance in the ER (Ma and Hendershot, 2004), 3. impaired function of ERAD, and 4. certain viral infections can also cause ER stress, and ultimately lead to cell death.

1.1.4.2 Three arms of the signalling pathway during UPR

In cells under normal homeostasis, resident chaperones are bound to transmembrane ER proteins. When ER stress occurs in the cell, accumulation of misfolded proteins causes release of the ER chaperone glucose regulated protein (GRP) 78 (Bip) to initiate the UPR (Figure 1.4). The UPR signaling pathway is composed of three sensors: double-stranded RNA-dependent protein kinase-like eukaryotic initiation

factor 2α kinase (PERK), inositol-requiring transmembrane kinase/endoribonuclease 1 (IRE1), and acting transcription factor 6 (ATF6).

1.1.4.2.1 PERK pathway

PERK is a serine/threonine kinase which contains a catalytic domain similar to the eukaryotic initiation factor 2α (eIF2α). PERK is activated when GRP78 dissociates at its luminal domain. This causes oligomerization and autophosphorylation of PERK (Bertolotti et al., 2000). Activated PERK then phosphorylates eIF2α, which leads to attenuation of global mRNA translation to ease the protein load. In addition, phosphorylated eIF2α leads to translation of the mRNA encoding transcription factor ATF4, which promotes transcription of many genes involved in the UPR including amino acid metabolism, ER stress induced apoptosis, and redox hemostasis (Ameri and Harris, 2008; Bertolotti et al., 2000; Harding et al., 2003). Under prolonged or unresolved ER stress conditions, ATF4 activates the transcription of proapoptotic factor, C/EBP Homologous Protein (CHOP). CHOP upregulates a number of downstream proapoptotic factors such as p53 upregulated modulator of apoptosis (PUMA) (Cazanave et al., 2010), and GADD34. GADD34 is a regulatory subunit of protein phosphate 1 (PP1), and activation of both dephosphorylates eIF2α, to resume the normal protein translation (Malhotra et al., 2008; Marciniak et al., 2004) (Figure 1.4). Together, PERK regulates amino acid metabolism, redox homeostasis, and ER stress-induced apoptosis to resolve ER stress (Ameri and Harris, 2008; Harding et al., 2003; Lange et al., 2008).

1.1.4.2.2 IRE1

The inositiol-requiring enzyme (IRE1) is a type I transmembrane protein which contains a serine/threonie kinase domain and an endoribonuclease (RNAse) domain (Hetz

and Glimcher, 2009). Two isoforms of IRE1 exist in vertebrates: IRE1α is ubiquitously expressed and IRE1β is only expressed in intestinal epithelial cells (Urano et al., 2000). Similar to PERK activation, IRE1 is also activated via dissociation of GRP78 from its luminal domain (Figure 1.4). This process leads to oligomerization and autophosphorylation of the kinase domain, which activates the RNAse domain via a conformational change (Gardner and Walter, 2011; Promlek et al., 2011). Activated IRE1 induces stress-sensitive splicing of X box protein 1 (XBP 1) mRNA, a transcriptional factor. Spliced XBP 1 then upregulates the expression of UPR target genes such as GRP78, GRP94, ERdj4, and ERP72 that are involved in protein folding, quality control, and ERAD (Nishitoh et al., 2002; Sriburi et al., 2007; Urano et al., 2000). Under prolonged ER stress, activated IRE1 interacts with tumor necrosis factor receptor associated factor 2 (TRAF2) to form a complex, which can activate the apoptosis signal-regulating kinase 1(ASK1), a member of the MAPKKK family (Nishitoh et al., 2002). Recruited ASK1 activates the JNK pathway to trigger apoptosis (Nishitoh et al., 2002). These results suggested a key role of IRE1 in apoptosis to resolve severe ER stress.

1.1.4.2.3 ATF6

ATF6 is a basic leucine zipper protein (bZIP) containing transcriptional factor. Two paralogs of ATF6 exist in mammals: ATF6α, and ATF6β, both are ubiquitously expressed (Haze et al., 2001). Activation of ATF6 is achieved through dissociating GRP78 from its N-terminus. However, instead of oligomerization or autophosphorylation, released ATF6 translocate to the Golgi to be sequentially cleaved by site-1 (S1P) and site-2 protease (S2P) in the luminal domain and transmembrane domain. As a result, the cleaved N-terminal cytosolic domain containing the bZIP domain

is translocated to the nucleus to activate UPR target genes including ER chaperones, ERAD, and XBP1. In addition, ATF6 is found to interact with Sterol regulatory element-binding protein (SREBP) -2 to regulate the expression of SREBP-2 and its target genes involved in cholesterol synthesis (Zeng et al., 2004). Overall, the link between the UPR marker ATF6 and SREBP-2 indicates a potential role of ER stress in the pathology of diseases such as metabolic disease and obesity.

1.1.4.3 ERAD

ER-associated degradation (ERAD) is a conserved mechanism adapted by eukaryotic cells to eliminate misfolded proteins from the ER. ER chaperones recognize misfolded proteins and relocate them to the cytosol to be degraded via the ubiquitin-proteasome complex (Haze et al., 2001). Three distinct ERAD pathways exist and can be classified based on the location where structural defect are found in misfolded substrate proteins: ERAD-C (proteins with misfolded cytosolic domains), ERAD-L (proteins with misfolded luminal domains), and ERAD-M (proteins with misfolded transmembrane domains) (Carvalho et al., 2006; Haze et al., 2001). In yeast, the ERAD-C pathway is mediated by the Doa10p complex, the ERAD-L pathway is mediated by the Hrd1p complex, and the ERAD-M pathway is mediated by both Doa10p and Hrd1p complexes (Kadowaki and Nishitoh, 2013). Both Doa10p and Hrd1p are ER resident E3 ligases with a cytosolic RING finger domain (Kadowaki and Nishitoh, 2013). In mammalian cells, a number of E3 ligases including HRD1, gp78, TRC8, RMA1/RNF5, and TEB4 (homolog of yeast Doa10p) are found to function in human ERAD pathway (Smith et al., 2011), however, the exact molecular mechanisms on how these E3 ligases function in each ERAD pathway are unclear in human.

1.1.5 Early secretory pathway and disease

Genes in the early secretory pathway are highly conserved across species. Mutations in secretory pathway proteins are associated with human diseases. These mutations occur in genes coding for COPII and COPI coat complex proteins, cargo receptors, and UPR pathway. In this section, I will describe mutations that affect the normal function of early secretory pathway and cause phenotypes and diseases in mammalian systems.

1.1.5.1 Mutations in COP II coat complex proteins

Many mutations in genes coding for COPII coat complex proteins are found to be associated with human diseases. In mammals two paralogues for SAR1, SAR1A and SAR1B, share 89% amino acid identity and similar secondary structures (Bi et al., 2002; Huang et al., 2001). However, mutation in SAR1B, but not in SAR1A in human, causes chylomicrons (a large lipid particles) retention disease because SAR1B is required for efficient packaging of chylomicrons (Jones et al., 2003). Further study has shown that SAR1B can facilitate the formation of larger COPII vesicles with large lipid capsules (Loftus et al., 2012).

Mammals also express two paralogues for SEC23, SEC23A and SEC23B (Paccaud et al., 1996). Human patients with heterozygous and homozygous mutations in SEC23A have craniolenticulosutural dysplasia (CLSD) (OMIM #607812) syndrome (Boyadjiev et al., 2006; Foley et al., 2012). A *Sec23a* knockout mouse model for human CLSD syndrome exists but the heterozygous mice do not exhibit the phenotype found in human patients. The *Sec23a* homozygous mutation causes embryonic lethality and neural

tube defects (Boyadjiev et al., 2006). However, *sec23a*-knockdown in zebrafish presents phenotypic features found in human patients with CLSD (Boyadjiev et al., 2006).

Patients with homozygous or compound heterozygous mutations in SEC23B present congenital dyserythropoietic anemia type (CDA) II (OMIM #224100) with inefficient erythropoiesis, lysis of red blood cells, and hypoglycosylation of red blood cell membrane proteins (Bianchi et al., 2009). A *Sec23b* knockout mouse model also exists and heterozygotes are viable, fertile with no phenotypic characteristics found in human patients. *Sec23b* homozygous mice die shortly after birth with severe developmental defects in the pancreas and other exocrine glands (Tao et al., 2012). Although the *Sec23b* knockout mice do not recapitulate the anemia phenotype in human patients with CDA II, and given the fact that those mice die at birth, it is possible that those mutant mice die before they develop a CDA II phenotype (Tao et al., 2012). Furthermore, molecular analysis of *Sec23b* knockout mice also shows dilated ER, activation of the UPR pathway, and increased apoptosis in the secretory tissues (Tao et al., 2012).

Human SEC24 family has four members: SEC24A, SEC24B, SEC24C, and SEC24D (Wendeler et al., 2007). Mutations in SEC24A are not associated with human diseases. However, mice with homozygous mutation in *Sec24a* have reduced plasma cholesterol and increased LDLR level due to deficiency in PCSK9 (Chen et al., 2013). Missense heterozygous mutation in human SEC24B causes neural tube defects, and *sec24b* knockdown in zebrafish results in convergent extension defects during neural tube development (Yang et al., 2013). *Sec24b* null mice have severe neural tube phenotypes such as craniorachischisis and deficiency in convergent extension (Merte et al., 2010;

Wansleeben et al., 2010). These observations suggest a conserved role for SEC24B in neural tube development.

Similar to SEC24A, human deficiency in SEC24C is not found to be associated with human diseases, however, mouse *Sec24c* is required for normal embryonic development. Mouse embryos with null mutation in *Sec24c* die between implantation and E8.5 (Adams et al., 2014).

Compound heterozygous mutations in SEC24D cause a disease called Osteogenesis Imperfecta with severely disturbed ossification of the skull (OMIM# 112240 and 616294) (Garbes et al., 2015). Deficiency in *sec24d* in zebrafish share similar phenotypes to human patients with severe defects in craniofacial morphogenesis due to failure of secreting type II collagen and matrilin, components of the extracellular matrix (ECM) (Sarmah et al., 2010). However, *Sec24d* homozygous mutation in mouse results in early embryonic lethality at 8-cell stage, and *Sec24d* heterozygous mice are viable with no phenotypic abnormality (Baines et al., 2013). Those results suggest an evolutionarily conserved role of *Sec24d* in embryogenesis.

1.1.5.2 Mutations in COPI coat complex proteins

Mutations in COPI coat complex proteins are also associated with human diseases. Deleterious mutations in the coatomer subunit alpha (*COPA*) gene were identified through whole exome sequencing (WES) in several families (Watkin, 2015). Patients with *COPA* mutations present with hereditary autoimmune-associated lung, joint, and kidney disease (OMIM# 616414) (Watkin, 2015).

Loss-of-function heterozygous mutation in *ARCN1*, which encodes the δ subunit of COPI, results in a craniofacial disorder characterized by facial dysmorphisms, rhizomelic shortening, severe micrognathia, microcephilic dwarfism, and mild developmental delay in patients (Izumi et al., 2016). A mouse model with a missense mutation in *ARCN1* presents with the neurodegeneration defect (ataxia), and diluted coat color but not any facial dysmorphisms seen in human patients (Xu et al., 2010).

Other studies suggest δ-COP affects the biology of amyloid precursor proteins (APP), a hallmark of Alzheimer's disease (AD) such as trafficking, metabolism, subcellular localization, and cell surface expression (Bettayeb et al., 2016a). Further investigation of whole genome study (WGS) on a cohort of 954 patients (B. Zhang et al., 2011) with Alzheimer's disease identified 12 single nucleotide polymorphisms (SNPs) and 24 mutations in COPI genes to be associated with increased AD risk (Bettayeb et al., 2016b).

1.1.5.3 Mutations in cargo receptor proteins

Mutations in cargo receptor protein, ERGIC53, cause a combined deficiency of coagulation factors V and factor VIII (F5F8D) disease in patients (~70% of F5F8D patients) (Nichols et al., 1998; Zhang et al., 2009). Homozygous mutation of *Ergic53* in mouse exhibits phenotypes of human patients with FV and FVIII deficiencies (B. Zhang et al., 2011).

In addition, mutations in a ERGIC-53-like protein, LMAN2L/VIPL which is responsible for sorting glycoproteins at ER, are found to be associated with an autosomal recessive mental retardation-52 (MRT52) disease (OMIM#616887) (Rafiullah et al., 2015). Mutations in TMED proteins are also implicated in diseases and phenotypes

associated with human patients and mouse models. In sections 1.2.5 and 1.2.6, knockout mouse models and human pathology of TMED proteins will be further described.

1.1.5.4 Mutations in genes involved in UPR pathway.

Mutations in genes involved in the UPR pathway are associated with attenuated UPR, which results in prolonged or unresolved ER stress in the cell. These mutations are identified in a number of phenotypes and diseases in mammals. Homozygous mutation of *CHOP* or *GADD34* in cells fail to activate ER-stress induced apoptosis, indicating a crucial role of PERK pathway in cell apoptosis (Malhotra et al., 2008; Marciniak et al., 2004; Song et al., 2008). Homozygous mutation of *Chop* in mouse models of type 2 diabetes promotes β cell survival and function (Song et al., 2008). Mice with homozygous deletion in *Ire1α* are embryonic lethal due to impaired labyrinth layer development (Iwawaki et al., 2009), whereas mice with homozygous mutation in *Ire1β* are viable with no obvious phenotypes except for a higher susceptibility to induced colitis, since *Ire1β* is only expressed in the intestinal epithelium (Bertolotti et al., 2001). Deletion in *Xbp1,* downstream effector of the IRE arm, results in embryonic lethality between embryonic days 10.5 to 14.5 due to cellular necrosis of cardiac myocytes (Masaki et al., 1999). Mice with single knockout mutation in either *Atf6α* or *Atf6β* are viable, however, mice with double homozygous mutations in both *Atf6α* and *Atf6β* are embryonic lethal before birth, the reason for which is unknown (Yamamoto et al., 2007). Another study using a medaka fish model of double *Atf6α* and *Atf6β* knockout, but not *Atf6α* or *Atf6β* single knockout, has also shown embryonic lethality as in the mouse model, due to impaired notochord development caused by profound ER stress and lack of ATF6α/β mediated chaperones (Ishikawa et al., 2013). These results suggest the

possibility of some redundancy yet independent roles of *Atf6α* and *Atf6β* during early vertebrate development. Furthermore, introduction of ER stress via injection of tunicamycin into *Atf6α* knockout mouse leads to steatosis and liver dysfunction (Yamamoto et al., 2010). Molecules involved in ER stress are associated with many human diseases including neurodegenerative diseases, metabolic diseases, inflammatory disease, diabetic diseases, cancer, and cardiovascular disease (Table1.1) (Kadowaki and Nishitoh, 2013).

1.2 TMED protein family

In this section, I will further describe one transmembrane protein family of cargo receptor proteins, TMED proteins. My PhD project focuses on understanding the function and developmental roles of one TMED proteins, TMED2. I will discuss the classification, structure, function, localization, developmental requirement during mouse embryogenesis, and pathology of *Tmed* genes in this section.

1.2.1 Overview of TMED protein family

TMED proteins are endoplasmic reticulum (ER) resident proteins that help sort cargo proteins between ER and Golgi through interaction with COP proteins in COP vesicles. So far, ten *Tmed* genes have been identified in vertebrates and they can be grouped into four subfamilies based on the similarity in amino acid sequence: α (*Tmed4*, *Tmed9*, *Tmed11*), β (*Tmed2*), γ (*Tmed1*, *Tmed3*, *Tmed5*, *Tmed6*, *Tmed7*) and δ (*Tmed10*) (Schuiki and Volchuk, 2012; Strating and Martens, 2009b). To function properly, a member of each subfamily is recruited to form a heterotetramer (Marzioch et al., 1999). All TMED family members are structurally related and share an N-terminus, a luminal region containing the Golgi-Dynamic (GOLD) domain (Anantharaman and Aravind,

2002), a coiled-coiled domain, a transmembrane region, and a short cytosolic C-terminus (Figure 1.5). TMEDs function as cargo receptors involved in trafficking of glycosylphosphatidylinositol-anchored proteins (GPI-Aps), such as folate receptor alpha (Bonnon et al., 2010), Wnt proteins, such as *Drosophila* Wingless (Wg) (Port et al., 2011b), G-protein-coupled receptors (GPCRs), such as protease-activated receptor-2 (PAR-2) (Zhao et al., 2014), and toll-like receptors (TLRs), such as TLR-4 (Zhao et al., 2014).

1.2.2 Structure and functional domains of TMED proteins

The N-terminus of TMED proteins contains the signal peptide sequence for translocation of TMED proteins to ER (Anantharaman and Aravind, 2002). The GOLD domain contains a putative disulfide bridge of two cysteine residues and is proposed to mediate cargo recognition and protein-protein interactions (Anantharaman and Aravind, 2002). The coiled-coil domain was originally shown to be crucial for oligomerization with other TMED proteins (Ciufo and Boyd, 2000), however, some recent work has shown that the coiled-coil domain can also recognize and transport GPI-APs (Ciufo and Boyd, 2000). The transmembrane region helps anchor proteins into the ER membrane and recently has been shown to also interact with SM18, a single sphingomyelin to regulate COPI vesicle transport (Contreras et al., 2012). The C-terminus contains a short cytosolic domain with conserved signals for interactions with COPI and COPII subunits during vesicle formation (Aniento et al., 2006). Most TMED proteins contain a dibasic ΦFXXBB(X)n motif (Φ refers a hydrophobic residue, B is a basic residue, and X refers to any amino acids, N≥2), which allows TMED proteins bind to COPII vesicles (Aniento et al., 2006; Barlowe, 2003; Belden and Barlowe, 2001; Contreras et al., 2004;

Dominguez et al., 1998). In addition TMED4, TMED9, and TMED11 have a KKXX and , TMED10 has a KK(H) motif for binding to COPI subunits (Belden and Barlowe, 2001; Béthune et al., 2006b; Dominguez et al., 1998; Fiedler et al., 1996; Ma and Goldberg, 2013; Popoff et al., 2011). TMED proteins can function either as heterotetramer or as heterodimer through interaction with each other through the coiled-coil domains (Ciufo and Boyd, 2000; Liaunardy-Jopeace et al., 2014; Ma and Goldberg, 2013). Oligomerization of TMED proteins is crucial for their function as well as stability, for instance, co-immunoprecipitation experiments have demonstrated that TMED2 interacts with TMED10 to form a complex in Chinese hamster ovary (CHO) cells (Gommel et al., 1999). A more recent study has shown crystal structures of TMED2 and TMED10 and they interact with each other at GOLD domains in HEK293 cells (Figure 1.6) (Nagae et al., 2016). Furthermore, overexpression of TMED10 enhances the interaction with TMED2 and this interaction is also important for each other's stability (Gommel et al., 1999). In the absence of one TMED protein, the expression of other TMED members is also reduced (Denzel et al., 2000; Jenne et al., 2002).

1.2.3 *Localization and expression of TMED proteins*

TMED proteins were first identified as cargo receptor proteins localized in the ER, ERGIC, and Golgi apparatus for both anterograde and retrograde transport (Belden and Barlowe, 1996; Blum et al., 1996; Dominguez et al., 1998; Emery et al., 2000; Füllekrug et al., 1999; Gommel et al., 1999; Nickel et al., 1997; Rojo et al., 2000, 1997; Schimmoller et al., 1995; Sohn et al., 1996; M A Stamnes et al., 1995). In addition, TMED2 protein also localizes to peroxisomes (Marelli et al., 2004), and TMED10

protein is found in secretory granules (Hosaka et al., 2007), and at plasma membrane (Blum and Lepier, 2008; Chen et al., 2006; Langhans et al., 2008).

Most *Tmed* genes are ubiquitously expressed in adult mouse tissues. Except for *Tmed11* and *Tmed6*, eight out of ten *Tmed* transcripts are widely expressed in various mouse tissues by real time-PCR (RT-PCR) (Strating et al., 2009b). Expression of *Tmed11* is restricted to lung, liver, kidney, small intestine, colon, and spleen, whereas *Tmed6* is only expressed in pancreas tissue (Strating et al., 2009b). However, during development, some *Tmed* genes showed spatial or temporal differences in their expression. The Jerome-Majewska group has shown that expression of *Tmed2* in the embryo is dynamic during gastrulation and becomes spatially restricted at embryonic day E6.5 (Jerome-Majewska 2010). In addition, *Tmed2* is widely expressed in the extraembryonic derived placental tissues throughout placental development (Jerome-Majewska et al., 2010). TMED2 is also found to be widely expressed in human placental tissues including syncytiotrophoblast, cytotrophoblast, and stromal cells during human placental development (Zakariyah et al., 2011)

1.2.4 *TMED protein functions*

1.2.4.1 Facilitating COPII and COPI vesicle formation

TMED proteins facilitate COPII and COPI vesicle formation in early secretory pathway. During anterograde transport, TMED proteins directly interact with SEC24 to promote COPII vesicle formation (Miller et al., 2002; Mossessova et al., 2003; Mark A Stamnes et al., 1995). In addition, TMED proteins are asymmetrically expressed in the ER membrane, and are able to alter the physical properties of the ER membrane to promote COPII vesicle budding (Čopič and Miller, 2012).

During retrograde transport, TMED proteins are required for the budding of COPI vesicles in an *in vitro* Golgi vesicle budding assay (Aguilera-Romero et al., 2008). In addition, both TMED2 and TMED10 are highly expressed in COPI vesicles and can interact with ARF1 through their cytoplasmic tails (Gommel et al., 1999; Majoul et al., 2001; Sohn et al., 1996). TMED10 can interact with GDP-bound form of ARF1 (inactive form) (Gommel et al., 1999), whereas TMED2 can interact with the ARF GTPase-activating protein 1 (GAP1) to prevent hydrolysis of ARF1 and premature vesicle uncoating to allow cargo selection within the COPI vesicles (Goldberg, 2000; Lanoix et al., 2001; Majoul et al., 2001). Thus, TMED proteins interact with both ARF1 and ARF1 activating GEF to regulate the COPI vesicle formation process.

1.2.4.2 Cargo receptor function

1.2.4.2.1 GPI-APs

In yeast, EMP24p (ortholog of vertebrate TMED2), Erv25p (ortholog of vertebrate TMED10), Erp1p (ortholog of vertebrate TMED11), and Erp2p (ortholog of vertebrate TMED1) have been shown to bind Gas1p, a GPI-AP, and are responsible for proper transport of Gas1p (Schimmoller 1995, Belden and Barlowe 1996, Marzioch 1999, Muniz 2000). In mammalian CHO cells, silencing TMED10 leads to delayed transport of two GPI-APs, vesicular stomatitis virus G protein (VSVG), and decay-accelerating factor (DAF) (Takida et al., 2008). In Hela cells, silencing either TMED2 or TMED10 blocks the trafficking of another GPI-AP, folate receptor alpha, from ER to Golgi (Bonnon et al., 2010).

1.2.4.2.2 WNT proteins

WNT proteins are crucial secretory glycoproteins during embryogenesis. In *Drosophila*, Éclair (ortholog of vertebrate TMED11) and Emp24 (ortholog of vertebrate TMED2) are required for proper secretion of the *Drosophila* WNT protein, Wingless (Wg), in a genome-wide RNAi screen (Port et al., 2011a). In a different RNAi screen, *Drosophila* Opm (ortholog of vertebrate TMED5) is found to also interact with Wg (Buechling et al., 2011). Knockdown of TMED5 in HEK293T cells significantly reduces normal trafficking of WNT proteins (Buechling et al., 2011). A more recent study also shows that *Drosophila* P24δ (ortholog of vertebrate TMED10) colocalizes and interacts with Wg (Liao et al., 2015). The interaction of multiple TMED proteins with WNT proteins suggests a regulatory role of TMED proteins on normal WNT protein secretion. Mutations and abnormal expression which interfere the TMED function may impact the Wnt pathway during early embryogenesis process.

1.2.4.2.3 G-protein-coupled receptors (GPCRs)

Both TMED2 and TMED10 have been shown to regulate the transport of protease-activated receptor 2 (PAR-2), a GPCR protein, from Golgi to the plasma membrane (Luo et al., 2007). In HEK293T cells, TMED2 binds PAR-2 via interaction between the N-terminal region of TMED2 and the second extracellular loop of PAR-2 (Luo et al., 2007).

1.2.4.2.4 Toll-like receptors (TLRs)

TMED7 has been shown to regulate the expression of TLR-4, a key regulator in innate immunity and inflammation (Bryant et al., 2010; Liaunardy-Jopeace et al., 2014). Silencing of TMED7 inhibits cell surface expression of TLR-4, whereas overexpression

of TMED7 enhances its expression. However, the mechanism of interaction between TMED7 and TLR-4 remains unclear (Liaunardy-Jopeace et al., 2014).

1.2.4.3 Quality control

TMED proteins have also been suggested to function in ER quality control to prevent misfolded proteins from exiting the ERES, and retrieve escaped misfolded proteins back to ER via COPI vesicles. Wen et al. showed that reduction in *Sel-9* (ortholog of vertebrate TMED2) in *C. elegans* leads to increased secretion of a mutated and misfolded LIN-12/NOTCH receptor protein, GLP-1, suggesting a role of TMEDs in quality control mechanism (Wen and Greenwald, 1999). In yeast, p24/TMED protein complex acts in the quality control of GPI-anchored proteins through recycling incompletely remodeled GPI-anchored proteins back to ER by COPI vesicles and retains them in the ER until complete remodeling (Castillon et al., 2011).

1.2.5 TMED proteins in mouse development

Several mouse models have suggested that TMED proteins are required in early mouse embryogenesis. Loss of TMED10 leads to early embryonic lethality at E3.5 (Denzel et al., 2000), and loss of TMED2 shows embryonic lethality at E11.5 (Jerome-Majewska et al., 2010).

1.2.5.1 Tmed10 in mouse embryonic development

Denzel et al. showed that homozygous mutation in *Tmed10* results in early embryonic loss. No *Tmed10*$^{-/-}$ blastocysts are found at E3.5, indicating *Tmed10* is required for very early embryonic survival. The *Tmed10*$^{+/-}$ mice appear normal with no obvious abnormalities. However, molecular analysis shows a reduction in both mRNA and protein levels of *Tmed10* in *Tmed10*$^{+/-}$ mice compared to wildtype (WT) littermate

control (Denzel et al., 2000). In addition, reduced levels of TMED10 also lead to reduced TMED9 and TMED3 protein levels. The structure of the Golgi apparatus in *Tmed10*$^{+/-}$ mice also appears more dilated compared to controls in both kidney and liver tissues (Denzel et al., 2000).

1.2.5.2 Tmed2 in mouse embryonic development

The Jerome-Majewska group described a mouse model carrying a point mutation in the signal peptide of TMED2 (the 99J mouse line) made through an N-Ethyl-N-nitrosourea (ENU) mutagenesis screen (Jerome-Majewska et al., 2010). Mouse embryos with *Tmed2* homozygous mutation (herein referred to *Tmed2*$^{99J/99J}$) do not express TMED2 proteins by western blot and exhibit a variety of embryonic defects. At E8.5, *Tmed2*$^{99J/99J}$ embryos are developmentally delayed having fewer somites, an open neural tube, short and abnormal tail bud, ball-shaped allantois, and remain unturned when compared to wildtype littermates (Figure 1.7). At E9.5, *Tmed2*$^{99J/99J}$ embryos have abnormal heart looping and a truncated posterior body when compared to a wildtype E9.5 control embryo (Figure 1.7). By E10.5, *Tmed2*$^{99J/99J}$ embryos are much smaller with a truncated posterior and smaller tail (Figure 1.7). No *Tmed2*$^{99J/99J}$ embryos survive beyond E11.5 due to defects in placental development. *Tmed2*$^{99J/99J}$ embryos do not have a functional placenta due to impaired placental labyrinth layer development (Jerome-Majewska et al., 2010). The phenotypes associated with *Tmed2*$^{99J/99J}$ placenta will be further described in section 1.3.3.

1.2.6 TMED proteins in pathology.

In human, both TMED10 and TMED9 are found to play a role in the pathogenesis of Alzheimer's disease (AD) via modulating beta-amyloid (Aβ) production, a hallmark for

AD (Chen et al., 2006; Hasegawa et al., 2010; Vetrivel and Thinakaran, 2008). TMED6 and TMED10 proteins are highly expressed in secretory cell types such as rat pancreatic islets and insulinoma cells (Wang et al., 2012; Zhang and Volchuk, 2010). Knockdown of TMED6 or TMED10 in insulinoma cell lines prohibits proinsulin biosynthesis and decreased insulin level in the cell, suggesting that TMED proteins play a role in insulin biosynthesis (Wang et al., 2012; Zhang and Volchuk, 2010).

In addition, altered expression of several *Tmed* genes has been associated with tumorigenic process. TMED2 is hypomethylated in the metastatic breast adenocarcinoma cell line (Rodenhiser et al., 2008). TMED10 is highly expressed in human hepatocellular carcinoma (HCC) cells, and knockdown of TMED10 by shRNA significantly increases HCC cell apoptosis (Saran et al., 2015). Nonetheless, in a different study, TMED10 is suggested to be a negative regulator of TGF-β-induced prooncogenic signaling in the breast cancer cells, and gain-of-function for TMED10 leads to decreased tumor size in xenograft cancer model (Nakano et al., 2017). Similarly, TMED3 is identified as a colon cancer metastatic suppressor through a genome-wide *in vivo* screen (Duquet et al., 2014a), whereas in another study, TMED3 was shown to promote HCC metastasis through IL-11/STAT3 signaling (Zheng et al., 2016). The opposite effects of TMED proteins in various cancer models suggest that TMED proteins may be involved in different pathways and have distinct roles specific to the disease.

1.3 Mouse placental development

In this section, I will describe the developmental steps and establishment of crucial cell lineages in order to form a mouse placenta. *Tmed2*$^{99J/99J}$ embryos die due to impaired placental development and function, I will discuss the expression pattern of

Tmed2 during mouse placental development, and phenotypes associated with *Tmed2*$^{99J/99J}$ placenta. Then I will introduce two existing models of *ex vivo* culture of placental explants and their application in the study of tissue-specific requirement for genes in the placental development.

1.3.1 Overview of placenta

The placenta is essential for normal embryonic growth and development in mammalian animals. The placenta contains two vascular systems: fetal circulation and maternal circulation which are in close proximity. The placenta functions as the interface for normal nutrients and gas exchange, and fetal waste disposal between two vascular systems. The placenta produces pregnancy-associated hormones and growth factors that can impact maternal and fetal physiology, and form a protective barrier against maternal immune system to maintain normal pregnancy (Cross et al., 2003; Watson and Cross, 2005). The process of placental development is tightly regulated: any chemical, environmental insult, or genetic mutations that affect normal placental development may impair placental function, which can lead to abnormalities such as intrauterine fetal growth retardation and death, or maternal pregnancy related complications (Rai and Cross, 2014).

Based on the gross morphology and physiology of the maternal-fetal interface, mammalian placenta can be classified as four types: diffused (horse, pig), multicotyledonary (ruminants), zonary (carnivores), and discoid/bidiscoid (primates, rodents, rabbits) (Grigsby, 2016). Though the gross architecture between the human and the mouse placenta is different, the molecular mechanisms of placental development and overall structure are similar (Rossant and Cross, 2001). Both human and mouse placenta

belong to the discoid/bidiscoid group and are composed of three layers (Grigsby, 2016). In mouse, the mature placenta is composed of the outer maternal decidual layer, the junctional layer, and the inner labyrinth layer. The outer maternal layer includes decidual cells derived from uterine stromal cells as well as maternal vasculatures; the middle junctional layer helps connect fetal placenta to the uterus and contains spongiotrophoblast and trophoblast giant cells (GCs) that are essential for keeping normal placental function; the inner labyrinth layer is a highly vascularized layer and the main functional layer of placenta where nutrient exchange, gas exchange and waste disposal take place (Figure 1.8) (Rai and Cross, 2014; Watson and Cross, 2005). The human placenta also has three similar layers: the outer decidual layer, the middle basal plate layer which is analogous to murine junctional layer, and the placental villi, which is similar to murine labyrinth layer (Figure 1.8) (Rai and Cross, 2014).

1.3.2 Development of the placenta

1.3.2.1 Early development of human placenta

The early development of human placenta includes 5 typical stages: prelacunar, lacunar, primary villous, secondary villous, and tertiary villous (Benirschke et al., 2012). In the prelacunar stage, day 4.5 postcoitus (p.c.), a layer of cytotrophoblast cells is formed from the blastocyst (Selwood and Johnson, 2006). On day 6-7 p.c., a subgroup of cytotrophoblast cells differentiates to syncytiotrophoblast, which then invade into the uterine epithelium to initiate implantation (Figure 1.9a) (Benirschke et al., 2012). Implantation triggers the decidualization of maternal stroma cells to form the decidual layer. Soon after implantation, small vacuoles (Figure 1.9b, pink) appear within the syncytiotrophoblastic mass and continue to enlarge to form lacunae (Figure 1.9c, pink)

(Benirschke et al., 2012). The lacunae will eventually form the intervillous space, which is crucial for maternal blood circulation. The primary villous stage takes place on about day 13 p.c. where branches of cytotrophoblast cells are formed through increased cytotrophoblast cell proliferation (Figure 1.9d) (Benirschke et al., 2012). These branches form the primary villi, which, are composed of an outer layer of syncytiotrophoblast and an inner core of cytotrophoblast (Figure 1.9d). Two days later, mesenchymal cells originally derived from extraembryonic mesenchyme begin to invade the primary villi to form the secondary villi (Figure 1.9e) (Benirschke et al., 2012). In addition to secondary villi formation, cytotrophoblast cells located at the tip of the primary villi differentiates into column cytotrophoblast cells, which then differentiate into extravillous trophoblast cells in the basal layer (Figure 1.9e, f). On day 18 p.c., mesenchymal cells from the secondary villi differentiate into fetal capillaries to form the tertiary villi (Figure 1.9f) (Demi et al., 1989; Dempsey, 1972).

1.3.2.2 Early development of mouse placenta

The process of mouse placental development is well studied at both cellular and molecular levels (Rossant and Cross, 2001; Simmons and Cross, 2005; Watson and Cross, 2005). The development of mouse placenta initiates from the trophectoderm layer of the blastocyst at embryonic (E) day 3.5, until the fully matured placenta at E12.5. The development of three layers initiates at different time points: similar to the human placenta, the maternal layer is triggered by the implantation of embryos at E4.5 via invasion into the stroma of the endometrium. Following this process, hormones like estrogen and progesterone promote a process named decidualization in which the stromal cells surrounding the implanted embryo proliferate, and differentiate into decidual cells to

later form the decidual layer (Bagchi and Ph, 2011). Both the junctional and labyrinth layers are developed from two extraembryonic origins: 1. trophectoderm which gives rise to trophoblast giant cells, the ectoplacental cone (EPC), and extraembryonic ectoderm; and 2. extraembryonic mesoderm which forms the allantois (Cross et al., 2002) (Figure 1.8). At implantation stage (E4.5), the mural trophectoderm cells which are distal to the ICM become trophoblast giant cells (Rossant and Cross, 2001). The giant cells are critical for normal pregnancy and produce factors to regulate maternal blood flow to the implantation site, as well as factors involved in angiogenic, anti-angiogenic and vasoactive processes (Cross et al., 2002). They separate the EPC from the maternal decidua and express specific markers such as *Prolactin-3D1* (*Pr3d1)* and *Proliferin* (*Plf*).Both the EPC and the extraembryonic ectoderm are derived from the polar trophectoderm cells which are adjacent to the ICM at E5.5 (Cross et al., 2002; Rossant and Cross, 2001). By E7.5, the extraembryonic ectoderm gives rise to the chorionic ectoderm that will later form the chorion, a crucial tissue required for labyrinth layer formation. On the other hand, the EPC develops into spongiotrophoblast cell layer which is sandwiched between the giant cell layer and the chorion (Watson and Cross, 2005). The spongiotrophoblast cells also express a specific marker named *Trophoblast-specific protein alpha* (*Tpbpα).* They are pluripotent cells that can differentiate into several giant cell subtypes for structural support of the placenta (Cross et al., 2002; Simmons et al., 2007; Watson and Cross, 2005).

The allantois is derived from a subset of extraembryonic mesoderm cells which were originally derived from ICM. At E8.0, the allantois extends from the posterior end of the embryo towards the chorion. At E8.5, the allantois and the chorion join together through

a process named chorioallantoic attachment. It is well known that the attachment of chorion and allantois depends on expression of the cell adhesion molecule VCAM1 in the allantois and its receptor, α4-integrin in the mesothelium of the chorion (Gurtner et al., 1995; Kwee et al., 1995; Yang et al., 1995). Following chorioallantoic attachment, the chorion folds to form villi-like structure, and the chorionic mesothelial is displaced. Similar to the secondary villi invasion in human placenta, murine fetal blood vessels differentiated from the allantois migrate into the chorionic space to form the chorionic villi (Rossant and Cross, 2001; Watson and Cross, 2005) (Figure 1.10). Branch points on the chorion are determined by the expression of a specific transcription factor, *glial cells missing-1* (*Gcm1)*, in a subset of chorionic cells (Anson-Cartwright et al., 2000). During the branching process, *Gcm1* expression is maintained in the tips of the chorionic villi, which triggers chorionic trophoblast cell differentiation: *Gcm1* activates expression of the cell fusion factor *Syncytin B* (Syn B) in a subset of chorionic trophoblast cells to induce differentiation of Syncytiotrophoblast (SynT) layer II cells. Chorionic trophoblast cells which are close to SynT layer II cells express a different cell fusion factor *Syncytin A* (SynA) and differentiate into SynT layer I cells (Simmons et al., 2008). Both SynT layer I and II cells work in close proximity to form the "barrier" trophoblast cells between the maternal and fetal circulations in a way that the gas and nutrients exchange takes place between the endothelial and SynT cells without having mixing between two vasculatures.

1.3.2.3 Chorioallantoic attachment in labyrinth layer development

The process of chorioallantoic attachment is the first step in labyrinth layer development, and is a crucial step for normal placental function. Defects in chorioallantoic attachment are commonly associated with midgestation embryonic

lethality (Rossant and Cross, 2001). Many molecules are shown to be required in this process including the bone morphogenetic proteins (BMPs), fibroblast growth factor receptor 2 (FGFR2), adhesion molecule VCAM1, and its receptor α4-integrin (Fujiwara et al., 2002; Gurtner et al., 1995; Kwee et al., 1995; Lechleider et al., 2001; Mahlapuu et al., 2001; Solloway and Robertson, 1999; Xu et al., 1998; Yang et al., 1995; Ying and Zhao, 2001). BMPs are particularly important in allantoic development: knockout of *Bmp2, 4, 5, 7* and *Smad1*, downstream effector of *Bmp4*, as well as deficiency in the forkhead transcription factor 1 (FOXF1), an upstream regulator of *Bmp4*, show abnormal allantoic development (Fujiwara et al., 2002; Lechleider et al., 2001; Mahlapuu et al., 2001; Steingrimsson et al., 1998; Ying and Zhao, 2001). In addition, T-box transcription factor, BRACHYURY (T), and Lim domain transcription factor, LIM1, are also required in normal allantoic development (Galceran et al., 2001; Shawlot and Behringer, 1995). Both FGFR2 and ERR2/ERRβ, a nuclear hormone receptor, are crucial in the extraembryonic ectoderm-derived chorion development (Luo et al., 1997; Xu et al., 1998).

In addition to genes that are required for normal growth of the allantois and the chorion, many genes are important for the process of chorioallantoic attachment even when both tissues grow normally. For instance, knockout in either *Vcam1* or *α4-integrin* results in failure of chorioallantoic attachment and impaired labyrinth layer formation (Gurtner et al., 1995; Kwee et al., 1995). However, neither knockout shows complete blocking of chorioallantoic attachment, suggesting that other possible molecules exist to facilitate this process. For instance, homozygous mutation in a co-chaperone protein, MRJ, results in the failure of chorioallantoic attachment, although normal expression of

VCAM1 and α4-integrin is observed in *Mrj* null placenta (Hunter et al., 1999). Similarly, knockout in the cargo receptor protein, *Tmed2*, also shows failure of chorioallantoic attachment, albeit both VCAM1 and α4-integrin are expressed in *Tmed2* null placenta (Jerome-Majewska et al., 2010). In addition, *Wnt* signaling pathway has been shown to be required in the placental development. Knockout of *Wnt7b* (Parr et al., 2001), and *Tcf1* (Galceran et al., 1999), a transcription factor downstream of *Wnt*, show failed chorioallantoic attachment, knockout in *Wnt2*, and *Fzd5* (a Wnt receptor) show defects in subsequent branching morphogenesis in the chorionic villi (Lu et al., 2013; Monkley et al., 1996). Knockout of *Gcm1* completely blocks branching initiation in the chorion and the placenta fails to form the labyrinth layer (Anson-Cartwright et al., 2000); and knockout in both SynA and SynB leads to unfused SynT I and SynT II cells, which results in abnormal labyrinth layer formation (Anson-Cartwright et al., 2000; Dupressoir et al., 2011, 2009).

1.3.3 Role of Tmed2 in labyrinth layer development

In section 1.2.5, I described phenotypes associated with the $Tmed2^{99J/99J}$ embryos. All $Tmed2^{99J/99J}$ embryos die due to impaired placental development. The allantois from $Tmed2^{99J/99J}$ embryos is malformed with a bullous shape (Figure 1.7D), and only 50% of $Tmed2^{99J/99J}$ embryos undergo chorioallantoic attachment. Those *Tmed2* null embryos with abnormal chorioallantoic attachment show abnormal and limited contact between allantois and chorion when compared to the wildtype controls (Figure 1.11), and all $Tmed2^{99J/99J}$ embryos fail to form a labyrinth layer subsequently (Figure 1.11). These results indicate that *Tmed2* is required for proper labyrinth layer development.

In situ hybridization analysis on transcripts of the parietal GC marker, *Pr3d1*, the spongiotrophoblast cell marker, *Tpbpa*, and the SynT layer II marker, *Gcm1,* shows expression of all three markers in both wildtype and *Tmed2*$^{99J/99J}$ placenta (Jerome-Majewska et al., 2010). However, the expression of both *Gcm1* and *Tpbpa* is abnormal and mis-localized in the *Tmed2*$^{99J/99J}$ placenta, albeit the parietal GC marker, *Pr3d1*, appears normal (Figure 1.12) (Jerome-Majewska et al., 2010).

1.3.3.1 Expression of Tmed2 in mouse labyrinth layer

Jerome-Majewska group has shown the mRNA expression of *Tmed2* during labyrinth layer development. At E8.5, *Tmed2* is expressed in both the chorion and the allantois (Figure 1.13). Following chorioallantoic attachment, *Tmed2* is predominantly expressed in the labyrinth layer, spongiotrophoblast, and giant cells. By E10.5, *Tmed2* is highly expressed in the labyrinth layer and spongiotrophoblast cells, but its expression in giant cells is further reduced (Figure 1.13) (Jerome-Majewska et al., 2010).

1.3.3.2 Ex vivo culturing models to study chorioallantoic attachment

1.3.3.2.1 Whole-embryo culture

There are a number of *ex vivo* culturing models existing to study the process of chorioallantoic attachment. One particular example is the whole-embryo culturing technique, which has been greatly improved and widely used in the last two decades. This technology enables the study of the early organogenesis *in vitro*, and allows direct manipulation on the embryos (Tam, 1998). Combining with the micro-manipulation of certain tissues, whole-embryo culture have provided new information on lineage differentiation, tissue interaction and morphogenetic mechanisms during development (Tam, 1998). The whole-embryo culturing technique is also commonly used in the

placental studies (Downs, 2006; Downs and Gardner, 1995). Downs et al. have demonstrated that a donor allantois can be transplanted into mouse conceptuses in which their allantoides have been removed, and chorioallantoic attachment can take place when the allantois is stage-matched with the recipient chorion under whole-embryo culturing (Downs and Gardner, 1995). Furthermore, Downs et al. have shown that engrafting the wildtype allantoic core domain that is required for normal elongation of the allantois into the host with homozygous mutation in *Brachyury* (T^c/T^c), a transgenic mouse line with defects of shortened allantois, can rescue the defect and restore allantoic elongation (Downs and Enders, 2009).

1.3.3.2.2 Ex vivo culture of pre-placental tissues

Stecca et al. (2002) showed another *ex vivo* model and successfully demonstrated the physical attachment of explants of chorion and allantois using pre-chorioallantoic attachment tissues under common tissue culture conditions (10% fetal bovine serum supplemented RPMI1640 culture medium). These explants of chorion with allantois faithfully recapitulate the expression pattern of *Gcm1 in vivo.* Expression of *Gcm1* is quickly attenuated when pre-attachment chorions, dissected out of decidual tissues, are cultured without allantoides; similar to what has been found *in vivo* in embryos with abnormal chorioallantoic attachment (Hunter et al., 1999). This data suggests that the physical attachment of allantois is required to maintain the expression of *Gcm1* in the chorion.

In a third *ex vivo* model by Proctor et al. (2009) post-chorioallantoic attachment placenta are cultured using whole embryo culture conditions (50% rat serum supplemented DMEM). Upon culture, these explants demonstrate a decrease in

expression of genes associated with labyrinth layer formation, such as *Gcm1* and *SynA*, and an increase in expression of the junctional zone marker *Tpbpα* (Proctor et al., 2009). In addition, columnar epithelial cells of the chorion undergo apoptosis, and the distinct arc-like shape of the chorion is compromised in these post-attachment explants. Thus, culturing post-attachment placenta explants under whole-embryo culturing conditions is not sufficient to recapitulate events associated with labyrinth layer development.

1.4 Non-alcoholic liver disease (NAFLD)

Non-alcoholic fatty liver disease (NAFLD) is a common liver condition that affects 25-30% of the general population (Bellentani, 2017). In this section, I will briefly introduce the phenotypic changes associated with NAFLD, causes and current treatment of NAFLD, ER stress and its role in NAFLD, and progression of NAFLD to more severe diseases such as non-alcoholic steatohepatitis (NASH), cirrhosis, and cancer. The *Tmed2*$^{99J/+}$ adult mice develop phenotypes associated with NAFLD and may serve as a mouse model of human NAFLD, which will be further elaborated in chapter IV.

1.4.1 Overview of NAFLD

The human liver is located to the upper right of the abdominal cavity and consists of two main lobes. It is the largest vital organ in the body, and has a wide range of functions including bile synthesis, protein metabolism, glucose storage and metabolism, blood filtration and detoxification, as well as production of cholesterol and proteins involved in fat metabolism. Several liver diseases that impair normal liver function and mortality are commonly found in human: hepatitis, cirrhosis, ascites, gallstones, hemochromatosis and hepatocellular carcinoma (HCC). Liver cancer is the third leading cause of cancer deaths worldwide, with over 500,000 patients affected (Cicalese, L. 2017). HCC is the most

common primary liver cancer and approximately 70%-90% of HCC patients have chronic liver disease and cirrhosis, which can be developed from chronic infection by hepatitis B and C viruses, alcoholic fatty liver disease (AFLD), NAFLD, or NASH (El-Serag and Rudolph, 2007; Wong et al., 2009).

NAFLD is a spectrum of liver pathology characterized by excessive accumulation of fatty acids and triglycerides within the cytoplasm of the hepatocytes (Cuadrado et al., 2005). In addition to increased fat deposition in the liver, histological diagnosis of early NAFLD shows evidence of hepatocyte injury, manifested as ballooned hepatocytes, and infiltration of inflammatory cells, such as neutrophils (Day and Saksena, 2002). NAFLD is the most common cause of chronic liver disease (40-70%) as a consequence of increasing cases of obesity, diabetes, hyperdyslipemia, and insulin resistance, the main aspects of the metabolic syndrome (Cusi, 2012; de Lédinghen et al., 2004; Madan et al., 2004; Skelly et al., 2001; Torezan-Filho et al., 2004). NAFLD does not usually have any serious implications in patients, however, it can progress to non-alcoholic steatohepatitis (NASH), which is a more severe liver injury and is a caused by a combination of steatosis, inflammation, and 'ballooning' characterized by degeneration of cytoplasm within hepatocytes (Day and Saksena, 2002). To date, no non-invasive tests exist that can distinguish NAFLD from NASH have been developed. Therefore, it is difficult to know the exact incidence and prevalence of this disorder. A subset of patients with NASH eventually develops fibrosis/cirrhosis and are at a higher risk for developing HCC (Figure 1.14).

1.4.2 Causes and treatment of NAFLD in patients

The presence of NAFLD is highly related to risk factors for insulin resistance and metabolic syndromes such as central or visceral obesity, Type 2 diabetes, hypertriglyceridaemia, low high-density lipoprotein-cholesterol (Bellentani, 2017; Hübscher, 2006). The etiology of NAFLD is not fully clear but a 'two-hit' model has been suggested (Adams et al., 2005; ANDREA E. REID, 2001; Cortez-Pinto et al., 2006; Day and James, 1998; Diehl, 2004; Ramesh and Sanyal, 2005). Increased deposition of fat in hepatocytes is thought as the first "hit". Factors affecting increased free fatty acid absorption, and impaired fatty acid metabolism in the hepatocytes are the main components for accumulation of fat in liver. Cellular stresses such as oxidative stress, activated inflammatory cascades, and gut-derived endotoxins are suggested to act as the second "hit" to induce inflammation and fibrosis (Hübscher, 2006; Leamy et al., 2013; Takaki et al., 2013; Tolman and Dalpiaz, 2007) (Figure 1.15). Experiments of immunohistochemistry (IHC) have shown increased staining of lipid oxidation products in the liver to be associated with fat increase and a further increase of the oxidation products is associated with more severe phenotype of NASH (Le et al., 2004; Sanyal et al., 2001). In addition, immune responses to lipid peroxidation products can also contribute to disease progression (Albano et al., 2005). For instance, an increase in proinflammatory cytokine, tumour necrosis factor (TNF)-α, and decrease in anti-inflammatory cytokine, adiponectin, are associated with biopsy of NAFLD and NASH patients (Bugianesi, 2005; Diehl et al., 2005; Eckel et al., 2005; Kaser et al., 2005). Endotoxins generated by gut microbiota can also reach the liver via the portal vein and induce inflammation (Amar et al., 2008; Cani et al., 2007).

More evidence suggests the "two-hit" model cannot explain the complexity of the NAFLD and a "multiple hit" hypothesis has been proposed (Figure 1.16). Patients with polymorphisms in *Patatin-like phospholipase 3* (*PNPLA3*), a triacylglycerol lipase which facilitate triacylglycerol hydrolysis in adipocytes, are found to have higher risks of developing NASH (Jenkins et al., 2004; Tian et al., 2010). In addition, ER stress has been shown to be involved in many aspects of NAFLD including lipid accumulation, adipogenesis, inflammation, and insulin resistance (Ozcan et al., 2009; Sha and Qi, 2009). This data suggests that ER stress may be the link between steatosis, insulin resistance and inflammation (Tilg and Moschen, 2010). The detailed role of ER stress in NAFLD will be further discussed in the following section 1.4.3.

The treatment of NAFLD involves weight loss and pharmacologic therapy towards insulin resistance, dyslipidemia (Tolman and Dalpiaz, 2007). Lifestyle interventions including dietary modification and physical activities show improvement in obese patients with insulin resistance and fatty liver (Goopaster et al., 2010). Pharmacological therapies against insulin resistance have also been shown to be effective in treating NAFLD and NASH patients. Two peroxisome proliferator-activated receptor alpha (PPAR α) agonist drugs, metformin and pioglitazone, have clinically improved NASH (Takaki et al., 2013). Other studies have shown that antioxidants such as vitamin E, with thiazolidinediones and 1-aminobenzotriazole, two insulin sensitizers, can improve patients with NAFLD or NASH (Bugianesi et al., 2005; Musso et al., 2010; Nan et al., 2009; Arun J. Sanyal et al., 2010). In addition, a methylaxanthine derivative drug, pentoxyphylline, also has anti-oxidative effects and is shown to improve NASH in clinical (Daniell, 2012; Trial et al., 2012).

1.4.3 ER stress and NAFLD

Hepatocytes are ER-rich cells that synthesize a number of proteins including lipoprotein, very-low-density lipoprotein (VLDL), and cholesterol. As a result, factors such as ER stress and UPR have been shown to be involved in pathological changes in NAFLD. UPR has been shown to directly upregulate the transcription of genes encoding enzymes and lipogenic factors to enhance *de novo* lipogenesis and lipid formation (Lee et al., 2012). First, the PERK-eIF2a-ATF4 pathway regulates lipogenesis and hepatic steatosis. Deletion in PERK inhibits expression of lipogenic enzymes, such as fatty acid synthase (FAS) in mouse embryonic fibroblast cells (Ashraf and Sheikh, 2015). A recent study shows that activation of PERK-pathway signalling in hepatocytes enhances the expression of sterol regulatory element-binding protein (SREBP)1c and 2, which are key transcription factors in regulating *de novo* lipogenesis including fatty acid, triglyceride, and cholesterol metabolism (Amemiya-Kudo et al., 2002; Brown and Goldstein, 1997; Lauressergues et al., 2012). In addition, attenuation of eIf2α phosphorylation leads to a decrease in adipogenic nuclear receptor peroxisome proliferator-activated receptor gamma (PPAR γ) as well as its upstream transcription factors CCAAT/enhancer-binding protein α and β (C/EBPα, C/EBPβ) (Oyadomari et al., 2009). Mice with null mutation in *Atf4*, the downstream effector of PERK pathway, are protective of diet-induced obesity, hypertriglyceridemia as well as steatosis, and expression of PPAR γ, SREBP1c, FAS, and acetyl CoA is decreased in adipose tissues and liver (Li et al., 2011; Seo et al., 2009; Wang et al., 2010; Xiao et al., 2013). In addition, the proapoptotic protein C/EBP homologous protein (CHOP), JNK and other ER stress response genes have been found to be activated in mouse models of steatohepatitis (Ji and Kaplowitz, 2004; Rahman et

al., 2007; Schattenberg et al., 2006; Yang et al., 2007) and alcohol fed $CHOP^{-/-}$ mice have complete absence of hepatocellular apoptosis in response of alcohol stress. These results suggest that activation of PERK-eIF2a-ATF4 pathway is involved in steatosis via enhancing *de novo* lipogenesis.

The IRE1α-Xbp1 pathway has been shown to be required for regulating hepatic lipid metabolism. Deletion of *IRE1α* in mouse hepatocytes leads to severe steatosis phenotype under ER stress conditions (K. Zhang et al., 2011). In addition, IRE1α is required in the synthesis of apolipoprotein B (ApoB), which are key proteins involved in VLDL synthesis and secretion. A liver-specific knockout of *Xbp1* in mouse results in hypocholesterolemia, hypotriglyceridemia, and reduced production of lipids in the liver (Lee et al., 2008).

The ATF6 arm of the UPR pathway also plays a role in ER stress-induced lipid accumulation. The nuclear ATF6 interacts with nSREBP2 and thereby antagonize the transcription of downstream lipogenic genes and lipid accumulation by SREBP2 (Zeng et al., 2004). In *Atf6α* knockout mice with tunicamycin induced ER stress, an increase of accumulation in neutral lipids (triacylglycerol and cholesterol) in the liver as a result of reduced fatty acid β-oxidation and attenuated VLDL is observed. These mice exhibit steatosis with increased lipid droplets in the hepatocytes and die three days after injection due to unresolved ER stress (Yamamoto et al., 2010). When fed with high fat diet, *Atf6α* knockout mice exhibit tendency for a higher degree of insulin intolerance, steatosis with increased SREBP1c in the liver, indicating a preventive role of ATF6 in steatosis (Usui et al., 2012).

Puri et al. have demonstrated that activation of several UPR genes including the PERK pathway marker, eIF2α, is found in patients with NAFLD and NASH (Puri et al., 2008). Patients with NASH are associated with failure of making spliced XBP 1 protein and activation of JNK, effectors of IRE1 pathway (Puri et al., 2008). Taken together, all three UPR sensors, PERK, IRE1α, and ATF6α, are involved in lipid regulation in the liver. Disruption in any arms may result in ER stress induced steatosis.

1.4.4 From NAFLD to NASH and clinical scoring systems

An estimated 50% of NAFLD patients will progress to NASH, and small amount of NASH patients can develop cirrhosis and in some cases, HCC (Figure 1.14). The effective approach to establish a diagnosis of NASH and distinguishing it from NAFLD is the liver biopsy. A number of histologic scoring systems have been developed for diagnosing NAFLD and NASH including two studies by Kleiner et al. 2005, and Mendler et al. 2005. The scoring system suggested by the pathology committee of the NASH clinical research network from Kleiner's study uses the unweighted sum of Steatosis (0-3), lobular inflammation (0-3), and hepatocellular ballooning (0-2) scores. A score of ≥ 5 is defined as NASH (Kleiner et al., 2005). The Mendler's scoring system uses the sum of lobular inflammation and necrosis (0-3), Mallory bodies (0-3), hepatocyte ballooning (0-3), presinusoidal fibrosis (0-3), together with independent score of portal fibrosis (PF) (0-6) for diagnosis. The severity of NAFLD is characterized as: Grade 1 (PF <2 and Sum <4), Grade 2 (PF =3 or Sum =5-7), and Grade 3 (PF =4-6 or Sum =8-12) (Mendler et al., 2005). However, neither of these studies can distinguish alcoholic from non-alcoholic fatty liver diseases on histologic basis (Tolman and Dalpiaz, 2007).

1.4.4 Progression to cirrhosis, and HCC

Development of cirrhosis requires long periods of chronic liver disease. The main causes of cirrhosis are alcohol (60-70%), chronic hepatitis B or C virus (10%), biliary obstruction (5%-10%), and NAFLD (10%) (Heidelbaugh and Bruderly, 2006). Cirrhosis can be characterized by a decrease in hepatocyte proliferation which is associated with an increase in fibrotic tissue and a destruction of liver cells (Caillot et al., 2009; Delhaye et al., 1996; Sanyal et al., 2010). To date, a number of possible mechanisms underlining the development of HCC in patients with cirrhosis have been shown, such as telomere shortening, and cellular proliferation (El-Serag and Rudolph, 2007). In cirrhotic liver, telomere lengths are significantly shorter than the non-cirrhotic liver, and this shortening also links to a decrease in hepatocyte proliferation and fibrotic process (Ande et al., 2002). In addition, cirrhosis also activates stellate cells, which lead to increased production of cytokines, growth factors, products of oxidative stress (Bataller and Brenner, 2005), and later affect the hepatocyte proliferation (El-Serag and Rudolph, 2007). The decrease in hepatocyte proliferation can enhance cancer formation in cirrhotic liver, which was demonstrated in a rat study (Van Gijssel et al., 1997).

The current treatment for HCC includes liver transplantation, surgical resection, local ablative therapies, radiation therapy, and targeted systemic chemotherapy, such as Sorafenib, which can inhibit multiple kinases involved in tumor progression (Raza and Sood, 2014). Liver transplantation is the best treatment option for patients who had cirrhosis, with a 5-year overall survival rate of 75% with a low risk of recurrence (patients with one lesion <5cm, or 3 lesions<3 cm) (Mazzaferro, 2011, 2007; Mazzaferro et al., 1996). Surgical resection is another option for patients with single nodules, and no

cirrhosis (Raza and Sood, 2014). Patients who had surgical resection have an overall 70% five-year survival but with a high risk of recurrence. Local ablative therapies with Percutaneous Radiofrequency Ablation (RFA) are considered to be more effective than surgical resections for patients with early stage tumours.

1.5 Objectives of study

TMED2 mainly functions as a cargo receptor protein in early secretory pathway (Bonnon et al., 2010; Luo et al., 2007; Port et al., 2011b). Several studies have shown that disruption in TMED2 can lead to abnormal trafficking of proteins and ER stress (Bonnon et al., 2010; Luo et al., 2007; Port et al., 2011b). *Tmed2* homozygous mutation in mice leads to early embryonic death at mid-gestation and abnormal placental development (Jerome-Majewska et al., 2010). In addition, ER stress plays a key role in pathology of NAFLD and liver health in human (Amemiya-Kudo et al., 2002; Ashraf and Sheikh, 2015; Brown and Goldstein, 1997; Lauressergues et al., 2012; Puri et al., 2008; Usui et al., 2012; Yamamoto et al., 2010). Therefore, I hypothesize that TMED2 is required in the chorion for normal chorioallantoic attachment and subsequent placental labyrinth layer development and change in TMED2 levels in the liver leads to disrupted ER homeostasis and NAFLD in mouse liver.

To address this hypothesis, I have three objectives presented in chapter II, III, and IV. The first objective was to develop a novel *ex vivo* model of pre-placental explants that allows me to study placental labyrinth formation. The work associated with this objective is presented in chapter II. The second objective was to use this *ex vivo* model to study the tissue-specific requirement of *Tmed2* during the labyrinth layer development. Chapter III covers this part of my work. The third objective was to characterize and analyze

phenotypes of ER stress and NAFLD in livers of TMED2 heterozygous mice presented in chapter IV.

1.6 Figures

Figure 1.1 Schematic of protein secretory pathway in Eukaryotic cells.

Newly synthesized transmembrane and secretory proteins receive post-translational modification at the ER. Properly folded and modified proteins gather at ER exit sites (ERES) and are packaged into COPII-coated transport vesicles. After budding, those COPII vesicles can fuse to form the ER-Golgi intermediate compartment (ERGIC), and move to the Golgi along microtubules in the anterograde transport. ER-resident proteins including chaperones and cargo-receptor proteins and some misfolded proteins can be packaged into COPI vesicles to transport back to ER via retrograde transport. Transmembrane and secretory proteins transported to the Golgi are further sorted to their destinations including endosomal/lysosomal system (ELS) or the plasma membrane. This figure was modified from Strating and Martens, 2009.

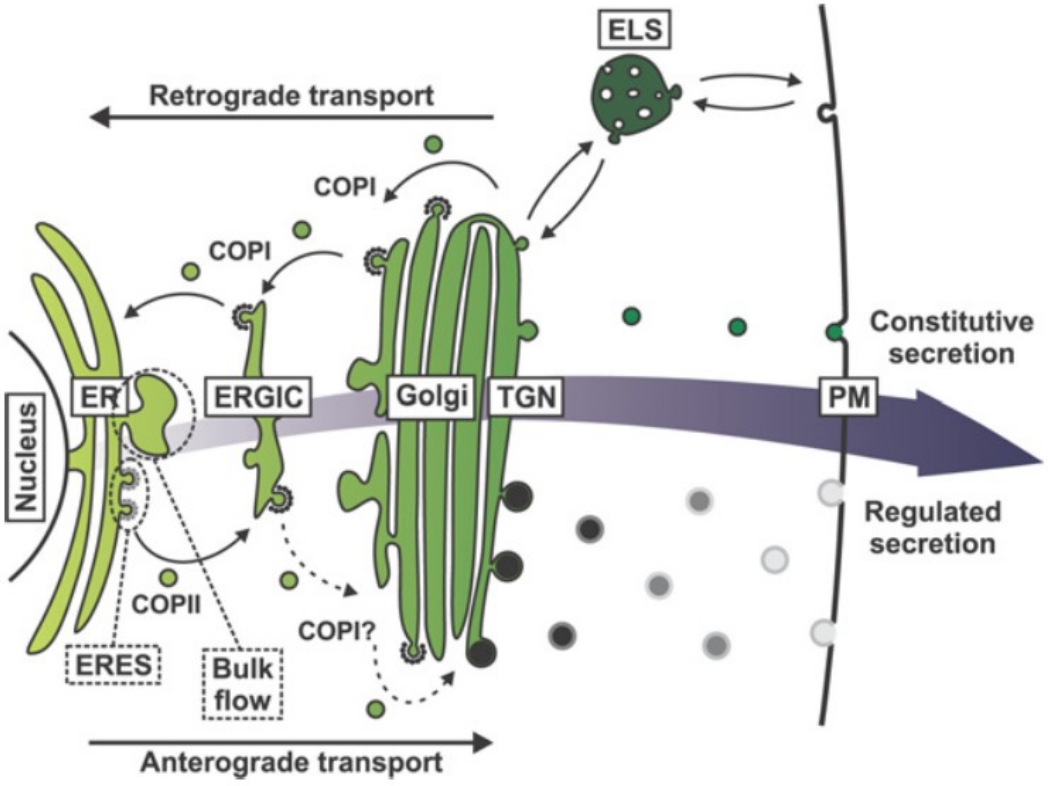

Figure 1.2 The COPII coat complex formation.

The COPII coat complex is composed of five components: the GTPase, SAR1, inner coat complex of SEC23/24, and outer coat complex of SEC13/SEC31. The initial step of COPII vesicle formation starts with the activation of SAR1 via an ER resident GEF, SEC12. The activated SAR1 (GTP-bound) recruits the heterodimeric protein complexes, SEC23/24 and SEC13/31. The SEC13/31 protein complex imposes curvature of the membrane to allow vesicle budding. This figure was modified from Brandizzi and Barlowe, 2013.

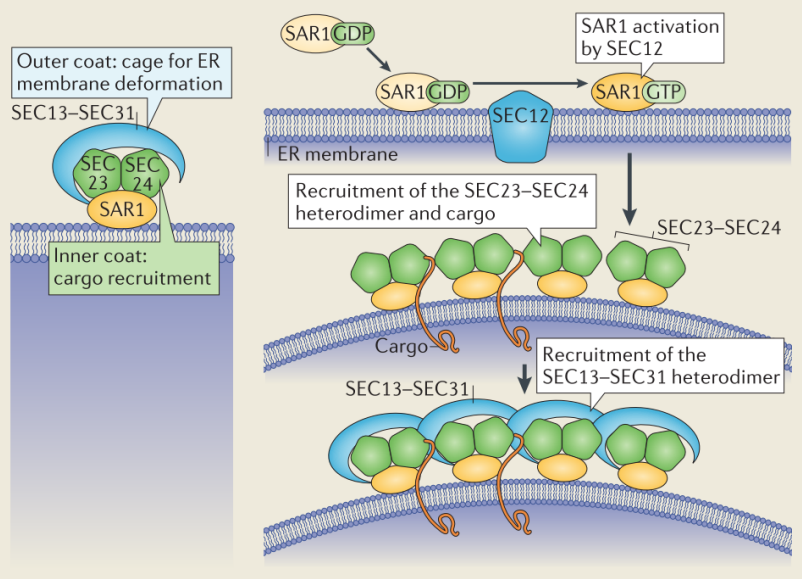

Figure 1.3 The structure of the COPII cage.

The COPII coating complex is composed of the SEC23/24 and SEC13/31 subcomplexes with flexible architecture. A. Structural model of the SEC13/31 outer cage, α and β represent vertex angles in between different SEC13/31 subcomplexes. B. Schematic represents the various vertex points of the SEC13/31 subcomplex. Variations in the α, β vertex and SEC31 hinge angles are associated with different COPII vesicle architecture. This figure was modified from Brandizzi and Barlowe, 2013.

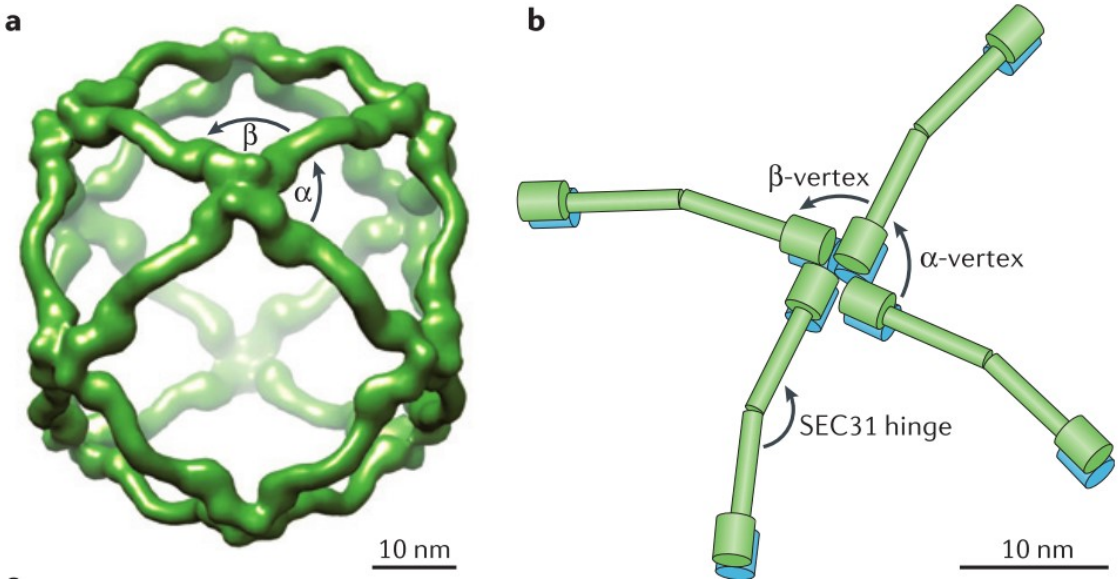

Figure 1.4 Schematic of activation of Unfolded Protein Response (UPR) pathway. Accumulation of misfolded proteins can activate three ER stress sensors including PERK, IRE1, and ATF6 through interaction with released BIP. PERK phosphorylate eIF2α to activate downstream ATF4, which is a transcription factor to block general protein synthesis and activation of transcriptions of genes involved in the ER quality control. Activation of IRE1 induces splicing of *Xbp1,* the spliced form of XBP1 is a transcription factor to induce transcription of ER-resident chaperones, ERAD, and lipogenesis proteins. Activation of ATF6 requires cleavage with S1P and S2P in the Golgi. The cleaved, active ATF6 is a transcription factor to induce ER chaperones, and XBP1 proteins. This figure was modified from Kadowaki and Nishitoh, 2013.

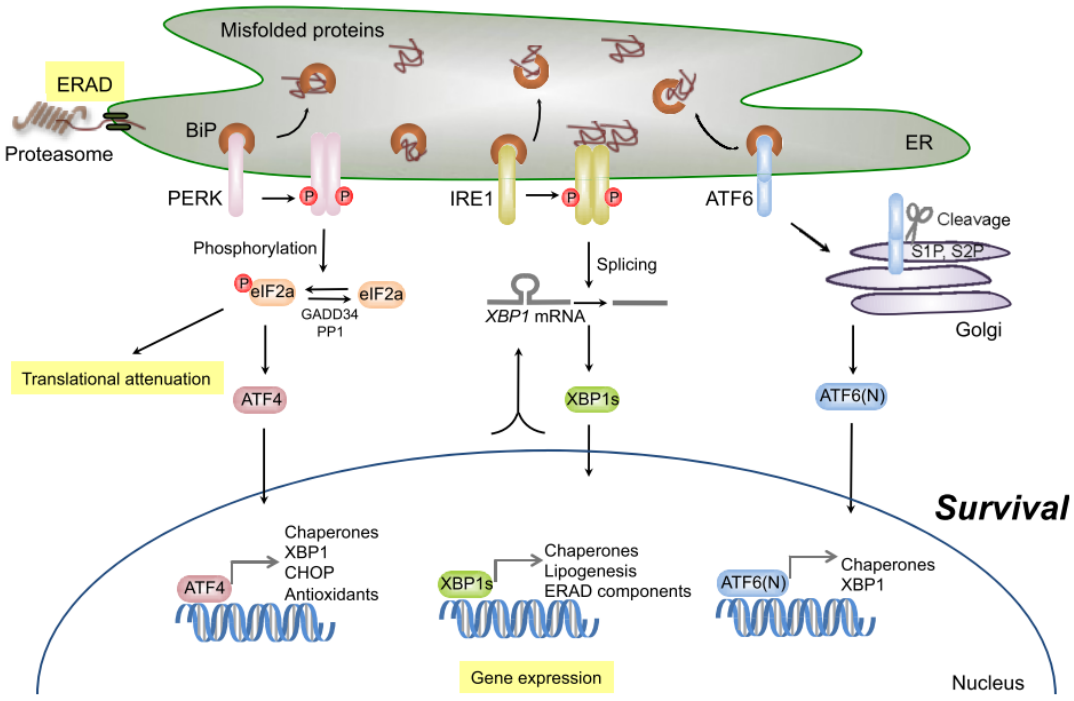

Figure 1.5 Function domains of TMED/P24 proteins.

All TMED proteins contain a large luminal region including a signal sequence at the N-terminus to translocate the protein into the ER, a GOLD domain functioning in interactions with cargo proteins and other TMED protein members (in yellow), a coiled-coil domain which is responsible for interactions between different TMED proteins as well as GPI-APs (in dark green), and a linker region (in white); a single transmembrane domain for anchoring protein in the ER membrane (in red); and a short cytoplasmic domain at C terminus for interaction with COP coating complex proteins (in light green).

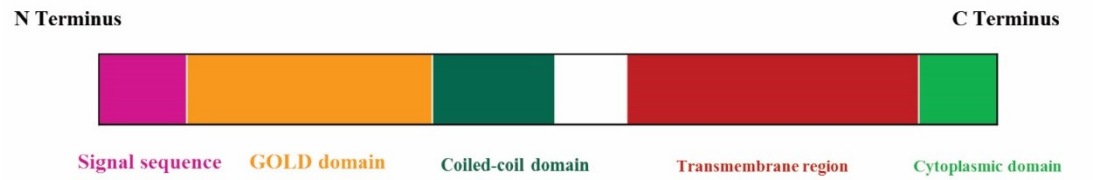

Figure 1.6 Crystal structure of TMED2 and TMED10 GOLD domains.

Overall structure of GOLD domains of TMED2 (left) and TMED10 (right). Protein and disulfide bond are shown in ribbon and stick for both proteins. The four β-sheets are labeled with letter and number code. Figure was modified from Nagae et al., 2016.

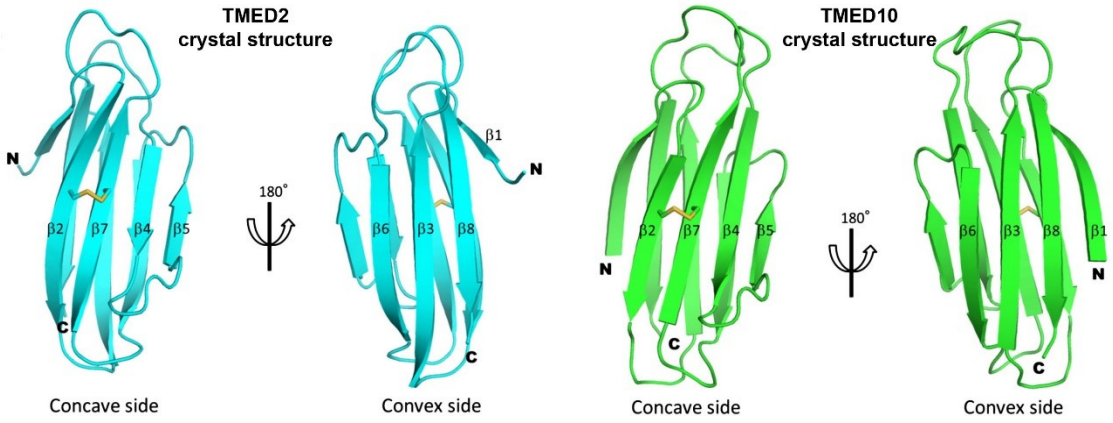

Figure 1.7 Phenotypes associated with *Tmed2* homozygous mutant embryos.

A. Representative image of a wildtype normally-developed E8.5 embryo with normal *sonic hedgehog (Shh)* mRNA expression in the node and midline. B. An E8.5 *Tmed2* homozygous mutant embryo resembles an egg cylinder with no somites, and expression of *Shh* in the head process. C. Representative images of the E9.5 wildtype embryo (on the left) that is turned and has over 20 somites, and the E9.5 *Tmed2* homozygous mutant littermate (on the right) who is unturned with an unlooped heart tube (arrow), smaller tail bud, and less somites. D. Representative images of the E10.5 *Tmed2* homozygous mutant embryo (on the right) who is now turned but remains developmentally delayed with a smaller sized torso and unattached allantois when compared to the wildtype littermate on the left. E. The posterior region of an E10.5 wildtype embryo (up) compared to a shortened posterior region of a E10.5 *Tmed2* homozygous mutant embryo at the bottom. H=heart, s=somite, al=allantois, tb=tail bud, fb=forebrain, ot= otic vesicle, fl=forelimb bud, hl=hindlimb bud, Scale bar=50 μm. This figure was modified from Jerome-Majewska et al., 2010.

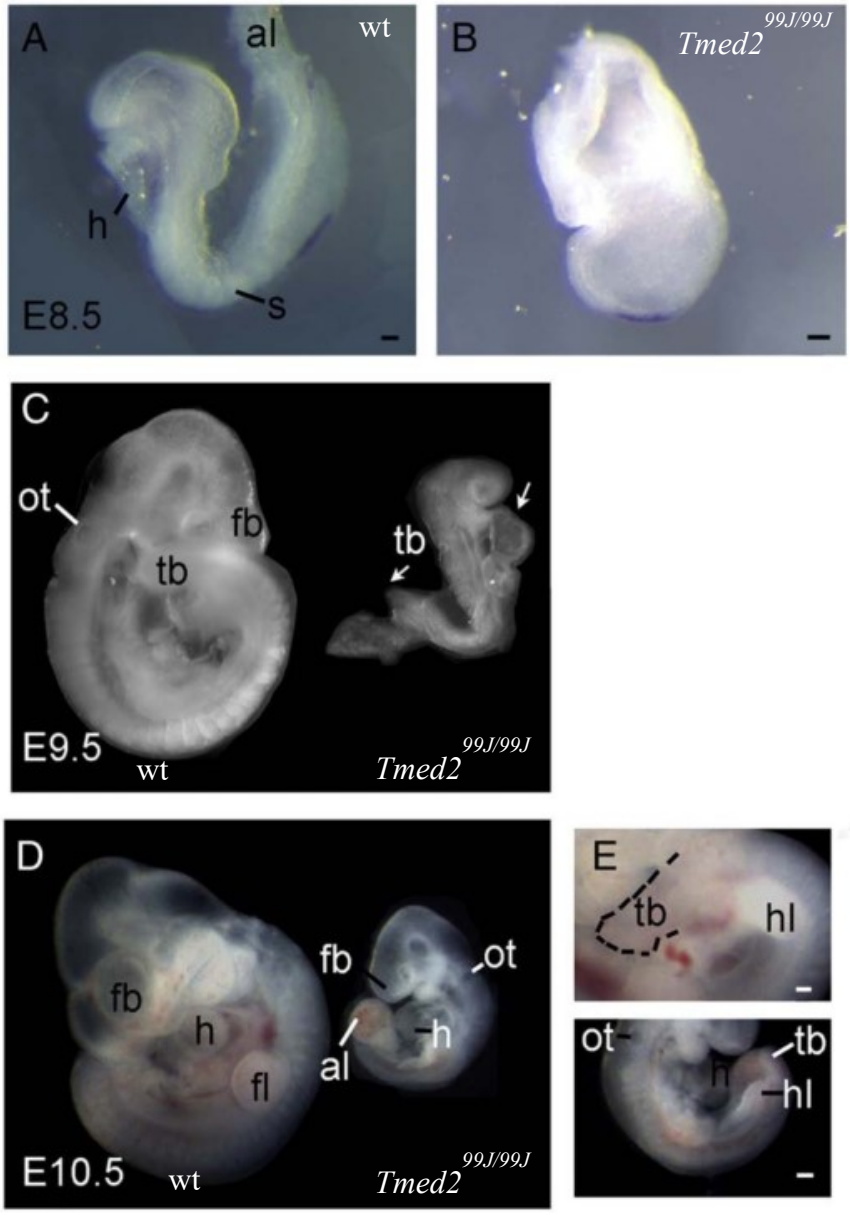
A
al
wt
h
E8.5
s
B
99J/99J
Tmed2
C
ot
fb
tb
tb
E9.5
wt
99J/99J
Tmed2
D
fb
fb
ot
h
h
al
fl
E10.5
wt
99J/99J
Tmed2
E
tb
hl
ot
tb
h
hl

Figure 1.8 Developmental origins of structures and cell types in mouse placenta. The presence of different cell lineages at various developmental stages. The right-side of the image shows the location of these cell types in different placental layers. This figure was modified from Cross et al., 2002.

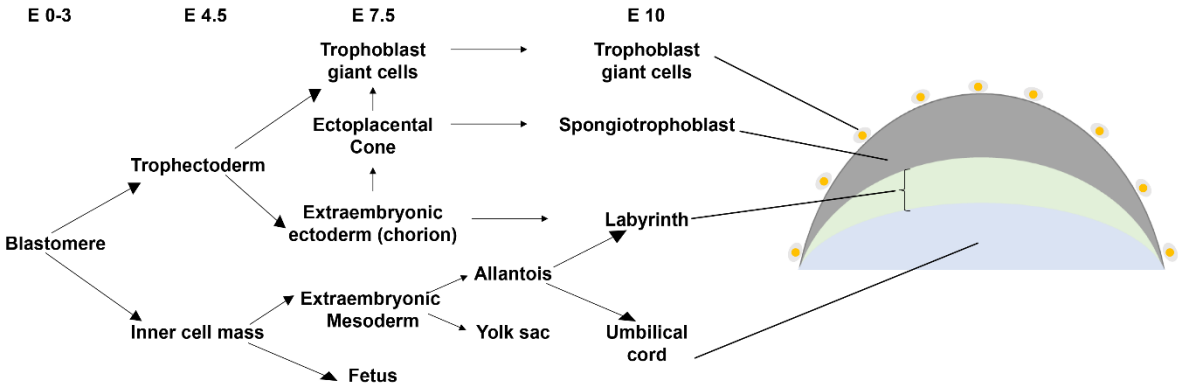

Figure 1.9 Diagram of 5 stages of early human placental development

(a) Prelacunar stage; (b-c) Lacunar stage; (d) Primary villous stage; (e) secondary villous stage; (f) tertiary villous stage. *Ac* amniotic cavity, *eg* endometrial glad, *ys* yolk sac, *eem* extraembryonic mesoderm, *eec* extraembryonic coelom, *ivs* intervillous space. This figure was modified from Benirschke et al., 2012.

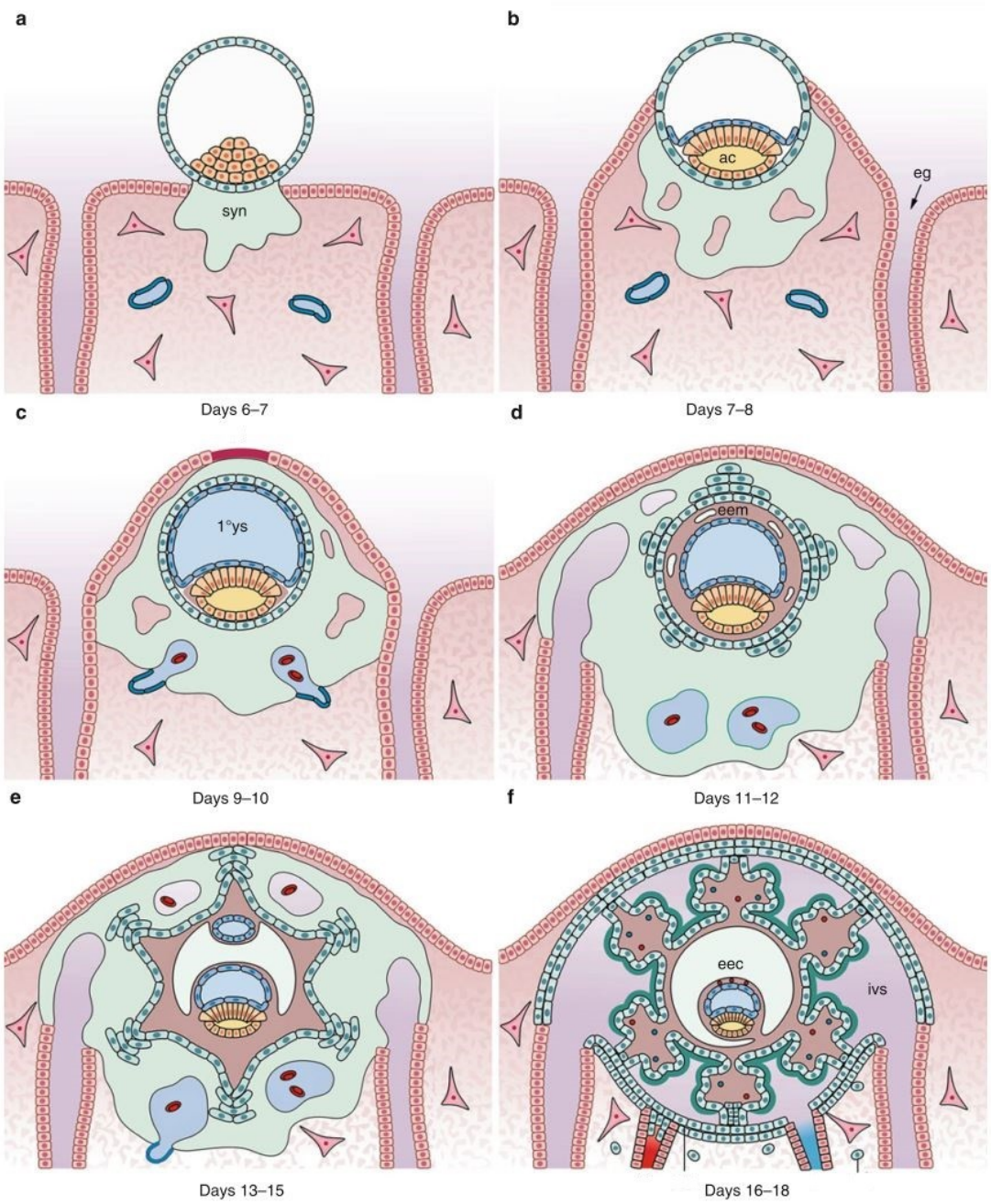

Figure 1.10 Scheme of the labyrinth layer development.

The allantois projects from the posterior end of the embryo towards the chorion at E8.0. At E8.5, the chorion and the allantois attach via a process called chorioallantoic attachment. This process is mediated by interaction between an adhesion molecule named VCAM1 and its receptor α4-integrin. Chorioallantoic attachment initiates the invagination of fetal blood vessels from the allantois into the chorion. In addition, the thin elongated cells of the mesothelium become morphologically dismissed and indistinguishable from the allantoic cells at E9.0 (Figure is adapted from D.P. Sarikaya, 2009, MSc thesis).

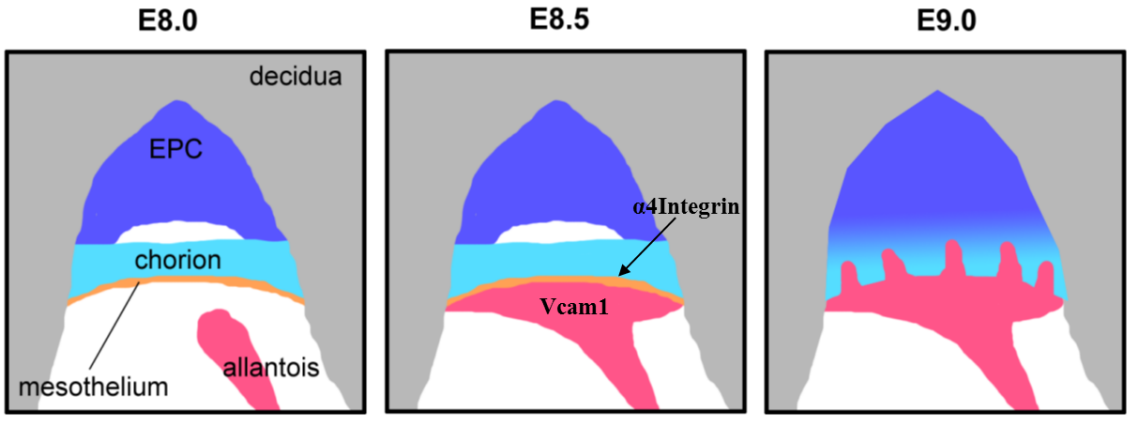

Figure 1.11 Abnormal labyrinth layer development in *Tmed2* homozygous mutant (*Tmed2*$^{99J/99J}$) placenta.

A. A normal E9.5 placenta with a fan shaped allantois (al) fusing with the chorion (ch). B. A representative image of a *Tmed2*$^{99J/99J}$ (99J) placenta with limited interaction between chorion and allantois. C. E. A normal E10.5 placenta showing distinguishable giant cells (gc), spongiotrophoblast (sp), and labyrinth (la) with maternal blood sinusoids (ms) in close proximity with fetal blood vessels (fv). D.F. A *Tmed2*$^{99J/99J}$ E10.5 placenta with no distinct spongiotrophoblast or labyrinth layer, but visible giant cells (arrow). Maternal blood sinusoids (ms) remained to be associated with chorion, and fetal blood vessels remained within the allantois. Scale bars =100µm (A, B),50µm (C, D), and 20µm (E, F). This figure was modified from Jerome-Majewska et al., 2010.

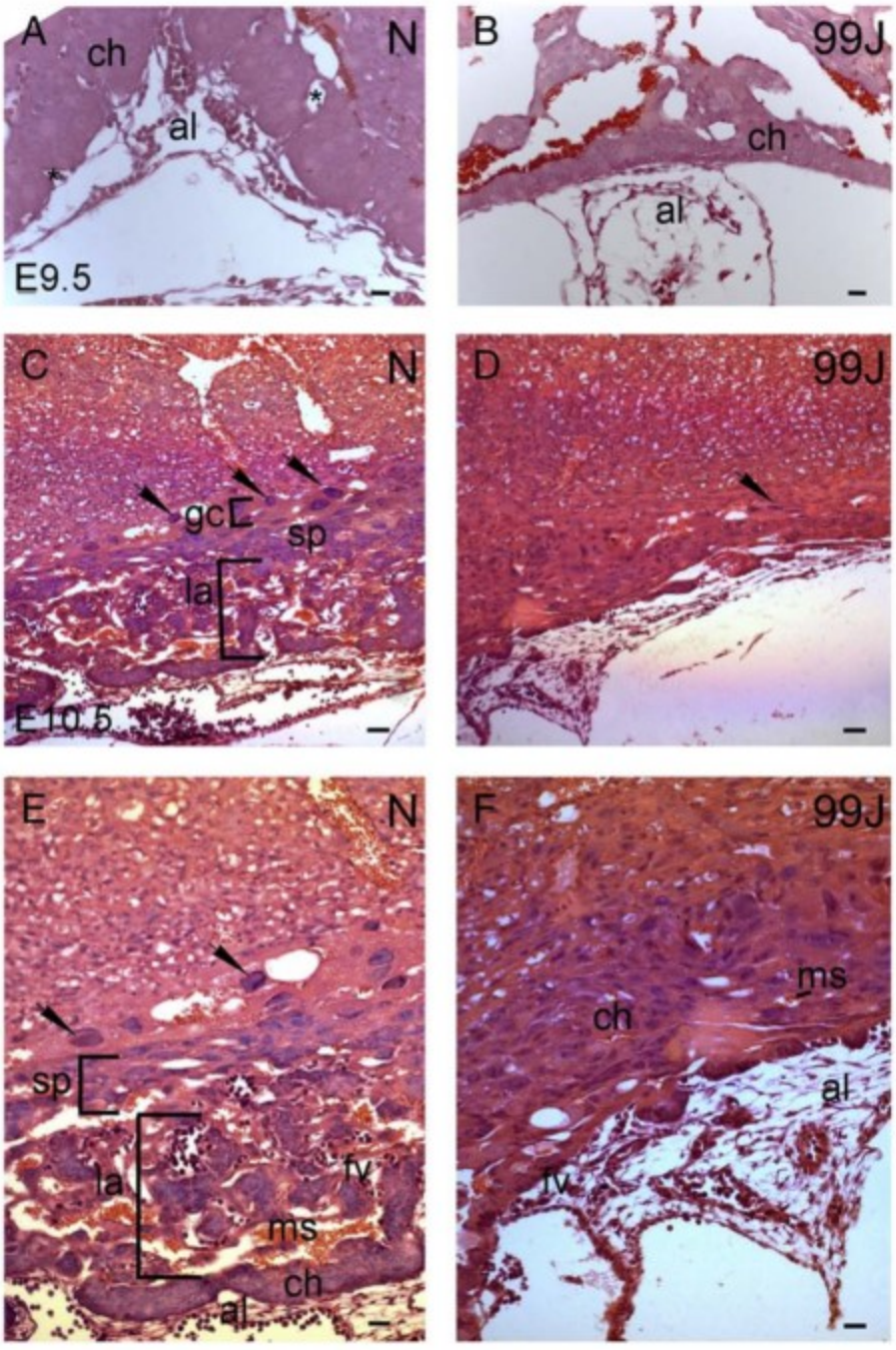
A
ch
N
al
E9.5
B
99J
ch
al
C
N
gc
sp
la
E10.5
D
99J
E
N
sp
la
fv
ms
ch
al
F
99J
ms
ch
al
fv

Figure 1.12 Abnormal expression of placental markers *Tpbpα*, and *Gcm1* in *Tmed2*$^{99J/99J}$ placenta.

Representative images showing the expression of the syncytiotrophoblast cell marker, *Gcm1*, in the E8.5 A. wildtype; B. *Tmed2*$^{99J/99J}$ chorionic trophoblast cells. Representative images showing C. expanded expression of *Gcm1* in the wildtype placenta; D. reduced expression of Gcm1 in the *Tmed2*$^{99J/99J}$ placenta at E9.5. Parietal giant cell marker pl-1 is expressed in E9.5 E. wildtype, and F. *Tmed2*$^{99J/99J}$ placenta. Expression of the spongiotrophoblast cell marker, *Tpbpα*, is located in the G. wildtype E9.5 placenta below the labyrinth layer; H. however, is resided immediately above the chorionic plate in the *Tmed2*$^{99J/99J}$ placenta at E9.5 (Arrows indicate the presence of the allantois). Dec=decidua, N=normal, 99J= *Tmed2*$^{99J/99J}$, la=labyrinth, fv=fetal vessels, ch=chorion, al=allantois. Scale bars =100μm. This figure was modified from Jerome-Majewska et al., 2010.

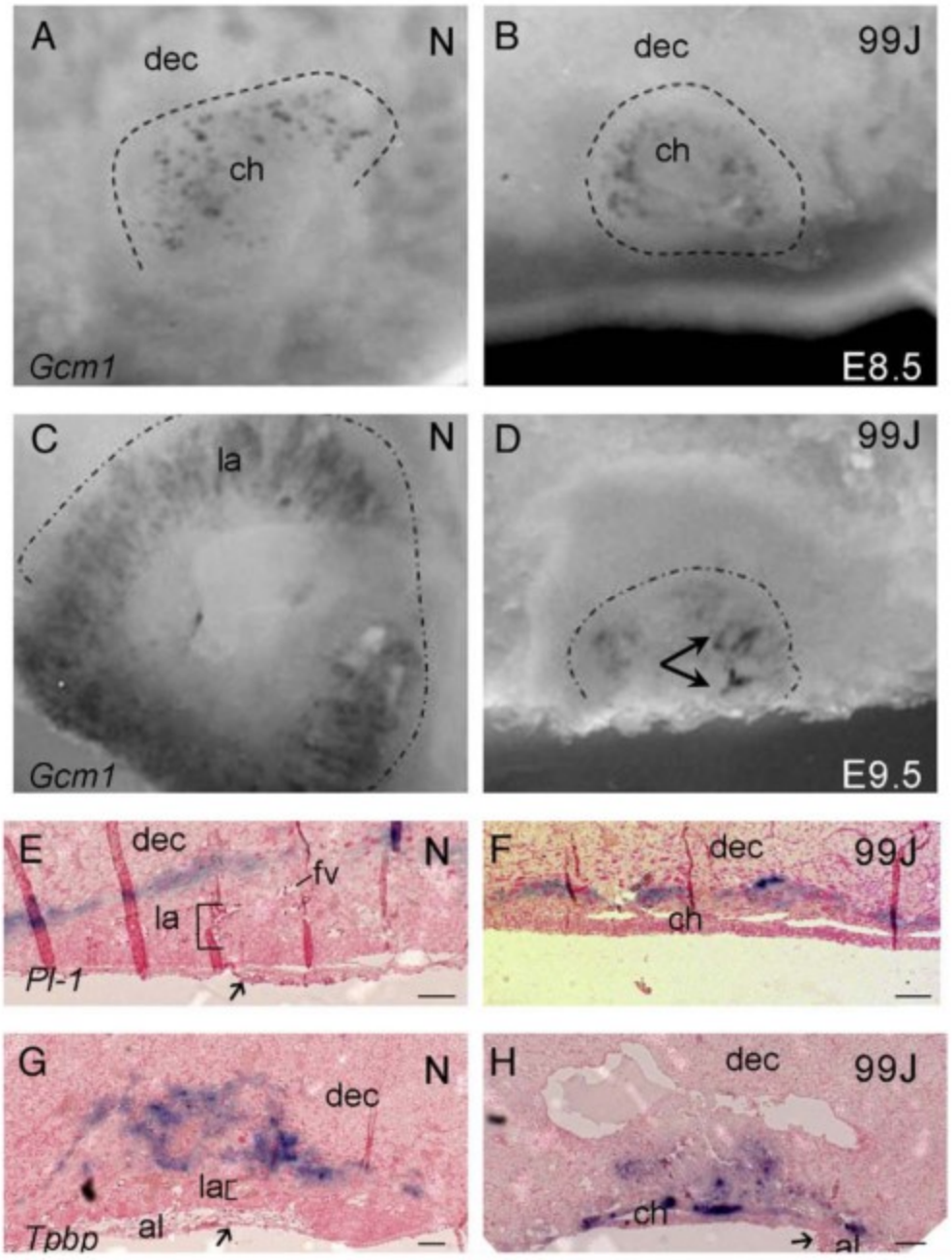
A
dec
N
ch
Gcm1
B
dec
99J
ch
E8.5
C
la
N
Gcm1
D
99J
E9.5
E
dec
N
fv
la
Pl-1
F
dec
99J
ch
G
N
dec
la
al
Tpbp
H
dec
99J
ch
al

Figure 1.13 *Tmed2* mRNA expression in the developing labyrinth layer from a wildtype embryo.

A. *Tmed2* is expressed in the chorion (ch) and giant cells (gc) after wholemount *in situ* hybridization (*ISH*) at E8.5. B. Expression of *Tmed2* is localized to the giant cells (gc), spongiotrophoblast (sp), and the labyrinth layer (lab), but not in the allantois (al) at E9.5 after section *ISH*. C.D. *Tmed2* is highly expressed in the spongiotrophoblast (sp), the labyrinth layer (lab), and weakly expressed in the giant cells (gc) or decidua (dc) at E10.5 after section *ISH*. Fv=fetal vessels, ms=maternal sinusoids, scale bar=20µm. This figure was modified from Jerome-Majewska et al., 2010.

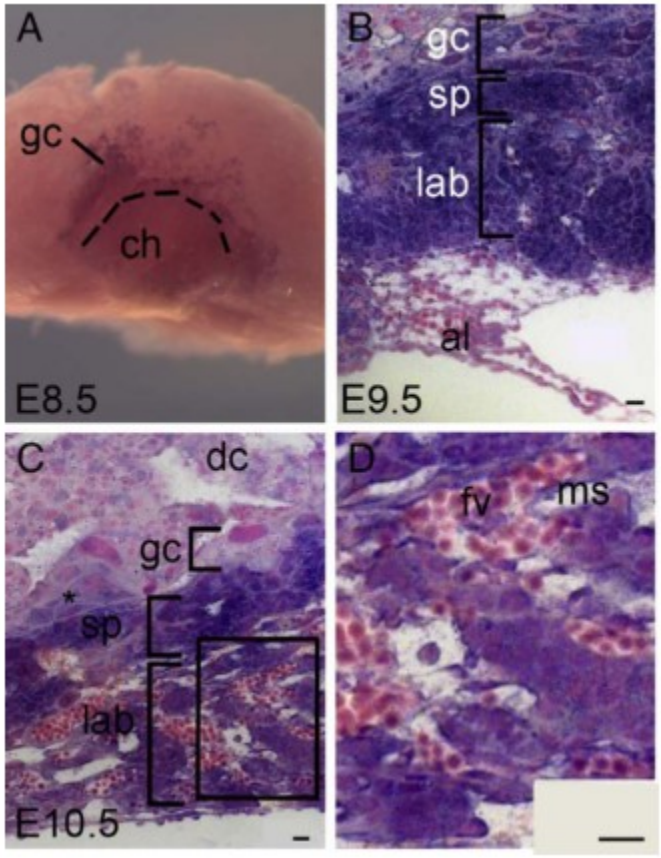

Figure 1.14 Progression of hepatocellular carcinoma (HCC) from a normal liver. The majority of people who develop non-alcoholic fatty liver phenotype exhibit fat change. This is a reversible process to a normal liver. A subset of people can progress to a more severe liver condition named steatohepatitis/ fibrosis. This process is less reversible. A even smaller proportion of the patients may develop to Cirrhosis and eventually HCC, this process is irreversible. This figure was modified from Hübscher, 2006.

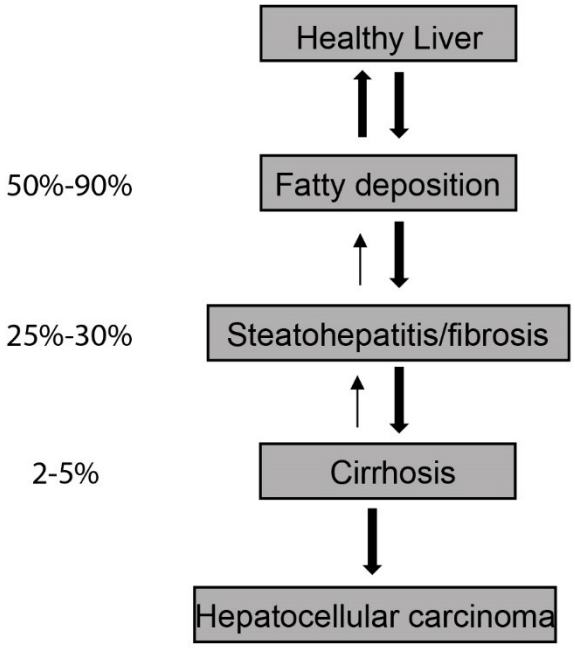

Figure 1.15 Two-hit model for pathological development of HCC.

The first hit, which is the development of steatosis due to alcoholic or non-alcoholic stimuli. Oxidative stress is believed to be the second hit in patients with steatosis, which will result in steatohepatitis, and some patients can eventually develop into more severe liver diseases including cirrhosis, carcinoma or portal hypertension, and eventually death. This figure was modified from Tolman and Dalpiaz, 2007.

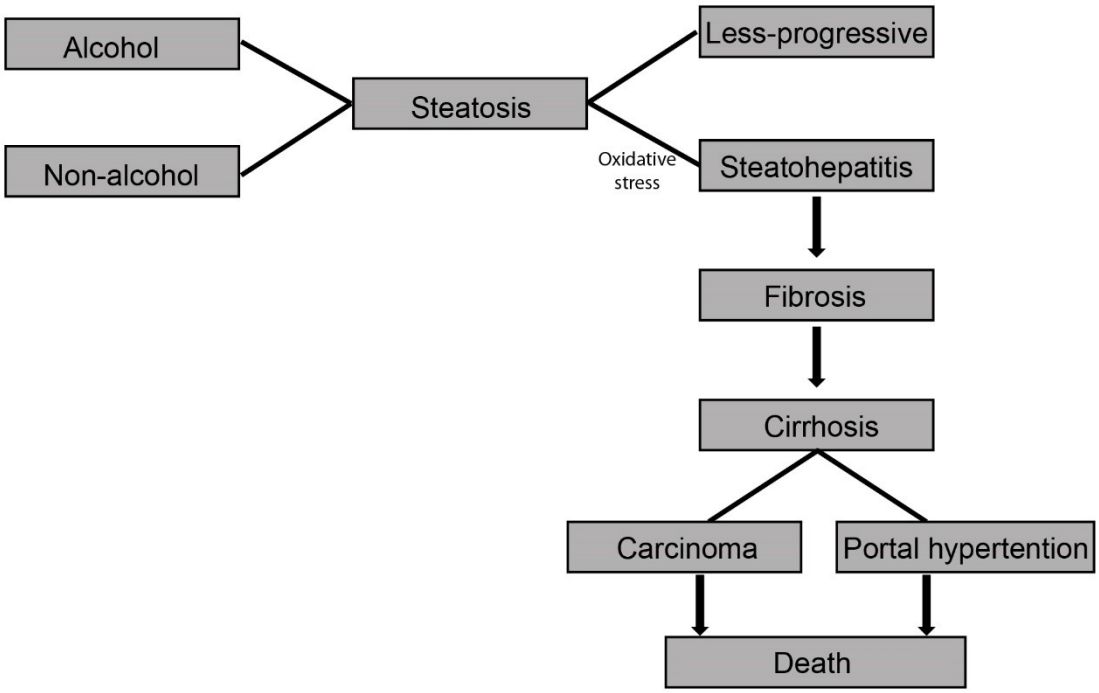

Figure 1.16 Multiple hits model for pathological development of HCC.

The first hit refers to the development of steatosis due to increased deposition of fat in hepatocytes. Patients with steatosis can have multiple hits including cellular stresses such as oxidative stress, apoptosis, gut-derived lipopolysaccharide, and inflammation, *PNPLA3* polymorphism, as well as increased ER stress to progress to steatohepatitis. Some patients eventually develop into more severe liver diseases including cirrhosis, carcinoma or portal hypertension, and eventually death. This figure was modified from Tolman and Dalpiaz, 2007.

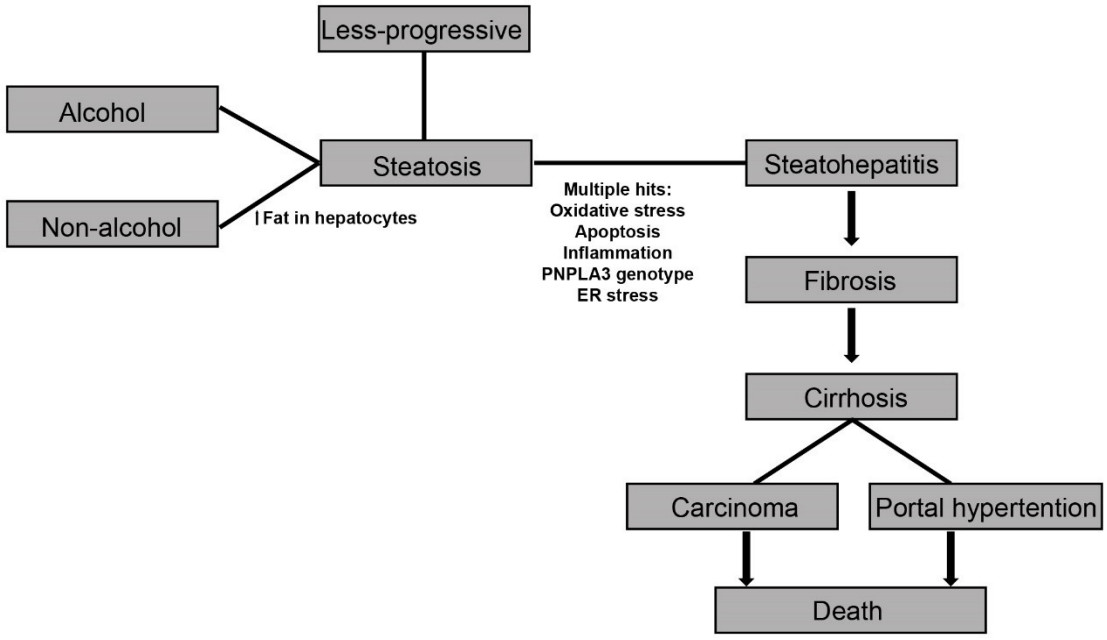

Table 1.1 ER stress related molecules in human diseases.

This table was modified from Kadowaki and Nishitoh, 2013.

Diseases	Key factors	The UPR signaling related physiological function &pathogenesis
Neurodegenerative disease		
Alzheimer's disease	Amyloid β (Aβ), IRE1, XBP1, PERK, eIF2α, CHOP	-Ab-induced activation of IRE1-XBP1 and PERK-eIF2αCHOP pathway
PolyQ diseases	Polyglutamine (polyQ), p97, IRE1, TRAF2, ASK1, JNK	- ERAD dysfunction by interaction of polyQ with p97 - Proteasomal inhibition and activation of IRE1-TRAF2-ASK1-JNK pathway by polyQ
Amyotrophic lateral sclerosis	SOD1, Derlin-1, ASK1	- ERAD dysfunction and ASK1 activation by interaction of mutant SOD1 with Derlin-1
	XBP1	- Digestion of mutant SOD1 by XBP1-mediated autophagy
Metabolic disease		
Hypertriglyceridemia	CREBH	- CREBH-induced expression of lipid metabolism genes
Inflammatory disease		
Inflammatory bowel disease	IRE1β, XBP1	- Protective effects against intestinal inflammation by IRE1β and XBP1
Diabetes mellitus		
Type 1 diabetes	CHOP, NO	- NO-induced β cell apoptosis through ER stress induced CHOP activation
Type 2 diabetes	PERK, eIF2α,ATF6	-Maintenance of ER function in β cell through PERK-eIF2α and ATF6
	CHOP	-Proapoptotic effects of CHOP in β cell
	XBP1	-Role of XBP1 in proinsulin processing and insulin secretion
	IRE1α	- IRE1αinduced *proinsulin* mRNA degradation under the condition of chronic high glucose exposure
Wolcott-Rallison syndrome	PERK	- Mutations of *PERK* related to β cell dysfunction in patients
Wolfram syndrome	WFS1	- Mutations of *WFS1* in patients, Control of ER Ca2+ homeostasis by WFS1
	ATF6	- Negative regulation of ATF6 and control in production and secretion of insulin by WFS1
Cancer		
Cancer	BiP, PERK, eIF2α	- Protective effects of BiP, the PERK-eIF2α pathway and the IRE1-XBP1 pathway in proliferation and progression of tumors
	IRE1, XBP1	pathway in proliferation and progression of tumors
Cardiovascular disease		
Atherosclerosis	CHOP atherosclerosis	- CHOP-induced Mφapoptosis and plaque necrosis in

Connecting text between Chapter I and II

In *Tmed2* null (*Tmed2*$^{99J/99J}$) embryos, the chorion and the allantois failed to undergo chorioallantoic attachment and the labyrinth layer also failed to form. The purpose of the study presented in chapter II is to create a novel *ex vivo* model of pre-placental tissues, which can investigate the tissue-specific requirement of TMED2 during chorioallantoic attachment. In the following chapter, I will describe the establishment of a novel condition to co-culture explants of wildtype pre-attachment placental tissues with wildtype pre-attachment allantois. The established *ex vivo* culturing conditions and analysis are also presented in this chapter.

Chapter II：*Ex vivo* culture of pre-placental tissues reveals that the allantois is required for maintained expression of *Gcm1* and *Tpbpα*

Wenyang Hou, Didem P. Sarikaya, Loydie A. Jerome-Majewska

Placenta **47,** 12–23 (2016). DOI: http://dx.doi.org/10.1016/j.placenta.2016.08.091

2.1 Abstract

Introduction:

Chorioallantoic fusion is essential for development of the labyrinth layer of the mouse placenta. However, events that occur after chorioallantoic attachment remain poorly described, partly due to difficulties of conducting *ex vivo* analysis of the placenta. Herein, we report conditions for *ex vivo* culture of the developing murine placenta.

Methods:

Mesometrial halves of decidua containing pre-attachment chorions were cultured alone or with explants of allantoides from stage-matched controls and analyzed by confocal and immunofluorescence (IF) microscopy. Expression and levels of marker genes associated with specific placental cell types were measured by *in situ* hybridization and qRT-PCR, respectively.

Results:

After 24 hours(hr) of co-culture, a mosaic pattern of $eGFP^+$ (enhanced Green Fluorescent $Protein^+$) and $eGFP^-$ cells were found when explants of pre-attachment chorions from $eGFP^+$ embryos were co-cultured with stage-matched allantoides from $eGFP^-$ embryos or vice versa. In addition, proliferation increased in the allantoic region and folds formed on the chorionic plate. Platelet endothelial cell adhesion molecule1 (PECAM1)-positive cells derived from the allantois were found in the chorionic region. Levels of the SynT-II marker, *Gcm1,* significantly increased at 24hr, although expression of *Gcm1,* was only found in explants co-cultured with an allantois at 12hr and 24hr. In addition, though levels of *Tpbpα* were not altered by co-culture with an allantois, *Tpbpα* was only detected in explants co-cultured with an allantois for 24hr.

Discussion:

Our data show that chorioallantoic fusion and events associated with initiation of labyrinth layer formation can be modeled *ex vivo,* and reveal a previously unsuspected requirement of chorioallantoic fusion for *Tpbpα* expression.

2.2 Introduction

The placenta is the interface for normal metabolic and gas exchange between the fetal and the maternal circulation, and is essential for rapid growth of mammalian embryos (Cross, 2000). In mouse, the mature placenta consists of multiple cell types that are organized into three histologically distinct zones: the maternal deciduum, the junctional zone, and the inner labyrinth layer. The labyrinth layer is a highly branched structure consisting of trophoblast-derived syncytiotrophoblast and giant cells which forms a trilaminar layer to separate fetal blood vessels and maternal sinuses. The junctional zone consists predominantly of spongiotrophoblast and glycogen cells that originate from the ectoplacental zone. Exchanges of nutrients, gas, and waste occur in the labyrinth layer, while the junctional zone provides support for placental growth and hormone production (Hu and Cross, 2010).

Formation of the labyrinth layer depends on chorioallantoic attachment and subsequent fusion of the chorion and allantois. Prior to chorioallantoic attachment, the allantois emerges as a bud of mesoderm cells from the posterior end of the embryos and grows towards the chorion. Trophoblast cells of the chorion undergo rapid proliferation which results in folding at the center of the chorionic plate and obliteration of the ectoplacental cavity (EC) (Hernandez-Verdun and Legrand, 1975). Chorioallantoic attachment is mediated by interactions between extraembryonic mesoderm cells in the

allantois and on the basal surface of the chorion; and occurs between embryonic day (E) 8.0 and E9.0 in embryos with 6 or more somite pairs (s) (Downs and Gardner, 1995). Recombination of allantois and chorion from embryos of asynchronous developmental stages showed that the chorion is competent to fuse with an allantois starting at the 1s stage, whereas the allantois exhibits maximal fusion in embryos with 3 - 5s (Downs et al., 2001; Downs and Gardner, 1995).

During chorioallantoic fusion, the mesothelial layer of the chorion which mediates the initial contact between the chorion and allantois is thought to degenerate (Downs et al., 2001), and a subset of chorionic trophoblast cells downregulate expression of tight-junction proteins, such as zona occluden 1 (ZO1) (Lu et al., 2013). On the other hand, the allantois spreads on the surface of the chorion to initiate the process of labyrinth layer formation (Watson and Cross, 2005). The primary vascular plexus of the allantois, consisting of endothelial cells expressing *Pecam1*, *Vcam1,* and *Flk1* invades the chorion by sprouting angiogenesis (Arora and Papaioannou, 2015; Drake and Fleming, 2000). In addition, chorionic trophoblasts that express the transcription factor *Gcm1* exit the cell cycle and initiate branching morphogenesis (Cross et al., 2006; Rossant and Cross, 2001). *Gcm1* expressing cells differentiate into one of the two syncytiotrophoblast cell-types, SynT-II, which separates allantois-derived embryonic blood vessels and maternal sinuses. In mutant embryos where chorioallantoic fusion fails to occur or in mice with loss of function mutations in *Gcm1,* branching morphogenesis is not initiated. In these mutants, both SynT-II and SynT-I cell types fail to differentiate and consequently the labyrinth layer of the placenta does not form (Anson-Cartwright et al., 2000; Gurtner et al., 1995; Jerome-Majewska et al., 2010; Yang et al., 1995).

In addition to chorioallantoic fusion, signals from the ectoplacental cone/ spongiotrophoblast are also required for labyrinth layer development. Mutations in genes required for maintenance of spongiotrophoblast lead to abnormal labyrinth layer development, and subsequently results in embryonic death (Adelman et al., 2000; Guillemot et al., 1994; Hitz et al., 2005). The specific contribution of the spongiotrophoblast to labyrinth layer formation is not clear, although it is postulated that these cells may provide signals or structural support important for labyrinth layer formation (Tanaka et al., 1997).

E*x vivo* organ cultures are widely used and provide insights into developmental processes such as kidney and lung morphogenesis (Gupta et al., 2003; Moral and Warburton, 2010; Piscione et al., 1997). A number of *ex vivo* placental models have been described, but are not well characterized. *Ex vivo* culture of embryos and their associated pre-placental tissues (ectoplacental cone, chorion and allantois) after chorioallantoic fusion supports syncytiotrophoblast differentiation and branching morphogenesis in static cultures (Hernandez-Verdun and Legrand, 1975). However, the ectoplacental cleft remains open and levels of *Syncytin A,* a marker of SynT-I decreases within 12hr (Proctor et al., 2009). In *ex vivo* cultures of pre-placental tissues after chorioallantoic fusion and without an embryo, the allantoic mesoderm degenerates and trophoblast differentiation is perturbed, as indicated by decreased expression of *Gcm1* and *Syncytin A*. Although expression of *Tpbpα,* a spongiotrophoblast marker, significantly increased in these *ex vivo* cultures, explants of pre-placental tissues post chorioallantoic fusion do not mimic the molecular differentiation events normally found *in vivo* (Proctor et al., 2009). Furthermore, explants of ectoplacental cone and chorion before chorioallantoic fusion

showed that *Gcm1* expression was only found if these explants are co-cultured with an allantois such that there is physical contact between the chorion and allantois (Stecca et al., 2002). Although, additional molecular and histological analysis of these explants were not performed, this finding suggests that explants of pre-placental tissues before chorioallantoic fusion may be a better model for studying the early events associated with placental development (Stecca et al., 2002).

We set out to determine if pre-attachment ectoplacental cones (EPCs) and chorions left in their associated decidua can be cultured with pre-attachment allantoides to mimic some of the events associated with early morphogenesis of the labyrinth layer. Herein, we report conditions for an *ex vivo* recombination system that recapitulate many of the changes associated with chorioallantoic fusion including: molecular changes, such as increased *Gcm1* expression and maintained expression of *Tpbpα,* morphogenic changes and trophoblast differentiation, including mixing of chorionic and allantoic cells and initiation of branching morphogenesis. We propose that this *ex vivo* model can be used to study chorionic and allantoic-specific contribution of genes required for early placental development.

2.3 Material and methods

2.3.1 Animals

All procedures and experiments were performed according to the guidelines of the Canadian Council on Animal Care and approved by the Animal Care Committee of the Montreal Children's Hospital. CD1 (*Charles River*) mice were used to collect wild type tissues, and Tg(HIST1H2BB/EGFP)1Pa (Hadjantonakis and Papaioannou, 2004) - a transgenic line on a mixed genetic background that ubiquitously expresses an H2B-eGFP

fusion protein in the nucleus - was used for collecting eGFP+ tissues. Tg(HIST1H2BB/EGFP)1Pa was a kind gift from Dr. K. Hadjantonakis. Retired stud male rats were purchased from *The Jackson Laboratory* for serum collection.

2.3.2 Rat serum collection

Blood was collected from the dorsal aorta of anesthetized rats. Rat serum was obtained after immediate centrifugation of the blood and stored at -80°C until preparation of the culture medium.

2.3.3 Isolation of allantoides and chorions for explant cultures

Female and male mice were mated overnight, and the presence of a plug the following morning was noted as E0.5. Pregnant females were euthanized at E8.0. On the day of dissection, decidua was removed from the uterus (Figure 2.1A). To remove embryos, an incision was made on the anti-mesometrial side of each decidua to remove the overlying tissue (Figure 2.1B**)**. After the anti-mesometrial portion of the decidua was removed, EGFP $^{+}$ embryos were distinguished from eGFP^{-} embryos under a stereo microscope with a GFP filter. Fine forceps were used to separate embryos from their associated yolk sacs (Figure 2.1B'). Embryos of 3-5s did not have chorioallantoic attachment and were easily separated from their extraembryonic tissues. The full allantois was cut from the tail-bud with a pair of fine forceps (Figure 2.1C'). All dissections were performed in 1xPBS. Tissues were either processed for explant cultures as described below (section 2.3.4) or collected for day 0. Decidua/EPC/chorion samples collected at day 0 were individually fixed in 4% Paraformaldehyde (PFA) overnight for immunohistochemistry or *in situ* hybridization. 3 pools of two chorion-only explants or

two chorions and allantois explants were stored in Trizol (Invitrogen) and used for qRT-PCR.

2.3.4 Explant of decidua/EPC/chorion or decidua/EPC/chorion with allantoides

For decidua/EPC/chorion only explants, samples were placed with the distal side containing the chorionic plate up, in 500ul of medium in 24-well tissue culture plates (Falcon) (Figure 2.1D). For decidua/EPC/chorion and allantois explants, $eGFP^+$ or negative decidua/EPC/chorion were placed as described above and a single $eGFP^-$ or positive allantoides were placed on top of the chorion, at an approximately 45-degree angle (Figure 2.1D'). Due to the convex morphology of the chorionic plate, the allantois remains associated with the chorion and can then be moved to 24-well tissue culture plates (Falcon) with 500ul of medium for culture (Figure 2.1D'). Presence of the allantois associated with the chorion was confirmed under a Leica dissecting scope (model MZ6), before culturing. Wholemount pictures were taken with an Infinity 1 Leica camera.

2.3.5 Culture conditions

Culture medium consisted of RPMI 1640, 50% rat serum, 4 μM L-Glutamine, and 50 μg/mL penicillin/streptomycin. Explants were cultured for 12 or 24 hours at 37°C in humidified tissue culture incubator (Fisher) with 5% CO_2.

2.3.6 Tissue processing and staining

Explants were fixed in 4% PFA/1x PBS overnight and were embedded with Shandon Cryomatrix (Thermo Scientific) and stored at -80°C freezer for frozen section analysis (Simmons et al., 2007), or dehydrated and embedded in paraffin. Paraffin embedded samples were sectioned at 5 μm thickness, and cryo-embedded samples were

sectioned at 10 µm thickness. Hematoxylin and Eosin (H&E) staining (Cardiff et al., 2014) was used for morphological analysis.

2.3.7 *In Situ Hybridization*

Plasmids containing *Prl3d1, PlF, Gcm1,* and *Tpbpα* riboprobes were kindly provided by Dr. Jay Cross (University of Calgary). *In situ* hybridization were performed as previously described (Simmons et al., 2008, 2007).

2.3.8 RNA extraction and quantitative RT-PCR

Cultured samples were washed once in 1xPBS and stored in Trizol. Pools of two explants were minced for RNA extraction according to manufacturer's protocol. Total RNA was treated with DNAse (NEB, according to manufacturer's protocol) and used for reverse transcription with the iScript^{TM} cDNA synthesis kit (Bio-rad Cat. #170-8890, according to manufacturer's protocol). qRT-PCR was performed using the QuantiFast SYBR Green PCR kit (Qiagen, Cat. #204054) on a Roche LightCycle 480 PCR machine. qPCR experiments were performed in triplicates to ensure technical replicability. Relative gene expression was determined using the $2^{-\Delta\Delta CT}$ method (Roche). RT-PCR program included a hot start at 95 °C for 5 min, followed by 40 cycles of a denaturation step at 95 °C for 10 s and an annealing/extension step at 60 °C for 30 s. The house keeping gene *Gapdh* was used for normalization. The data was normalized using the ratio of *Tpbpa*, *Gcm1* or *Syncytin A* to that of the *Gapdh* RNA. The following primers were used:

Gapdh (CTCATGACCACAGTCCATGC, CACATTGGGGGTAGGAACAC),
Gcm1 (AGAGGAAGGCCGCAAGATTTA, GGGGTCCATTGCAGTTGGG),
Tpbpa (CACAGTAGCGAAAATGACCAGG, TCCTCCTCTTCAAACATTGGGT), and

Syncytin A (CTGGGAATATGAACCCACTGTTA, GAGTTGAGGCAGAAGGAGTATG).

2.3.9 Immunofluorescence

Immunofluorescence experiments were performed according to standard protocols (Zakariyah et al., 2011). The following primary antibodies were used: phosphohistone H3 (Ser10) (1:200 dilution, Millipore, 06-570), ZO1 (1:50 dilution, Invitrogen, 339100), PECAM1 (CD31) (1:100 dilution, Abcam, ab28364), and cleaved caspase-3 (1:200 dilution, Asp175, Cell signaling, 9661). Alexa Fluor 568 and 594 conjugated secondary antibodies (ThermoFisher, 1:500 dilutions) were used. Slides were mounted with VECTASHIELD hard-set mounting medium with DAPI (Vector Labs, H-1500) to visualize the nuclei. Images were captured on a Leica microsystem (model DM6000B) and Leica camera (model DFC 450 C). Confocal images were obtained via a Zeiss LSM780 laser scanning confocal microscope.

2.3.10 Mitotic Index, Apoptotic Index and Statistical analysis

For each sample, 2 - 3 sections stained for phosphohistone H3 and DAPI or cleaved caspase-3 and DAPI were used for cell counts. Cell number was calculated with ImageJ software (Fiji, http://fiji.sc/).The mitotic index (MI) was determined by calculating the percentage of phosphohistone H3 positive cells over total number of chorionic and allantoic cells counted per section (Table 2.1). Apoptotic index (Ap. I) is a percentage of cleaved caspase-3 positive cells and was determined by calculating the number of cleaved caspase-3 positive cells over total number of chorionic and allantoic cells counted per section (table 2.2).

2.3.11 Statistical analysis

One-way ANOVA followed by the Tukey-Kramer multiple comparison from the Prism Software (http://www.graphpad.com/scientific-software/prism/) was used to calculate statistical differences. Significant p-values are represented as * for <0.05, ** for <0.01, *** for <0.001.

2.4 Results

2.4.1 Chorionic and allantoic cells are mixed in explants of pre-attachment decidua/EPC/chorion and allantois

Since EPC cells immediately differentiate into giant cells when explanted (Carney et al., 1993; Rossant and Tamura-lis, 1981), we postulated that excess differentiation of EPC cells contributed to loss of expression of syncytiotrophoblast markers in previously described placental culture systems (Hernandez-Verdun and Legrand, 1975; Proctor et al., 2009). Furthermore, since decidua derived cells block excess giant cell differentiation (Babiarz et al., 1992), we chose to leave the EPC and chorions associated with the decidua. We used transgenic embryos with widespread expression of CAG:H2B-EGFP ($eGFP^+$) in the precursors of the developing placenta (Figure 2.2) (Hadjantonakis and Papaioannou, 2004) to track cells from the chorion or the allantois after culture.

To determine if the allantois and chorion attach *ex vivo*, we cultured mesometrial halves of decidua containing EPCs and pre-attachment chorions of $eGFP^-$ embryos with 3-5s alone or with explants of $eGFP^+$ allantoides from stage-matched embryos, or vice versa, as illustrated in Figure 2.1A-D and depicted in Figure 2.1A'-D' for 12 hours (hr) (n=6, Figure 2.1E) or 24hr (n=10, Figure 2.1F). To confirm that the allantois remained attached to the chorion and to determine if any morphological changes occurred as a

consequence of chorioallantoic attachment, we performed histological analysis of these explants with hematoxylin and eosin staining. In chorion only samples, the epithelial layer of the chorionic plate was discernable but the mesothelial layer was no longer associated with the ectoderm after 12hr of culture (Figure 2.1G, n=5). A day later, the ectoderm was folded and appeared as a thin layer of epithelium with condensed nuclei (Figure 2.1H, n=5) in 24hr cultures. In contrast, after 12hr of culture, a distinct mesothelial layer was found between the chorionic plate and allantoic cells of decidua/EPC/chorion explants cultured with an allantois (Figure 2.1E', arrowheads, n=6). However, a mesothelial layer was no longer distinguishable at the junction in explants analyzed after 24hr of culture with an allantois (n=10) (Figure 2.1F').

To determine the extent of mixing between allantoic and trophoblast cells, we used confocal microscopy to examine distribution of cells labeled with the eGFP marker in cryosection of explants cultured for 12hr and 24hr (n=16, Figures 2.3 and 2.4). Analysis of explants consisting of decidua/EPC/chorions from $eGFP^-$ embryos and allantoides from $eGFP^+$ embryos after 12hr, revealed $eGFP^+$ allantoides in cylindrical shape, similar to pre-attachment allantoides of E8.0 embryos (Figure 2.3 A1-A6). In addition, allantoides remained mostly separated from chorions with little mixing of $eGFP^+$ and $eGFP^-$ cells (Figure 2.3 A7-A9). In contrast, in explants cultured for 24hr, allantoides spread to cover the surface of chorions (Figure 2.3 B1-B6), and significantly more mixing of $eGFP^+$ allantoic and $eGFP^-$ chorionic cells was found, when compared to 12hr cultures (Figure 2.3 B7-B12).

In the complementary experiment, explants of decidua/EPC/chorions from $eGFP^+$ embryos with 3-5s were co-cultured with $eGFP^-$ allantoides from stage-matched embryos

(Figure 2.4). In all cases, $eGFP^+$ giant cells were found migrating on the surface of the decidua (Figure 2.4 A1 and B1). In addition, after 12hr of culture the mesothelial cells - morphologically distinguishable with brighter eGFP signal and oblong shaped nuclei (Figure 2.4A7, A9) - formed a border between most of the allantois and chorion (Figure 3A9, arrowhead). Mixing of $eGFP^+$ chorionic cells and $eGFP^-$ allantoic cells was limited to regions where the mesothelium was no longer continuous (Figure 2.4A9 inset, white star). After 24hr of culture, the mesothelium could not be distinguished, and significantly increased mixing of $eGFP^-$ and $eGFP^+$ cells was observed (Figure 2.4 B7-B12). Thus, chorioallantoic fusion occurred *ex vivo,* and after 24hr of culture the mesothelium was no longer discernable with significant mixing between chorionic and allantoic cells.

To quantify the extent of mixing between allantoic and trophoblast cells, we analyzed 4 -5 cryosections at the midline of explants and calculated the percentage of $eGFP^+$ or $eGFP^-$ allantoic cells in the chorionic region of decidua/EPC/chorions from $eGFP^-$ or $eGFP^+$ embryos, respectively, cultured for 12hr or 24hr. On average 5.4% of cells in the chorionic region were of allantoic origin explants cultured for 12hr (n=5). This increased significantly, to approximately 14.3% after 24hr of culture (n=4). This data confirms the significant increase in mixing of allantoic and chorionic cells observed between explants cultured for 24hr compared to 12hr.

2.4.2 Expression of ZO1 *was maintained in decidua/EPC/chorion explants co-cultured with an allantois*

The tight junction protein, ZO1, uniformly expressed on the apical surface of trophoblast cells before chorioallantoic, is downregulated in regions of branching morphogenesis after chorioallantoic attachment (Lu et al., 2013). We performed

immunofluorescence microscopy using an antibody specific to ZO1 to determine if expression of this protein was modified in explants cultured with an allantois for 24hr, when we find significant mixing. In non-cultured pre-placental tissues, ZO1 was expressed on the epithelial surface of the chorionic plate (Figure 2.5A1-A3), similar to that previously reported (Lu et al., 2013). Immediately after chorioallantoic attachment, robust expression of ZO1 demarcated regions of branching on the chorionic plate (Figure 2.5A4-A9). In chorions cultured without an allantois, reduced expression of ZO1 was found in the chorionic region of explants (n = 2 out of 3, Figure 2.5 B1-B6). In explants cultured with an allantois, expression of ZO1 was also variable, with expression in 3 of 4 samples examined. In addition, ZO1 expression demarcated regions of branching on the chorionic plate (Figure 2.5B7 – B12). Thus, expression of this tight junction protein was not modified in our explant model system and differs from what was previously reported (Lu et al., 2013; Thiery and Sleeman, 2006).

2.4.3 PECAM1 positive cells are found in the chorionic region of decidua/EPC/chorion explants co-cultured with an allantois

The endothelial-specific protein, PECAM1 marks blood vessel formation in the labyrinth placenta (Drake and Fleming, 2000). Expression of PECAM1 was examined to determine if this protein was expressed in GFP^- derived allantoic cells found mixing with GFP^+ chorionic trophoblast. A core group of GFP^- allantoic cells expressed PECAM1 (Figure 2.6). In addition, expression of PECAM1 was also found in a subset of GFP^- cells in the chorionic region (white star, Figure 2.6B3, B4) as well as in a subset of GFP^+ trophoblast cells (purple star, Figure 2.6B3, B4). Our data shows that angiogenesis is initiated in this explant model.

2.4.4 The allantois is required for maintained expression of Tpbpα and *Gcm1*

In situ hybridization and qRT-PCR were performed to compare expression of genes that mark trophoblast giant cells, spongiotrophoblast, SynT-1 and SynT-II in explants cultured with or without an allantois for 12hr and 24hr. *Prl3d1*and *Plf* mark trophoblast giant cells, and were expressed in parietal trophoblast giant cells of all explants analyzed after 12hr (n=6) and 24hr of culture (n=7) (Figure 2.7). In addition, the domain of *Prl3d1* and *Plf* expression was comparable in explants cultured without (Figure 2.7 A, C, E, G) or with an allantois (Figure 2.7 B, D, F, H), suggesting that trophoblast giant cells were maintained in these *ex vivo* conditions.

In contrast to *Prl3d1* and *Plf*, expression of *Tpbpα*, a marker of spongiotrophoblast, was modulated by chorioallantoic fusion (Figure 2.7I-L). In explants of decidua/epc/chorions cultured without (n=5) or with an allantois (n=6) for 12hr, *Tpbpα* expression was distally restricted to the region of the EPC (Figure 2.7I and 2.7J). In explants analyzed after 24hr of culture with an allantois, *Tpbpα* expression was reduced, although the pattern was similar to what was found at 12hr (Figure 2.7L, n=6/7). However, explants cultured without an allantois showed no expression of this gene (n=0/5) (Figure 4K). To quantify the observed changes in *Tpbpα* level, qRT-PCR was performed on cDNA of explants with or without an allantois after 12hr and 24hr of culture (n= 3). However, no significant change was found in *Tpbpα* level in explants cultured with an allantois for 12hr or 24hr (Figure 2.7M). Our data indicate that chorioallantoic fusion does not modulate *Tpbpα* level, but is required for maintained expression *ex vivo*.

To assess syncytiotrophoblast differentiation, we examined expression of *Gcm1* as a marker for SynT-II, and *Syncytin A* as a marker for SynT-I. Consistent with the findings of *Stecca et al.* (Stecca et al., 2002), *Gcm1* was not expressed in explants cultured without an allantois for 12hr (n=0/5, Figure 2.8A) or 24hr (n=0/5, Figure 2.8C). In explants cultured with an allantois, *Gcm1* was expressed in clusters of trophoblast cells at the base of the chorionic plate (n=6, Figure 2.8B and 2.8B') at 12hr. After 24hr of culture, *Gcm1* was expressed in clusters of cells that were similar to those found at 12hr, and also in a subset of cells that line vessels in the explants (n=6, Figure 2.8D and 2.8D').

To determine if absence of *Gcm1* expression in explants cultured without an allantois reflects a decrease in *Gcm1* level, we performed qRT-PCR and compared levels of this gene in explants cultured with or with an allantois for 12hr and 24hr. No significant difference was found in *Gcm1* level in explants cultured with or without an allantois for 12hr. However, *Gcm1* level increased 2.2-fold in explants cultured with an allantois for 24hr, when compared to explants cultured without an allantois for 24hr ($p<0.001$, One-Way ANOVA, Figure 2.8E). Thus, the lack of *Gcm1* expression in explants cultured without an allantois for 12hr did not correlate with a significant difference in *Gcm1* transcript level in explants cultured with or without an allantois. Nonetheless, in this *ex vivo* system, co-culture with an allantois for 24hr resulted in a significant increase in *Gcm1* level, similar to what has been observed *in vivo.*

In contrast to *Gcm1*, *Syncytin A* expression was not detected by *in situ* hybridization in any explants analyzed at 12hr or 24hr (n=3, at each time point). Nor, did we find any significant difference in level of *Syncytin A*, in explants cultured without or

with an allantois for 12hr and 24hr (Figure 2.9). Thus, expression of the Type-I syncytiotrophoblast marker was not induced under this *ex vivo* culture condition.

2.4.5 The mitotic index (MI) of cells in the allantoic region is significantly increased after 24 hours of culture

Since, trophoblast cells at the branch point exit the cell cycle as a precursor to syncytiotrophoblast differentiation, immunofluorescence microscopy with antibody to Phosphohistone H3 (PH3) was performed to examine the pattern of proliferation in explants cultured with or without an allantois. The majority of PH3 positive cells were found in the chorionic plate, in the distal portion of explants cultured for 24hr without an allantois (Figure 2.10A, B). Few mitotic cells were found in the more proximal EPC. In explants cultured with an allantois, the pattern of PH3 positive cells was similarly restricted to the allantoic and chorionic region after 12hr and 24hr (Figure 2.10C and D). In addition, the mitotic index in explants cultured for 24hr with an allantois, was significantly increased, when compared to explants cultured without an allantois for 24 hours (Table 2.1A: MI=1.14, Stand error of mean (SEM)=0.13; $P<0.001$) or 12hr (Table 2.1A: MI=1.73, SEM=0.28, $P<0.01$) (Figure 2.10A-D; Table 2.1A). To quantify the relative distribution of mitotic cells after co-culture with an allantois, the mitotic index in the chorionic and allantoic regions of explants were calculated after 12hr and 24hr of culture. No significant difference was found between mitotic index of the allantoic and chorionic region at 12hr. A significant increase in mitotic index was found in the allantoic region after 24hr of culture (Table 2.1B: MI=6.90, SEM=0.33) when compared to the chorionic region of the same explants (MI=3.62, SEM=0.74) and the allantoic region of explants cultured for 12hr (Table 2.1B MI=1.41, SEM=0.46; $P<0.01$, Figure

2.10C and 2.10D; Table 2.1B). Thus, cells in the chorionic region have reduced mitosis when compared to the allantoic regions at 24hr.

2.4.6 Apoptotic index (Ap. I) significantly increased in explants cultured with an allantois for 24 hours

To examine apoptosis in these cultures, we performed immunofluorescence microscopy with antibody specific to cleaved caspase3. Apoptosis was increased in explants after 24hr of culture when compared to explants analyzed after 12hr of culture with or without an allantois (Figure 2.11). The apoptotic index was significantly higher in explants cultured with an allantois for 24 hours (Table 2.2A, Ap.I=9.66, SEM=1.56) when compared to explants cultured with an allantois for 12hr (Table 2.2A; Ap.I=1.51, SEM=1.14, $P<0.01$) and explants cultured without an allantois for 12hr (Table2.2A; Ap.I=1.04, SEM=0.33, $P<0.001$) and 24hr (Table 2.2A, Ap.I=2.74, SEM=0.44, $P<0.05$). To quantify the relative distribution of caspase3 positive cells in explants co-cultured with an allantois, we calculated the apoptotic index in the chorionic or allantoic regions of these samples. A significant increase was found in the allantoic region of explants co-cultured with an allantois for 24hr when compared to the chorionic region of explants co-cultured with an allantois for 12hr (Table 2.2B, $p<0.01$). In addition, no significant difference was found in the apoptotic index of the allantoic region of explants co-cultured with an allantois after 24hr when compared the chorionic region of the same explants (Table 2.2B). Thus, apoptosis increased over culture time but was distributed between the chorionic and allantoic region of explants co-cultured with an allantois for 24hr.

2.5 Discussion

In this study, we described culture conditions for explants of pre-placental tissues before chorioallantoic fusion, and showed that some of the early morphogenic and molecular events associated with labyrinth layer formation are observed in these explants. Using a fluorescent marker, eGFP, we showed that chorioallantoic fusion occurs and that allantoic cells mix with chorionic trophoblasts after 24hr of culture. Branching morphogenesis was initiated and marked by down-regulation of ZO1 in basal chorionic cells and presence of PECAM1 positive cells in the chorionic plate. qPCR showed no change in the expression of the SynT-I marker, *Syncytin A* and a significant increase in expression of the SynT-II marker *Gcm1* after 24hr of culture with an allantois. *In situ* hybridization showed that an allantois was required for sustained expression of the spongiotrophoblast marker *Tpbpα* at 24hr and for expression of *Gcm1* at both 12hr and 24hr. Cell proliferation and apoptosis increased in both the chorionic and allantoic regions during the 24hr culture period.

Stecca *et al.* previously reported that *Gcm1* expression depended on physical contact between the chorion and allantois using a transgenic line with a LacZ reporter in the *Gcm1* gene (Stecca et al., 2002). They further showed that maintenance of *Gcm1* expression was downstream of interaction between α4-integrin positive chorionic trophoblast and VCAM1 positive allantoic cells. Our qRT-PCR data revealed that expression of *Gcm1* was not significantly different between explants cultured with or without an allantois for 12hr, but significantly increased after 24hr in explants cultured with an allantois. Nonetheless, *Gcm1* was detectable by *in situ* hybridization only when the explants were co-cultured with an allantois at 12hr and 24hr. Similar to our observations in regard to *Gcm1* expression at 12hr, expression of *Tpbpα* was comparable

in explants cultured with or without an allantois for 24hr, by qRT-PCR. However, expression of this gene was only detected by *in situ* hybridization in the presence of an allantois. There are several potential explanations for these seemingly contradictory results: The first trivial explanation that primers for *Tpbpα* were not specific, were ruled out by sequencing the resulting product and confirming that the expected gene was amplified. The second trivial explanation that the samples used were contaminated with RNAse - therefore destroying the integrity of mRNA in these tissues - was also ruled out since all explants, including explants without expression of these two genes, showed expression of the parietal giant cell marker, *Pl1*. A third non-trivial explanation is a difference in the stability of *Gcm1* and *Tpbpα* mRNA in the chorion. We postulate that signals downstream of chorioallantoic attachment may result in stabilization of a subset of transcripts in the chorion. Although the mechanism underlying this stabilization signal from the allantois remains to be identified, several genes important in mRNA stability and decay are required for labyrinth layer development(Katsanou et al., 2009; Stumpo et al., 2004).

Our findings and those of Stecca *et al.* are opposite those of Proctor *et al.* who showed decreased expression of both *Gcm1* and *Syncytin A* when pre-placental tissues were cultured without an embryo(Hernandez-Verdun and Legrand, 1975; Proctor et al., 2009; Stecca et al., 2002). We propose three different reasons for these differences: (1) the time at which the explants were analyzed; (2) the amount of allantoic tissue explanted with pre-placental tissues after chorioallantoic fusion was not sufficient to generate or maintain the signal(s) required for *Gcm1* expression; or (3) one or more signals present in a pre-attachment allantois cannot be maintained when the allantois is explanted after

chorioallantoic fusion. Our data does not support the first two scenarios, since *Gcm1* expression was detectable by *in situ* hybridization when we explanted pre-placental tissues post-chorioallantoic fusion (data not shown). We favor the third hypothesis, although the identification of these signals remained to be determined.

Our study further suggests that though signals in the pre-attachment allantois were sufficient to maintain and increase expression of *Gcm1*, expression of *Syncytin A* was not affected by these culture conditions. We did not detect *Syncytin* A expression by *in situ* hybridization and qRT-PCR indicated no differences between samples cultured with or without an allantois at 12hr or 24hr. Furthermore, although *Gcm1* and *Syncytin A* were used as markers of the two distinct syncytiotrophoblast cell types in these studies, both genes are also required for differentiation of SynT-II and SynT-I, respectively (Simmons et al., 2008). Therefore, we predict that SynT-II differentiation and to a lesser extent SynT-I differentiation can occur under the conditions described in this paper, this remains to be determined by electron microscopy in future studies.

Surprisingly, we found that the allantois was required for *Tpbpα* expression after 24hr of culture, uncovering a previously unsuspected role for the allantois in spongiotrophoblast maintenance. It is known that labyrinth layer formation requires normal expansion of *Tpbpα* positive spongiotrophoblasts, and that mutants with abnormal labyrinth layer development often have decreased numbers of *Tpbpα* positive cells (Adelman et al., 2000; Du et al., 2014; Mould et al., 2012). Our findings suggest that abnormal expansion of *Tpbpα* positive spongiotrophoblasts could also be due to abnormal signaling from the allantois.

Herein, we reported an *ex vivo* murine placental model that captures early stages of placental development, including chorioallantoic fusion and trophoblast differentiation. This model is easily adapted for most laboratories and does not require any additional or specialized machines. In our hands, the most difficult aspect of this model was due to loss of eGFP signal in samples embedded in paraffin or when antibodies that required antigen retrieval were used. The explant model described successfully captures some of the key interactions between the chorion and allantois, and will be useful for future studies of early placental development. The simplicity of *ex vivo* models has accelerated research in studies of kidney and lung development (Gupta et al., 2003; Moral and Warburton, 2010; Piscione et al., 1997), therefore a successful protocol for *ex vivo* culture will advance our knowledge of placental development. We expect that the conditions described in this study, combined with future live imaging of explants, will shed much needed insights into the cellular events occurring during branching morphogenesis of the developing placenta.

2.6 Acknowledgement

We would like to thank Dr. James Cross for his generous gifts of *Prl3d1*, *Plf*, *Gcm1*, *Tpbpα,* and *Syncytin A* plasmids for *in situ* hybridization experiments. We would also like to thank Dr. K. Hadjantonakis for the kind gift of the Histone-H2B-eGFP reporter mouse line. We would like to thank MC Beauchamp, V Keser, S Bader, and A Fields for helpful feedback on the manuscript. This work was supported by grants from the Natural Sciences and Engineering Council of Canada (NSERC – grant number 214976) to L.JM. L.J.M. is a member of the Research Institute of the McGill University Health Centre,

which is supported in part by the FRQS. W.H. was supported in part by Centre for Research in Reproduction and Development of McGill University.

2.7 Figures

Figure 2.1 Chorioallantoic fusion occurs when explants of decidua/epc/chorion are co-cultured with an allantois.

Illustration (A – D) and representative images (A'-D') of experimental steps for explanting pre-placental tissues before chorioallantoic fusion, as described in the Materials and Methods. (E-H) Representative images of H&E stained sections of decidua/epc/chorion explants after 12 hours (E, E') and 24 hours (F, F') of culture with an allantois. E' and F' are higher magnification pictures of boxed regions in panels E and F. Representative images of H&E stained sections of decidua/epc/chorion explants after 12 hours (G, G') and 24 hours (H, H') of culture without an allantois. G' and H' are higher magnification pictures of boxed regions in panels G and H. Chorion (ch), allantois (al); black arrows indicate mesothelium in panel E', G'. Scale bar for A'-D'= 200μm, scale bar for E-H =50μm

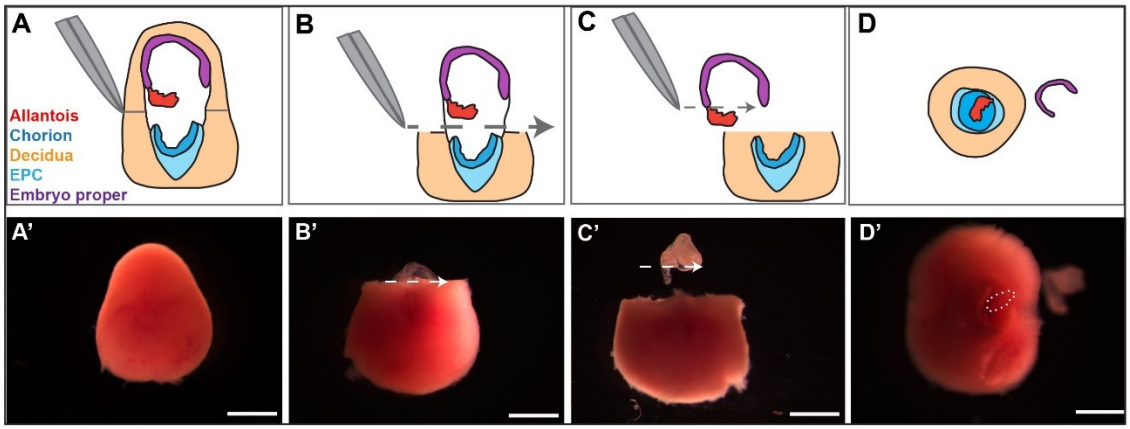
A
B
C
D
Allantois
Chorion
Decidua
EPC
Embryo proper
A'
B'
C'
D'

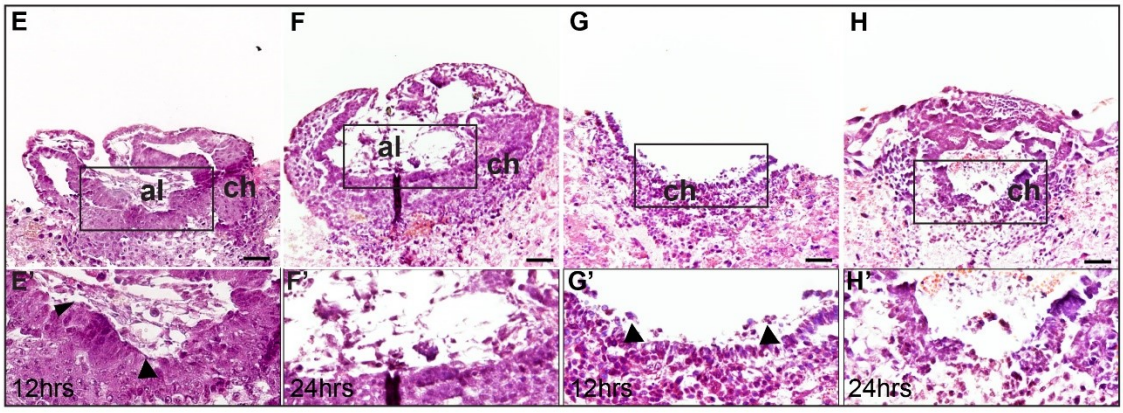
E
F
G
H
al
ch
ch
ch
E'
F'
G'
H'
12hrs
24hrs
12hrs
24hrs

Figure 2.2 Representative images of E8.5 H2B-eGFP+ embryos and placentas. Tg(HIST1H2B/EGFP)1Pa is a transgenic line that constitutively expresses the H2B-eGFP fusion protein in all nucleated cells. A1-A3: $eGFP^-$ (left) and $eGFP^+$ (right) embryos after removal of the anti-mesotmetrial side of the decidua (A1: eGFP; A2:bright field, A3: merge). B1-B3: Representative images of developing placentas from E8.5 $eGFP^+$ embryos after chorioallantoic attachment (B1: eGFP, B2: DAPI, B3: merged, all nucleated cells were positive in green for eGFP and in megenta for Dapi staining). C1-C3: Higher magnification images of boxed region in B3 showing expression of eGFP in all DAPI positive nuclei. Scale bar =200μm for A1-A3, scale bar=50μm for B1-C3.

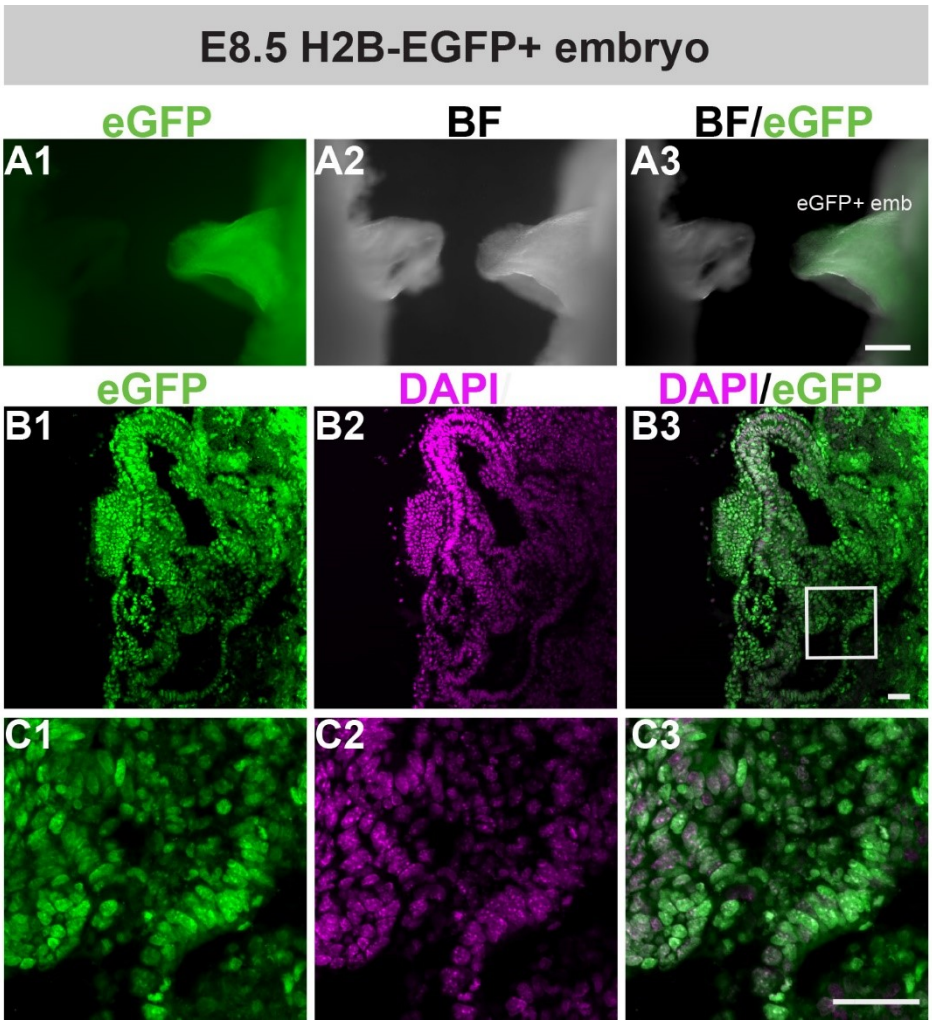

Figure 2.3 Representative images of eGFP- decidua/epc/chorion explants co-cultured with an eGFP+ allantois after 12 (A1-A9) and 24 (B1-B12) hours.

$eGFP^+$ allantois attached to a decidua/epc/chorion explants after 12 (top view: A1-A3, side view: A4-A6) and 24 (top view: B1-B3, side view: B4-B6) hours of culture. Representative image of cryosection from a different explant showing limited mixing of $eGFP^+$ allantoic cells after 12 hours of culture (A7-A9). Representative cryosection of the explant shown in panels B1-B6 showing dispersal of $eGFP^+$ allantoic cells and mixing with eGFP- trophoblasts (B7-B9). Higher magnification of regions in white box is shown below each panel. White stars indicate examples of $eGFP^+$ allantoic cells that are adjacent to $eGFP^-$ trophoblast at 12 hours and 24hours; Chorion (ch), allantois (al), bright field (BF), eGFP =green; DAPI =magenta; scale bar =200μm for A1-A6, B1-B6 and 20μm for A7-A9, B7-B12.

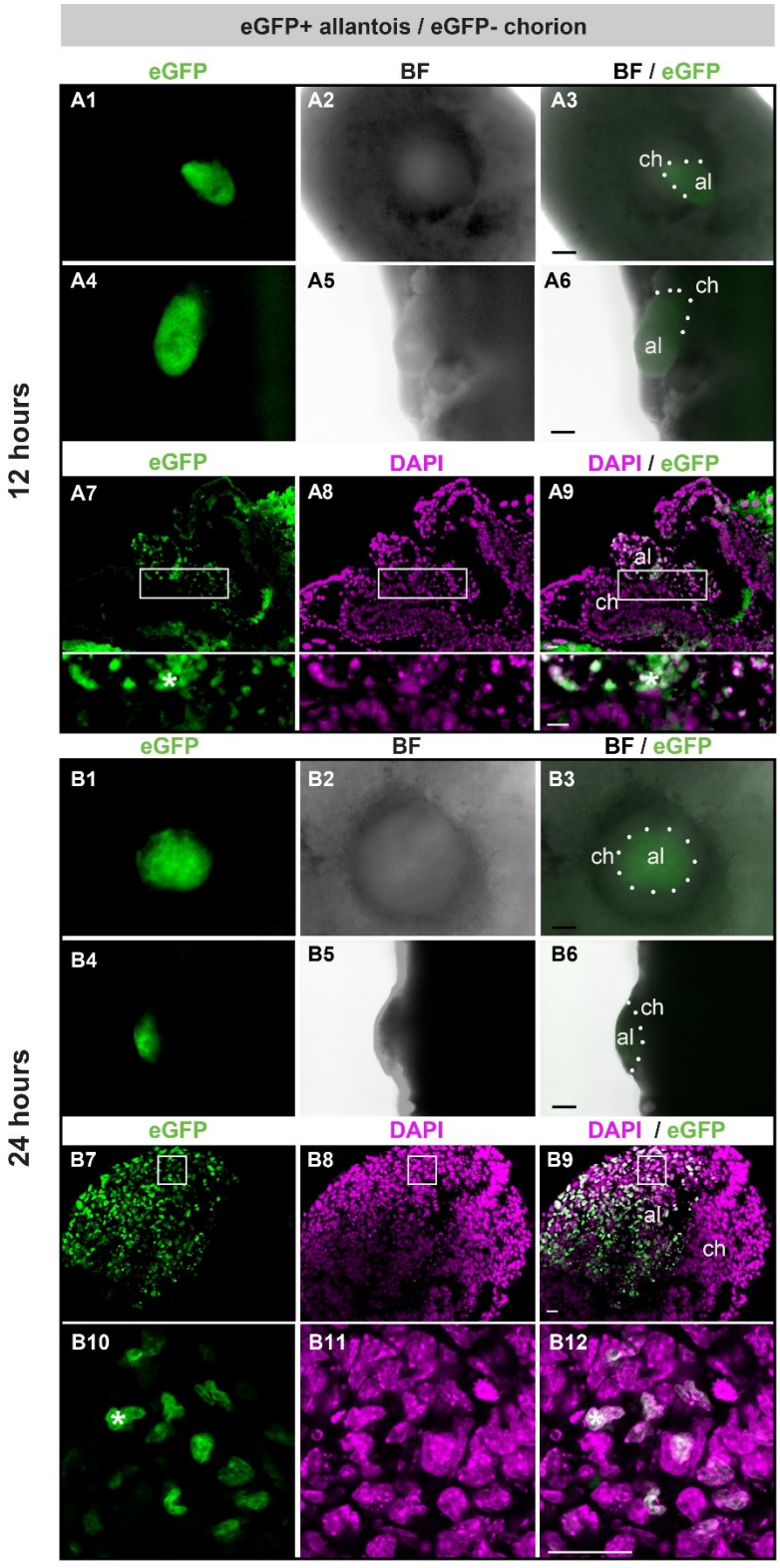
eGFP+ allantois / eGFP- chorion
12 hours
24 hours
eGFP
BF
BF / eGFP
DAPI
DAPI / eGFP
A1
A2
A3
A4
A5
A6
A7
A8
A9
B1
B2
B3
B4
B5
B6
B7
B8
B9
B10
B11
B12
ch
al

Figure 2.4 Representative images of eGFP+ decidua/epc/chorion explants co-cultured with an eGFP- allantois after 12 (A1-A9) and 24 (B1-B12) hours.

After 12 and 24 hours of culture $eGFP^+$ trophoblast giant cells are found spreading on the surface of $eGFP^-$ deciduas (A1 and B1). Images of $eGFP^-$ allantois attached to $eGFP^+$ chorion after 12 (top view: A1-A3, side view: A4-A6) and 24 (top view: B1-B3, side view: B4-B6) hours of culture. Representative images of cryosections from the explant shown in panels A1 –A6 showing the distinct mesothelial cells (white arrow in panel A9) and limited mixing between $eGFP^-$ allantoic cells (white stars) and $eGFP^+$ trophoblasts. Representative images of cryosections from the explant shown in panels B1 –B6 showing increased dispersal of $eGFP^+$ trophoblast cells and increased mixing with $eGFP^-$ allantoic cells. Higher magnification of regions in white box is shown below each panel. White stars indicate examples of eGFP- allantoic cells that are adjacent to $eGFP^+$ trophoblast cells. Chorion (ch), allantois (al), bright field (BF), eGFP =green; DAPI =magenta; scale bar =200μm for A1-A6, B1-B6, and 20μm for A7-A9, B7-B12.

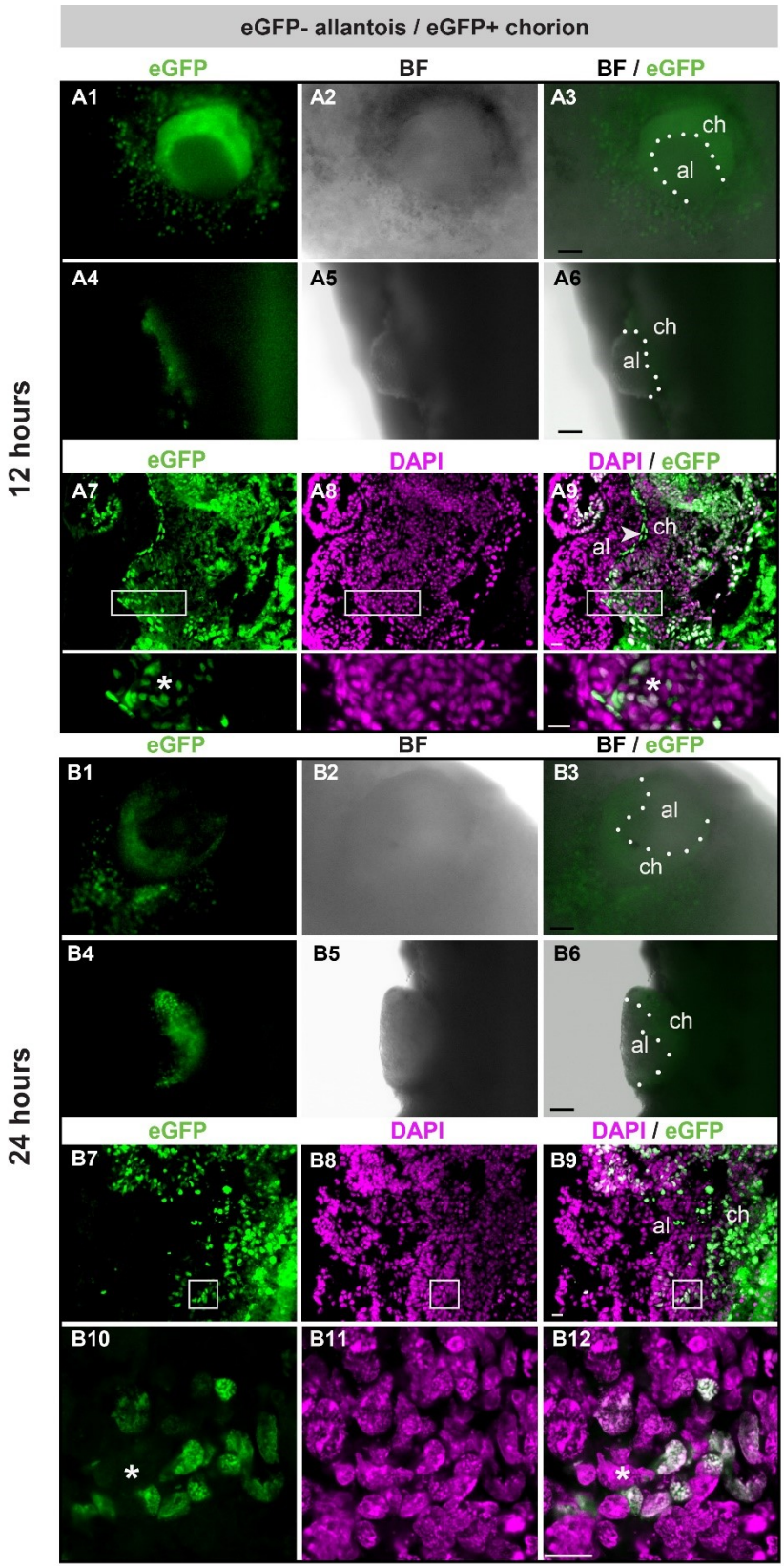
eGFP- allantois / eGFP+ chorion
12 hours
24 hours
eGFP
BF
BF / eGFP
DAPI
DAPI / eGFP
A1
A2
A3
A4
A5
A6
A7
A8
A9
B1
B2
B3
B4
B5
B6
B7
B8
B9
B10
B11
B12
ch
al

Figure 2.5 Representative images showing ZO1 expression.

ZO1 expression of non-cultured decidua/epc/chorion prior chorioallantoic fusion (A1-A3), non-cultured decidua/epc/chorion/allantois post chorioallantoic fusion(A4-A9), cultured explants of decidua/epc/chorion without an allantois (B1-B6), and cultured explants of decidua/epc/chorion with an allantois (B7 – B12) for 24hours. Expression of ZO1 was found on the epithelial surface of chorionic plate in non-cultured pre-placental tissues (A1-A3). In non-cultured post chorioallantoic fusion placental tissues, robust ZO1 expression demarcates the regions of branching on the chorionic plate (A4-A9). In cultured explants of chorion without an allantois, reduced expression of ZO1 was found in the chorionic plate (B1-B6). In explants cultured with an allantois, expression of ZO1 demarcates regions of branching on the chorionic plate (B7-B12), comparable to *in vivo* placental tissues post chorioallantoic fusion (A4-A9). Chorion (ch), allantois (al), dot line marks the expression of ZO1 staining. Scale bar =50μm.

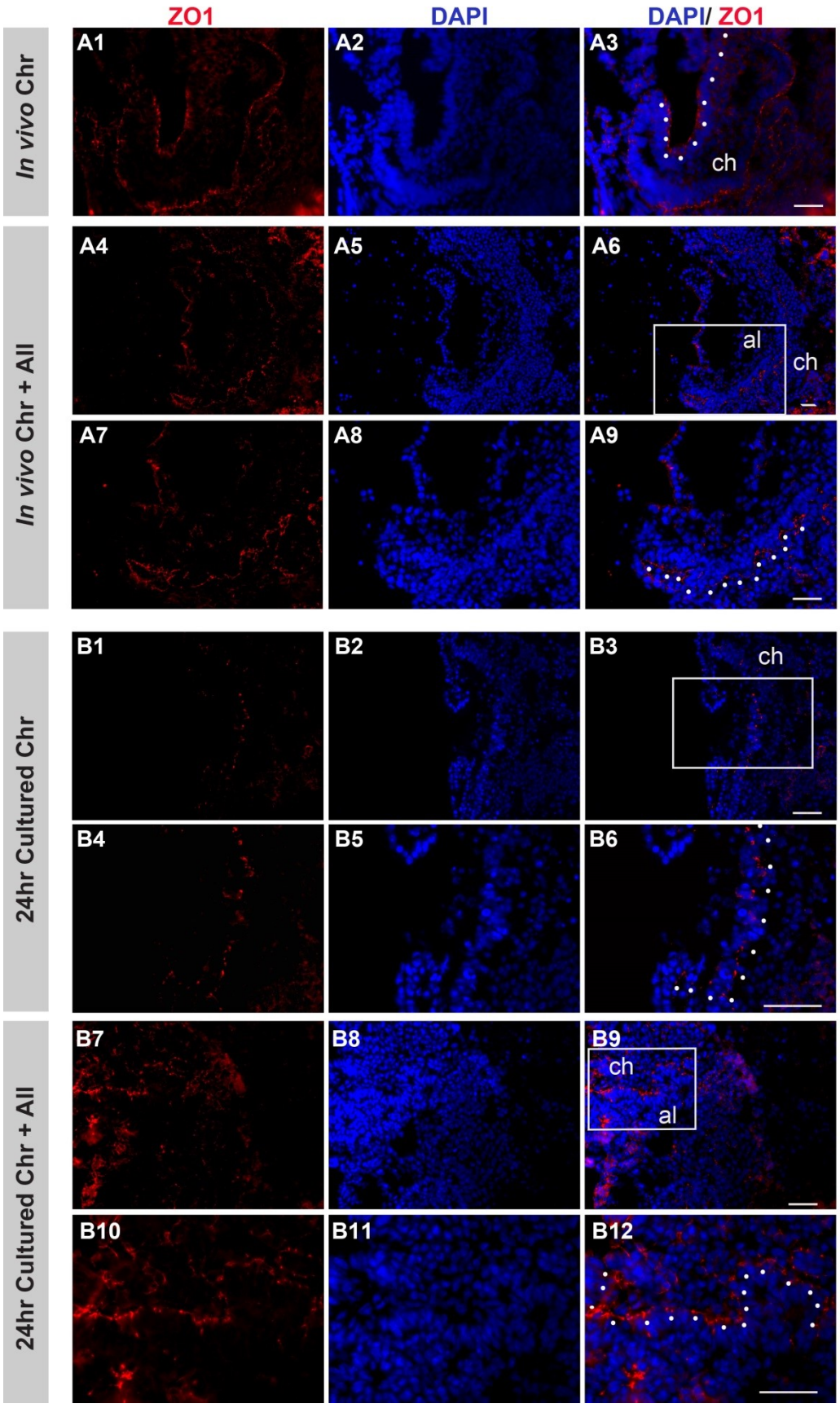
ZO1
DAPI
DAPI/ ZO1
In vivo Chr
In vivo Chr + Ali
24hr Cultured Chr
24hr Cultured Chr + Ali
A1
A2
A3
ch
A4
A5
A6
al
ch
A7
A8
A9
B1
B2
B3
ch
B4
B5
B6
B7
B8
B9
ch
al
B10
B11
B12

Figure 2.6 Representative images showing expression of the endothelial marker PECAM1.

A1-A4: $PECAM1^+$ endothelial cells (red) are found in the allantoic and chorionic region of decidua/epc/chorion explants cultured with an allantois after 24 hours. B1-B4: Higher magnification images of boxed region in A4 show PECAM1 expression in $eGFP^-$ allantoic cells (B3) surrounded by $eGFP^+$ trophoblast cells (white stars) as well as in a subset of GFP^+ trophoblast cells (purple star)in the chorionic region (A4 and B4). Chorion (ch), allantois (al). Scale bar =50μm.

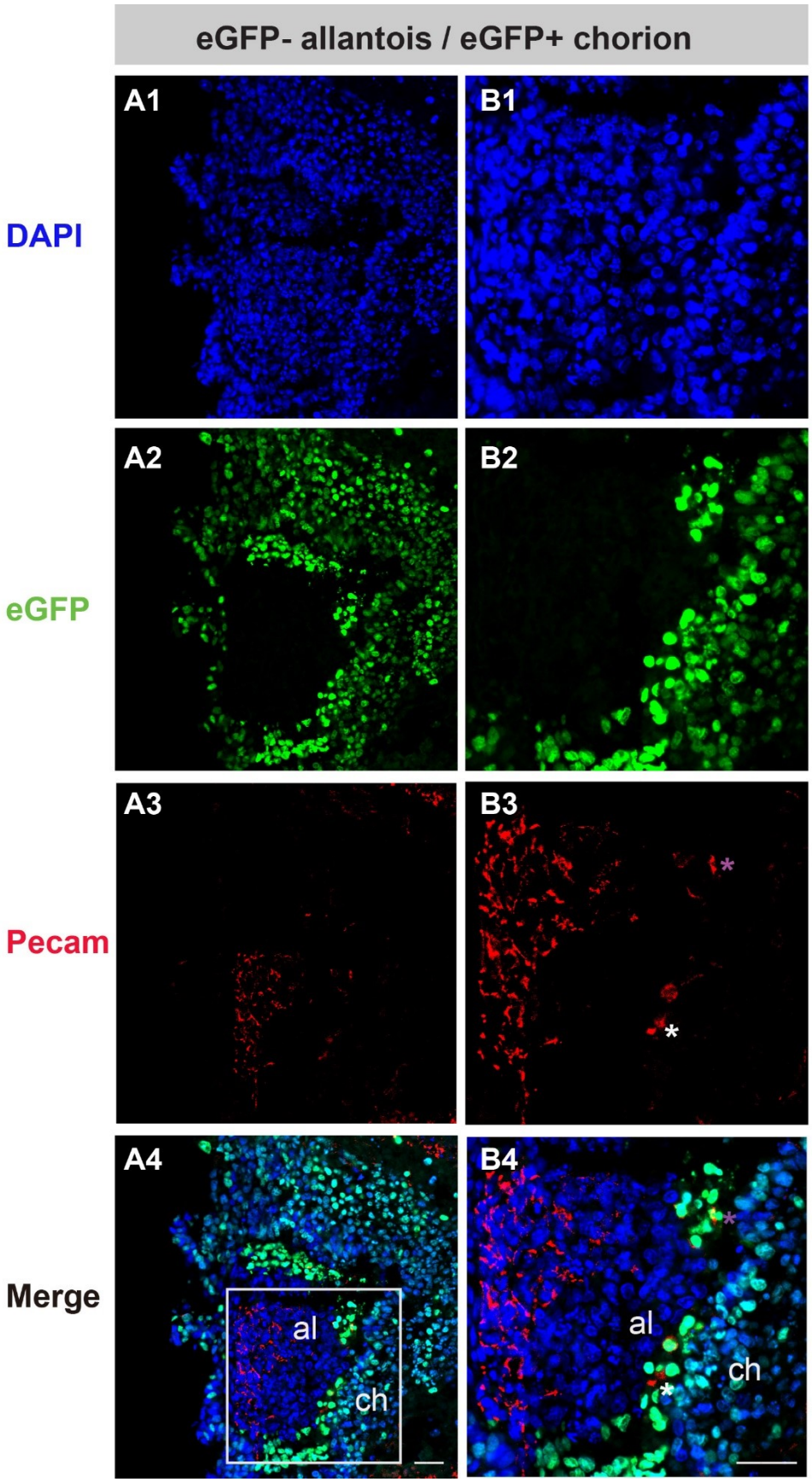
eGFP- allantois / eGFP+ chorion
DAPI
eGFP
Pecam
Merge
A1
B1
A2
B2
A3
B3
A4
B4
al
ch
al
ch

Figure 2.7 Expression of the parietal giant cell markers *Plf*, *Prl3d1* and spongiotrophoblast marker *Tpbpα* in pre-placental explants.

(A-H): representative images of pre-placental explants after section *in situ* hybridization with probe to detect expression of the parietal giant cell marker *Plf* and *Plr3d1*. *Plf* was expressed in cells in the proximal regions of decidua/epc/chorion explants cultured without (A, C) or with an allantois (B, D) for 12 (A, B) and 24 hours (C, D). (E-H): *Prl3d1* was expressed in cells in the proximal and distal regions of decidua/epc/chorion explants cultured without (E, G) or with an allantois (F, H) for 12 (E, G) and 24 hours (F, H). (I-L): Representative images of placental explants after *in situ* hybridization showing *Tpbpα* expression in the distal region of decidua/epc/chorion explants cultured for 12 hours without (I) or with an allantois (J). After 24 hours of culture, *Tpbpα* expression was not expressed in explants cultured without an allantois (K) but was expressed in explants cultured with an allantois (L). Purple color indicates regions with expression, Nuclei were counterstained red with nuclear fast red. Quantification of *Tpbpα* level in pre-placental explants indicated as fold change relative to explants of decidua/epc/chorion cultured without an allantois (M) (n=3). *Tpbpα* level was similar in decidua/epc/chorion explants cultured with or without an allantois for 12 and 24 hours. Error bars represent standard error of the mean. Chorion (ch), allantois (al), and ectoplacental cavity (EC). Scale bar =50μm.

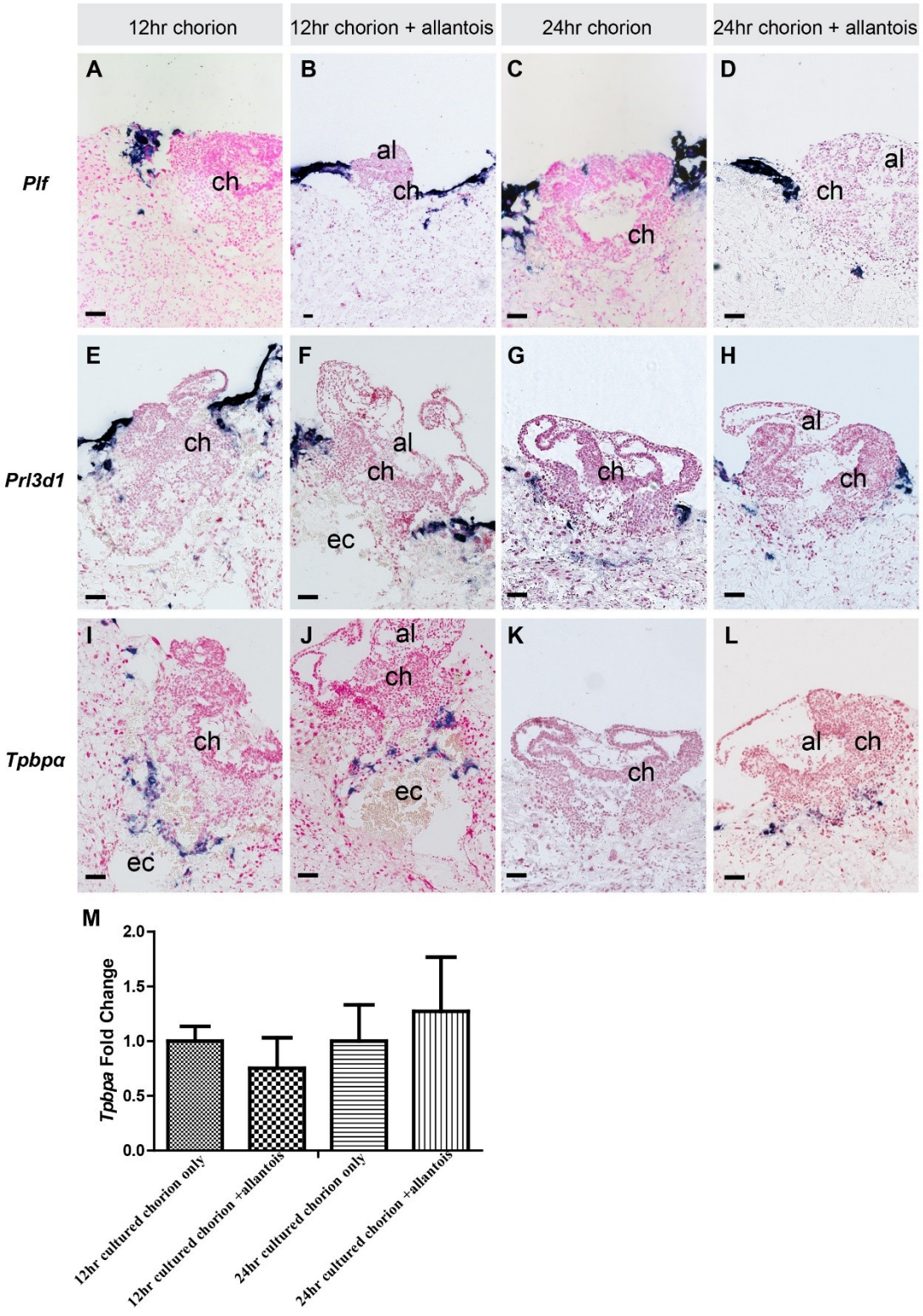
12hr chorion
12hr chorion + allantois
24hr chorion
24hr chorion + allantois
Plf
Prl3d1
Tpbpα
A
B
C
D
E
F
G
H
I
J
K
L
ch
al
ec
M
Tpbpa Fold Change
2.0
1.5
1.0
0.5
0.0
12hr cultured chorion only
12hr cultured chorion +allantois
24hr cultured chorion only
24hr cultured chorion +allantois

Figure 2.8 Expression of the syncytiotrophoblast marker *Gcm1* in pre-placental explants.

Gcm1 expression was not found in decidua/epc/chorion explants cultured for 12 (A) or 24 (C) hours without an allantois. However, *Gcm1* expression was found in chorion of decidua/epc/chorion explants cultured with an allantois for 12hr (B and B')and 24h (D and D') hours. The higher magnification picture of the boxed region in B shows cluster of cells with expression of *Gcm1* (B') and a subset of cells that line vessels expressing *Gcm1* in (D'). Quantification of *Gcm1* level in pre-placental explants indicated as fold change relative to explants of decidua/epc/chorion cultured without an allantois for 12 and 24 hours (E) (n=3). A significant increase of *Gcm1*level was observed in decidua/epc/chorion explants cultured with an allantois for 24 hours. Significant P-values are represented as *** for <0.001, and error bars represent standard error of the mean. Chorion (ch), allantois (al), and ectoplacental cavity (ec). Scale bar =50μm.

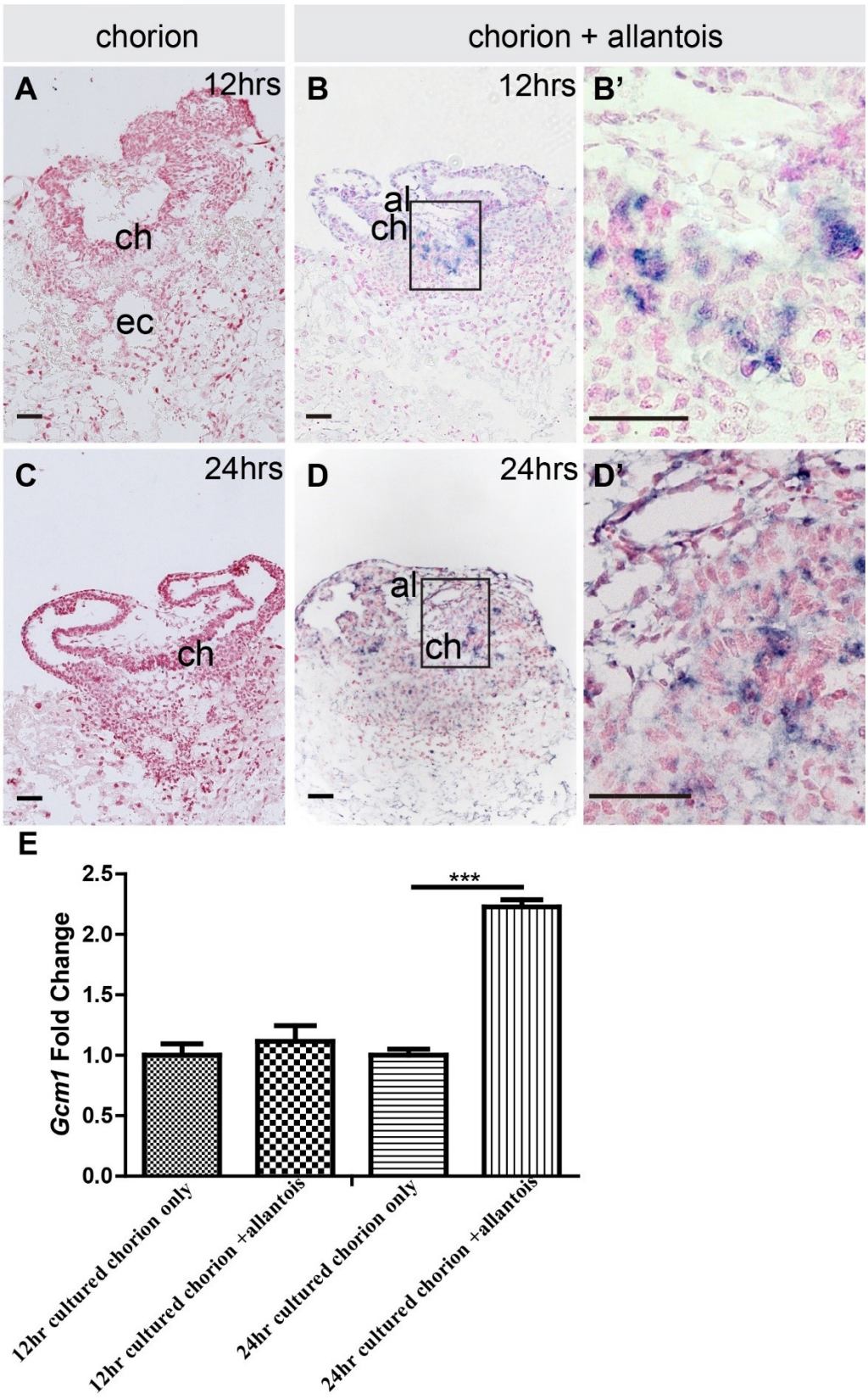
chorion
chorion + allantois
A
12hrs
ch
ec
B
12hrs
al
ch
B'
C
24hrs
ch
D
24hrs
al
ch
D'
E
Gcm1 Fold Change
2.5
2.0
1.5
1.0
0.5
0.0
***
12hr cultured chorion only
12hr cultured chorion +allantois
24hr cultured chorion only
24hr cultured chorion +allantois

Figure 2.9 Quantification of the levels of the syncytiotrophoblast Type-I marker Syncytin A in pre-placental explants.

Quantitative RT-PCR was performed to examine *Syncytin A* levels in pre-placental explants cultured after 12 and 24 hours. Levels are indicated as fold change relative to explants of decidua/epc/chorion cultured without an allantois. A non-significant increase in *SynA* level was found in both 12 and 24hr cultured explants of deicuda/epc/chorion with an allantois. Error bar represents standard error of the mean.

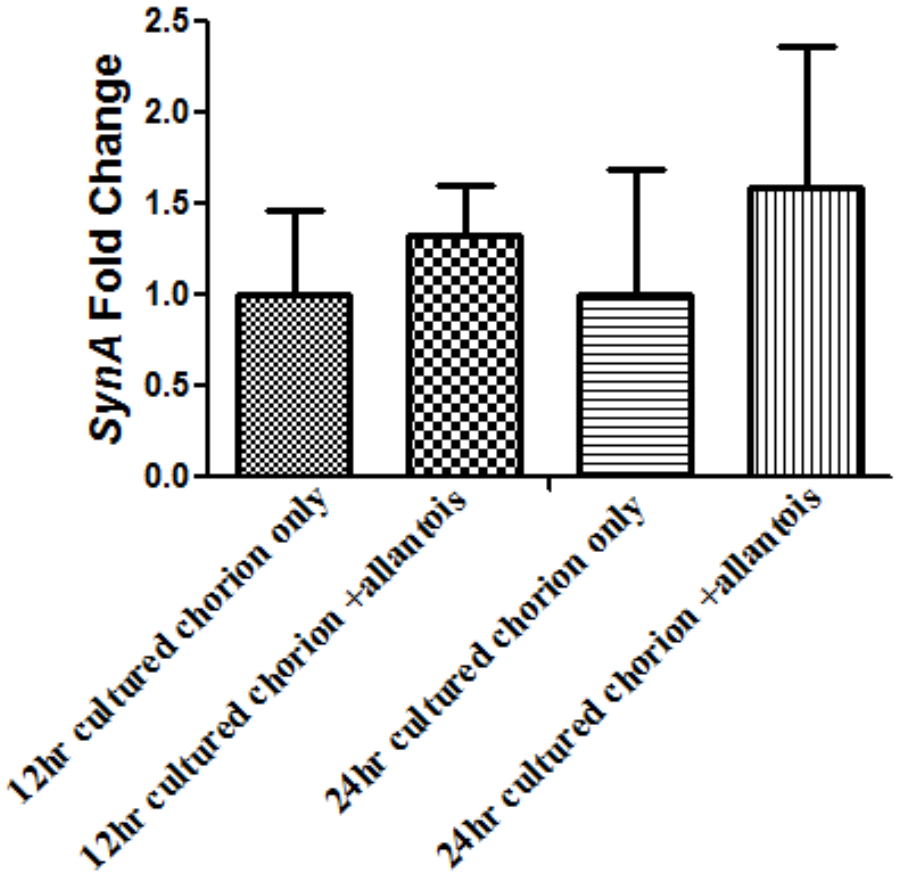

Figure 2.10 Expression of a mitotic marker, Phosphohistone H3 in pre-placental explants.

Representative images of phosphohistone H3 expression in explants of decidua/epc/chorion cultured for 12 (A-A'') and 24 (B-B'') hours wihtout an allantois (Chorion only); as well as in decidua/epc/chorion explants cultured with an allantois for 12 (C-C'') and 24 (D-D'') hours (Chorion+Allantois). Scale bar =50μm.

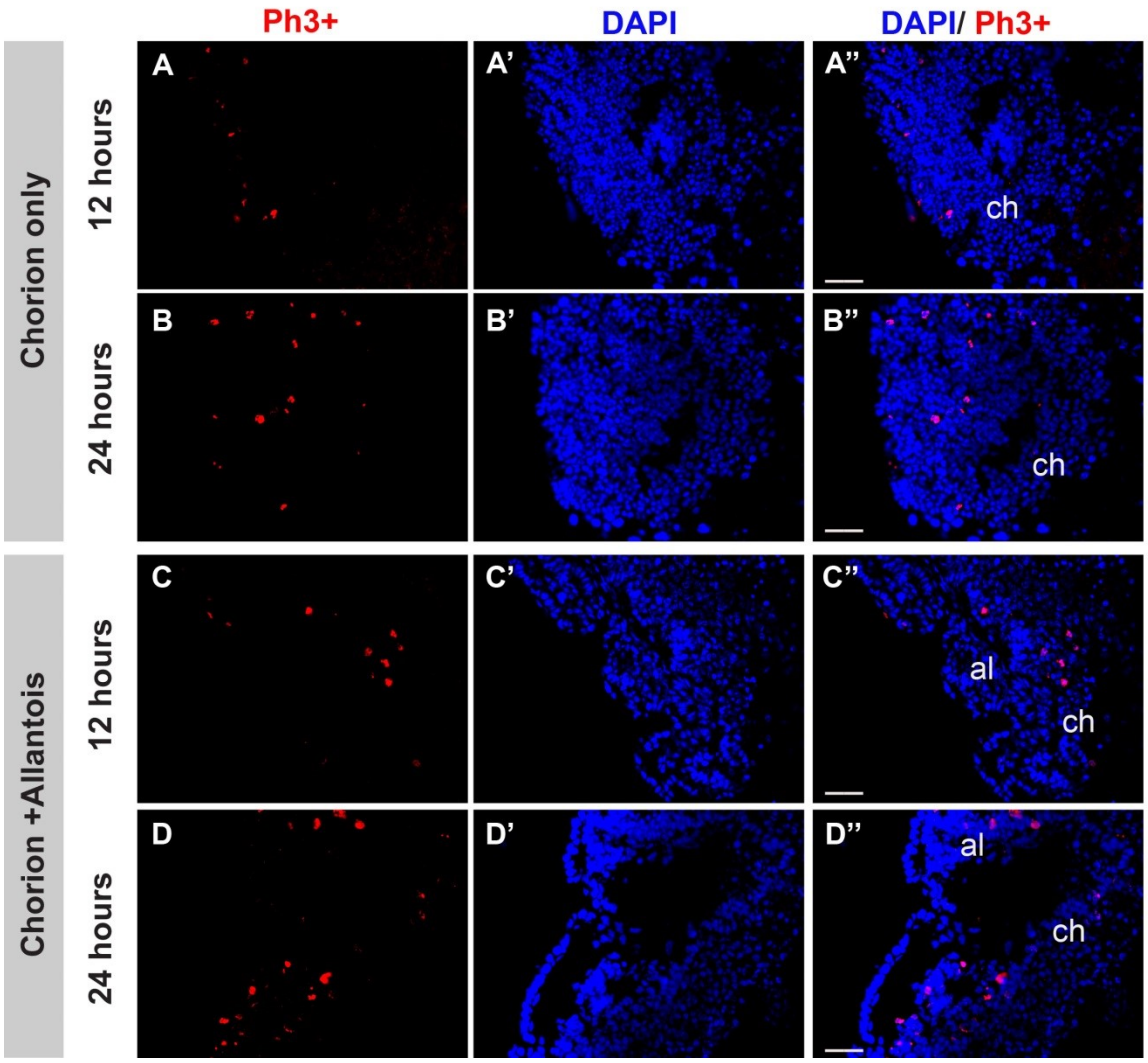

Figure 2.11 Representative images of explants stained with an apoptotic marker cleaved caspase-3.

cleaved caspase-3 was detected in explants of decidua/epc/chorion cultured without (Chorion only; A, B) or with an allantois (chorion+allantois; C, D) for 12 (A, C) or 24 hours (B, D). Apoptotic nuclei were found in the proximal region of pre-placental explants and the allantois. Chorion (Ch), allantois (al). Scale bar = 50 μm

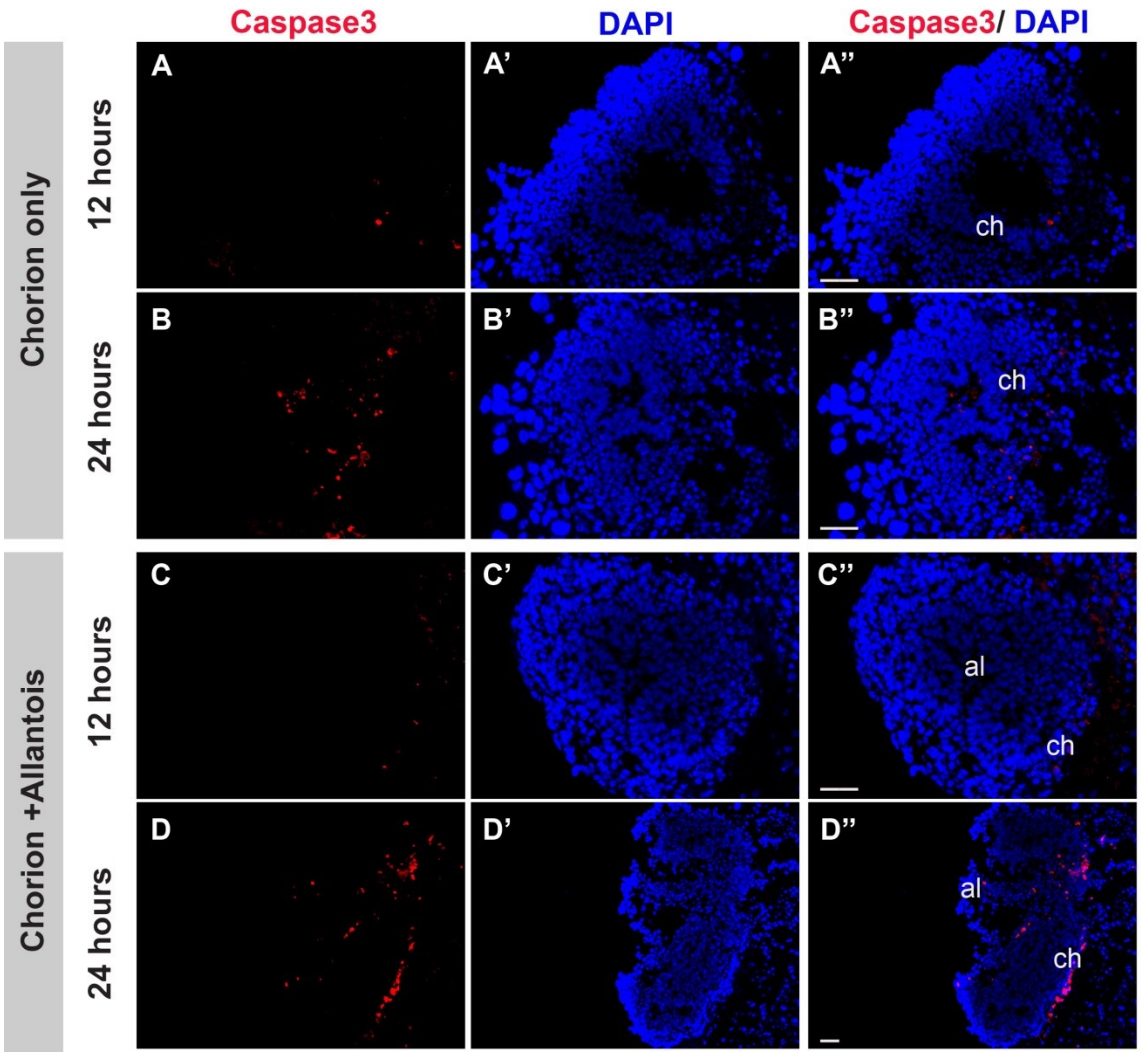

Table 2.1 Mitotic index of 12 and 24hr decidua/epc/chorion explants cultured with or without an allantois.

Table 2.1A: Counts for the total number of cells in explants, the number of PH3 positive cells, and the calculated mitotic index for explants of decidua/epc/chorion without (chorion) and with an allantois (chorion+allantois). Significant increase of proliferation was found in 24 hour cultured chorion + allantois shown in the bar graph in the lower left panel. Table 2.1B: Counts for the total number of cells in the chorionic and allantoic region of explants, the number of PH3 positive cells, and the calculated Mitotic index for the chorionic and allantoic region of decidua/epc/chorion explants cultured with an allantois (chorion+allantois) for 12 and 24 hours. Significant increase of proliferation was found in allantoic region after 24 hours of culture, shown in the bar graph in the lower right panel. Chorion (chr), allantois (all), P-values represented as **for <0.01, *** for <0.001 (1-way Anova).

Table 2.1A. Mitotic Index of cultured chorion explants and chorion + allantois explants for 12 and 24 hours

	Sample type	Number of samples (N)	Mean (M)	Standard Deviation (SD)	Standard Error of Mean (SEM)
Total cell count	Chorion (12hr)	3	732	120.82	34.88
	Chorion (24hr)	2	714.14	66.49	25.13
	Chorion+Allantois (12hr)	3	656.45	138.65	41.81
	Chorion+Allantois (24hr)	4	539.45	148.83	44.88
PH3+ cell count	Chorion (12hr)	3	11.83	6.63	1.91
	Chorion (24hr)	2	16.86	5.15	1.94
	Chorion+Allantois (12hr)	3	7.64	3.47	1.05
	Chorion+Allantois (24hr)	4	21.45	12.34	3.72
PH3+/total cell count (%)	Chorion (12hr)	3	1.73	0.98	0.28
	Chorion (24hr)	2	2.41	0.87	0.33
	Chorion+Allantois (12hr)	3	1.14	0.42	0.13
	Chorion+Allantois (24hr)	4	4.15	2.81	0.85

Table 2.1B. Mitotic Index of chorionic or allantoic region of co-cultured chorion +allatnois explants for 12 and 24 hours

	Sample type	Number of samples (N)	Mean (M)	Standard Deviation (SD)	Standard Error of Mean (SEM)
Total cell count	Allantoic(12hr)	3	81.55	61.52	18.55
	Allantoic(24hr)	4	114.27	107.28	32.35
	Chorionic (12hr)	3	574.91	102.59	30.93
	Chorionic (24hr)	4	425.18	141.20	42.57
PH3+ cell count	Allantoic(12hr)	3	1.0	1.10	0.33
	Allantoic(24hr)	4	6.82	5.42	1.63
	Chorionic (12hr)	3	6.64	3.72	1.12
	Chorionic (24hr)	4	14.64	9.98	3.01
PH3+/total cell count (%)	Allantoic(12hr)	3	1.41	1.54	0.46
	Allantoic(24hr)	4	6.90	6.30	0.33
	Chorionic (12hr)	3	1.12	0.53	0.16
	Chorionic (24hr)	4	3.62	2.44	0.74

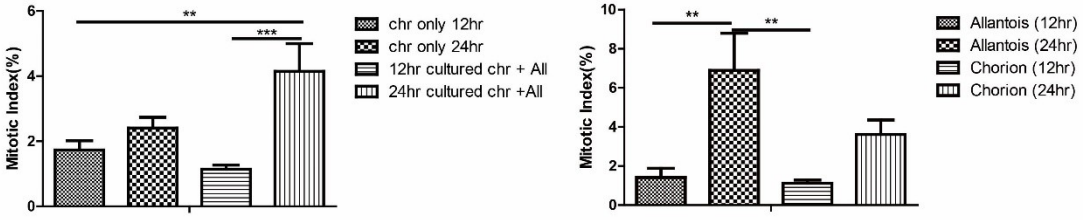

Table 2.2 Apoptotic index of 12 and 24hr decidua/epc/chorion explants cultured with or without an allantois.

Table 2.2A: Counts for the total number of cells in explants, the number of cleaved Caspase-3 positive cells, and the calculated apoptotic index for explants of decidua/epc/chorion without (chorion) and with an allantois (chorion+allantois). Significant increase of apoptosis was found in 24 hour cultured chorion + allantois shown in the bar graph in the lower left panel. Table 2.2B: Counts for the total number of cells in the chorionic and allantoic region of explants, the number of cleaved Caspase-3 positive cells, and the calculated apoptotic index for the chorionic and allantoic region of decidua/epc/chorion explants cultured with an allantois for 12 and 24 hours. Significant increase of apoptosis was found in allantoic region after 24 hours of culture, shown in the bar graph in the lower right panel Chorion (chr), allantois (All). P-values represented as *for <0.05, ** for <0.01, *** for <0.001 (1-way Anova).

Table 2.2A. Apoptotic Index of cultured chorion explants and chorion + allantois explants for 12 and 24 hours

	Sample type	Number of samples (N)	Mean (M)	Standard Deviation (SD)	Standard Error of Mean (SEM)
Total cell count	Chorion (12hr)	2	656.4	111.82	55.91
	Chorion (24hr)	2	724.5	41.72	29.5
	Chorion+Allantois (12hr)	2	393.25	148.61	85.8
	Chorion+Allantois (24hr)	3	645.2	160.58	80.29
Casp3+ cell count	Chorion (12hr)	2	6.4	3.43	1.72
	Chorion (24hr)	2	20	5.65	4
	Chorion+Allantois (12hr)	2	5.25	5.56	3.21
	Chorion+Allantois (24hr)	3	59.4	12.17	6.09
casp3+/total cell count (%)	Chorion (12hr)	2	1.04	0.66	0.33
	Chorion (24hr)	2	2.74	0.62	0.44
	Chorion+Allantois (12hr)	2	1.51	1.97	1.14
	Chorion+Allantois (24hr)	3	9.66	3.11	1.56

Table 2.2B. Apoptotic Index of chorionic or allantoic region of co-cultured chorion +allanois explants for 12 and 24 hours

	Sample type	Number of samples (N)	Mean (M)	Standard Deviation (SD)	Standard Error of Mean (SEM)
Total cell count	Allantoic(12hr)	2	60	27.72	16
	Allantoic(24hr)	3	106	26.15	13.08
	Chorionic (12hr)	2	333.25	125.55	72.49
	Chorionic (24hr)	3	539.2	141.44	70.72
Caps3+ cell count	Allantoic(12hr)	2	5.25	5.56	3.21
	Allantoic(24hr)	3	18.6	4.83	2.41
	Chorionic (12hr)	2	0	0	0
	Chorionic (24hr)	3	40.8	10.55	5.27
Casp3+/total cell count (%)	Allantoic(12hr)	2	7.84	9.28	5.36
	Allantoic(24hr)	3	18.25	6	3
	Chorionic (12hr)	2	0	0	0
	Chorionic (24hr)	3	7.93	2.85	1.4

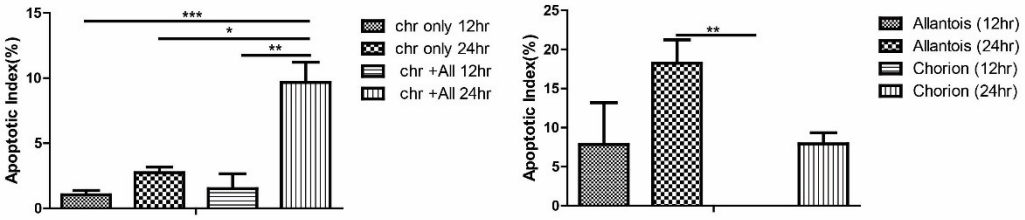

Connecting text between Chapter II and III

The successful establishment of the *ex vivo* cultured pre-placental explants allows us to examine gene specific requirement in the chorion and allantois during and after chorioallantoic attachment. In this chapter, through combining the allantois or the chorion of *Tmed2* null mutants with wildtype recipient placental tissues, I investigated the specific requirement of *Tmed2* in the allantois and the chorion during chorioallantoic attachment. I examined the events associated with the chorioallantoic attachment, including the physical association between the chorion and the allantois, mixing between the chorionic and the allantoic cells. I examined the expression of endothelial cell marker, Pecam1/CD31, in the allantois, as well as the spongiotrophoblast marker, *Tpbpα*, and the syncytiotrophoblast marker, *Gcm1*, in the chorion of the *Tmed2* null/ wildtype recombined pre-placental explants. In addition, I examined the state of proliferation and apoptosis in these explants, and the expression of one potential TMED2 cargo protein, an extracellular matrix (ECM) protein, fibronectin.

Chapter III：Trafficking protein TMED2 is required in both the chorion and the allantois for normal chorioallantoic fusion and labyrinth layer development

Wenyang Hou, Loydie A. Jerome-Majewska

Manuscript in preparation

3.1 Abstract

TMED2 belongs to the transmembrane emp24 domain (TMED) protein family, which is required for normal transport of secretory cargoes between the ER and Golgi. *Tmed2* is expressed in the allantois and the chorion, and null mutation in *Tmed2* results in abnormal chorioallantoic fusion and failure of placental labyrinth formation. We aimed to investigate the tissue-specific requirement for TMED2 using a previously established *ex vivo* explant model of chorion and allantois. *Ex vivo* explants of wildtype chorions and wildtype allantoides recapitulated the early events associated with chorioallantoic fusion, as previously published. *Ex vivo* explants of *Tmed2* null chorions and *Tmed2* null allantoides showed abnormal chorioallantoic fusion, and reduced expression of spongiotrophoblast marker, *Tpbp*α, and syncytiotrophoblast marker, *Gcm1,* as previously found in *Tmed2* null placenta. Explants of *Tmed2* null chorions and wildtype allantoides showed abnormal chorioallantoic fusion with no chorionic and allantoic cell mixing, reduced expression of *Tpbp*α and *Gcm1,* and reduced proliferation in the allantois compared to wildtype explants. Explants of wild type chorions and *Tmed2* null allantoides showed chorionic and allantoic cell mixing, reduced expression of *Tpbp*α and *Gcm1,* increased apoptosis in the allantois, and abnormal expression of an extracellular matrix protein, fibronectin, in the allantois. Our data indicates that *Tmed2* is required in both the chorion and the allantois during placental labyrinth development. In the chorion *Tmed2* is required for mixing of allantoic and chorionic cells. In the allantois *Tmed2* is required for cell survival, and proper secretion of fibronectin. Intriguingly, TMED2 is required in both the chorion and the allantois for normal expression of *Gcm1* and *Tpbpα*.

Our *ex vivo* explant model recapitulates phenotypes found in the *Tmed2* null placenta; and reveals a tissue-specific role of *Tmed2* in early labyrinth layer development.

3.2 Introduction

Members of the transmembrane emp24 domain (TMED)/p24 protein family of trafficking proteins are key components of coated vesicles. They are transported with cargo molecules via coat protein (COP) II vesicles from the endoplasmic reticulum (ER) to the Golgi complex and then returned to the ER via COPI vesicles (Strating and Martens, 2009a). Ten Tmed/ p24 genes have been identified in vertebrates and can be classified into four subfamilies: α, β, γ and δ (Dominguez et al., 1998). To function properly, a member of each subfamily is recruited to form a hetero-oligomeric complex, which is believed to function as receptors for specific secretory cargos (Anantharaman and Aravind, 2002). All Tmed/ p24 family members are structurally related and share four distinct functional domains; an N-terminal domain that contains the signal sequences for translocation to ER, a Golgi dynamics (GOLD) domain responsible for cargo recognition (Anantharaman and Aravind, 2002), a coiled-coil domain involved in interactions with other subfamily members (Blum et al., 1996; Emery et al., 2000; Greco et al., 2012; Liaunardy-Jopeace et al., 2014) as well as recognition of GPI-anchored proteins (Theiler et al., 2014), and a C-terminal domain that contains conserved binding motif to coat complexes in COPI and COPII vesicles (Dominguez et al., 1998; Editor and Robinson, 2007). *Tmed2* is the sole member of the β subfamily of the p24 family, and is conserved in human and mouse (Strating and Martens, 2009b). Jerome-Majewska et al. previously reported that a mouse line carrying a point mutation in the signal sequence of *Tmed2* (99J mouse line) generated via an ENU mutagenesis

presents with embryos arresting at mid-gestation and abnormal placenta (Jerome-Majewska et al., 2010). They showed that 50% of *Tmed2* homozygous mutant (herein referred as *Tmed2*$^{99J/99J}$) embryos did not have chorioallantoic fusion, and all *Tmed2*$^{99J/99J}$ embryos failed to form the labyrinth layer of the placenta (Jerome-Majewska et al., 2010). *In situ* hybridization *(ISH)* experiments showed reduced mRNA expression of the spongiotrophoblast cell marker *Tpbp*α and syncytiotrophoblast cell marker *Gcm1* in *Tmed2*$^{99J/99J}$ placenta (Jerome-Majewska et al., 2010). *ISH* experiments using a *Tmed2* probe showed *Tmed2* expression in the chorion throughout placental development and in the allantois transiently before chorioallantoic attachment in wildtype embryos. While *Tmed2*$^{99J/99J}$ embryos arrest at mid-gestation, *Tmed2* heterozygous (herein referred as *Tmed2*$^{99J/+}$*)* embryos exhibited no obvious embryonic or placental phenotypes, and are viable and fertile.

We previously reported conditions for *ex vivo* culture of pre-attachment decidua/ectoplacental cone/chorion (herein referred as chorion) and allantois. Under the reported conditions, explants of pre-attachment chorion and allantois fused after 12 hours of culture, and an eGFP positive marker allowed us to visualize increased chorionic and allantoic cell mixing after 24 hours of culture (Hou et al., 2016). *ISH* experiments using probes specific to the spongiotrophoblast cell marker *Tpbp*α and the syncytiotrophoblast marker *Gcm1* showed expanded mRNA expression in co-cultured explants of chorion and allantois (Hou et al., 2016).

In the current study, we utilized our validated *ex vivo* culture conditions to investigate the tissue-specific requirement for *Tmed2* during chorioallantoic fusion. In addition to the nuclear eGFP marker, a cytoplasmic RFP marker was introduced into the 99J line in

order to trace the behavior of chorionic and allantoic cells. We recombined pre-placental tissues from *Tmed2*$^{99J/99J}$ embryos with those from somite-matched wild type or *Tmed2*$^{99J/+}$ embryos. To determine if *Tmed2* is required in the chorion or the allantois, *Tmed2*$^{99J/99J}$ chorions were co-cultured with wildtype allantoides and in complementary experiments, *Tmed2*$^{99J/99J}$ allantoides were co-cultured with wild type chorions. These recombinant explants revealed a tissue-specific requirement for *Tmed2* in the chorion for: mixing of allantoic and chorionic cells, and proliferation of the allantois. In contrast, *Tmed2* was required in the allantois for cell survival, and proper localization of fibronectin, an ECM protein. Intriguingly, we also found that *Tmed2* was required in both the chorion and the allantois for normal mRNA expression of *Gcm1* and *Tpbpa* in the chorion and for expression of Pecam1/CD31, a maker of the endothelial lineage, in the allantois. In this study, we validated the utility of our previously published *ex vivo* explant model of pre-placental tissues and identified novel tissue-specific requirement for TMED2 in the chorion and allantois during early labyrinth layer development.

3.3 Material and methods

3.3.1 Animals

All procedures and experiments were performed according to the guidelines of the Canadian Council on Animal Care and approved by the Animal Care Committee of the RI-MUHC. C3Heb/FeJ (*The Jackson Laboratory*) mice were used to collect wild type tissues, Tg(HIST1H2BB/EGFP)1Pa (Hadjantonakis and Papaioannou, 2004) - a transgenic line on a mixed genetic background that ubiquitously expresses an H2B-eGFP fusion protein in the nucleus - was used for collecting eGFP+ tissues, and ROSA-tdTomato- a transgenic line on a mixed genetic background that ubiquitously express

mCherry in the cytoplasm of all cells- was used for collecting RFP+ tissues. Tg(HIST1H2BB/EGFP)1Pa was a kind gift from Dr. K. Hadjantonakis, and ROSA-tdTomato was a kind gift from Dr. Yojiro Yamanaka. Retired stud male rats were purchased from *The Jackson Laboratory* for serum collection.

3.3.2 Rat serum collection

Blood was collected from the dorsal aorta of anesthetized rats. Rat serum was obtained after immediate centrifugation of the blood and stored at -80°C until preparation of the culture medium.

3.3.3 Culturing Explant of decidua/ectoplacental cone/chorions with allantoides

Dissecting procedures and culturing conditions for decidua/ectoplacental cone/chorion and allantois were previously described (Hou et al. 2016). The presence of the allantois associated with the chorion was confirmed under a Leica dissecting scope (model MZ6), before culturing. All explants were assessed after culture for the success of chorioallantoic attachment under a Leica stereo microscope (LEICA M205 FA).

3.3.4 Tissue processing and staining

Explants were fixed in 4% PFA/1x PBS overnight and were embedded with Shandon Cryomatrix (Thermo Scientific) and stored at -80°C freezer for frozen section analysis (Simmons et al., 2007), or dehydrated and embedded in paraffin. Paraffin embedded samples were sectioned at 5 μm thickness, and frozen samples were sectioned at 10 μm thickness. Hematoxylin and Eosin (H&E) staining (R.D. Cardiff, 2014) was used for morphological analysis.

3.3.5 *In Situ Hybridization*

Plasmids containing *Prl3d1, Plf, Gcm1,* and *Tpbpα* riboprobes were kindly provided by Dr. Jay Cross (University of Calgary). *In situ* hybridization was performed as previously described (Simmons et al., 2008, 2007).

3.3.6 Immunofluorescence

Immunofluorescence experiments were performed according to standard protocols (Zakariyah et al., 2011). The following primary antibodies were used: Phosphohistone H3 (Ser10) (1:200 dilution, Millipore, 06-570), PECAM1 (CD31) (1:100 dilution, Abcam, ab28364), fibronectin (1:100 dilution, Abcam, ab2413), VCAM1 (1:100 dilution, BD bioscience 553330) and cleaved caspase-3 (1:200 dilution, Asp175, Cell signaling, 9661). Alexa Fluor 488, 568, and 647 conjugated secondary antibodies (ThermoFisher, 1:500 dilutions; Jackson ImmunoResearch, 1:250 dilution) were used to detect signals. Slides were mounted with VECTASHIELD hard-set mounting medium with DAPI (Vector Labs, H-1500) to visualize the nuclei. Images were captured on a Leica microsystem (model DM6000B) and Leica camera (model DFC 450 C). Confocal images were obtained using a Zeiss LSM780 laser scanning confocal microscope.

3.3.7 Mitotic Index, and Apoptotic Index

For each sample, 2 - 3 sections stained with either phosphohistone H3 and DAPI or cleaved Caspase-3 and DAPI were used for the analysis. Cell number was calculated with ImageJ software (Fiji, http://fiji.sc/). The mitotic index was determined by calculating the percentage of phosphohistone H3 positive cells over total number of chorionic and allantoic cells counted per section (Table 3.1). Apoptotic index was calculated as the percentage of cleaved caspase-3 positive cells over total number of chorionic and allantoic cells counted in each section.

3.3.8 Statistical analysis

Student t-test from the Prism Software (http://www.graphpad.com/scientific-software/prism/) was used to calculate statistical differences. Significant p-values are represented as * for <0.05, ** for <0.01, *** for <0.001.

3.4. Results

3.4.1 TMED2 localization differs in allantoic and chorionic cells.

To examine localization of TMED2 protein in the chorion and the allantois, immunofluorescence experiments with a TMED2 antibody was performed. TMED2 was found in both the chorion and the allantois of wildtype placentas, after chorioallantoic attachment (Figure 3.1). However, the localization of TMED2 differed between allantoic and chorionic cells. In allantoic cells, TMED2 was found close to the nucleus; and in chorionic cells, TMED2 appeared in scattered dots (Figure 3.1 B1-B3, C1-C3). This observation suggests that TMED2 may localize to different organelles in the chorion and allantois.

3.4.2 Ex vivo explants of Tmed2 null chorion with Tmed2 null allantois recapitulate abnormal chorioallantoic fusion found in $Tmed2^{99J/99J}$ *embryos.*

To track allantoic and chorionic cells after recombination, a transgenic mouse lines with tdTomato red reporter in the cytoplasm (herein referred as RFP) and an eGFP reporter in the nucleus (herein referred as eGFP, Hadjantonakis and Papaioannou, 2004) were crossed into the *Tmed2* mutant mouse line, 99J. Explants of eGFP + wild type or $Tmed2^{99J/+}$ allantoides were cultured with RFP+ wild type or $Tmed2^{99J/+}$ chorions for 24hours as controls. In control explants chorioallantoic fusion with mixing of eGFP+ allantoic and RFP+ chorionic cells (n=8, Figure 3.2 A-C) was found. RFP+ mesothelial

cells were also found to migrate into the allantoic region from the chorionic plate (Figure 3.2B3, B4), and the chorionic plate underwent morphological change at the contact points with allantoic cells, as previously reported (Figure 3.2 B1-B4, C1-C4).

In explants of *Tmed2*$^{99J/99J}$ allantoides and *Tmed2*$^{99J/99J}$ chorions, attachment between the mutant chorion and mutant allantois was observed, however, no mixing of RFP + chorionic and eGFP+ allantoic cells were observed (n=5, Figure 3.2 D-F). Thus, *ex vivo* explant culture of *Tmed2*$^{99J/99J}$ allantoides and *Tmed2*$^{99J/99J}$ chorions recapitulated the abnormal chorioallantoic fusion phenotype previously reported in *Tmed2*$^{99J/99J}$ placenta (Jerome-Majewska et al., 2010). Furthermore, DAPI staining and nuclear eGFP revealed increased cellular debris and fragmented nuclei in *Tmed2*$^{99J/99J}$ explants (Figure 3.2F1, F4), indicating a possible increase of cell death in *Tmed2* mutant explants. This was confirmed by staining with an apoptotic marker, cleaved Caspase-3 (Figure 3.7D – D"). In addition, expression of *Tpbp*α and *Gcm1*, and not *Plf* and *Prl3d1*, (Figure 3.5D-D'") were reduced in mutant explants, as previously found in *Tmed2*$^{99J/99J}$ placentas (Jerome-Majewska et al., 2010). Thus*, ex vivo* culture of pre-attachment *Tmed2*$^{99J/99J}$ chorion and *Tmed2*$^{99J/99J}$ allantois recapitulates the *in vivo Tmed2*$^{99J/99J}$ placental phenotypes including abnormal chorioallantoic fusion, failure of chorionic and allantoic cell mixing, and reduced expression of *Tpbp*α and *Gcm1*.

3.4.3 Tmed2 is required in the chorion for mixing of chorionic and allantoic cells.

To examine the requirement of *Tmed2* in the allantois during chorioallantoic fusion, we used *Tmed2*$^{99J/99J}$ RFP+ allantoides to co-culture with wild type eGFP+ chorions, and in complimentary experiments *Tmed2*$^{99J/99J}$ eGFP+ allantoides to co-culture with wild type RFP+ chorions for 24 hours (n=6). Chorioallantoic fusion occurred in

those explants (Figure 3.3 B4) with mixing of mutant allantoic cells and wild type chorionic cells (Figure 3.3 C4, Inset). However, regions of cell mixing appeared reduced when compared to wildtype explants (Figure 3.2 B4, C4).

To determine if *Tmed2* was required in the chorion for normal chorioallantoic fusion, we performed the complementary recombination experiments using explants of eGFP+ wild type allantoides with RFP+ *Tmed2*$^{99J/99J}$ chorions, and vice versa explants of RFP+ wild type allantoides with eGFP+ *Tmed2*$^{99J/99J}$ chorions cultured for 24 hours (n = 5). Those explants showed no mixing between RFP+ *Tmed2*$^{99J/99J}$ mutant chorionic cells and eGFP+ wild type allantoic cells (Figure 3.3 E4, F4). Thus, we concluded that *Tmed2* was required in the chorion for normal chorioallantoic fusion and mixing of allantoic and chorionic cells.

3.4.4 Endothelial cell marker Pecam1/CD31 was not maintained in explants of Tmed2$^{99J/99J}$ *pre-placental tissues.*

Normal placental labyrinth layer development requires proper vasculogenesis and angiogenesis (Arora and Papaioannou, 2015; Rossant and Cross, 2001). *De novo* endothelial cell differentiation is initiated in the distal allantois and is characterized by expression of the Flk1, Pecam1, and VE-Cadherin (Drake and Fleming, 2000). The endothelial cell maker Pecam1/CD31 is expressed in a subpopulation of allantoic angioblasts before chorioallantoic fusion (Inman and Downs, 2006; Naiche and Papaioannou, 2003) and we previously showed the expanded expression of Pecam1/CD31 in allantoic cells of explants of wildtype chorion and allantois (Figure 3.4A4) (Hou et al., 2016). In order to understand if endothelial cells were present in *Tmed2*$^{99J/99J}$ mutant placentas and maintained in explants with *Tmed2*$^{99J/99J}$ tissues,

immunofluorescence against a Pecam1/CD31 antibody was performed. *CD31* expression was detected in wildtype explants (Figure 3.4 A1- A6) and in allantois of *Tmed2*$^{99J/99J}$ placentas, before culture (data not shown). However, Pecam1/CD31 was not found in any explant with *Tmed2*$^{99J/99J}$ pre-placental tissues (Figure 3.4 B-4D). These results suggest that TMED2 is required in both the chorion and the allantois for maintaining endothelial cells in the allantois.

3.4.5 Tmed2 is required in the chorion and the allantois for expanded expression of Tpbpa and Gcm1.

ISH revealed comparable expression of *Prl3d1* and *Plf* in all explants (Figure 3.5 A-E, A'-E'). However, though *Tpbpα* and *Gcm1* were also expressed in explants with *Tmed2*$^{99J/99J}$ pre-placental tissues (Figure 3.5 B"-E" for *Tpbpα*, and Figure 3.5 B'"-E'" for *Gcm1*), expression of these genes was reduced when compared to the control (Figure 3.5 A'' and A'"). These results suggest that *Tmed2* is required in both the chorion and the allantois for maintaining the spongiotrophoblast and syncytiotrophoblast lineage.

3.4.6 Allantoic cell proliferation was abolished in explants with Tmed2$^{99J/99J}$ *tissues.*

The growth of allantois before chorioallantoic fusion requires both cell proliferation and addition of cells from the primitive streak , and is critical for the allantois to reach the chorion during chorioallantoic attachment (Kimberly and Downs, 2007). The mitotic index of the allantois stays at about 10% in embryos with 2 somites and gradually declines to ~6% at 5-6 somites stage, when chorioallantoic attachment takes place (Downs and Bertler, 2000). To examine the state of proliferation in explants with *Tmed2*$^{99J/99J}$ tissues, we performed immunofluorescence with an antibody to Phosphohistone H3 (PH3). We calculated the mitotic index (MI) and found reduced

proliferation in all explants with *Tmed2*$^{99J/99J}$ tissues when compared to control explants with wildtype tissues (Table 3.1A), particularly in explants of *Tmed2*$^{99J/99J}$ chorions with wildtype allantoides (Table 3.1A, P-value=0.004). The majority of PH3+ cells were found in the allantoic rather than the chorionic region of both wildtype and *Tmed2*$^{99J/99J}$ mutant tissues (Figure 3.6). We calculated the mitotic index in the chorionic and the allantoic regions, respectively. In the chorionic region, the mitotic index was comparable between control explants with wildtype tissues and explants with *Tmed2*$^{99J/99J}$ tissues (Table 3.1B). However, in the allantoic region, the mitotic index was significantly decreased in explants of *Tmed2*$^{99J/99J}$ chorions with wildtype allantoides (Table 3.1C, MI=3.59, SEM=1.21, P-value=0.008), and explants of *Tmed2*$^{99J/99J}$ chorions with *Tmed2*$^{99J/99J}$ allantoides (Table 3.1C, MI=3.53, SEM=1.66, P-value=0.01) when compared to wildtype explants (Table 3.1C, MI=10.25, SEM=0.99). These results suggest TMED2 is required in the chorion for allantoic proliferation.

3.4.7 Increased apoptosis was found in explants of Tmed2$^{99J/99J}$ *chorions with Tmed2*$^{99J/99J}$ *allantoides*

To quantify apoptosis in cultured explants, we performed immunofluorescence against an apoptotic marker, cleaved caspase-3. We calculated the apoptotic index (AI) and found an increase of cell death in all explants with *Tmed2*$^{99J/99J}$ tissues, particularly in explants of *Tmed2*$^{99J/99J}$ chorions with *Tmed2*$^{99J/99J}$ allantoides (Table 3.2A, AI=13.55, SEM=2.26) when compared to the wildtype explants (Table 3.2A, AI=8.77, SEM=0.69, P-value= 0.03) (Figure 3.7 A-A'' versus D-D''). To quantify the distribution of apoptotic cells in these explants, we calculated the apoptotic index associated with either chorionic or allantoic regions. In the chorionic region, the apoptotic index was increased in explants

of *Tmed2*$^{99J/99J}$ chorions cultured with *Tmed2*$^{99J/99J}$ allantoides (Table 3.2B, AI=9.88, SEM=1.51) when compared to wildtype controls (Table 3.2B, AI=4.59, SEM=0.34, P-value=0.03). In the allantoic region, the apoptotic index was increased in explants of wildtype chorions cultured with *Tmed2*$^{99J/99J}$ allantoides (Table 3.2C, AI=31.82, SEM=0.88) when compared to wildtype controls (Table 3.2C, AI=21.41, SEM=1.93, P-value=0.003). Thus, TMED2 is required in both the chorion and the allantois for cell survival.

3.4.8 Abnormal expression of ECM protein fibronectin and adhesion molecule VCAM1 were found in Tmed2$^{99J/99J}$ *allantois.*

Fibronectin is a highly expressed extracellular matrix protein in the murine allantois. Null mutation in *fibronectin* is embryonic lethal and homozygous mutant embryos have impaired embryonic and extraembryonic vasculature formation and reduced placenta (George et al., 1993). We postulate that fibronectin is a potential cargo protein of TMED2 and that its expression may be disrupted in *Tmed2*$^{99J/99J}$ allantoides. Thus, immunofluorescence against a fibronectin antibody was performed in both wildtype and *Tmed2*$^{99J/99J}$ placenta (Figure 3.8 A1-A4, B1-B4). We found that fibronectin was abnormally accumulated in allantoides of *Tmed2*$^{99J/99J}$ placentas when compared to wildtype controls (Figure 3.8 A4 versus B4, arrows indicate protein accumulation). We further characterized expression of fibronectin in cultured explants and found abnormal accumulation of fibronectin in all explants with *Tmed2*$^{99J/99J}$ allantois (Figure 3.8 E4, F4, arrows). This observation indicates that fibronectin localization is disrupted in *Tmed2*$^{99J/99J}$ allantoides and that this may contribute to abnormal chorioallantoic fusion and impaired labyrinth layer formation in *Tmed2*$^{99J/99J}$ placenta.

The adhesion molecule VCAM1 and its receptor α4-integrin were previously shown to be required for normal chorioallantoic attachment (Gurtner et al., 1995; Kwee et al., 1995; Yang et al., 1995). Immunohistochemistry revealed that VCAM1 and α4-integrin were found in *Tmed2*$^{99J/99J}$ mutant placentas (Jerome-Majewska et al., 2010). Therefore, we performed immunofluorescence to examine localization of VCAM1 in *Tmed2*$^{99J/99J}$ placentas and pre-placental explants (Figure 3.9). In wildtype placenta, polarized expression of VCAM1 was found in a single layer of cells surrounding the allantois Figure 3.9 A1-A4). In *Tmed2*$^{99J/99J}$ placentas, VCAM1 expression was no longer polarized as in the wildtype placenta (Figure 3.9 B1-B4). In addition, abnormal accumulation of VCAM1 was observed in some allantoic cells of *Tmed2*$^{99J/99J}$ placentas (Figure 3.9 B4, arrows). Localization of VCAM was also examined in cultured explants with wildtype or *Tmed2*$^{99J/99J}$ pre-placental tissues, however, VCAM1 was not found in any cultured explants (data not shown). Our data indicates that VCAM1 localization was disrupted in *Tmed2*$^{99J/99J}$ placentas and that the current *ex vivo* explant model is unable to sustain expression of VCAM1.

3.5. Discussion

3.5.1 TMED2 is required in both the chorion and the allantois during labyrinth layer development.

In this study, we discovered a tissue-specific requirement of TMED2 in the chorion for chorioallantoic fusion using a previously established *ex vivo* explant model (Hou et al., 2016). Molecular analysis showed increased apoptotic index, decreased mitotic index and deceased expression of placental markers *Tpbp*α as well as *Gcm1* in explants with *Tmed2*$^{99J/99J}$ pre-placenta tissues when compared to explants with wildtype

tissues. Immunofluorescence experiments on two potential cargo proteins of TMED2, fibronectin and VCAM1, showed abnormal expression in the allantois of *Tmed2*$^{99J/99J}$ placenta. These data suggest a tissue-specific requirement of TMED2 in both the chorion and the allantois for normal labyrinth layer development.

3.5.2 Potential roles of TMED2 during labyrinth layer development.

Increased apoptosis was observed in the allantoic region of explants with *Tmed2*$^{99J/99J}$ tissues when compared to explants of wildtype control: a range of 25% to 32% of apoptotic index was observed in explants with *Tmed2*$^{99J/99J}$ tissues and ~20% of apoptotic index was observed in explants of wildtype control. One possible explanation is that TMED2 could play a role in UPR-induced cell apoptosis. Future investigations on proteins involved in the UPR-induced cell apoptosis, such as ATF4, CHOP, IRE1, and TRAF2 could address this question. On the other hand, decreased proliferation was observed in the allantoic region of explants with *Tmed2*$^{99J/99J}$ tissues when compared to explants of wildtype control. This data suggests that TMED2 may regulate proteins involved in the cell cycle and in proliferation. In addition, the increase in apoptosis and the decreased in proliferation in explants with *Tmed2*$^{99J/99J}$ tissues could be due to mis-communication between the chorion and the allantois. For instance, absence of TMED2 protein in either the allantois or the chorion could result in the abnormal transport of one or more signaling molecules required for proliferation and survival in the chorion and/or the allantois.

We have previously shown that maintained expression of the spongiotrophoblast cell marker *Tpbpα* and the syncytiotrophoblast cell marker *Gcm1* requires physical contact between chorion and allantois under *ex vivo* culturing conditions (Hou et al.,

2016). Although chorioallantoic attachment occurred with *Tmed2*$^{99J/99J}$ mutant explants, *ISH* experiments revealed reduced expression of *Tpbpα* and *Gcm1* in explants with *Tmed2*$^{99J/99J}$ tissues when compared to controls, indicating that TMED2 is required in both the chorion and the allantois for sustained and expanded expression of *Tpbpα* and *Gcm1*. The mechanism via which TMED2 regulates expansion of the spongiotrophoblast and syncytiotrophoblast lineages remains to be determined.

The transmembrane adhesion protein VCAM1 and the extracellular matrix protein fibronectin, were abnormally expressed in allantoides of *Tmed2*$^{99J/99J}$ placenta. VCAM1 has been shown to interact with its receptor α4integrin in the chorionic mesothelium and is required for chorioallantoic attachment (Gurtner et al., 1995; Kwee et al., 1995; Watson and Cross, 2005; Yang et al., 1995). However, neither *Vcam1* nor *α4integrin* null embryos showed complete failure of chorioallantoic attachment (Gurtner et al., 1995; Yang et al., 1995). This suggests that other mechanisms co-exist to facilitate chorioallantoic attachment. Although abnormal localization of VCAM1 was observed in *Tmed2*$^{99J/99J}$ placenta, we could not determine if this disrupted pattern was due to a requirement for TMED2 in the chorion or the allantois. On the other hand, abnormal fibronectin localization was also observed in *Tmed2*$^{99J/99J}$ placenta and our data indicates that this is a cell-autonomous requirement in the allantois. Fibronectin was known to be required for mesodermal differentiation and extraembryonic vasculature development (George et al., 1993). In addition, formation of extracellular fibrils requires interaction between fibronectin and its receptors such as α5β1 and α5β3 integrins (Moursi et al., 1997). Since both VCAM1 and fibronectin relies on their interactions with integrins for their normal localization, it is possible that abnormal localization of their co-receptor,

integrins, explain the abnormal expression of both proteins in *Tmed2*$^{99J/99J}$ placenta. In addition, further experiments to refine localization of VCAM1 and fibronectin in the allantoic cells of the *Tmed2*$^{99J/99J}$ allantois may shed insight of whether those proteins are abnormally trafficked and thus retained inside of the cell due to the absence of TMED2.

In this study, we used a previously established *ex vivo* model of pre-placental explants to recapitulate placental abnormalities observed in *Tmed2*$^{99J/99J}$ placenta. Co-culturing explants of *Tmed2*$^{99J/99J}$ chorions with wildtype allantoides, revealed that *Tmed2* is required cell-autonomously in the chorion for chorioallantoic fusion and cell-autonomously in the allantois for normal expression of fibronectin. These data suggest that our *ex vivo* model is able to reveal tissue specific requirement of genes involved in early labyrinth layer development.

3.6 Acknowledgment

We would like to thank Dr. James Cross for his generous gifts of *Prl3d1*, *Plf*, *Gcm1*, and *Tpbpa* plasmids for in situ hybridization experiments. We would also like to thank Dr. K. Hadjantonakis for the kind gift of the Histone-H2B-eGFP reporter mouse line and Dr. Yojiro Yamanaka for the tdTomato-RFP reporter mouse line.

3.7 Figures

Figure 3.1 Representative images of TMED2 expression in wildtype placenta post chorioallantoic attachment.

A1-A3:TMED2 was expressed in both the chorion and the allantois after chorioallantoic attachment. TMED2 expression showed different patterns between allantoic (B1-B3) and chorionic cells (C1-C3). Chorion (ch), allantois (al), TMED2=green, DAPI=magenta; scale bar = 50μm.

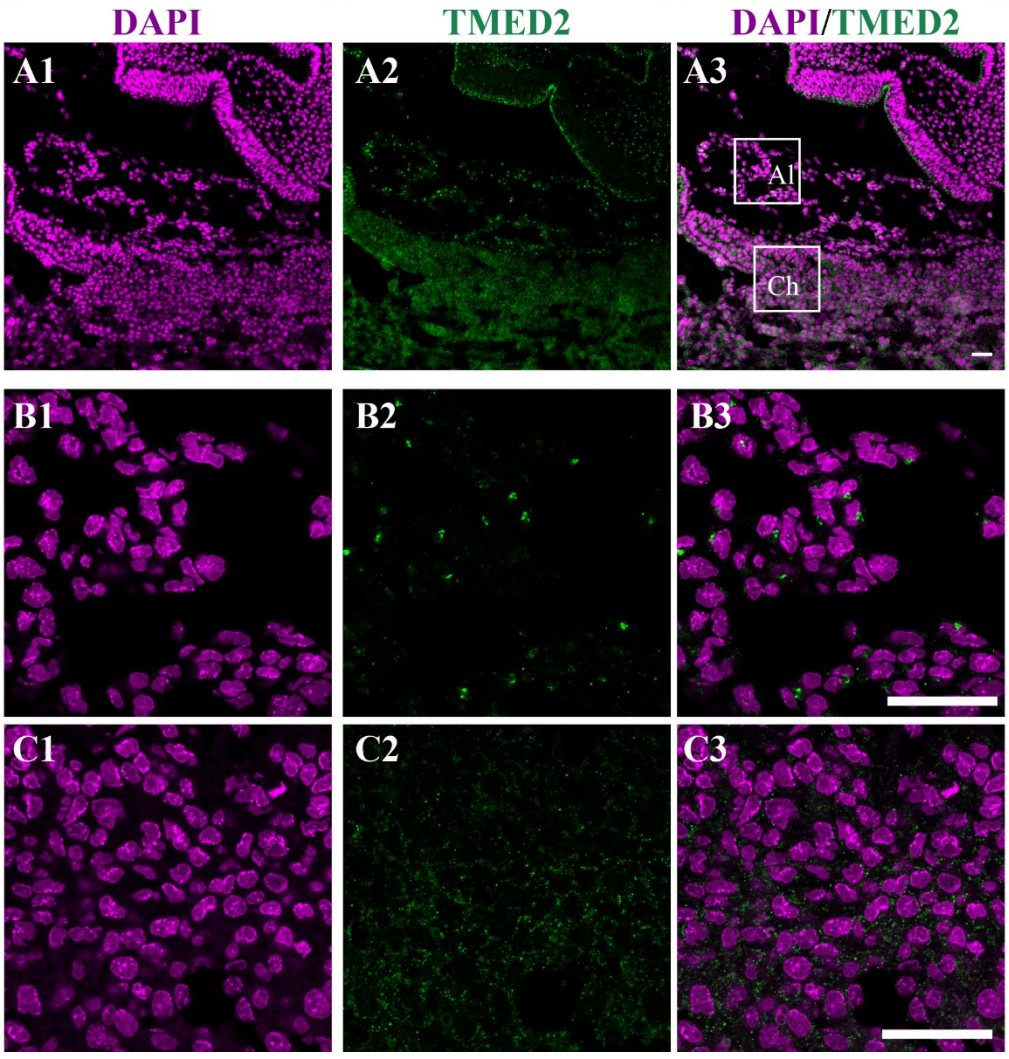

Figure 3.2 Representative images of explants of wildtype RFP+ chorion with an eGFP+ allantois and *Tmed2*$^{99J/99J}$RFP+ chorion with a *Tmed2*$^{99J/99J}$eGFP+ allantois.

Wt eGFP+ allantois is attached to the wildtype chorion explant (Wholemount view, A1-A4). Representative midline section of the same explant showed mixing between the eGFP+ allantoic and RFP+ chorionic cells along the chorionic plate (B1-B4, inset: C1-C4). Explant sample shows that *Tmed2*$^{99J/99J}$ eGFP+ allantois is attached to the *Tmed2*$^{99J/99J}$ chorion (Wholemount view, D1-D4). Representative midline section of the same explant showed no mixing between eGFP+ allantoic and RFP+ chorionic cells at the chorionic plate (E1-E4, inset: F1-F4). Chorion (ch), allantois (al), bright field (BF), eGFP=green, RFP= red, DAPI=magenta; * represents site of mixing; scale bar = 200μm for A1-A4, and D1-D4, and 50μm for B1-C4, and E1-F4.

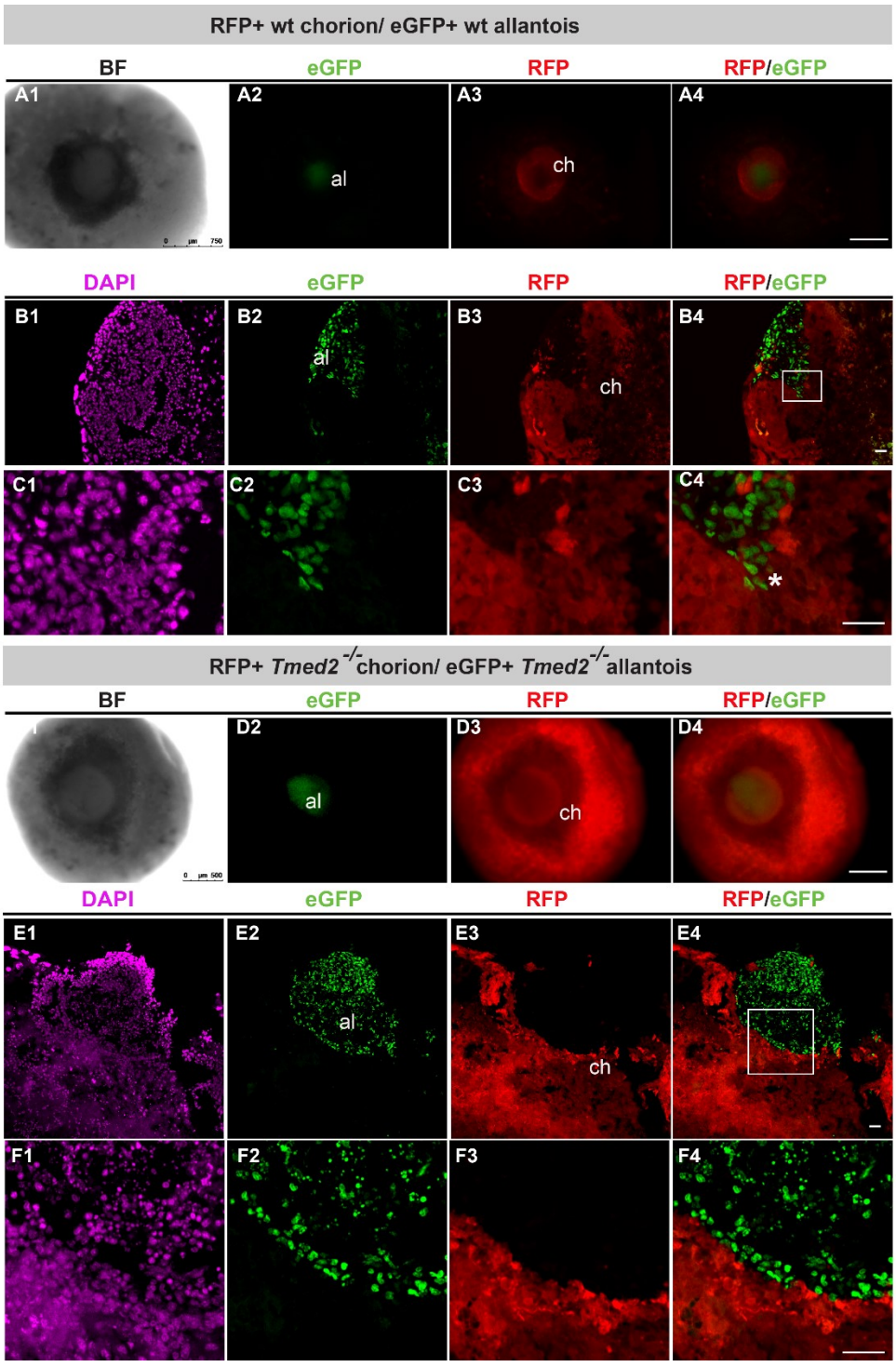
RFP+ wt chorion/ eGFP+ wt allantois
BF
eGFP
RFP
RFP/eGFP
A1
A2
A3
A4
al
ch
DAPI
eGFP
RFP
RFP/eGFP
B1
B2
B3
B4
al
ch
C1
C2
C3
C4
*
RFP+ Tmed2 -/- chorion/ eGFP+ Tmed2 -/- allantois
BF
eGFP
RFP
RFP/eGFP
D2
D3
D4
al
ch
DAPI
eGFP
RFP
RFP/eGFP
E1
E2
E3
E4
al
ch
F1
F2
F3
F4

Figure 3.3 Representative images of explants of a *Tmed2*$^{99J/99J}$ RFP+ allantois with wildtype eGFP+ chorion and a wildtype eGFP+ allantois with *Tmed2*$^{99J/99J}$ RFP+ chorion.

Tmed2$^{99J/99J}$ RFP+ allantois is attached to the wildtype chorion explant (Wholemount view, A1-A4). Representative midline section of the same explant showed mixing between the *Tmed2*$^{99J/99J}$ RFP+ allantoic and eGFP+ chorionic cells at the chorionic plate (B1-B4, inset: C1-C4). Wildtype eGFP+ allantois is attached to the *Tmed2*$^{99J/99J}$ chorion explant (Wholemount view, D1-D4). Representative midline section of the same explant showed no mixing between the eGFP+ allantoic and RFP+ *Tmed2*$^{99J/99J}$ chorionic cells at the chorionic plate (E1-E4, inset: F1-F4). Chorion (ch), allantois (al), bright field (BF), eGFP=green, RFP= red, DAPI=magenta; scale bar = 200μm for A1-A4, and D1-D4, and 50μm for B1-C4, and E1-F4.

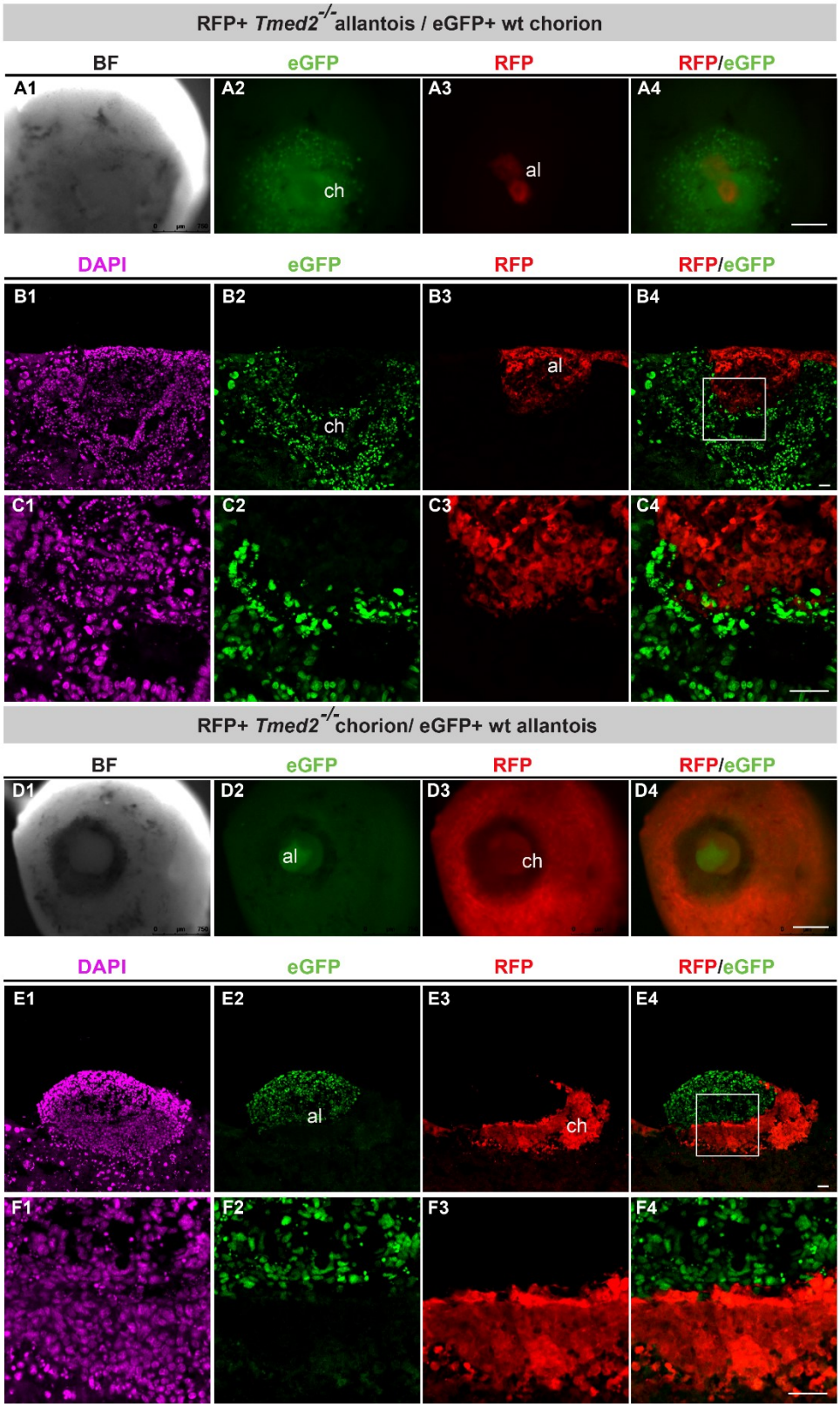
RFP+ Tmed2-/- allantois / eGFP+ wt chorion
BF
eGFP
RFP
RFP/eGFP
A1
A2
A3
A4
ch
al
DAPI
eGFP
RFP
RFP/eGFP
B1
B2
B3
B4
al
ch
C1
C2
C3
C4
RFP+ Tmed2-/- chorion/ eGFP+ wt allantois
BF
eGFP
RFP
RFP/eGFP
D1
D2
D3
D4
al
ch
DAPI
eGFP
RFP
RFP/eGFP
E1
E2
E3
E4
al
ch
F1
F2
F3
F4

Figure 3.4 Representative images showing expression of the endothelial marker PECAM1/CD31.

A1-A6: $CD31^{+}$ endothelial cells (yellow) are found in a subset of allantoic cells of the wildtype explant control after 24 hours. A6: Higher magnification images of boxed region in A5 show CD31 expression in eGFP+ allantoic cells. CD31 expression was not found in all explants with *Tmed2*$^{99J/99J}$ tissues (B4, C4, D4). Chorion (ch), allantois (al). Scale bar =50μm; green= eGFP, red= RFP, magenta= DAPI, yellow=CD31.

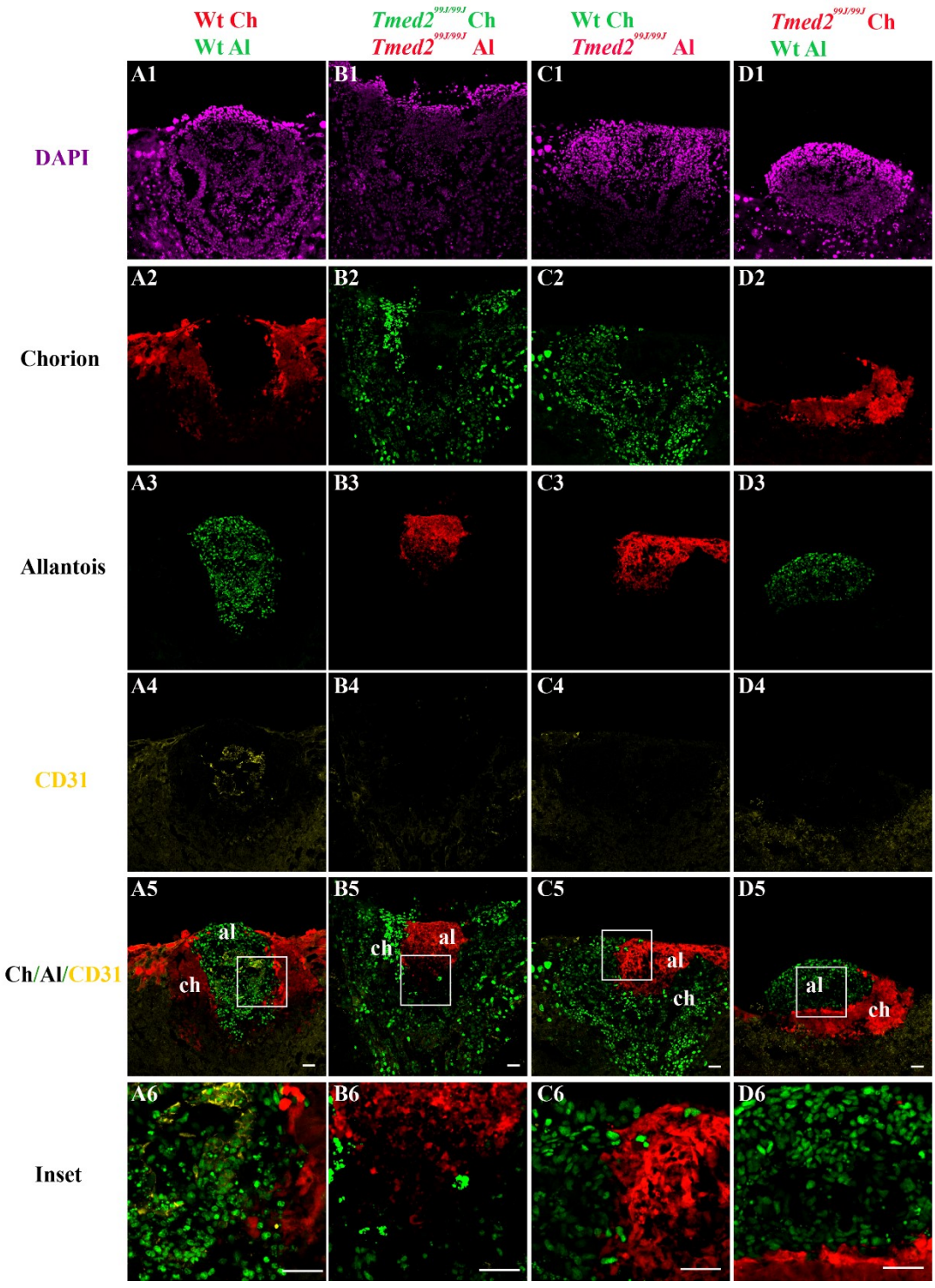
Wt Ch
Wt Al
Tmed2 99J/99J Ch
Tmed2 99J/99J Al
Wt Ch
Tmed2 99J/99J Al
Tmed2 99J/99J Ch
Wt Al
DAPI
Chorion
Allantois
CD31
Ch/Al/CD31
Inset
A1
B1
C1
D1
A2
B2
C2
D2
A3
B3
C3
D3
A4
B4
C4
D4
A5
B5
C5
D5
A6
B6
C6
D6
al
ch

Figure 3.5 mRNA expression of parietal giant cell markers *Prl3d1*, *Plf*, spongiotrophoblast marker *Tpbpα*, and syncytiotrophoblast maker *Gcm1* in cultured explants.

Expression of both parietal giant cell markers *Prl3d1* and *Plf* was detected by *in situ* hybridization in all explants of wildtype control and explants with *Tmed2*$^{99J/99J}$ tissues (A-E, A'-E'). Spongiotrophoblast marker *Tpbpα* was detected in all explants of wildtype control and explants with *Tmed2*$^{99J/99J}$ tissues (A"-D"), however, *Tpbpα* was not expressed in explants of *Tmed2*$^{99J/99J}$ chorion only without an allantois (E"). Syncytiotrophoblast maker *Gcm1* was also detected all explants of wildtype control and explants with *Tmed2*$^{99J/99J}$ tissues (A'"-D'"), but not in explants of *Tmed2*$^{99J/99J}$ chorion only without an allantois (E'"). Expression of *Tpbpα* and *Gcm1* was reduced in all explants with *Tmed2*$^{99J/99J}$ tissues when compared to the explant of wildtype control (B", C", D" versus A"; B'", C'", D'" versus A'"). Chorion (ch), allantois (al). Scale bar =50μm.

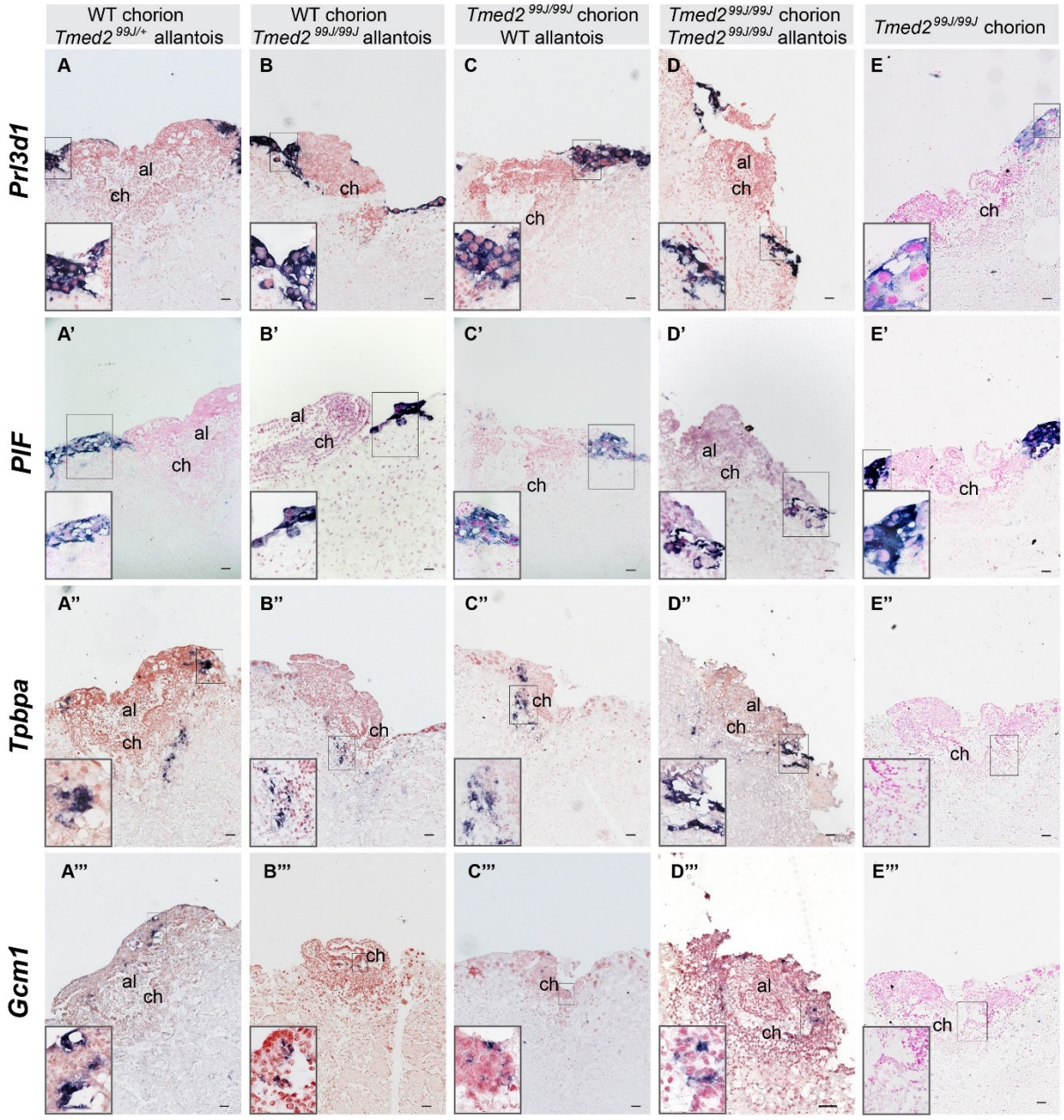
WT chorion
Tmed2 99J/+ allantois
WT chorion
Tmed2 99J/99J allantois
Tmed2 99J/99J chorion
WT allantois
Tmed2 99J/99J chorion
Tmed2 99J/99J allantois
Tmed2 99J/99J chorion
Prl3d1
PlF
Tpbpa
Gcm1
A
B
C
D
E
A'
B'
C'
D'
E'
A''
B''
C''
D''
E''
A'''
B'''
C'''
D'''
E'''
al
ch

Figure 3.6 Expression of a mitotic marker, phosphohistone H3 in cultured explants. Representative images of phosphohistone H3 (Ph3) expression in (A-A") a control explant of wildtype chorion with a wildtype allantois; (B-B") an explant of wildtype chorion with a *Tmed2*$^{99J/99J}$ allantois; (C-C") an explant of *Tmed2*$^{99J/99J}$ chorion with a wildytpe allantois; (D-D") an explant of *Tmed2*$^{99J/99J}$ chorion with a *Tmed2*$^{99J/99J}$ allantois. Chorion (ch), allantois (al). Green=Ph3, Magenta=DAPI. Scale bar =50μm.

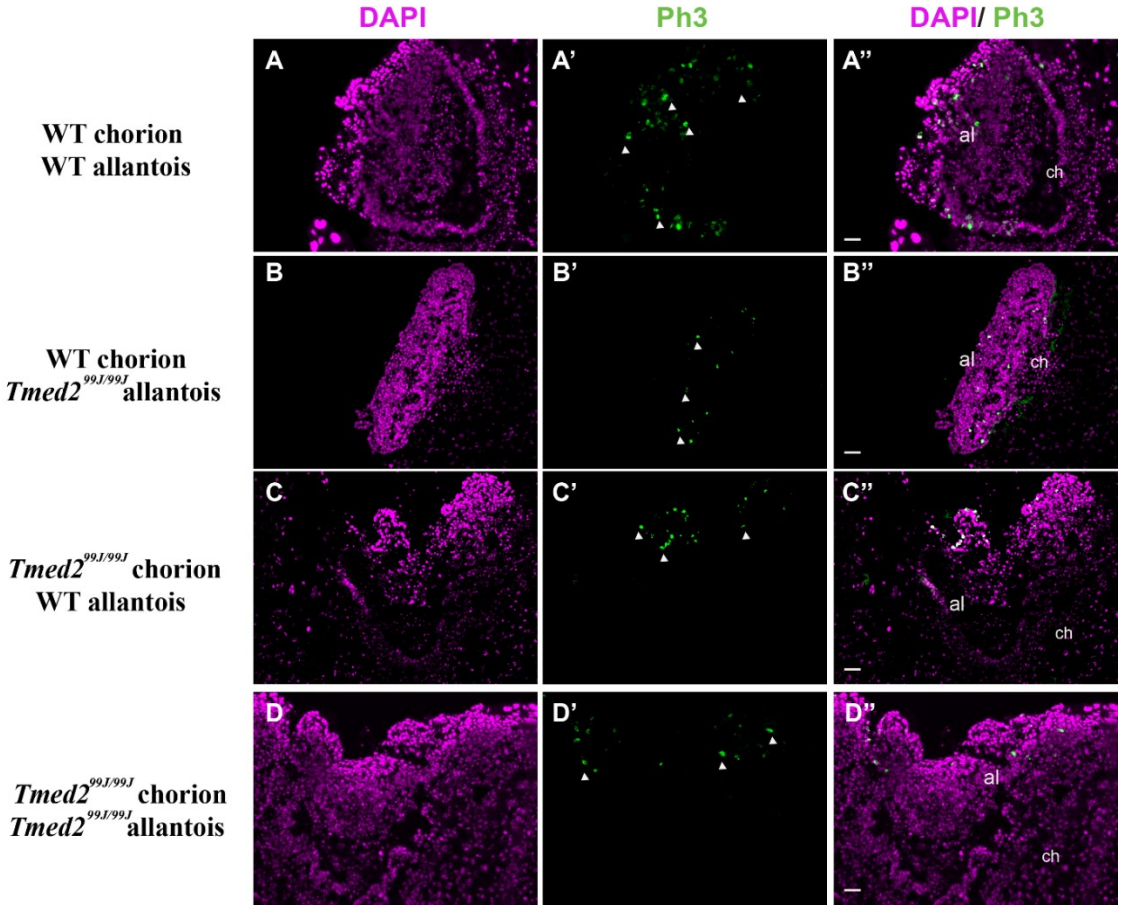

Figure 3.7 Expression of an apoptotic marker, cleaved Caspase-3 in cultured explants.

Representative images of cleaved Caspase-3 expression in (A-A") a control explant of wildtype chorion with a wildtype allantois; (B-B") an explant of wildtype chorion with a *Tmed2*$^{99J/99J}$ allantois; (C-C") an explant of *Tmed2*$^{99J/99J}$ chorion with a wildytpe allantois; (D-D") an explant of *Tmed2*$^{99J/99J}$ chorion with a *Tmed2*$^{99J/99J}$ allantois. Chorion (ch), allantois (al). Green=cleaved Caspase3, Magenta=DAPI. Scale bar =50μm.

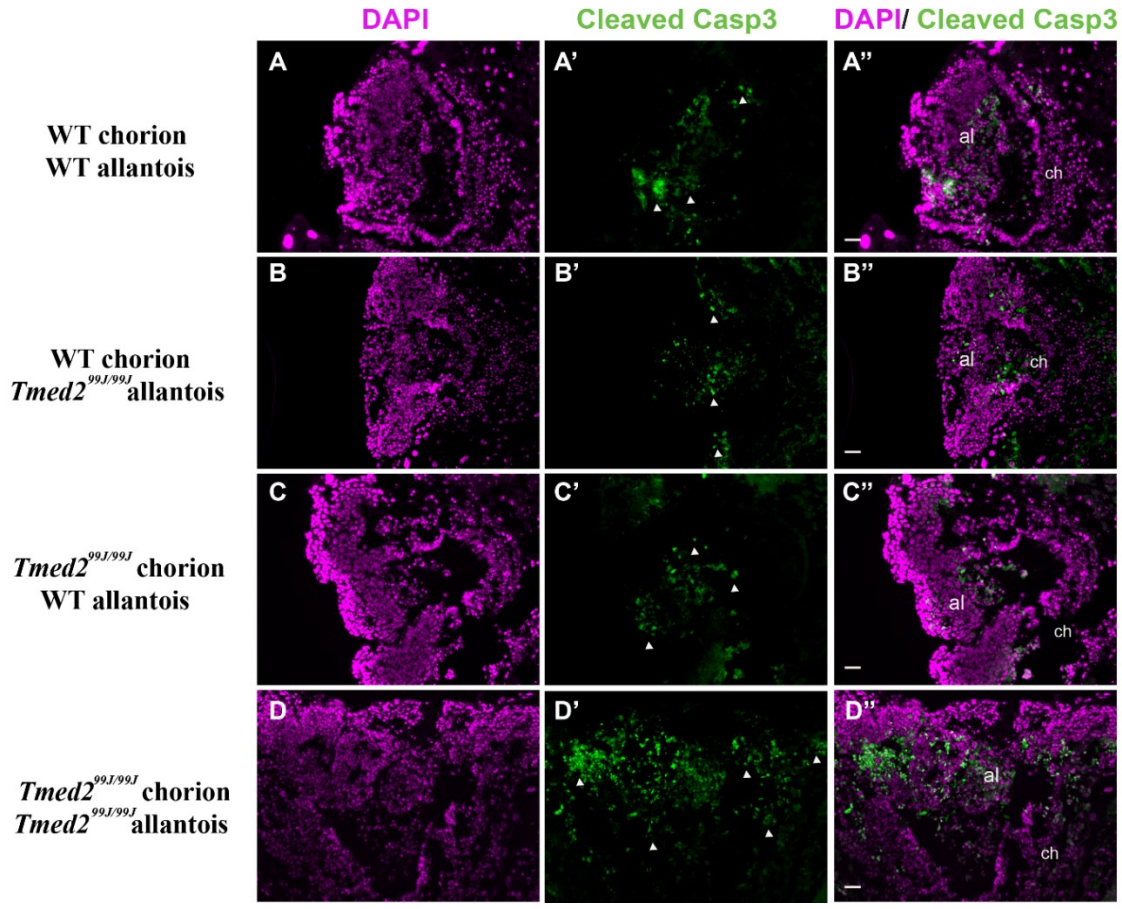

Figure 3.8 Representative images showing expression of ECM protein fibronectin in wildtype, *Tmed2*$^{99J/99J}$placenta and explants after culture.

A1-A4: fibronectin was expressed in the allantois of a wildtype placenta post chorioallantoic attachment. B1-B4: Abnormal expression of fibronectin was found in the allantois of *Tmed2*$^{99J/99J}$ placenta post chorioallantoic attachment, arrows indicate increased expression of fibronectin protein. Fibronectin was expressed normally in: (C1-C4) the control explant of wildtype chorion with a wildtype allantois, and (D1-D4) the explant of *Tmed2*$^{99J/99J}$ chorion with a wildtype allantois. Abnormal fibronectin expression was found in: (E1-E4) the explant of wildtype chorion with a *Tmed2*$^{99J/99J}$ allantois, and (F1-F4) the explant of *Tmed2*$^{99J/99J}$ chorion with a wildtype allantois. Chorion (Ch), Allantois (Al), DAPI= magenta, fibronectin= green. Scale bar =50μm, Arrows indicate increased expression of fibronectin.

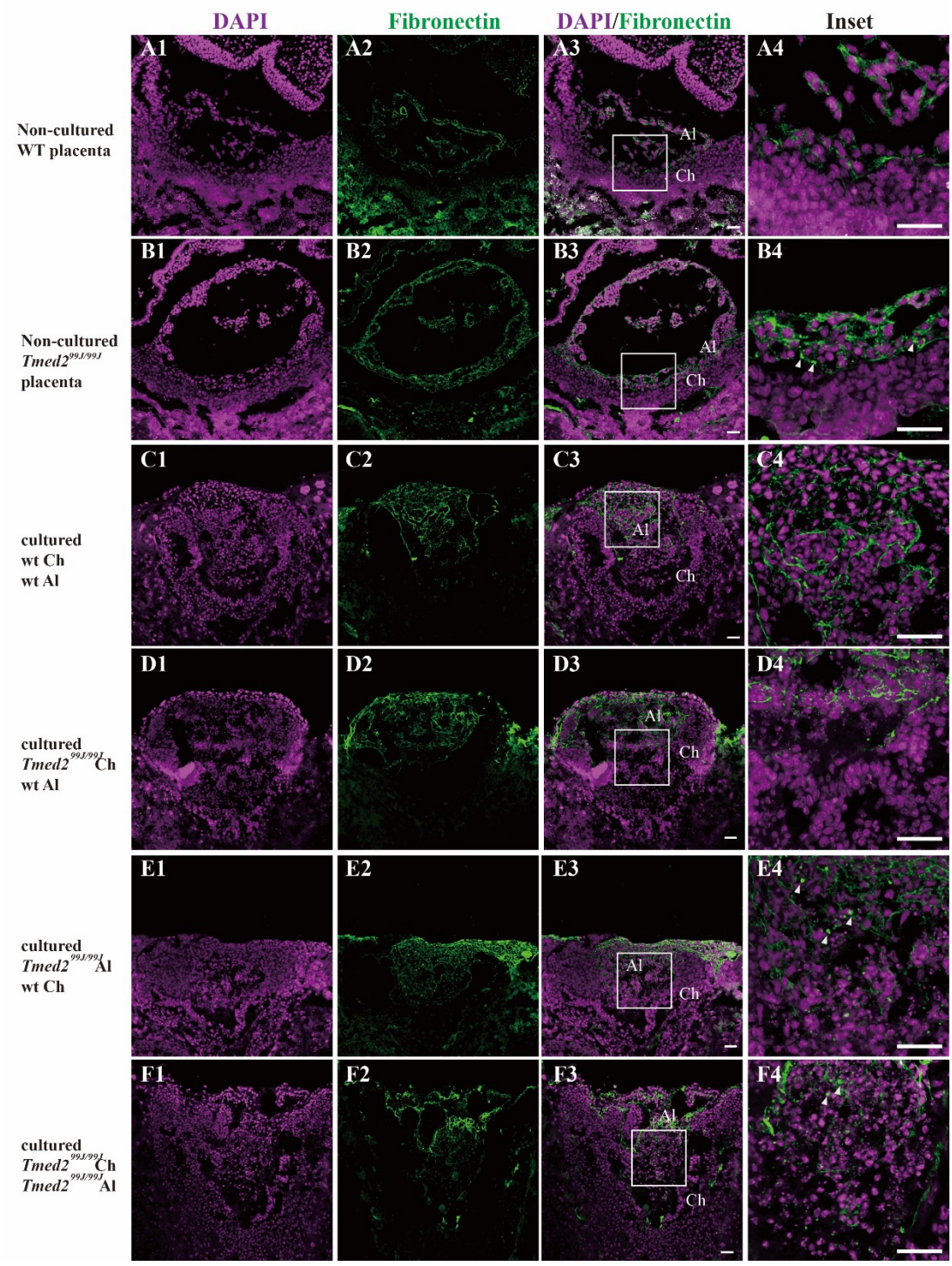
DAPI
Fibronectin
DAPI/Fibronectin
Inset
Non-cultured WT placenta
Non-cultured Tmed2 99J/99J placenta
cultured wt Ch wt Al
cultured Tmed2 99J/99J Ch wt Al
cultured Tmed2 99J/99J Al wt Ch
cultured Tmed2 99J/99J Ch Tmed2 99J/99J Al
A1
A2
A3
A4
B1
B2
B3
B4
C1
C2
C3
C4
D1
D2
D3
D4
E1
E2
E3
E4
F1
F2
F3
F4
Al
Ch

Figure 3.9 Representative images showing expression of adhesion molecule VCAM1 in wildtype and *Tmed2*$^{99J/99J}$placenta.

A1-A4: VCAM1 was localized at the apical surface of a monolayer of allantoic cells in wildtype placenta post chorioallantoic attachment. B1-B4: in the allantois of a *Tmed2*$^{99J/99J}$ placenta post-chorioallantoic attachment, VCAM1 showed abnormal expression in the allantoic cells. arrows indicate increased expression of VCAM1. Chorion (Ch), Allantois (Al), DAPI= blue, VCAM1= red. Scale bar =50µm.

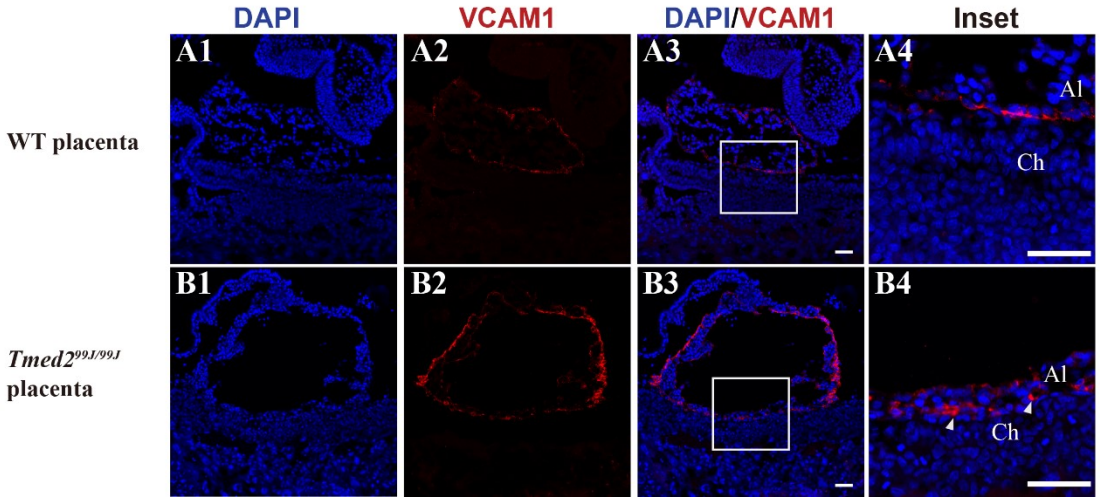

Table 3.1 Mitotic index in explants of wildtype control and explants with *Tmed2*$^{99J/99J}$ tissues.

A: The average sum of total number of cells counted, the average number of PH3+ cells, and the average mitotic index in cultured explants. Significantly less proliferation was found in explants of *Tmed2*$^{99J/99J}$ chorion cultured with a wildtype allantois when compared to wildtype control (bar graph). B: The average sum of total number of cells counted in the chorionic region, the average number of PH3+ cells in the chorionic region, and the average mitotic index in the chorionic region of cultured explants. No significant difference was found in mitotic index among all sample types (bar graph). C: The average sum of total number of cells counted in the allantoic region, the average number of PH3+ cells in the allantoic region, and the average mitotic index in the allantoic region of cultured explants. Reduced proliferation was found in explants of *Tmed2*$^{99J/99J}$ chorion with a wildtype allantois, and explants of *Tmed2*$^{99J/99J}$ chorion cultured with a *Tmed2*$^{99J/99J}$ allantois when compared to wildtype control (bar graph). P-values represented as*for <0.05, ** for <0.01 (student t-test).

Table 3.1A Mitotic Index of cultured *Tmed2* null and wildtype chorion/allantois explants for 24 hours

	Sample type	Number of samples (N)	Mean (M)	Standard Deviation (SD)	Standard Error of Mean (SEM)
Total cell count	*Tmed2*$^{+/+}$chorion+*Tmed2*$^{+/+}$allantois	4	1095.50	220.09	110.04
	Tmed2$^{+/+}$chorion+*Tmed2*$^{-/-}$allantois	4	689.9	204.43	102.21
	Tmed2$^{-/-}$chorion+*Tmed2*$^{+/+}$allantois	3	740.56	58.06	33.52
	Tmed2$^{-/-}$chorion+*Tmed2*$^{-/-}$allantois	4	1203.56	386.67	193.33
PH3+ cell count	*Tmed2*$^{+/+}$chorion+*Tmed2*$^{+/+}$allantois	4	74.21	17.07	8.54
	Tmed2$^{+/+}$chorion+*Tmed2*$^{-/-}$allantois	4	27.35	24.07	12.03
	Tmed2$^{-/-}$chorion+*Tmed2*$^{+/+}$allantois	3	15.78	7.42	4.28
	Tmed2$^{-/-}$chorion+*Tmed2*$^{-/-}$allantois	4	45.33	38.33	19.16
PH3+/total cell count (%)	*Tmed2*$^{+/+}$chorion+*Tmed2*$^{+/+}$allantois	4	6.83	1.25	0.62
	Tmed2$^{+/+}$chorion+*Tmed2*$^{-/-}$allantois	4	4.40	4.38	2.19
	Tmed2$^{-/-}$chorion+*Tmed2*$^{+/+}$allantois	3	2.20	1.08	0.62
	Tmed2$^{-/-}$chorion+*Tmed2*$^{-/-}$allantois	4	3.93	3.99	2.00

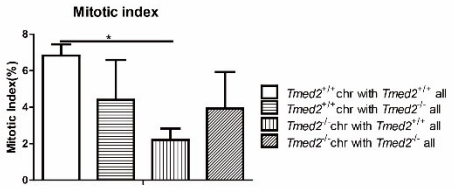

Table 3.1B Mitotic Index of chorion of cultured *Tmed2* null and wildtype chorion/allantois explants for 24 hours

	Sample type	Number of samples (N)	Mean (M)	Standard Deviation (SD)	Standard Error of Mean (SEM)
Total cell count	*Tmed2*$^{+/+}$chorion+*Tmed2*$^{+/+}$allantois	4	640.13	123.11	61.56
	Tmed2$^{+/+}$chorion+*Tmed2*$^{-/-}$allantois	4	496.50	188.74	94.37
	Tmed2$^{-/-}$chorion+*Tmed2*$^{+/+}$allantois	3	472.67	104.33	60.23
	Tmed2$^{-/-}$chorion+*Tmed2*$^{-/-}$allantois	4	834.15	415.15	207.57
PH3+ cell count	*Tmed2*$^{+/+}$chorion+*Tmed2*$^{+/+}$allantois	4	29.46	16.23	8.12
	Tmed2$^{+/+}$chorion+*Tmed2*$^{-/-}$allantois	4	18.56	17.52	8.76
	Tmed2$^{-/-}$chorion+*Tmed2*$^{+/+}$allantois	3	5.72	5.51	3.18
	Tmed2$^{-/-}$chorion+*Tmed2*$^{-/-}$allantois	4	34.14	32.60	16.30
PH3+/total cell count (%)	*Tmed2*$^{+/+}$chorion+*Tmed2*$^{+/+}$allantois	4	4.63	2.44	1.22
	Tmed2$^{+/+}$chorion+*Tmed2*$^{-/-}$allantois	4	4.55	5.49	2.75
	Tmed2$^{-/-}$chorion+*Tmed2*$^{+/+}$allantois	3	1.07	0.88	0.51
	Tmed2$^{-/-}$chorion+*Tmed2*$^{-/-}$allantois	4	4.03	4.55	2.28

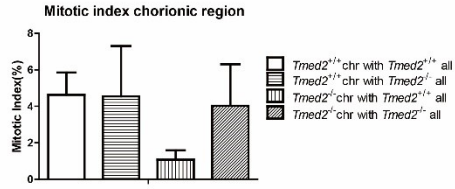

Table 3.1C Mitotic Index of allantoic region of cultured *Tmed2* null and wildtype chorion/allantois explants for 24 hours

	Sample type	Number of samples (N)	Mean (M)	Standard Deviation (SD)	Standard Error of Mean (SEM)
Total cell count	*Tmed2*$^{+/+}$chorion+*Tmed2*$^{+/+}$allantois	4	455.38	268.22	134.11
	Tmed2$^{+/+}$chorion+*Tmed2*$^{-/-}$allantois	4	193.40	82.34	41.17
	Tmed2$^{-/-}$chorion+*Tmed2*$^{+/+}$allantois	3	267.89	127.30	73.50
	Tmed2$^{-/-}$chorion+*Tmed2*$^{-/-}$allantois	4	369.41	170.52	85.26
PH3+ cell count	*Tmed2*$^{+/+}$chorion+*Tmed2*$^{+/+}$allantois	4	44.75	23.03	11.51
	Tmed2$^{+/+}$chorion+*Tmed2*$^{-/-}$allantois	4	8.79	8.26	4.13
	Tmed2$^{-/-}$chorion+*Tmed2*$^{+/+}$allantois	3	10.06	10.08	5.82
	Tmed2$^{-/-}$chorion+*Tmed2*$^{-/-}$allantois	4	11.19	8.06	4.03
PH3+/total cell count (%)	*Tmed2*$^{+/+}$chorion+*Tmed2*$^{+/+}$allantois	4	10.25	1.99	0.99
	Tmed2$^{+/+}$chorion+*Tmed2*$^{-/-}$allantois	4	4.98	4.63	2.32
	Tmed2$^{-/-}$chorion+*Tmed2*$^{+/+}$allantois	3	3.59	2.09	1.21
	Tmed2$^{-/-}$chorion+*Tmed2*$^{-/-}$allantois	4	3.53	3.32	1.66

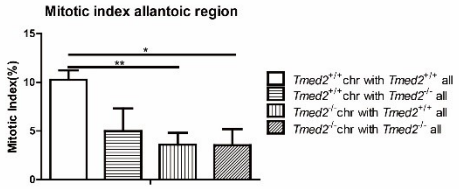

Table 3.2 Apoptotic index in explants of wildtype control and explants with *Tmed2*$^{99J/99J}$ tissues.

A: The average sum of the total number of cells counted in explants, the average number of cleaved Casp3+ cells, and the average apoptotic index in cultured explants. Increased cell death was found in explants of *Tmed2*$^{99J/99J}$ chorion cultured with a *Tmed2*$^{99J/99J}$ allantois when compared to the wildtype control (bar graph). B: The average sum of the total number of cells counted in the chorionic region, the average number of cleaved Casp3+ cells in the chorionic region, and the average apoptotic index in the chorionic region of cultured explants. Increased cell death was found in explants of *Tmed2*$^{99J/99J}$ chorion cultured with a *Tmed2*$^{99J/99J}$ allantois when compared to the wildtype control (bar graph). C: The average sum of the total number of cells counted in the allantoic region, the average number of cleaved Casp3+ cells in the allantoic region, and the average apoptotic index in the allantoic region of cultured explants. Increased cell death was found in explants of wildtype chorion cultured with a *Tmed2*$^{99J/99J}$ allantois when compared to wildtype control (bar graph). P-values represented as*for <0.05, ** for <0.01 (student t-test).

Table 3.2A Apoptosis Index of cultured *Tmed2* null and wildtype chorion/allantois explants for 24 hours

	Sample type	Number of samples (N)	Mean (M)	Standard Deviation (SD)	Standard Error of Mean (SEM)
Total cell count	*Tmed2*$^{+/+}$chorion+*Tmed2*$^{+/+}$allantois	3	1032.28	119.08	68.75
	Tmed2$^{+/+}$chorion+*Tmed2*$^{-/-}$allantois	4	843.42	318.10	159.05
	Tmed2$^{-/-}$chorion+*Tmed2*$^{+/+}$allantois	3	1071.67	77.17	44.56
	Tmed2$^{-/-}$chorion+*Tmed2*$^{-/-}$allantois	3	1264.00	379.75	219.25
Casp3+ cell count	*Tmed2*$^{+/+}$chorion+*Tmed2*$^{+/+}$allantois	3	89.44	13.49	7.79
	Tmed2$^{+/+}$chorion+*Tmed2*$^{-/-}$allantois	4	104.04	67.25	33.63
	Tmed2$^{-/-}$chorion+*Tmed2*$^{+/+}$allantois	3	116.22	47.30	27.31
	Tmed2$^{-/-}$chorion+*Tmed2*$^{-/-}$allantois	3	167.83	42.99	24.82
Casp3+ /total cell count (%)	*Tmed2*$^{+/+}$chorion+*Tmed2*$^{+/+}$allantois	3	8.77	1.19	0.69
	Tmed2$^{+/+}$chorion+*Tmed2*$^{-/-}$allantois	4	14.22	7.78	3.89
	Tmed2$^{-/-}$chorion+*Tmed2*$^{+/+}$allantois	3	11.42	5.72	3.30
	Tmed2$^{-/-}$chorion+*Tmed2*$^{-/-}$allantois	3	13.55	2.26	1.31

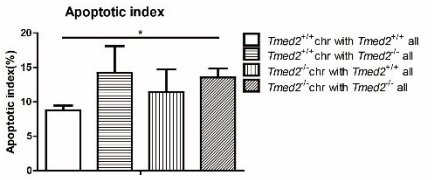

Table 3.2B Apoptosis Index of chorion of cultured *Tmed2* null and wildtype chorion/allantois explants for 24 hours

	Sample type	Number of samples (N)	Mean (M)	Standard Deviation (SD)	Standard Error of Mean (SEM)
Total cell count	*Tmed2*$^{+/+}$chorion+*Tmed2*$^{+/+}$allantois	3	765.44	78.33	45.23
	Tmed2$^{+/+}$chorion+*Tmed2*$^{-/-}$allantois	4	616.83	365.78	182.89
	Tmed2$^{-/-}$chorion+*Tmed2*$^{+/+}$allantois	3	805.11	74.02	42.73
	Tmed2$^{-/-}$chorion+*Tmed2*$^{-/-}$allantois	3	1043.78	411.00	237.29
Casp3+ cell count	*Tmed2*$^{+/+}$chorion+*Tmed2*$^{+/+}$allantois	3	34.22	2.04	1.18
	Tmed2$^{+/+}$chorion+*Tmed2*$^{-/-}$allantois	4	34.04	8.08	4.04
	Tmed2$^{-/-}$chorion+*Tmed2*$^{+/+}$allantois	3	55.22	31.51	18.19
	Tmed2$^{-/-}$chorion+*Tmed2*$^{-/-}$allantois	3	110.28	64.35	37.15
Casp3+/total cell count (%)	*Tmed2*$^{+/+}$chorion+*Tmed2*$^{+/+}$allantois	3	4.59	0.58	0.34
	Tmed2$^{+/+}$chorion+*Tmed2*$^{-/-}$allantois	4	7.45	4.88	2.44
	Tmed2$^{-/-}$chorion+*Tmed2*$^{+/+}$allantois	3	7.33	4.88	2.82
	Tmed2$^{-/-}$chorion+*Tmed2*$^{-/-}$allantois	3	9.88	2.62	1.51

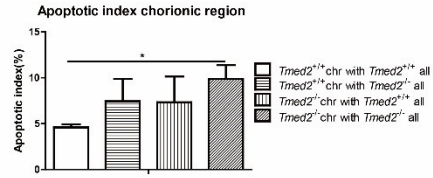

Table 3.2C Apoptosis Index of allantoic region of cultured *Tmed2* null and wildtype chorion/allantois explants for 24 hours

	Sample type	Number of samples (N)	Mean (M)	Standard Deviation (SD)	Standard Error of Mean (SEM)
Total cell count	*Tmed2*$^{+/+}$chorion+*Tmed2*$^{+/+}$allantois	3	266.83	58.50	33.78
	Tmed2$^{+/+}$chorion+*Tmed2*$^{-/-}$allantois	4	226.58	203.86	101.93
	Tmed2$^{-/-}$chorion+*Tmed2*$^{+/+}$allantois	3	266.56	55.06	31.79
	Tmed2$^{-/-}$chorion+*Tmed2*$^{-/-}$allantois	3	220.22	44.23	25.54
Casp3+ cell count	*Tmed2*$^{+/+}$chorion+*Tmed2*$^{+/+}$allantois	3	55.22	11.95	6.90
	Tmed2$^{+/+}$chorion+*Tmed2*$^{-/-}$allantois	4	70.0	60.22	30.11
	Tmed2$^{-/-}$chorion+*Tmed2*$^{+/+}$allantois	3	61.0	16.67	9.62
	Tmed2$^{-/-}$chorion+*Tmed2*$^{-/-}$allantois	3	57.56	26,37	15.23
Casp3+/total cell count (%)	*Tmed2*$^{+/+}$chorion+*Tmed2*$^{+/+}$allantois	3	21.41	3.34	1.93
	Tmed2$^{+/+}$chorion+*Tmed2*$^{-/-}$allantois	4	31.82	1.77	0.88
	Tmed2$^{-/-}$chorion+*Tmed2*$^{+/+}$allantois	3	24.42	9.68	5.59
	Tmed2$^{-/-}$chorion+*Tmed2*$^{-/-}$allantois	3	26.08	7.09	4.09

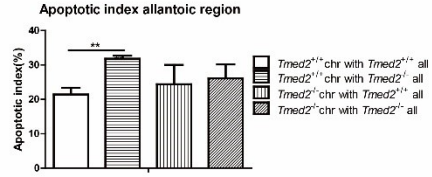

Connecting text between Chapter III and IV

In the previous chapter, I described the study of tissue-specific requirement of *Tmed2* during early labyrinth layer development using an established *ex vivo* pre-placental explant system. Though *Tmed2*$^{99J/99J}$ embryos arrested before E11.5 due to impaired placental development and function, *Tmed2*$^{99J/+}$ mice were viable and fertile. Although young adults of *Tmed2*$^{99J/+}$ animals (< 6 months old) did not have any obvious gross abnormalities, a number of *Tmed2* heterozygous mice developed liver cancer at older age (starting at 8 months). Histological analysis on liver samples from *Tmed2*$^{99J/+}$ and age-matched wildtype littermate mice revealed a significant increase in numbers of *Tmed2*$^{99J/+}$mice with the non-alcoholic fatty liver disease (NAFLD) phenotype at 6 months old. In this chapter, I described experiments and analysis performed to characterize the NAFLD phenotype and potential underlining mechanisms regulated by TMED2 in the *Tmed2*$^{99J/+}$ liver.

Chapter IV：Non-alcoholic Fatty Liver Disease in Mice with Heterozygous Mutation in TMED2

Wenyang Hou, Swati Gupta, Marie-Claude Beauchamp, Libin Yuan, Loydie A. Jerome-Majewska

PLoS ONE 12(8): e0182995. https://doi. org/10.1371/journal.pone.0182995

4.1 Abstract

The transmembrane emp24 domain/p24 (TMED) family are essential components of the vesicular transport machinery. Members of the TMED family serve as cargo receptors implicated in selection and packaging of endoplasmic reticulum (ER) luminal proteins into coatomer (COP) II coated vesicles for anterograde transport to the Golgi. Deletion or mutations of Tmed genes in yeast and Drosophila results in ER-stress and activation of the unfolded protein response (UPR). The UPR leads to expression of genes and proteins important for expanding the folding capacity of the ER, degrading misfolded proteins, and reducing the load of new proteins entering the ER. The UPR is activated in non-alcoholic fatty liver disease (NAFLD) in human and mouse and may contribute to the development and the progression of NAFLD. *Tmed2*, the sole member of the vertebrate Tmed β subfamily, exhibits tissue and temporal specific patterns of expression in embryos and developing placenta but is ubiquitously expressed in all adult organs. We previously identified a single point mutation, the 99J mutation, in the signal sequence of *Tmed2* in an N-ethyl-N-nitrosourea (ENU) mutagenesis screen. Histological and molecular analysis of livers from heterozygous mice carrying the 99J mutation, $Tmed2^{99J/+}$, revealed a requirement for TMED2 in liver health. We show that $Tmed2^{99J/+}$ mice had decreased levels of TMED2 and TMED10, dilated endoplasmic reticulum membrane, and increased phosphorylation of eIF2α indicating ER-stress and activation of the UPR. Increased expression of *Srebp1a* and *2* at the newborn stage and increased incidence of NAFLD were also found in $Tmed2^{99J/+}$ mice. Our data establishes $Tmed2^{99J/+}$ mice as a novel mouse model for NAFLD and supports a role for TMED2 in liver health.

4.2 Introduction

The ten TMED proteins in mouse and human are subdivided into four subfamilies based on sequence similarity (Strating and Martens, 2009a): three belong to the α subfamily (TMED4, 9, 11); one to the β family (TMED2); five to the γ subfamily (TMED1, 3, 5, 6, 7); and one to the δ family (TMED10). TMED proteins were found to form monomers, dimers and heterodimers (Jenne et al., 2002)and to regulate the stability of each other (Pastor-Cantizano et al., 2015). Thus, loss of one member of a subfamily resulted in loss of TMED proteins in other subfamilies (Denzel et al., 2000; Jenne et al., 2002; Jerome-Majewska et al., 2010).

Members of the TMED family serve as cargo receptors implicated in selection and packaging of endoplasmic reticulum (ER) luminal proteins into COP II coated vesicles for anterograde transport to the Golgi. TMED putative cargos include WNTs and glycosylphosphatidylinositol-anchored proteins (GPI-APs) (Pastor-Cantizano et al., 2015). Deletion or mutations of Tmed genes in yeast and Drosophila resulted in ER-stress and activation of the unfolded protein response (UPR) (Belden and Barlowe, 2001).The UPR leads to expression of genes and proteins important for expanding the folding capacity of the ER, degrading misfolded proteins, and reducing the load of new proteins entering the ER (Malhi and Kaufman, 2011) .

Tmed2, the sole member of the vertebrate Tmedβ subfamily exhibits tissue and temporal specific patterns of expression in embryos and developing placenta (Au et al., 2015; Jerome-Majewska et al., 2010; Zakariyah et al., 2011) but was ubiquitously expressed in all adult organs (Strating et al., 2009a). Our group identified a point mutation in the signal sequence of *Tmed2* in a mutant mouse line, 99J, generated in a

mutagenesis screen with N-ethyl-N-nitrosourea (ENU). We showed that the 99J mutation results in decreased TMED2 protein levels in heterozygous (*Tmed2*$^{99J/+}$) embryos and loss of TMED2 protein in homozygous mutant embryos (*Tmed2*$^{99J/99J}$) (Jerome-Majewska et al., 2010). *Tmed2* is required for morphogenesis of the embryo and its associated placenta, and consequently *Tmed2*$^{99J/99J}$ embryos arrest at mid-gestation, shortly after embryonic day (E)10.5 (Jerome-Majewska et al., 2010). Similarly, *Tmed10,* the sole member of the Tmed δ family is required for embryonic development and, *Tmed10* homozygous mutant embryos arrest early in development, before E3.5 (Denzel et al., 2000). Furthermore, *Tmed10* heterozygous mice showed dilated Golgi and reduced amount of at least two other members of the TMED family, TMED9 and TMED3. The consequences of reduced levels of TMED2 have not been described yet. Herein, we report that in adult mice, normal amount of TMED2 was required for liver health. Mice heterozygous for the ENU-induced *Tmed2*$^{99J/+}$ allele had decreased levels of TMED2 and TMED10, dilated endoplasmic reticulum membrane and increased phosphorylation of eIF2α indicating ER-stress and activation of the UPR, increased expression of *Srebp1a* and *2* at the newborn stage, and an increased incidence of non-alcoholic fatty liver disease (NAFLD).

NAFLD is the major cause of chronic liver disease worldwide in both developing and developed countries (Abd El-Kader and El-Den Ashmawy, 2015; Review T, LaBrecque DR, Abbas Z, Anania F, Ferenci P, Khan AG, Goh KL, Hamid SS, Isakov V, Lizarzabal M, Penaranda MM, Ramos JF, Sarin S, Stimac D, Thomson AB, UmarM, Krabshuis J, 2014). Although, the global prevalence of NAFLD is estimated to be 25.24%, with the highest prevalence in South America (30.45%) and the Middle East

(31.79%), no therapy exists to treat NAFLD. Lifestyle changes, including diet and exercise, can result in significant improvement in steatosis in a subset of patients and is the treatment currently recommend for NAFLD (S.Nahum, 2004). In addition, two drugs Pioglizatone and Obeticholic Acid, were also found to significantly improve histological signs of NAFLD in two separate randomized, placebo-controlled trials (Cusi et al., 2016; Louis et al., 2016). The thiazolidinedione, Pioglitazone, was shown to be safe and effective in patients with prediabetes or type 2 diabetes and non-alcoholic steatohepatitis (Cusi et al., 2016), however, concerns persist regarding the longterm safety of this drug. In addition, the Farnesoid X nuclear receptor ligand Obeticholic Aid, also resulted in significant improvement of histological features of NAFLD (Louis et al., 2016). Nonetheless, since many patients are refractory to these treatments and NAFLD is a heterogenous disease, identifying and characterizing novel models for NAFLD will aid in development of biomarkers and new therapeutic targets. Our work indicates that *Tmed2* heterozygous mice with the 99J mutation is a novel mouse model for NAFLD and supports a role for TMED2 in liver health.

4.3 Materials and Methods

4.3.1 Mice

All procedures and experiments were performed according to the guidelines of the Canadian Council on Animal Care and approved by the Animal Care Committee of the Montreal Children's Hospital. The 99J mouse line was generated on a C57/BL6J genetic background and maintained on a mixed C3H genetic background (C3HeB/FeJ and C3HeB/FeV). The 99J mutation was genotyped by PCR using primers to D5MIT95 and D5MIT213 as previously described (Jerome-Majewska et al., 2010). For newborns, the

date of birth was designated as P1. Liver analysis was performed on samples collected from mice between 1 – 17 months of age euthanized between 13h - 17h on the day of tissue collection. For molecular analysis, livers collected at P5 were classified as pre-weaning newborn, livers collected from animals between 1 and 2 months of age were classified as post-weaning juveniles, and livers collected from animals 3 – 6 months of age were classified as mature adults.

4.3.2 Cell Lines

Human hepatocellular carcinoma cells (HepG2) and the liver adenocarcinoma cells (SK-HEP-1) (ATCC, Manassas, VA, USA) were used in this study (Gifts of Dr. P. Metrakos). Both cell lines were grown in Minimal Essential Medium supplemented with 10% of FBS, 1% penicillin/streptomycin (Wisent, Saint-Bruno, Quebec, Canada). Each cell line was passaged every 4 to 6 days. Cells were maintained at 37 °C in a 5 % CO_2, 95 % air atmosphere incubator. Treatment with tunicamycin (Sigma, Oakville, Ontario, Canada), diluted in DMSO, was performed in cell medium at the indicated concentrations. DMSO was used as vehicle.

4.3.3 Tunicamycin

Tunicamycin was prepared in 150mM sucrose and was injected intraperitoneally at a dose of 0.75mg/kg in 10 weeks old wildtype (n=4) and *Tmed2*$^{99J/+}$ (n=6) mice at day 0. The weight of mice was monitored daily in the morning for 14 days at which point they were euthanized and organs collected.

4.3.4 Liver Collection

Liver samples collected from individual adult animals were used for multiple experiments. To standardize experiments between animals, the left lateral lobe of the

liver was used for histology, the left medial lobe was used for RNA analysis, and the rest of the liver tissue was used for Western blot analysis. Liver tissue was collected and fixed in 4% PFA or Bouin solution (Ricca Chemical, Texas, USA) for immuno-histochemical analyses and/or histology, respectively. For Western blot analysis, liver was flash frozen in liquid nitrogen before lysis in RIPA buffer. For RNA analysis, liver tissue was treated with Trizol and stored at -80ºC before RNA extraction. For Transmission Electron Microscopy (TEM) liver samples, mice were anesthetized, and the internal organs were perfused and fixed with 25% glutaraldehyde in 0.1 M cacodylate buffer.

4.3.5 Paraffin and Cryoembedding

Liver samples fixed in Bouin and/or PFA were dehydrated and embedded in paraffin, as previously described (Gupta et al., 2016; Hou et al., 2016; Jerome-Majewska et al., 2010). All samples were sectioned at 5µm thickness. For cryosection, liver samples were fixed in 4% PFA, cryoprotected in 30% sucrose, and cryoembedded in plastic molds before sectioning at 10µm thickness.

4.3.6 Transmission Electron Microscopy (TEM)

Livers collected from wild type (n=2) and *Tmed2*$^{99J/+}$(n=4) mice were washed in Phosphate Buffered Saline (PBS), fixed with 25% glutaraldehyde in 0.1 M cacodylate buffer (pH = 7.5), stained in 2% reduced osmium tetraoxide, and embedded in Epone. The samples were sectioned at the McGill FEMR facility. Imaging of sections was completed on the Tecnai T12 120 kV TEM microscope.

4.3.7 Scoring for NAFLD

Paraffin embedded samples were stained with Hematoxylin and Eosin (H&E) using standard protocols and scored for NAFLD using a scoring system adapted from

Kleiner et al., 2005, for details see Table 1 (Kleiner et al., 2005). Liver samples were scored using 20X objectives on a Zeiss Axiophot compound microscope. Minimum of two slides (four sections each) at least 100 µm apart were used for scoring liver samples. Representative images were taken for each sample using a Zeiss Axiophot compound microscope, AxioCamMRc camera and Axiovision v4.7.1.0 software. Samples with scores of ≥4 were considered sick and samples with scores of < 4 were diagnosed healthy. All livers were scored by two individuals blind to animal genotype.

4.3.8 Oil Red O Staining and Sudan Black B staining

Livers from subset of wild type (n = 4) and heterozygous (n=4) mice with macro and/or microvesicular steatosis scores of 0 - 3 were stained with Oil Red O or Sudan Black B to confirm presence of steatosis. Briefly**,** cryosectioned livers were washed with running tap water for 10 minutes, rinsed with 60% isopropanol and stained with Oil Red O (Sigma, Cat# O0625-25G) mixed with 60% isopropanol for 15 minutes. The sections were then rinsed with 60% isopropanol, and nuclei were stained with Mayer's Haematoxylin, rinsed in tap water and coversliped with aqueous mounting medium. For Sudan Black B staining, cryosectioned livers were washed in tap water for 10 minutes, rinsed in 70% ethanol for 1 minute and stained with Sudan Black B (Sigma, Cat# 199664-25G) diluted in 70% ethanol for 8 minutes. The sections were dipped in 70% ethanol for 2 minutes to remove any extra stain, and the nuclei were stained with 0.1% nuclear fast red. Sections were then washed in tap water for 10 minutes and coversliped with aqueous mounting medium. All samples were imaged using Leica microsystem (model DM6000B) and Leica camera (model DFC 450 C).

4.3.9 Biochemical Analysis

Cardiac puncture was performed to collect blood for biochemical analysis. Briefly, after euthanization, blood was collected in Vacuette potassium-EDTA tubes (VWR, Cat #454428) and centrifuged to isolate plasma. Plasma samples were stored at -20°C until analysis. Levels of cholesterol and triglycerides were measured by routine laboratory techniques at the McGill University Health Center core facility.

4.3.10 RT-PCR

RNA extraction was performed according to Trizol manufacturer's protocol (Invitrogen, Burlington, Ontario). Total RNA was treated with DNAse (NEB, according to manufacturer's protocol) and used for reverse transcription with the iScript™cDNA synthesis kit (Bio-rad, Cat. #170-8890, according to the manufacturer's protocol). qRT-PCR was performed using the ssoAdvanced universal SYBR green supermix (Bio-Rad, cat#172-5270) on a Roche LightCycle 480 PCR machine. qPCR experiments were performed in duplicates to ensure technical replicability. At least 4 animals of each genotype were analyzed for biological replicates. Target genes were normalized with the normalization factor as calculated by geNorm software (v3.4; Ghent university hospital center for medical genetics) (Vandesompele et al., 2002). Two to three house-keeping genes including B2M, GAPDH, and SDHA were used for the generation of the normalization factor as previously reported (Vandesompele et al., 2002). RT-PCR program included a hot start at 95 °C for 5 min, followed by 40 cycles of a denaturation step at 95 °C for 10s and an annealing/extension step at 60 °C for 30s. Primers used in the present study are listed on Table 4.1.

4.3.11 Western Blot analysis

Snap-frozen mice tissues were minced and lysed in RIPA buffer (25 mM Tris·HCl pH 7.6, 10 % glycerol, 420 mM NaCl, 2 mM $MgCl_2$, 0.5 % NP-40, 0.5 % Triton X-100, 1 mM EDTA, protease inhibitor) on ice. Approximately 50mg of liver tissue was sonicated and centrifuged at 13000rpm for 20 minutes at 4ºC. Clarified protein lysates were measured according to standard methods using a DC protein assay kit (Bio-Rad, Mississauga, Ontario, Canada). Cells were pelleted and lysed with RIPA buffer. 50µg of protein was resolved on 6 % and 12 % denaturing SDS-polyacrylamide gels and transferred to PVDF membranes, as previously described (Marques et al., 2015).
For protein samples resolved on TGX Stain-Free gels (Bio-Rad, Cat# 4568045), the gel was activated by exposure to UV light for 1 min to visualize total proteins. They were then transferred to Low Fluorescence PVDF membrane (Bio-Rad, Cat# 1620260), and a stain-free blot image was acquired to obtain a total protein profile. The total protein profile was used as a loading control to normalize the level of the protein of interest. When indicated, β-actin level was used as a loading control to normalize the level of the protein of interest.

After blocking in 5 % milk, all membranes were probed with indicated primary antibodies. Immunoblotted proteins were visualized using horseradish peroxidase-conjugated secondary antibodies (Cell Signaling), and antigen-antibody complexes were detected using the ECL system (ZmTech Scientifique, Montreal, Quebec, Canada).
All western blots were repeated at least twice on each sample, and at least 3 animals of each genotype were analyzed for biological replicates. Images of western blots were taken with Bio-Rad's ChemiDoc MP System. The bands for total proteins and the Chemi

images were digitally analyzed using Image Lab software. Primary antibodies used in this study are listed in Table 4.2.

4.3.12 Statistical Analysis

Two-tailed unpaired t-test analysis and Fisher's exact test were calculated using the Prism Software (http://www.graphpad.com/scientific-software/prism/). Significant p-values are represented as * for <0.05, ** for <0.01, *** for <0.001.

4.4 Results

4.4.1 TMED2 protein was significantly decreased in livers of newborn Tmed2$^{99J/+}$ mice.

We previously showed that embryos homozygous mutant for the 99J mutation in *Tmed2* have reduced mRNA and absent protein (Jerome-Majewska et al., 2010). To examine the requirement of TMED2 in heterozygous mice, we first quantified *Tmed2* mRNA levels in livers of heterozygous mice carrying the 99J mutation (*Tmed2*$^{99/+}$) using qRT-PCR. We predicted that TMED2 levels may correlate with the age and maturity of the mice. Therefore, we analyzed newborn pre-weaning (P5, n=4 per genotype), post-weaning juvenile (1 - 2 months, n=4 per genotype) and adult mice (3 - 6months, n=4 per genotype), separately. No significant difference was observed in levels of *Tmed2* mRNA in the liver of *Tmed2*$^{99/+}$ newborn, juvenile, and adult mice as compared to age-matched wild type mice (Figure 4.1A). However, TMED2 protein was reduced at all stages analyzed (n=3 per genotype per age group; Figure 4.1B – 1E), though this decrease was only statistically different when livers of newborn *Tmed2*$^{99/+}$mice where compared to age-matched wild type control (two-tailed, unpaired t-test, p=0.004; Figure 4.1B,1C). These data confirmed the previously reported discordance between expression of Tmed2 mRNA and protein, in *Tmed2*$^{99/99J}$ embryos (Jerome-Majewska et al., 2010).

4.4.2 TMED10 was significantly decreased in livers of newborn Tmed2$^{99J/+}$ mice.

TMED2 complexes with TMED10 (Blum et al., 1999; Füllekrug et al., 1999; Jenne et al., 2002), and is required for TMED10 stability and localization (Emery et al., 2000; Jerome-Majewska et al., 2010).We examined *Tmed10* mRNA level and found that it was not significantly different between wild type and *Tmed2*$^{99/+}$ mice (n=4 per genotype per age group; Figure 4.2A). However, TMED10 was reduced at all stages analyzed (n=3 per genotype per age group; Figure 4.2B – 4.2C), and this difference was statistically significant in newborn and adult mice (two-tailed, unpaired t-test, p=0.045 for newborn, and 0.024 for adult; Figure 4.2B – 4.2C). Thus, levels of both TMED2 and its associated partner, TMED10 are decreased in livers of *Tmed2*$^{99J/+}$ mice.

4.4.3 Normal level of TMED2 was not required for tunicamycin induced UPR.

Since TMED2 and TMED10 were implicated in rapid ER stress-induced export (RESET), an early step in the unfolded protein response (UPR) important for the degradation of misfolded GPI-anchored proteins (Satpute-Krishnan et al., 2014), we investigated a potential role for TMED2 in the UPR. Treating HepG2 and SKHep1 - human liver cancer cell lines - with tunicamycin for 24 hours resulted in a significant increase in glucose regulated protein (GRP)78, consistent with activation of UPR (two-tailed, unpaired t-test, p=0.048 for HepG2 and 0.029 for SKHep1). However, no significant modulation of TMED2 was found when HepG2 and SKHep1 cells were treated with tunicamycin for 24-hours (Figure 4.3 A – D). This indicates that TMED2 was not regulated during tunicamycin-induced UPR. In addition, wild type and *Tmed2*$^{99J/+}$ mice treated with tunicamycin, as described previously (Yamamoto and Mori, 2010) and in the materials and methods, showed a similar reduction in weight and

subsequent recovery (Figure 4.3 E). Overall, our data indicate that TMED2 is not modulated by tunicamycin and suggest that normal levels of TMED2 is not required for tunicamycin-induced UPR.

4.4.4 ER dilation and increased phosphorylated eIF2α in Tmed2$^{99J/+}$ livers.

Golgi of mice with heterozygous mutation in *Tmed10* are moderately dilated, (Denzel et al., 2000) therefore, we used transmission electron microscopy to examine the morphology of Golgi and ER in livers of *Tmed2*$^{99/+}$ mice. No morphological abnormalities were found in Golgi of *Tmed2*$^{99J/+}$ mice (data not shown). However, ER membranes in a subset of adult *Tmed2*$^{99J/+}$ mice were mildly dilated (n=3/4) (Figure 4.4B, D) when compared to age-matched wild type control (Figure 4.4A, C). In one case, severely dilated ER membranes was observed in a hepatocellular carcinoma found in one *Tmed2*$^{99J/+}$ mouse (data not shown).

Dilated ER membranes are an indication of ER-stress and are associated with activation of the UPR. Therefore, we examined expression of genes and proteins associated with the UPR (Malhi and Kaufman, 2011). During UPR, expression of chaperone proteins such as GRP78 and GRP94 are increased to reduce the load of unfolded proteins in the ER. In addition, activation of three canonical pathways: eukaryotic translation initiation factor (eIF)-2α Kinase 3 (PERK), endoplasmic reticulum to nucleus signaling/inositol-requiring enzyme (IRE)-1, and activating transcription (ATF)-6, result in transcriptional regulation of genes which will help to maintain ER homeostasis or to initiate cell death (Henkel and Green, 2013; Malhi and Kaufman, 2011). ER-stress was examined in juvenile and/or adult wild type and *Tmed2*$^{99J/+}$ mice. No significant differences were found in levels of the chaperone proteins GRP78 and

GRP94 (Figure 4.5 A, B) in juvenile and adult animals. In addition, splicing of the transcription factor *Xbp1* (Figure 4.5 E) - a surrogate for activation of the IRE-1, and accumulation of cleaved ATF 6 were comparable in livers of adult wildtype and *Tmed2*$^{99J/+}$ mice (Figure 4.5C, D). However, phosphorylated eIF2α (peIF2α) was significantly increased in livers of adult *Tmed2*$^{99J/+}$ mice, when compared to age-matched wild type mice (two-tailed, unpaired t-test, $p = 0.032$; Figure 4.4E-G), indicating that the PERK arm of the UPR was activated. Nonetheless, expression of *Atf4* and *Chop*, downstream targets of eIF2α were comparable between adult *Tmed2*$^{99J/+}$ and wild type mice (Figure 4.4H). Overall, our data indicate that dilation of ER membranes in *Tmed2*$^{99J/+}$ mice was associated with activation of the PERK arm of the UPR.

4.4.5 Heterozygous Tmed2 mice develops NAFLD.

During our studies, we noted that livers of *Tmed2*$^{99J/+}$ mice appeared abnormal and that a subset of mice developed hepatocellular carcinoma, in addition lung and stomach tumors were found in two different *Tmed2*$^{99J/+}$mice (manuscript in preparation). To systematically analyze livers of *Tmed2*$^{99J/+}$ mice and compare them to their wild type littermates we utilized a modified version of the Non-alcoholic Activity Score (NAS) described by the Non-alcoholic Steatohepatitis Clinical Research Network (Kleiner et al., 2005). Livers from wild type and heterozygous mice between 1 month – 17 months were scored for ballooning, macrosteaosis, and lobular inflammation after Haematoxylin and Eosin (H&E) staining (Table 4.3). In the course of our analysis, it became apparent that two additional phenotypes, microvesicular steatosis and portal inflammation (Figure 4.6)-associated with NAFLD (Tandra and Chalasani, 2011) and not included in the NAS scoring system, -were also present in wild type and *Tmed2*$^{99J/+}$ mice. Hence, these two

additional phenotypes were also incorporated into our scoring system (Table 4.3 and Figure 4.6). The average age of mice analyzed was not significantly different, 8.6 months and 8.4 months for *Tmed2*$^{99J/+}$ and wild type mice, respectively. However, significantly more *Tmed2*$^{99J/+}$ mice exhibited NAS activity scores of 4 or higher (n=21/55) when compared to wild type (n=4/40) mice (two-tailed, fisher's exact test, p=0.0021; Figure 4.6G). Accumulation of neutral lipids in animals with macrosteatosis score of ≥2 was confirmed after staining with Oil Red O and Sudan Black B (Figure 4.7). Although, 72 – 91% of male C3H/HeJ mice were reported to develop hepatomas at the age of 14 months (The Jackson Laboratory), increased susceptibility to liver cancer was not associated with liver disease (Gariboldi et al., 1993). Nonetheless, our data indicates that reduction of TMED2 resulted in a 28% increase (from 10% to 38%) in the number of mice with clinical features associated with NAFLD by the age of 6 months.

NAFLD is often associated with a metabolic syndrome (Williams, 2015). Therefore, features associated with a metabolic syndrome such as increased weight, increased plasma cholesterol and triglycerides were measured in post-weaning juvenile and adult wild type and *Tmed2*$^{99J/+}$ mice. No significant difference was found in any of these metabolic indicators when *Tmed2*$^{99J/+}$ mice were compared to their wild type littermates (Figure 4.8 and 4.9), although NAFLD was only scored in a subset of mice used for cholesterol and triglyceride studies (n=5/10 wild type and 3/10 *Tmed2*$^{99J/+}$ mice) none of the animals showed any overt liver diseases. However, we noted that plasma triglyceride level was higher and that plasma cholesterol level was lower in adult *Tmed2*$^{99J/+}$ mice when compared to age-matched wild type litter mates (Figure 4.9). Thus, our data indicates that *Tmed2*$^{99J/+}$ mice do not exhibit signs of a metabolic syndrome.

4.4.6 Levels of Srebp1a and Srebp2 are increased in Tmed2$^{99J/+}$ mice.

Srebp1f and *Srebp2* belong to a family of transcription factors that regulates fatty acid and cholesterol synthesis, respectively (Eberlé et al., 2004; Ferré and Foufelle, 2010; Shimano et al., 1997). The *Srebp1f* gene encodes for two alternative transcripts: *Srebp1c,* which primarily regulates expression of genes involved in fatty acid biosynthesis, and *Srebp1a* that regulates expression of genes implicated in both fatty acid and cholesterol biogenesis (JD Horton, 2002). No significant difference was found in *Srebp1c* expression or in generation of cleaved SREBP1C, when juvenile and adult *Tmed2*$^{99J/+}$ mice were compared to wild type age-matched controls (Figure 4.10B, D). Similarly, SREBP2 was comparable between juvenile and adult wild type and *Tmed2*$^{99J/+}$ mice (Figure 4.10E). However, levels of *Srebp1a* and *Srebp2* were significantly higher in livers of newborn *Tmed2*$^{99J/+}$ mice when compared to age-matched wild type littermates (two-tailed, unpaired t-test, p=0.017 for *Srebp1a*, and 0.016 for *Srebp2*; Figure 4.10A, C). Thus, expression of transcription factors associated with steatosis and NAFLD is increased in newborn *Tmed2*$^{99J/+}$ mice.

4.5 Discussion

4.5.1 A novel model of NAFLD.

Herein, we describe a novel model of NAFLD associated with haploinsufficiency for the cargo receptor TMED2. We showed that newborn mice carrying the 99J point mutation in *Tmed2* have a significant decrease in TMED2 and TMED10 with no associated change in the mRNAs. In addition, TMED2 was not regulated by the UPR and normal levels of TMED2 was not required for tunicamycin-associated UPR. However, livers from *Tmed2*$^{99/+}$ mice had dilated ER membranes and activation of the PERK arm of the UPR

pathway, as indicated by increased phosphorylation of eIF2α (Puri et al., 2008). Consistent with the established association of the UPR in liver disease, *Tmed2*$^{99/+}$ mice develop NAFLD with no associated metabolic disease (Malhi and Kaufman, 2011). Increased expression of *Srebp2* and *Srebp1a* in livers of newborn heterozygous mice is postulated also to contribute to the development of NAFLD in adult *Tmed2*$^{99J/+}$ mice.

4.5.2 TMED2 regulates stability of TMED10.

Expression levels of TMED proteins are interdependent (Denzel et al., 2000; Jenne et al., 2002; Jerome-Majewska et al., 2010; Pastor-Cantizano et al., 2015), and reduction of TMED2 was associated with a reduction of TMED10 in *Tmed2*$^{99J/+}$ mice. TMED2 and TMED10 form hetero-oligomeric complexes in the early secretory pathway (Jenne et al., 2002) and where TMED10 is predicted to aid in retrieval of TMED2 and other ER-resident proteins from the Golgi in TMED10-associated COPI-coated vesicles (Jenne et al., 2002; Lavoie et al., 1999; Pastor-Cantizano et al., 2015). In addition, although interactions between TMED proteins are essential for individual TMED protein stability, interacting-TMED proteins are not always expressed or required in the same cells and organelles (Au et al., 2015; Jerome-Majewska et al., 2010; Strating et al., 2009a; Zakariyah et al., 2011). In fact, Jenne et al. showed that TMED protein oligomeric complexes are organelle specific (Jenne et al., 2002), and Strating et al. proposed that through an unknown mechanism individual TMED proteins provide proper ER/Golgi sub-compartmental environment during transport (Strating et al., 2009a). Our studies and those of Denzel et al. showing that TMED2 and TMED10 are required for normal ER and Golgi morphology, respectively (Denzel et al., 2000; Strating et al., 2009a) are consistent with the hypothesis proposed by Strating et al. (Strating et al., 2009a). Current studies in

our laboratory aim to identify the TMED2 specific partners important for its dependent and independent functions in the liver.

4.5.3 Normal levels of TMED2 is required for normal ER-homeostasis but not for UPR.

In the presence of ER-stress, GRP78 dissociates from three ER-transmembrane resident proteins - PERK, IRE1α, and ATF6 - to initiate a cascade of activity that either resolves the stress or promotes cell death (Malhi and Kaufman, 2011). PERK phosphorylates eIF2α, which attenuates general protein translation to reduce the influx of nascent and unfolded polypeptide chains into the ER (Harding et al., 1999). In parallel, eIF2α phosphorylation increases the translation of a subset of mRNAs, for example, *Atf4* to activate expression of pro-apoptotic genes such as C/EBP homologous protein (*Chop*) and growth arrest and DNA damage-inducible protein (*Gadd34*) (Ma et al., 2002). Activation of IRE1α results in alternative splicing of the mRNA encoding for X-box binding protein 1 (*Xbp1*) that is involved in regulation of molecular chaperones such as *Grp78* and *Grp94* (Calfon et al., 2002). On the other hand, ATF6 translocates to the Golgi where it is proteolytically cleaved and released to the nucleus to activate transcription of target genes including ER chaperones and ER-associated protein degradation (ERAD) components (Yamamoto et al., 2007).

As cargo receptors are important for transport of proteins from the ER, it was expected that reduction or mutations in TMED proteins would lead to UPR, or be required to mount an effective UPR. In fact, deletion of emp24, the yeast ortholog of *Tmed2*, results in splicing of *Xbp1* and secretion of bip/Grp78, two markers of UPR (Belden and Barlowe, 2001). However, in drosophila, mutations in Tmed genes result in activation of the NF-κB pathway and expression of genes consistent with activation of the PERK arm

of the UPR. Intriguingly, no evidence of *Xbp1* alternative splicing was found suggesting that a specific arm of the UPR is activated in Tmed mutants (Boltz et al., 2007). Our group previously reported that homozygous loss of function mutations in *Tmed2* did not result in *Xbp1* alternative splicing, indicating that the IRE-1α arm of the UPR was not activated (Jerome-Majewska et al., 2010). In the current study, we confirmed that the IRE-1α and the ATF 6 arms of the UPR were not activated. However, we found that TMED2 was required for normal ER-morphology and that reduced levels of TMED2 was associated with activation of the PERK arm of the UPR. Considering the observations of Bolz and Carney (Boltz et al., 2007) and our findings, we propose that the activation of the PERK arm of the UPR is a conserved mechanism through which animal cells responds to perturbation of TMED protein levels. In addition, we found that expression of genes associated with activation of the PERK arm of the UPR, such as *Atf4, Chop*, and *GADD34* was not increased in these mice, as was reported in a subset of patients with NAFLD (Puri et al., 2008). Future work in our model will focus on determining if the NF-κB pathway is also activated and potentially contributing to development of NAFLD in $Tmed2^{99/+}$ mice. We will also investigate if failure to activate expression of genes downstream of the PERK arm of the UPR contributes to NAFLD in $Tmed2^{99/+}$ mice. Satpute-Krishan et al., showed a requirement for TMED10 in export of misfolded GPI-anchored proteins downstream of thapsigargin or Dithiothreitol (DTT)-mediated ER-stress, prior to UPR (Satpute-Krishnan et al., 2014). Since TMED2 and TMED10 interact, and levels of TMED10 were decreased in $Tmed2^{99/+}$ mice, we reasoned that TMED2 may be regulated by the UPR or like TMED10 be required for UPR. However, we found no evidence to support a similar requirement for TMED2 in UPR. Though

unlikely, it is possible that the type of ER-stress may dictate if TMED proteins are required. Thus, thapsigargin induced ER-stress - which disrupts calcium flux, and DTT induced ER-stress - which blocks disulfide bond formation in polypeptides, may be more dependent on the amount of TMED cargo receptors than tunicamycin induced ER stress, which blocks N-glycosylation and glycoprotein biosynthesis at the first step. Alternatively, RESET could be specifically dependent on TMED10 and not TMED2. Treating TMED10 heterozygous mice with ER-stress inducing reagents will help to resolve this discrepancy.

4.5.4 PERK activation and increased expression of Srebp2 and Srebp1a in Tmed2$^{99/+}$ mice.

Increased levels of *Srebp2* and *Srebp1a* in newborn *Tmed2*$^{99J/+}$ mice suggest that signals downstream of TMED2 regulate cholesterol and triglyceride metabolism in newborn mice. However, although we were unable to determine if increased *Srebp2* and *Srebp1a* was associated with an increase in active protein; levels of *Srebp1a* and *Srebp2* mRNA and proteins were comparable in juvenile and adult *Tmed2*$^{99J/+}$ mice, when compared to age-matched wild type mice, and hypercholestoremia and hypetriglyceridemia were not observed in *Tmed2*$^{99J/+}$ mice. These findings indicate that continued dysregulation of SREBP1 and SREBP2 was not responsible for NAFLD in this mutant mouse line. In contrast, a direct role for the PERK-peIf2α -ATF4 pathway has been established in steatosis in mouse models and corroborated in human. Thus, we propose that phosphorylated eIF2α partly contributes to NAFLD in *Tmed2*$^{99J/+}$ mice. We hypothesize that reduced TMED2 leads to abnormal ER homeostasis and UPR. Constitutive activation of UPR or an inability to trigger downstream events in the UPR in

Tmed2$^{99J/+}$ mice in turn increase susceptibility of these mice to unknown factors that promote NAFLD in a subset of *Tmed2*$^{99J/+}$ mice. Patients with NAFLD can be grouped base on four different phenotypes: obese, type 2 diabetes, metabolic syndrome, and lean patients (Romero-Gómez et al., 2017).We expect that this mouse model will be instrumental in future studies aimed to identify the genetic and cellular factors involved in non-obese or lean NAFLD patients (Kim and Kim, 2017).

4.5.5 TMED proteins in diseases.

Though discovered over twenty years ago, the requirement and function of the TMED family has long remained an enigma. However, recently, the contribution of TMED family members in diseases has begun to emerge. Disrupted expression of TMED proteins is associated with a diverse group of diseases ranging from cancer to Alzheimer's. TMED3 is an emerging tumor suppressor gene implicated in prostate cancer (Vainio et al., 2012), colon cancer (Duquet et al., 2014b) and hepatocellular carcinoma progression (Zheng et al., 2016). Intriguingly, in The Exome Aggregation Consortium no loss of function mutations has been reported in TMED2 and half the expected number of missense mutations have been found, suggesting that this gene is essential in human. Our work presented here indicates that TMED2 is a candidate gene in a human disease, specifically NAFLD.

4.6 Acknowledgments

We would like to thank MUHC laboratories for plasma analysis. We would also like to thank Jacek Majewski and Wesley Chan for helpful feedback on the manuscript. L.J.M. and M.C.B. are members of the Research Institute of the McGill University Health Centre, W.H. and S.G. are students of Human Genetics Department of McGill

University. L.J.M. is a member of the Research Institute of the McGill University Health Centre.

4.7 Figures

Figure 4.1 TMED2 level in livers of wildtype and *Tmed2*$^{99J/+}$ mice at P5, 1-2 months and 3-6 months.

A. RT-qPCR shows no difference in *Tmed2* in livers. B. Western blot analysis showed significantly reduced TMED2 in livers of P5 *Tmed2*$^{99J/+}$mice compared to wildtype littermates C. Representative images of Western blot showing expression of TMED2 and β-ACTIN, used as a loading control. D. Reduced TMED2 in livers of 1-2 months and 3-6 months *Tmed2*$^{99J/+}$mice compared to age-matched wildtype. E. Representative images of Western blot showing expression of TMED2 and total protein used as loading control. 3 animals of each genotype were analyzed per age group. **P<0.01 by t-test. WT=wildtype.

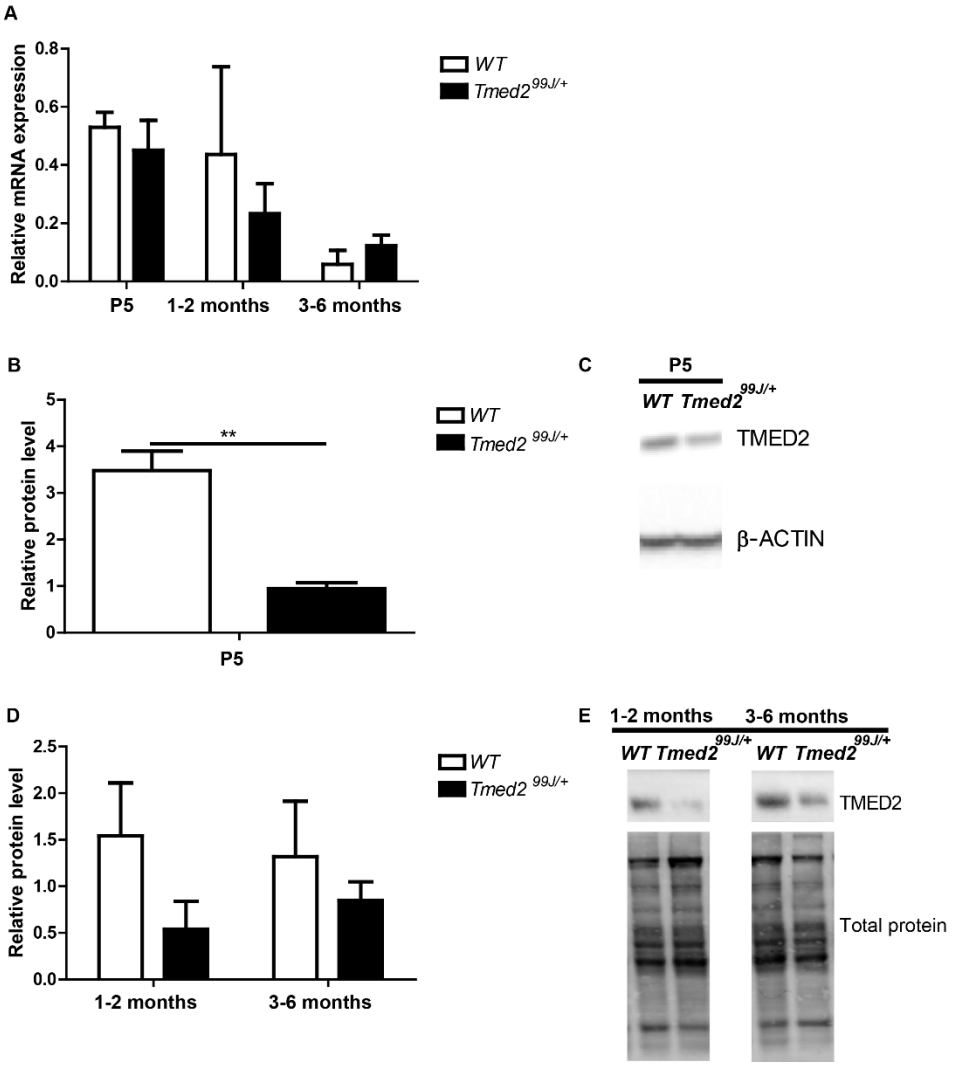
A
Relative mRNA expression
0.8
0.6
0.4
0.2
0.0
P5
1-2 months
3-6 months
WT
Tmed2 99J/+
B
Relative protein level
5
4
3
2
1
0
**
P5
WT
Tmed2 99J/+
C
P5
WT Tmed2 99J/+
TMED2
β-ACTIN
D
Relative protein level
2.5
2.0
1.5
1.0
0.5
0.0
1-2 months
3-6 months
WT
Tmed2 99J/+
E
1-2 months
3-6 months
WT Tmed2 99J/+
WT Tmed2 99J/+
TMED2
Total protein

Figure 4.2 TMED10 level in livers of wildtype and *Tmed2*$^{99J/+}$ mice at P5, 1-2 months and 3-6 months.

A. RT-qPCR shows no difference in *Tmed2* in livers. B. Western blot analysis revealed significantly decreased TMED10 in livers of *Tmed2*$^{99J/+}$mice compared to wildtype littermates at P5 and 3-6months. C. Representative images of Western blot gel showing expression of TMED10 and β-ACTIN, used as a loading control. *P<0.05 by t-test. WT=wildtype.

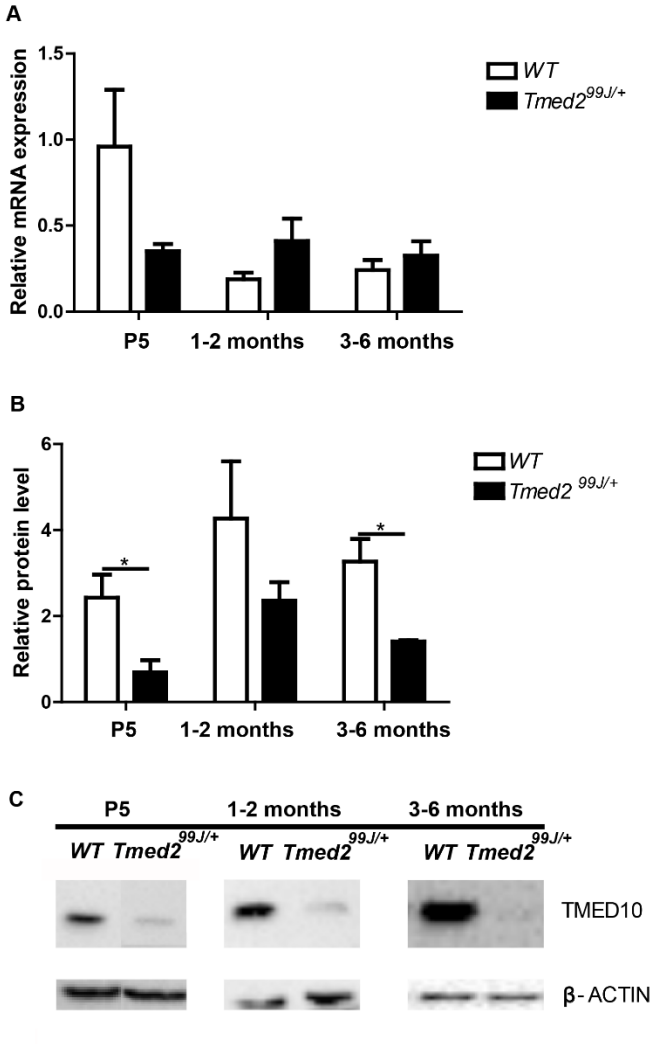

Figure 4.3 TMED2 expression is not regulated by Tunicamycin or required for Tunicamycin-induced stress.

A). Tunicamycin induces increased level of the unfolded protein response marker, GRP78 in HepG2 cells when compared to vehicle-treated controls. The same treatment did not affect TMED2. B). Representative images of Western blot gel showing expression of TMED2, GRP78 and β-actin loading control. C). Tunicamycin induces increased level of the unfolded protein response marker, GRP78 in tunicamycin treated SKHep1 cells when compared to vehicle-treated controls. The same treatment did not affect TMED2. D). Representative images of Western blot gel showing expression of TMED2, GRP78 and β-actin loading control. E). Percent weight loss in wildtype and *Tmed2*$^{99J/+}$ mice after tunicamycin injection at age of 10 weeks. n=4 for wildtype and n=6 for *Tmed2*$^{99J/+}$ mice. WT = wildtype, Veh = vehicle, Tuni = tunicamycin.

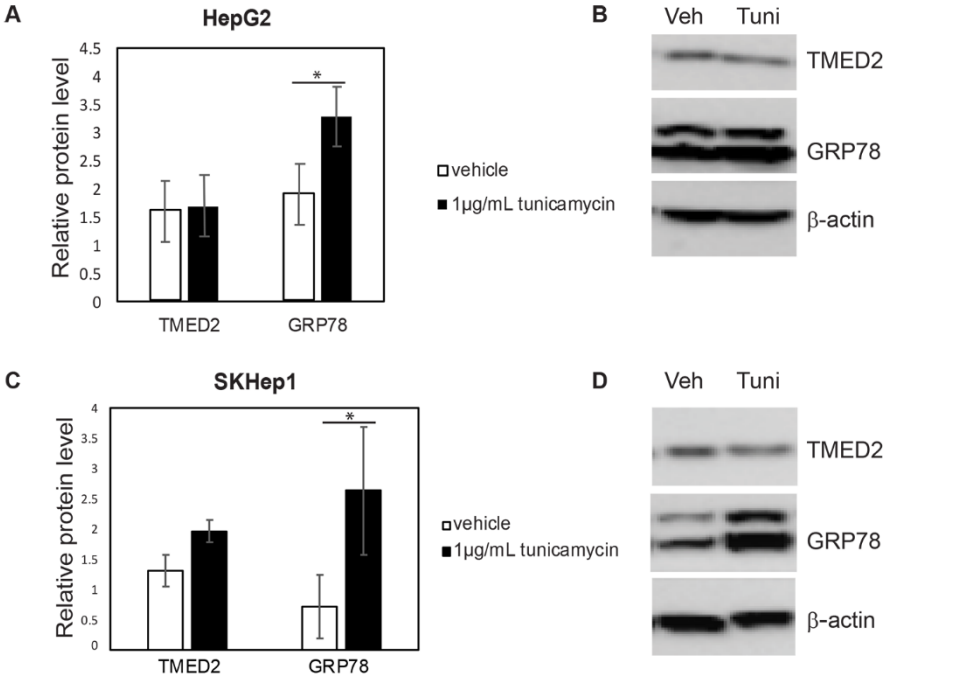
A
HepG2
Relative protein level
4.5
4
3.5
3
2.5
2
1.5
1
0.5
0
*
TMED2
GRP78
vehicle
1μg/mL tunicamycin
B
Veh
Tuni
TMED2
GRP78
β-actin
C
SKHep1
Relative protein level
4
3.5
3
2.5
2
1.5
1
0.5
0
*
TMED2
GRP78
vehicle
1μg/mL tunicamycin
D
Veh
Tuni
TMED2
GRP78
β-actin

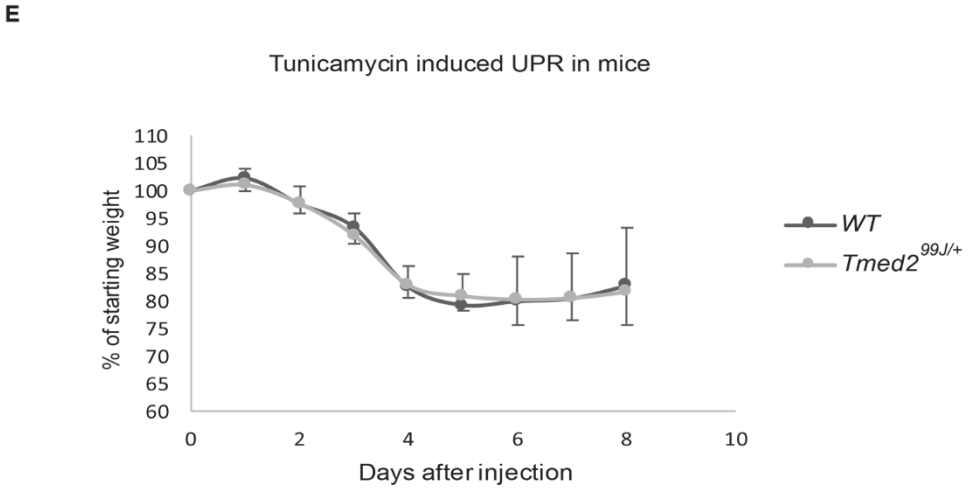
E
Tunicamycin induced UPR in mice
% of starting weight
110
105
100
95
90
85
80
75
70
65
60
0
2
4
6
8
10
Days after injection
WT
Tmed2 99J/+

Figure 4.4 *Tmed2*$^{99J/+}$ livers exhibit dilated ER and increased level of the UPR marker phosphorylated-eIF2α.

A-D. Transmission electron microscopy (TEM) pictures showing dilated ER (arrows) in hepatocytes of *Tmed2*$^{99J/+}$ mice (B, D) when compared to wildtype littermates (A, C; scale bar=500nm). E. Phosphorylated eIF2α (p-eIF2α) was significantly increased in livers of 3-6 months *Tmed2*$^{99J/+}$ mice when compared to age-matched wildtype controls. F. No significant difference was found in levels of total eIF2α when *Tmed2*$^{99J/+}$ mice were compared to age-matched wildtype controls. G. Representative images of Western blot gel showing expression of p-eIF2α, total eIF2α, and total protein loading control. H. RT-qPCR indicate no significant difference in levels of *Gadd34*, *Chop*, and *Atf4* in livers of 3-6 months *Tmed2*$^{99J/+}$ mice when compared to age-matched wildtype controls. 3 animals of each genotype were analyzed per age group, *P<0.05 by t-test. N= nucleus, ER= Endoplasmic Reticulum, WT=Wildtype. Arrows indicate dilated ER.

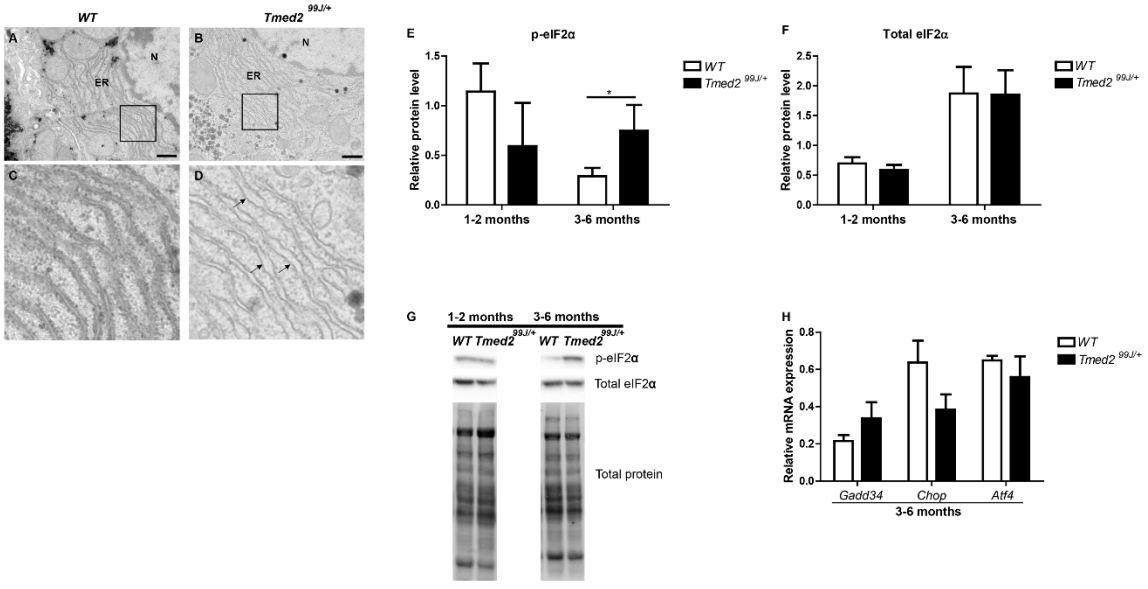

Figure 4.5 Expression of genes associated with the unfolded protein response (UPR) are not disrupted in *Tmed2*$^{99J/+}$ mice.

A). GRP78 level was comparable in livers of *Tmed2*$^{99J/+}$ and stage-matched wildtype controls. B). level of GRP94 was comparable in livers of *Tmed2*$^{99J/+}$ and stage-matched wildtype controls. C). Level of activated ATF6α was comparable in livers of 3 – 6 months *Tmed2*$^{99J/+}$ and stage-matched wildtype controls. D. Representative images of Western blot gel showing expression of GRP78, GRP94, cleaved ATF6α, total ATF6α and total protein internal controls. E.) Levels of spliced *Xbp1* and unspliced *Xbp1* were comparable in livers of 3- 6 months wildtype and *Tmed2*$^{99J/+}$ mice. n=3 for each genotype. WT = wildtype.

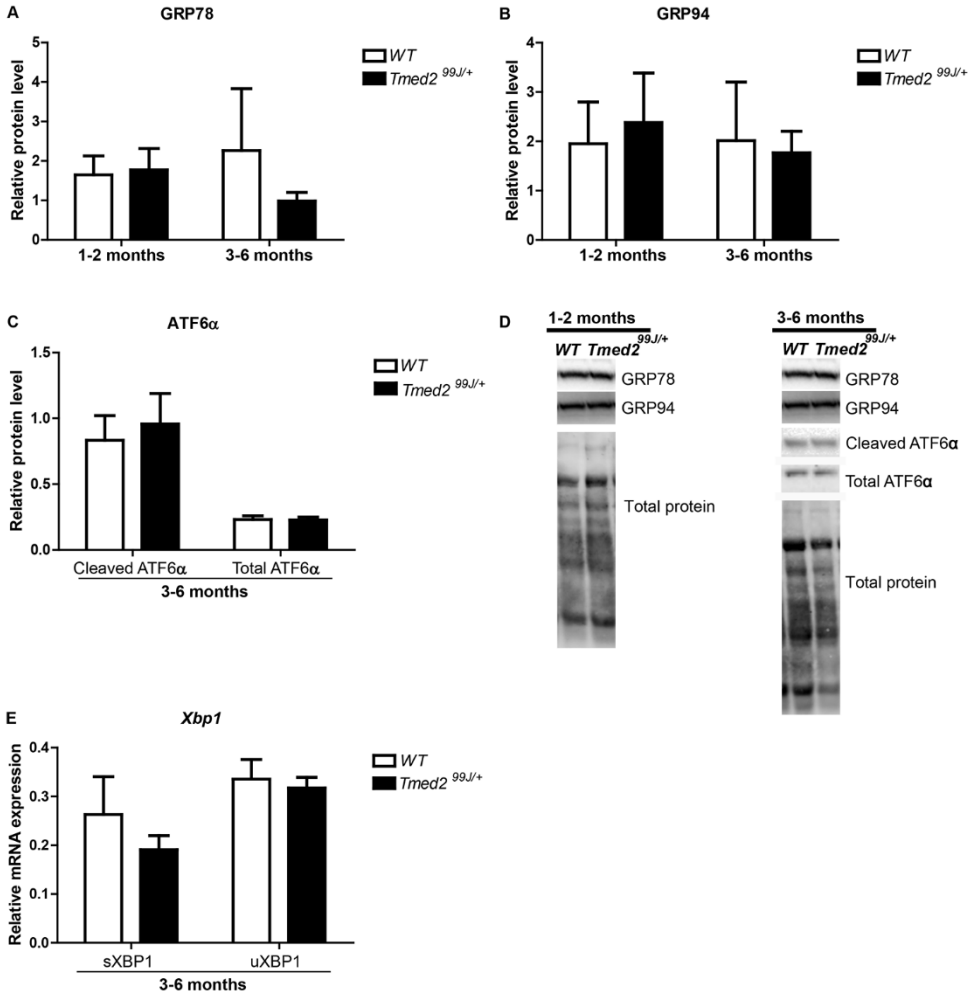
A
GRP78
Relative protein level
WT
Tmed2 99J/+
1-2 months
3-6 months
B
GRP94
C
ATF6α
Cleaved ATF6α
Total ATF6α
D
1-2 months
3-6 months
WT Tmed2 99J/+
GRP78
GRP94
Cleaved ATF6α
Total ATF6α
Total protein
E
Xbp1
Relative mRNA expression
sXBP1
uXBP1

Figure 4.6 Increased NAFLD in *Tmed2*$^{99J/+}$ mice.

Representative images of Hematoxylin & Eosin stained liver sections showing A). a healthy liver section; and phenotypes scored for on Table 1; B). macrosteatosis; C). microsteatosis D). lobular inflammation; E). portal inflammation; and F). ballooning. G. Significantly more *Tmed2*$^{99J/+}$ mice had NAFLD scores of ≥ 4 when compared to age-matched wildtype controls. **P<0.01 using Fisher exact t-test. Arrows indicate inflammatory cells. Scale bar =50um. WT=Wildtype.

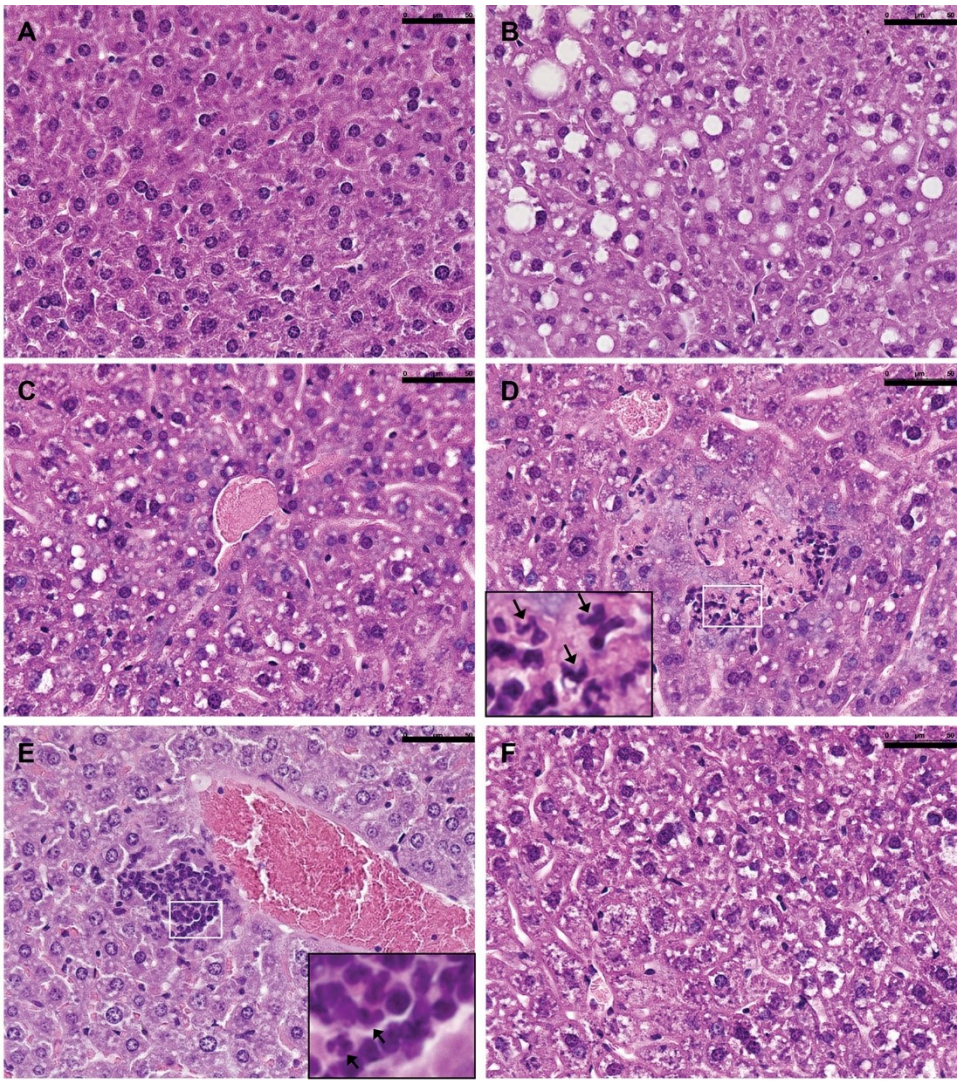
A
B
C
D
E
F

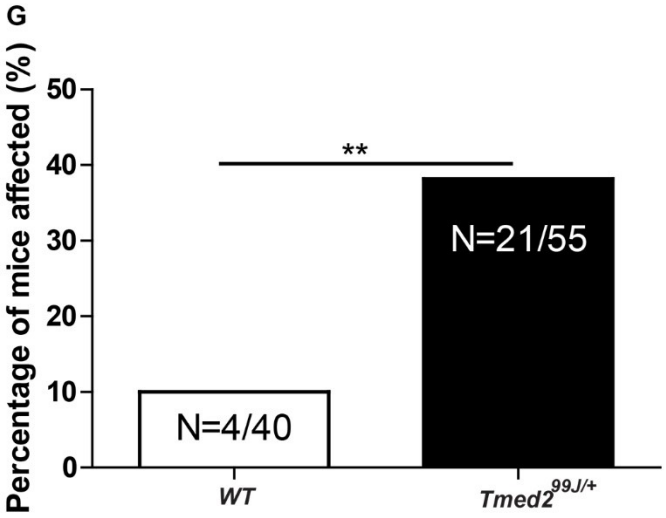
G
Percentage of mice affected (%)
50
40
30
20
10
0
**
N=21/55
N=4/40
WT
Tmed2 99J/+

Figure 4.7 Representative images of liver samples stained with Oil Red O and Sudan Black B.

A). wildtype liver with score of 1 had no Oil Red O staining. B). *Tmed2*$^{99J/+}$ liver with score of 5 had intense Oil Red O staining. C). Same wildtype sample as in A had no Sudan Black B staining. D). Same *Tmed2*$^{99J/+}$ sample as in B had intense Sudan Black B staining. Scale bar =50um. WT = wildtype, n = 4 for each genotype.

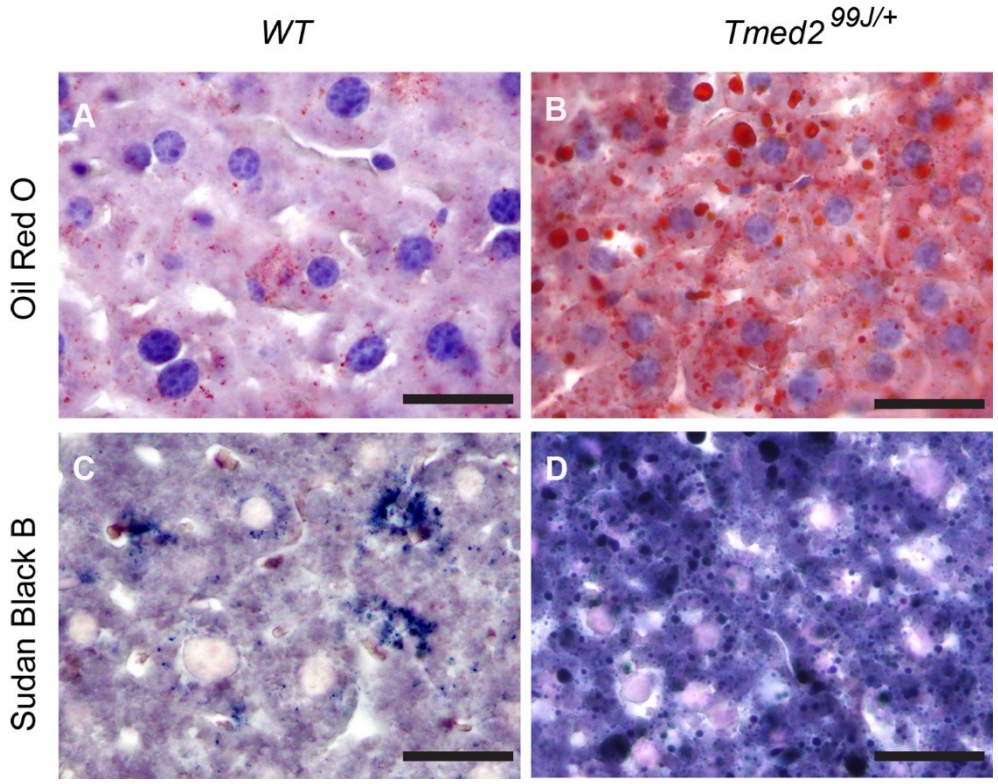

Figure 4.8 No significant differences in body and liver weight of *Tmed2*$^{99J/+}$ mice when compared to age-matched controls.

A). Bar graph showing body weight of *Tmed2*$^{99J/+}$ and age-matched wildtype controls. B). Bar graph showing liver weight of *Tmed2*$^{99J/+}$ and age-matched wildtype controls. C). Bar graph showing percentage of liver to body weight ratio in both wildtype and *Tmed2*$^{99J/+}$ mice. n=3 for wildtype and n=4 for *Tmed2*$^{99J/+}$ mice for 1-2 months age group; n=11 for wildtype and n=10 for *Tmed2*$^{99J/+}$ mice for 3-6 months age group. WT = wildtype.

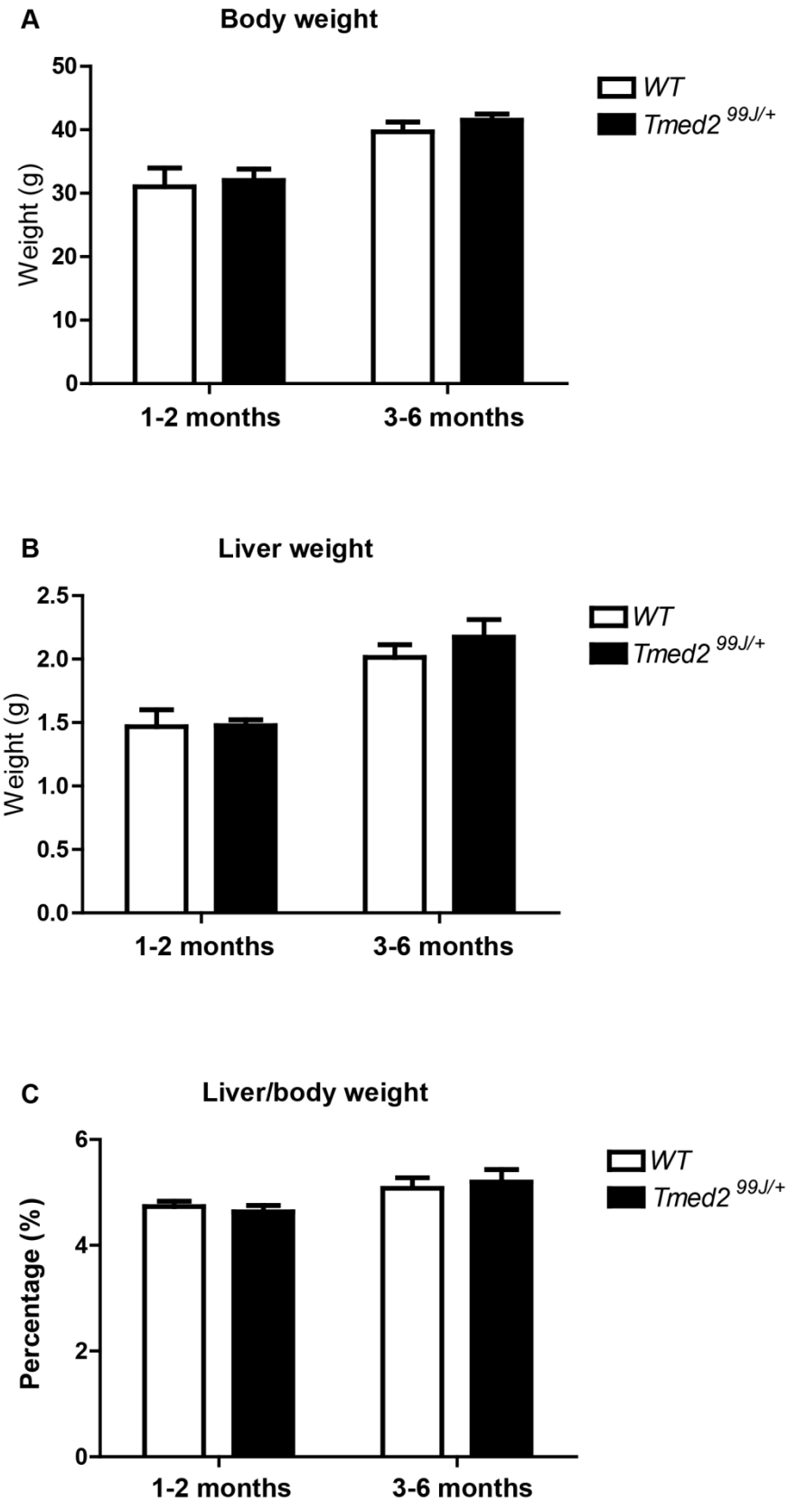
A
Body weight
Weight (g)
50
40
30
20
10
0
1-2 months
3-6 months
WT
Tmed2 99J/+
B
Liver weight
Weight (g)
2.5
2.0
1.5
1.0
0.5
0.0
1-2 months
3-6 months
WT
Tmed2 99J/+
C
Liver/body weight
Percentage (%)
6
4
2
0
1-2 months
3-6 months
WT
Tmed2 99J/+

Figure 4.9 No significant difference in circulating cholesterol and triglycerides levels in wildtype and *Tmed2*$^{99J/+}$ mice.

A). Plasma cholesterol levels were comparable between wildtype and *Tmed2*$^{99J/+}$ at 1 – 2 months, but B). decreased in *Tmed2*$^{99J/+}$ mice at 3 – 6 months age-matched wildtype controls (P=0.07, t-test). Plasma triglycerides levels were comparable between wildtype and *Tmed2*$^{99J/+}$ at 1 -2 months but D). increased in *Tmed2*$^{99J/+}$ mice at 3 – 6 months when compared to age-matched wildtype controls (P=0.06, t-test). n=5 for wildtype and n=4 for *Tmed2*$^{99J/+}$ mice for 1-2 months age group; n=5 for wildtype and n=6 for *Tmed2*$^{99J/+}$ mice for 3-6 months age group. WT = wildtype.

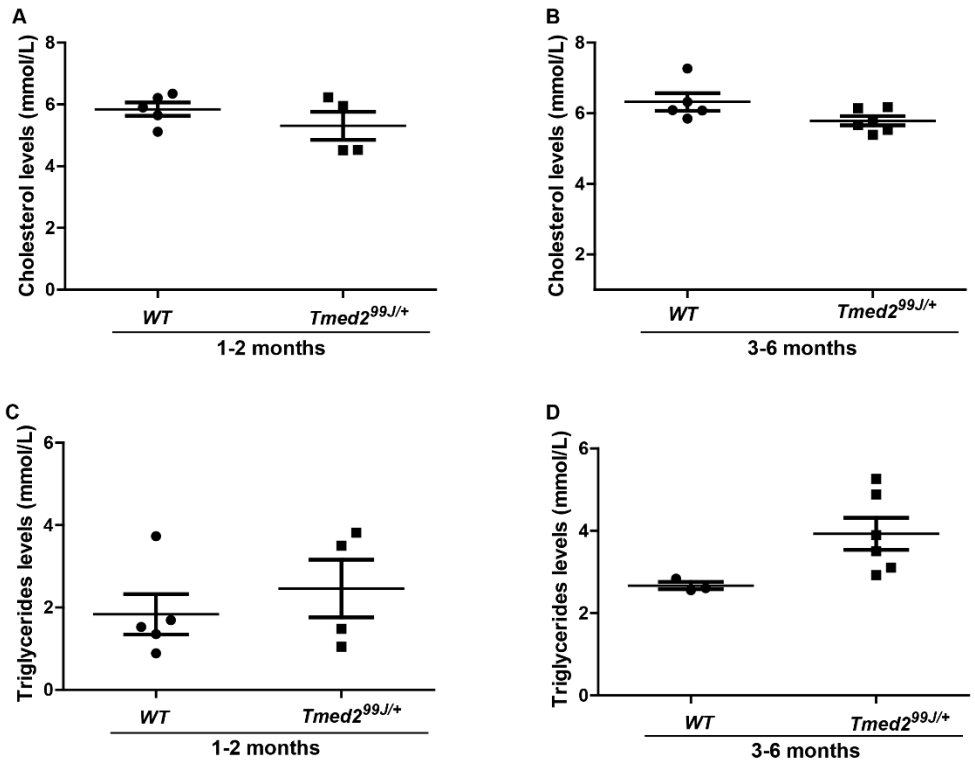

Figure 4.10 Expression of lipid biosynthesis regulators-SREBPs in wildtype and *Tmed2*$^{99J/+}$ livers.

A). *Srebp1α* level was increased in *Tmed2*$^{99J/+}$ increased in P5 *Tmed2*$^{99J/+}$ mice compared to age-matched wildtype controls. B). *Srebp1c* level was comparable in *Tmed2*$^{99J/+}$ and age-matched wildtype control mice at all stages. C). *Srebp2* level was increased in P5 *Tmed2*$^{99J/+}$ mice compared to age-matched wildtype controls. D). Levels of activated SREBP1C was comparable in *Tmed2*$^{99J/+}$ and age-matched wildtype control at 1 – 2 and 3 – 6 months. E). Levels of activated SREBP2 was comparable in *Tmed2*$^{99J/+}$ and age-matched wildtype control at 1 – 2 and 3 – 6 months. F). Representative images of Western blot showing expression of full SREBP1C, cleaved SREBP1C (active form), SREBP2, and total protein loading control. 3 animals of each genotype were analyzed per age group. WT = wildtype. *P<0.05 by t-test.

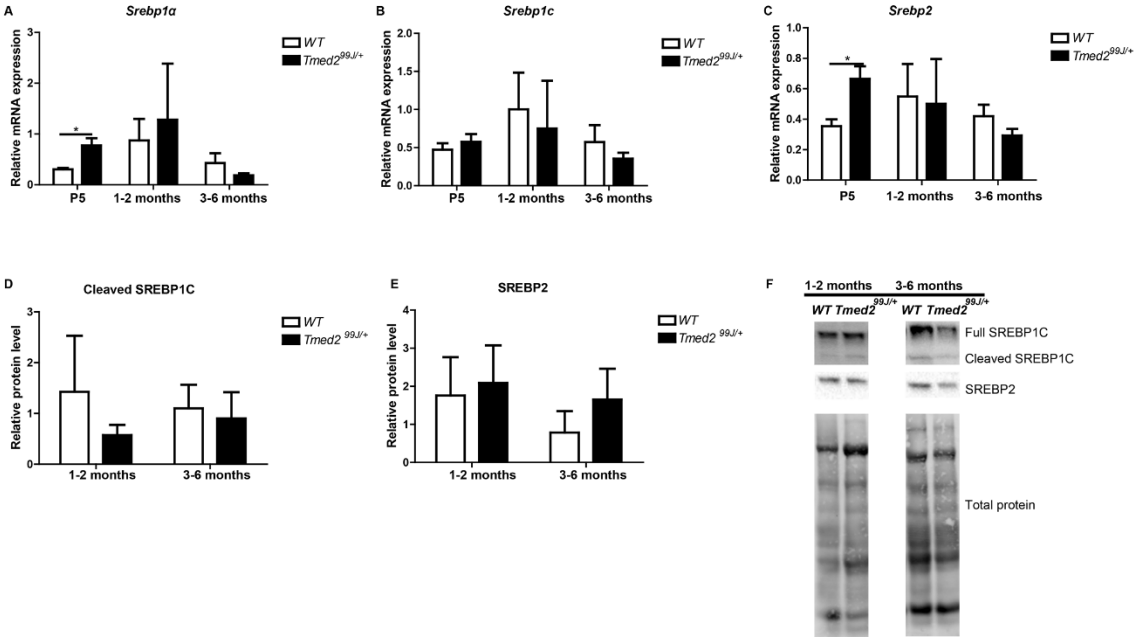
A
Srebp1α
Relative mRNA expression
WT
Tmed2 99J/+
P5
1-2 months
3-6 months
B
Srebp1c
C
Srebp2
D
Cleaved SREBP1C
Relative protein level
E
SREBP2
F
1-2 months
3-6 months
WT Tmed2 99J/+
Full SREBP1C
Cleaved SREBP1C
SREBP2
Total protein

Table 4.1 List of primers used in RT-qPCR analysis.

Gene	GenBank Accession Number[1]	Forward Primer	Reverse Primer
Gapdh	NM_001001303.1	ATGACATCAAGAAGGTCCTG	CATACCAGGAAATGAGCTTG
Sdha	NM_023281.1	GCTGTGGCCCTGAGAAAGATC	ATCATGGCCGTCTCTGAAATTC
B2m	NM_009735.3	ATGCTATCCAGAAAACCCCTCAA	GCGGGTGGAACTGTGTTACG
Tmed2	NM_019770.2	CGGACAACAGGAGTACATGGAAGTCCG	GACCAAAGGACCACTCTGCTGT
Tmed10	NM_026775.4	GGAGGTGGAGTTACGACGG	TGGACTCATTAGTGTCCCTCATC
Srebp1c	NM_001313979.1	GGAGCCATGGATTGCACATT	GGCCCGGGAAGTCACTGT
Srebp1a	NM_011480.4	TAGTCCGAAGCCGGGTGGGCGCCGGCG CCAT	GATGTCGTTCAAAACCGCTGTGTGTC CAGTTC
Srebp2	NM_033218.1	GATGAGCTGACTCTCGGGGACATC	GTGGGGTAGGAGAGACTTTGACCT

1National Center for Biotechnology Information (NCBI)

Table 4.2 List of antibodies used in Western blot analysis.

Antibody	Type	Host	Concentration or dilution	Supplier
TMED2	Polyclonal	Rabbit	1:4000	Majewska *et al.*
TMED10 (TMP21)	Polyclonal	Rabbit	1:1000	Cell Signaling
GRP78	Polyclonal	Rabbit	1:4000	Abcam
GRP94	Polyclonal	Rabbit	1:4000	Abcam
eIF-2α	Polyclonal	Rabbit	1:2000	Cell Signaling
eIF-2α P	Monoclonal	Rabbit	1:2000	Epitomics
ATF6α	Monoclonal	Mouse	1:1000	Novus Biolabs
SREBP2 (SREBF2)	Polyclonal	Rabbit	1:1000	Protein Tech
SREBP1c	Monoclonal	Mouse	1:1000	Abcam

Table 4.3 Scoring system used for phenotypic analysis of *Tmed2*$^{99J/+}$ and wildtype livers.

Histological Features		**Score**	
Steatosis	Macrovesicular	<5% of cells	0
		5%-33% of cells	1
		33%-66% of cells	2
		>66% of cells	3
	Microvesicular	<5% of cells	0
		5%-33% of cells	1
		33%-66% of cells	2
		>66% of cells	3
Inflammation	Lobular	No Foci	0
		<2 foci per 200X field	1
		2-4 foci per 200X field	2
		>4 foci per 200X field	3
	Portal	Absence	0
		Presence	1
Ballooning		<5% of cells	0
		5%-33% of cells	1
		>33% of cells	2

Chapter V: Discussion

5.1 General discussion

Transmembrane and secretory proteins are important molecules for intra and inter cellular communication and function. Proper secretion and concentration of those proteins to their destination sites are tightly and properly regulated by cellular machineries. The ER is the major site for proper protein synthesis, post-modification, and sorting. Many ER-resident enzymes, proteins, and molecules help various processes to maintain normal protein homeostasis. In this thesis, I am very interested in one such regulatory ER-resident proteins, TMED2. TMED2 is a transmembrane cargo receptor protein that help proper transport of luminal cargo proteins at the ER. Our previous laboratory work has demonstrated the requirement of TMED2 during early development of the embryo and the placenta. During the course of my PhD study, I aimed to understand the roles that TMED2 play in both embryonic and extraembryonic tissues. In chapter II and III, I investigated the tissue-specific requirement of TMED2 in the extraembryonic placenta using an *ex vivo* model of pre-placental tissues. In chapter IV, I investigated phenotypes associated with the liver in *Tmed2* heterozygous mice.

5.1.1 Developing ex vivo culture from explants of pre-placental tissues

In my first manuscript presented in chapter II, I described a novel *ex vivo* culturing system using pre-placental tissues of mesometrial halves of decidua containing pre-attachment chorions (chorions) and pre-attachment allantoides. Upon co-culturing chorions with allantoides, these explants underwent chorioallantoic attachment after 12 hours. I observed the event of cell mixing between chorionic and allantoic cells at the

chorionic plate via combining eGFP+ and GFP- tissues after culture. Significantly more mixing was observed in explants with longer period of culture (24 h).

After *ex vivo* culture of eGFP+ chorions and eGFP- allantoides for 12 hours, we observed that mesothelial cells on the surface of chorionic plate were usually associated with a brighter GFP intensity. During the course of culture, we observed gradual migration and dispersion of those mesothelial cells into the allantoic regions by tracking their brighter GFP signal. Previous studies have demonstrated that both the chorionic mesothelium and the allantois express the hematopoietic stem cell marker, Runx1, before chorioallantoic attachment at E7.5 (North et al., 2002; Zeigler et al., 2006). Runx1 expression in the chorionic mesothelium became more intense during chorioallantoic fusion, and was found at the chorion-allantois interface at E9.0 (Zeigler et al., 2006). Those results suggest that 1. Hematopoiesis from hematopoietic stem cells contribute to the development of the fetal vasculature system in the mature placenta, and 2. Runx1+ cell from the chorionic mesothelium may also participate in the formation of fetal vasculature. The dispersed pattern of the mesothelial cells found in the allantoic region of the explants also suggests that those cells may need to be positioned within the allantois before differentiation and branching of the allantoic vasculature.

The growth of allantois requires both cell proliferation and addition of cells from the primitive streak (Kimberly and Downs, 2007). We could not monitor the migratory state of cells from the primitive streak as the allantois was removed from the embryo. However, in immunofluorence experiments against an antibody to phosphohistone H3, a significant increase of cell proliferation was found in the allantoic region of cultured explants at 24 h, suggesting that the allantoic cell proliferation was maintained in our *ex*

vivo culture system. Furthermore, the endothelial cell marker, PECAM1, was also expressed in a subset of allantoic cells in the cultured explants. The expression pattern of PECAM1 in the allantois draws our attention: though majority of PECAM+ cells were found in the centre of the allantois, which is distal to the chorionic plate, a subset of PECAM1+ cells were found close to the chorionic plate. In fact, PECAM1 was expressed in allantoic cells prior to chorioallantoic attachment *in vivo*, thus, our experimental observation suggests: 1. The PECAM1+ cells in the allantoic centre of culture explants could be PECAM1+ allantoic cells prior to culture, and the culturing conditions were able to maintain or expand their expression; 2. PECAM1+ cells in the chorionic region could be results of either *De novo* or migration of endothelial cells from the central allantois to initiate fetal vasculatures in the chorionic plate.

Both *in situ* hybridization and RT-PCR experiments suggested the requirement of the allantois for maintaining transcripts of spongiotrophoblast marker, *Tpbpα*, as well as syncytiotrophoblast layer II marker, *Gcm1*. Furthermore, expression of *Gcm1* was significantly elevated after 24 h by RT-PCR, indicating that the physical attachment of the allantois to the chorion is crucial for subsequent chorionic cell differentiation. This observation could be due to the fact that chorioallantoic attachment brings the morphological folding to the chorionic plate. Since *Gcm1* is expressed at the branching points and its expression is crucial for Syn II cell differentiation and upregulation of Wint-Fzd5 to induce disassociation of tight junction markers, ZO-1, Claudin 4, and 7 (Lu et al., 2013). Furthermore, upregulated Frd5 can also enhance the *Gcm1* expression via nuclear β-catenin signaling (Lu et al., 2013). Taken together, the chorioallantoic attachment is crucial to set up the branching points during fetal vessel invagination, and

dissociation of the tight junctions in the chorionic trophoblast cells at those branching points on the apical surface of chorionic plate.

Prior to our *ex vivo* explant model, there are a couple of *ex vivo* models that exist to study the biology of chorioallantoic attachment. Downs et al. has demonstrated that via whole-embryo culturing technique, allantois can be transplanted into a mouse conceptus in which its allantois has been removed, and chorioallantoic attachment takes place when the allantois is stage-matched with the recipient chorion (Downs and Gardner, 1995). Further studies by Downs et al. have shown that engrafting a wildtype allantoic core domain into a *Brachyury* homozygous mutant embryo with shortened allantois can rescue the defect and restore allantoic elongation (Downs and Enders, 2009; Inman and Downs, 2006).

A different approach proposed by Stecca et al. has successfully demonstrated that explants of pre-chorioallantoic attachment chorion without ectoplacental cone nor decidual tissues with a stage-matched allantois underwent chorioallantoic attachment when co-cultured in common tissue culture conditions (10% fetal bovine serum supplemented RPMI1640 culture medium). In their study, they also showed that chorioallantoic attachment was required for maintained expression of *Gcm1* (Stecca et al., 2002).

Our *ex vivo* explant model took advantage of both techniques via co-culturing pre-attachment decidua/ectoplacental cone/chorion and allantois under whole-embryo culturing conditions. This model allowed us to study tissue-specific requirement of TMED2 during chorioallantoic fusion, and demonstrated that wildtype chorion can rescue failure of chorionic and allantoic cell mixing defects observed in *Tmed2*$^{99J/99J}$

placenta.

5.1.2 Implications of ex vivo culture of explants of pre-placental tissues from a TMED2 null mouse line, 99J.

In my second manuscript presented in chapter III, I addressed the tissue-specific requirement of TMED2 during chorioallantoic attachment using the established *ex vivo* culturing system presented in chapter II. I demonstrated that, via using the *ex vivo* culturing system, explants of *Tmed2*$^{99J/99J}$ chorions and *Tmed2*$^{99J/99J}$ allantoides show phenotypic features associated with *Tmed2*$^{99J/99J}$ placenta including abnormal chorioallantoic attachment, failed mixing between chorionic and allantoic cells, and reduced expression of *Tpbpα* and *Gcm1.* To investigate the tissue-specific requirement of TMED2 in the chorion or the allantois, I recombined *Tmed2*$^{99J/99J}$ chorions with wildtype allantoides, or reversely, wildtype chorions with *Tmed2*$^{99J/99J}$ allantoides in explants (herein referred as *Tmed2*$^{99J/99J}$/wildtype recombined explants). The morphological analysis of those *Tmed2*$^{99J/99J}$ /wildtype recombinants suggested that TMED2 was required in the chorion for normal chorioallantoic attachment and cell mixing, since recombination of *Tmed2*$^{99J/99J}$ allantoides and wildtype chorions showed chorionic and allantoic cell mixing.

Jerome-Majewska group previously showed that *Tmed2* mRNA was expressed in both the chorion and the allantois, however, the chorion-specific requirement of TMED2 for chorioallantoic attachment also suggested differential roles of TMED2 in two tissues. I performed immunofluorence experiments using a TMED2 antibody in wildtype placenta post-chorioallantoic attachment, and found the pattern of TMED2 expression differs between chorionic and allantoic cells. This preliminary data suggests that TMED2

may localize in different organelles between chorionic and allantoic cells. Future experiments to show co-localization of TMED2 and organelle markers will elucidate such a question.

In addition, immunofluorescence to the phosphohistone H3 antibody revealed reduced proliferation in the allantoic region of explants with *Tmed2*$^{99J/99J}$ tissues when compared to explants of wildtype control. The reason for this observation could simply be that TMED2 was required non-autonomously in the allantoic cells for normal proliferation: TMED2 may directly regulate molecules that are essential for cell division mechanisms, or be responsible for trafficking effector proteins involved in this process. Alternatively, though TMED2 may not be directly involved in the cell cycling process, it might be involved in mechanisms that can activate the apoptotic process in these highly active cells. I observed increased apoptotic index in explants of *Tmed2*$^{99J/99J}$ tissues cultured with wildtype tissues when compared to the control. Further investigation to specify whether these highly proliferative cells could activate apoptotic mechanism in *Tmed2*$^{99J/99J}$ tissues needs to be validated.

The endothelial cell marker, Pecam1, was absent in all explants with *Tmed2*$^{99J/99J}$ tissues but presented in the wildtype control. This suggests that TMED2 was required in both the chorion and the allantois to maintain Pecam1 expression under *ex vivo* culturing conditions. However, this phenotype could be culture-specific since Pecam1 expression was found in the *Tmed2*$^{99J/99J}$ placenta *in vivo*. However, it is also possible that maintenance of Pecam1 expression requires normal expression of TMED2, or Pecam1+ cells undergo apoptosis under the culture.

Instead of expanded expression of *Tpbpα* and *Gcm1* in the wildtype explants, both markers showed reduced expression in explants with *Tmed2*$^{99J/99J}$ tissues, similar to what we observed in the *Tmed2*$^{99J/99J}$ placenta. This result suggests that TMED2 is required in both the chorion and the allantois for expansion of both markers.

Lastly, I showed two potential cargos for TMED2, one secreted extracellular matrix protein, fibronectin, and one adhesion molecule, VCAM1, were abnormally expressed in the *Tmed2*$^{99J/99J}$ allantoises *in vivo* or *ex vivo*. TMED2 may possibly be responsible for normal transport of both proteins, or alternatively their common transmembrane receptor, β1 integrin. Further investigation on integrin expression in *Tmed2*$^{99J/99J}$ placenta could address this question. Through chapter II and III, I demonstrated the successful use of an *ex vivo* model of pre-placental tissues to investigate tissue-specific requirement of TMED2 during labyrinth layer development.

5.1.3 Implications of a mouse model of haploinsufficiency in TMED2 for NAFLD.

The third manuscript presented in chapter IV focused on a common human liver disease presented in mice with heterozygosity in *Tmed2*. Due to the embryonic lethality phenotype observed in *Tmed2*$^{99J/99J}$ embryos, we used *Tmed2* heterozygous (*Tmed2*$^{99J/+}$) animals as models to study the role of TMED2 in the liver. Although *Tmed2* mRNA level was the same between *Tmed2*$^{99J/+}$and wildtype littermates, TMED2 protein level was significantly reduced in the *Tmed2*$^{99J/+}$animals at P5. Several studies have been shown that TMED2 complexes with TMED10 (Blum et al., 1999; Füllekrug et al., 1999; Jenne et al., 2002), and is required for TMED10 stability and localization (Emery et al., 2000; Jerome-Majewska et al., 2010). We looked at the *Tmed 10* expression in livers of

99J animals. Similar to previously findings, TMED10 protein level but not mRNA level, was significantly reduced in the *Tmed2*$^{99J/+}$animals at P5.

Since mice with reduced TMED10 level present with moderately dilated Golgi (Denzel et al., 2000), we performed SEM to examine the morphology of ER and Golgi in liver cells of *Tmed2*$^{99J/+}$animals. No abnormal morphologies were found in the Golgi, however, a subset of *Tmed2*$^{99J/+}$animals had dilated ER morphology, which is often associated with ER stress. This observation of difference in dilated organelles between *Tmed2* and *Tmed10* heterozygous mice could be due to different functions of two proteins during secretory transport, as TMED10 was shown to be the key in COPI vesicle formation in the Golgi membrane (Gommel et al., 1999).

Then, we looked at the expression of all three UPR pathway sensors, PERK, ATF6, and IRE1α, and found a significant increase in one of PERK downstream effectors, p-eIF2α, albeit no differences found in the ATF6 or the IRE1α pathways. Mouse models of affected PERK-p-eIf2α-ATF4 have demonstrated NAFLD phenotype in these mice. Thus, TMED2 could serve as a downstream effector specific to the PERK pathway, and reduced TMED2 level could result in prolonged ER stress which leads to liver damage. Further study on the molecular mechanism of TMED2 in the PERK pathway could elucidate a clearer link between ER stress and NAFLD. Approximately 40% of *Tmed2*$^{99J/+}$animals developed NAFLD phenotypes compared to 10% in wildtype littermates by H&E staining. Further histological analysis including Oil red O and Sudan black B confirmed deposition of triglycerides in the hepatocytes of *Tmed2*$^{99J/+}$animals, which was consistent to observations of increased triglyceride level in the liver as the

main cause of NAFLD in patients. The fact that only 40% of animals with heterozygosity in TMED2 developed NAFLD phenotype illustrated the complexity of the NAFLD.

In addition, I observed higher incidence of NAFLD associated with older animals, suggesting the chronic progression characteristics of NAFLD. Fatty acid and cholesterol regulatory transcription factors, *Srebp1a*, and *Srebp2*, were significantly increased in the $Tmed2^{99J/+}$animals at P5 but not in the adult age when they became sick. Those results suggested that early disruption in the free fatty acid synthesis can predispose a higher risk of developing diseases at a later stage. However, whether TMED2 served as the link between the ER stress and mis-regulation in Srebp expression remains unclear. In this chapter, we described a novel mouse model of NAFLD due to haploinsufficiency in TMED2.

5.2 Future directions

5.2.1 Improving the ex vivo culturing conditions

Our *ex vivo* explants model system is an excellent experimental approach for our research questions, albeit it presents a number of shortcomings for improvement. 1. Maintained explant health under longer culturing time. We would like to extend the culturing time longer than 24hours to examine the status of mixing between two tissues, and trophoblast differentiation required for labyrinth layer function following the chorioallantoic fusion. In a pilot experiment, we cultured wildtype explants for extended 36 hours, and observed more mixing between eGFP- allantoic and eGFP+ chorionic cells as well as more cell death (data not shown). Those data suggest that modifications to the culturing media or conditions are necessary for maintaining healthy explants in extended culturing period. 2. Limitations of using allantoic explants. Our culturing system requires

engrafting pre-chorioallantoic attachment allantois to the chorion for culture, thus, it can not capture and study allantois growth defects such as addition of cells into the allantois via primitive streak (Kimberly and Downs, 2007). Explants of both primitive streak and allantois may be used to address such questions in the *ex vivo* system.

5.2.2 Potential TMED2 cargo proteins which are known players during placental development

5.2.2.1 Wnt

Wnt glycoproteins are potential cargos of TMED2, and have been shown to be required during murine labyrinth layer development. Knockout of *Wnt7b* (Parr et al., 2001) shows failure of chorioallantoic attachment, and knockout in *Wnt2*, *Fzd5* shows branching defects in the chorionic villi (Lu et al., 2013; Monkley et al., 1996). Thus, investigating the expression of Wnt proteins in *Tmed2* null placenta could demonstrate the protein interaction between TMED2 and Wnt proteins during placental development.

5.2.2.2 Extracellular matrix proteins and adhesion molecules

Mouse models with mutations in extracellular matrix proteins such as fibronectin, and Collagen IV have demonstrated a crucial role of ECM in the labyrinth layer development (George et al., 1993; Pöschl et al., 2004). In the $Tmed2^{99J/99J}$ placenta, fibronectin showed increased and disrupted expression pattern. Whether this disruption in fibronectin expression contributed to the phenotype observed in the $Tmed2^{99J/99J}$ placenta needs further investigation. However, those results suggest a previously unknown role of TMED proteins in regulating extracellular matrix proteins, and normal levels of certain extracellular matrix proteins in the placenta are crucial for normal placental development.

Knockout mouse models with null mutation in an adhesion molecule VCAM1 showed abnormal chorioallantoic attachment and failure of labyrinth layer formation (Gurtner et al., 1995). The immunofluorence experiment against the VCAM1 antibody showed abnormal VCAM1 expression in the *Tmed2*$^{99J/99J}$ placenta compared to wildtype controls. *Vcam1* has two isoforms in mouse and human, and one of the two is a GPI-AP (Kumar et al., 1994; Terry et al., 1993; Ulyanova et al., 2005), which could be a potential cargo of TMED2. The disrupted expression pattern of fibronectin and VCAM1 suggests that TMED2 may be responsible for the transport of multiple secretory proteins that are required during chorioallantoic attachment and subsequent labyrinth layer development. Further investigation on interactions between TMED2 and those secretory molecules may provide more insights towards the phenotype observed in *Tmed2* null placenta. Another potential category of proteins are integrins, which are transmembrane receptors interacting with extracellular matrix proteins, collagens, and adhesion molecules. For instance, β1integrin is a common receptor for both fibronectin and VCAM1. The mouse model with homozygous mutation in α4β1 integrin shows failure of chorioallantoic attachment and impaired labyrinth layer formation. Whether TMED2 regulates integrins to attribute subsequent modifications in the expression of ECM and adhesion proteins remains to be answered.

5.2.2.3 Runx1

Expression of Runx1 in the chorionic mesothelium suggests a role of mesothelium in the fetal hematopoiesis. Further investigation on the expression of Runx1 in explants of wildtype control and explants with *Tmed2*$^{99J/99J}$ tissues could address the following questions:1. are mesothelial cells observed in the allantoic region of the

wildtype explants expressing Runx1; 2. is the expression of Runx1 in the mesothelium maintained in the *Tmed2*$^{99J/+}$ placenta.

5.2.3 TMED2 during the early development of liver.

We have demonstrated in chapter IV that a significant reduction in protein levels of TMED2 and TMED10 was found in E17.5 (data not shown) and P5 *Tmed2*$^{99J/+}$ liver and kidney samples. In addition, two regulators of free fatty acid synthesis, Srebp1a and Srebp2, were found to be elevated in P5 *Tmed2*$^{99J/+}$ liver samples, although the NAFLD phenotype only initiated in mice who were at least five months old. Those results suggest that an early mis-regulation of molecules and proteins by haploinsufficiency in TMED2 can lead to a later-stage, chronic liver condition. Thus, understanding the morphological changes associated with early liver development in the *Tmed2*$^{99J/+}$ mice may provide better knowledge towards pathological progress of NAFLD. In addition, incomplete penetrance of NAFLD in *Tmed2*$^{99J/+}$ mice (40%) may due to the heterogeneity of TMED protein expression in the liver. We looked at the link between NAFLD scores and TMED2 protein levels by western blot, and found no obvious association between differences in NAFLD scores and TMED2 protein level. To understand what roles of TMED2 play during embryonic liver development and pathological causes of NAFLD, a mouse model of liver-specific knockout is necessary.

5.2.4 TMED2-regulated proteins and liver homeostasis

In *Tmed2*$^{99J/+}$ animals, we observed an increase in UPR sensor in p-eIF2α in the young adult animals. Since UPR can regulate the expression of *Srebp* genes, a further dissection of the roles that TMED2 plays in ER stress and *Srebp* genes can better address which mechanism is affected by TMED2. In addition, although we did not observe any

severe phenotypes in Tunicamycin-induced *Tmed2*$^{99J/+}$ animals, TMED2 may be involved in other forms of ER stress. After all, TMED10 has been shown to be required in export of misfolded GPI- anchored proteins downstream of thapsigargin or Dithiothreitol (DTT)-mediated ER-stress, prior to UPR (Satpute-Krishnan et al., 2014). Lastly, some known TMED2 cargos were found to be associated with NAFLD. For instance, disrupted Wnt signaling in mice leads to hyperlipidemia phenotypes (Go et al., 2014). In addition, two folate receptors, FRα and FRβ, are known GPI-AP cargos of TMED2 responsible for folate transport. Folate deficiency was reported to contribute NAFLD in mouse (Christensen et al., 2010). Mis-regulation in other TMED known cargos such as PAR-1, and TLR4, was also shown to contribute to liver diseases such as NASH and fibrosis (Hritz et al., 2008; Luyendyk et al., 2010; Pradere et al., 2010). Investigation over these known cargos of TMED2 will be equally important to better understand functions of TMED2 in normal liver homoeostasis.

5.3 Concluding summary

TMED proteins are key components of early secretory pathway in eukaryotic cells. They interact with coatomer proteins during COPI and COPII vesicle formation and regulate secretory and transmembrane cargo proteins which are required in many intracellular and intercellular processes. A couple of TMED members have shown to be required during embryogenesis, and many TMED proteins are found to be implicated in human diseases. During the course of my PhD study, I focused on *Tmed2*, the sole member of *Tmed* β subfamily, in murine labyrinth layer development and liver conditions in the adults. I observed distinct tissue-specific requirements of TMED2 in the chorion and the allantois during the chorioallantoic attachment process using a novel *ex vivo* culturing model. Molecular analysis on cellular processes such as proliferation, apoptosis, and cell migration, as well as the expression of many proteins/cell markers including PECAM1, VCAM1, fibronectin, *Tpbpα*, and *Gcm1*, were affected in explants with *Tmed2* null pre-placental tissues. Although *Tmed2* homozygous embryos die at mid-gestation, we looked at the role of TMED2 in the liver of *Tmed2* heterozygous animals. We observed decreased levels of TMED2 and TMED10, dilated endoplasmic reticulum membrane and increased phosphorylation of eIF2α, increased expression of *Srebp1a* and *Srebp2* at the newborn stage, and an increased incidence of NAFLD in *Tmed2* heterozygous mice, providing a novel mouse model of NAFLD.

References

Abd El-Kader, S.M., El-Den Ashmawy, E.M.S., 2015. Non-alcoholic fatty liver disease: The diagnosis and management. World J. Hepatol. 7, 846–858. doi:10.4254/wjh.v7.i6.846

Adams, E.J., Chen, X.W., O'Shea, K.S., Ginsburg, D., 2014. Mammalian COPII coat component SEC24C is required for embryonic development in mice. J. Biol. Chem. 289, 20858–20870. doi:10.1074/jbc.M114.566687

Adams, L.A., Sanderson, S., Lindor, K.D., Angulo, P., 2005. The histological course of nonalcoholic fatty liver disease: A longitudinal study of 103 patients with sequential liver biopsies. J. Hepatol. 42, 132–138. doi:10.1016/j.jhep.2004.09.012

Adelman, D.M., Gertsenstein, M., Nagy, A., Simon, M.C., Maltepe, E., 2000. Placental cell fates are regulated in vivo by HIF-mediated hypoxia responses. Genes Dev. 14, 3191–3203. doi:10.1101/gad.853700

Aguilera-Romero, A., Kaminska, J., Spang, A., Riezman, H., Muñiz, M., 2008. The yeast p24 complex is required for the formation of COPI retrograde transport vesicles from the Golgi apparatus. J. Cell Biol. 180, 713–720. doi:10.1083/jcb.200710025

Albano, E., Mottaran, E., Vidali, M., Reale, E., Saksena, S., Occhino, G., Burt, A.D., Day, C.P., 2005. Immune response towards lipid peroxidation products as a predictor of progression of non-alcoholic fatty liver disease to advanced fibrosis. Gut 54, 987–93. doi:10.1136/gut.2004.057968

Amar, J., Burcelin, R., Ruidavets, J.B., Cani, P.D., Fauvel, J., Alessi, M.C., Chamontin, B., Ferriéres, J., 2008. Energy intake is associated with endotoxemia in apparently healthy men. Am J Clin Nutr 87, 1219–1223.

Amemiya-Kudo, M., Shimano, H., Hasty, A.H., Yahagi, N., Yoshikawa, T., Matsuzaka, T., Okazaki, H., Tamura, Y., Iizuka, Y., Ohashi, K., Osuga, J., Harada, K., Gotoda, T., Sato, R., Kimura, S., Ishibashi, S., Yamada, N., 2002. Transcriptional activities of nuclear SREBP-1a, -1c, and -2 to different target promoters of lipogenic and cholesterogenic genes. J. Lipid Res. 43, 1220–1235. doi:10.1194/jlr.M100417-JLR200

Ameri, K., Harris, A.L., 2008. Activating transcription factor 4. Int. J. Biochem. Cell Biol. 40, 14–21. doi:10.1016/j.biocel.2007.01.020

Anantharaman, V., Aravind, L., 2002. The GOLD domain, a novel protein module involved in Golgi function and secretion. Genome Biol. 3, research0023.

Ande, S., Wiemann, S., Tashuridu, M., 2002. HEPATOCYTE TELOMERE SHORTENING AND SENESCENCE ARE GENERAL MARKERS OF HUMAN LIVER CIRRHOSIS 44.

ANDREA E. REID, 2001. Nonalcoholic steatohepatitis. Gastroenterology 127, 410–411. doi:10.1053/gast.2001.27126

Aniento, F., Matsuoka, K., Robinson, D.G., 2006. ER-to-Golgi Transport : The COPII-

Pathway.

Anson-Cartwright, L., Dawson, K., Holmyard, D., Fisher, S.J., Lazzarini, R. a, Cross, J.C., 2000. The glial cells missing-1 protein is essential for branching morphogenesis in the chorioallantoic placenta. Nat. Genet. 25, 311–4. doi:10.1038/77076

Appenzeller, C., Andersson, H., Kappeler, F., Hauri, H.P., 1999. The lectin ERGIC-53 is a cargo transport receptor for glycoproteins. Nat. Cell Biol. 1, 330–4. doi:10.1038/14020

Arora, R., Papaioannou, V.E., 2015. The murine allantois : a model system for the study of blood vessel formation. Blood 120, 2562–2573. doi:10.1182/blood-2012-03-390070.

Ashraf, N.U., Sheikh, T.A., 2015. Endoplasmic reticulum stress and Oxidative stress in the pathogenesis of Non-alcoholic fatty liver disease. Free Radic. Res. 49, 1405–18. doi:10.3109/10715762.2015.1078461

Au, C.E., Hermo, L., Byrne, E., Smirle, J., Fazel, A., Simon, P.H.G., Kearney, R.E., Cameron, P.H., Smith, C.E., Vali, H., Fernandez-Rodriguez, J., Ma, K., Nilsson, T., Bergeron, J.J.M., 2015. Expression, sorting, and segregation of Golgi proteins during germ cell differentiation in the testis. Mol. Biol. Cell 26, 4015–32. doi:10.1091/mbc.E14-12-1632

Babiarz, B.S., Romagnano, L.C., Kurilla, G.M., 1992. , 0o t 500–508.

Bacia, K., Futai, E., Prinz, S., Meister, A., Daum, S., Glatte, D., Briggs, J.A.G., Schekman, R., 2011. Multibudded tubules formed by COPII on artificial liposomes. Sci. Rep. 1, 17. doi:10.1038/srep00017

Bagchi, I.C., Ph, D., 2011. NIH Public Access 28, 17–26. doi:10.1055/s-0029-1242989.ENDOMETRIAL

Baines, A.C., Adams, E.J., Zhang, B., Ginsburg, D., 2013. Disruption of the Sec24d gene results in early embryonic lethality in the mouse. PLoS One 8, e61114. doi:10.1371/journal.pone.0061114

Bannykh, S.I., Rowe, T., Balch, W.E., 1996. The organization of endoplasmic reticulum export complexes. J. Cell Biol. 135, 19–35. doi:10.1083/jcb.135.1.19

Barlowe, C., 2003. Signals for COPII-dependent export from the ER: What's the ticket out? Trends Cell Biol. 13, 295–300. doi:10.1016/S0962-8924(03)00082-5

Barlowe, C., Orci, L., Yeung, T., Hosobuchi, M., Hamamoto, S., Salama, N., Rexach, M.F., Ravazzola, M., Amherdt, M., Schekman, R., 1994. COPII: A membrane coat formed by sec proteins that drive vesicle budding from the endoplasmic reticulum. Cell 77, 895–907. doi:10.1016/0092-8674(94)90138-4

Barlowe, C., Schekman, R., 1993. SEC12 encodes a guanine-nucleotide-exchange factor essential for transport vesicle budding from the ER. Nature 365, 347–349. doi:10.1038/365347a0

Bataller, R., Brenner, D., 2005. Liver fibrosis. J. Clin. Invest. 115, 209–218. doi:10.1172/JCI200524282.The

Beck, R., Ravet, M., Wieland, F.T., Cassel, D., 2009. The COPI system: Molecular mechanisms and function. FEBS Lett. 583, 2701–2709. doi:10.1016/j.febslet.2009.07.032

Belden, W.J., 2001. Role of Erv29p in Collecting Soluble Secretory Proteins into ER-Derived Transport Vesicles. Science (80-.). 294, 1528–1531. doi:10.1126/science.1065224

Belden, W.J., Barlowe, C., 1996. Erv25p, a component of COPII-coated vesicles, forms a complex with Emp24p that is required for efficient endoplasmic reticulum to Golgi transport. J. Biol. Chem. 271, 26939–26946. doi:10.1074/jbc.271.43.26939

Belden, W.J., Barlowe, C., 2001. Role of Erv29p in Collecting Soluble Secretory Proteins into ER-Derived Transport Vesicles Published by : American Association for the Advancement of Science Stable URL : http://www.jstor.org/stable/3085135 Linked references are available on JSTOR for thi 294, 1528–1531.

Belden, W.J., Barlowe, C., 2001. Deletion of yeast p24 genes activates the unfolded protein response. Mol. Biol. Cell 12, 957–69.

Belden, W.J., Barlowe, C., 2001. Distinct Roles for the Cytoplasmic Tail Sequences of Emp24p and Erv25p in Transport between the Endoplasmic Reticulum and Golgi Complex. J. Biol. Chem. 276, 43040–43048. doi:10.1074/jbc.M108113200

Bellentani, S., 2017. The epidemiology of non-alcoholic fatty liver disease. Liver Int. 37, 81–84. doi:10.1111/liv.13299

Benirschke, K., Burton, G.J., Baergen, R., 2012. Pathology of the Human Placenta, Springer. doi:10.1097/00000478-199604000-00026

Bertolotti, A., Wang, X., Novoa, I., Jungreis, R., Schlessinger, K., Cho, J.H., West, A.B., Ron, D., 2001. Increased sensitivity to dextran sodium sulfate colitis in IRE1beta-deficient mice. J. Clin. Invest. 107, 585–93. doi:10.1172/JCI11476

Bertolotti, A., Zhang, Y., Hendershot, L.M., Harding, H.P., Ron, D., 2000. Dynamic interaction of BiP and ER stress transducers in the unfolded-protein response. Nat. Cell Biol. 2, 326–332. doi:10.1038/35014014

Béthune, J., Kol, M., Hoffmann, J., Reckmann, I., Brügger, B., Wieland, F., 2006a. Coatomer, the coat protein of COPI transport vesicles, discriminates endoplasmic reticulum residents from p24 proteins. Mol. Cell. Biol. 26, 8011–21. doi:10.1128/MCB.01055-06

Béthune, J., Kol, M., Hoffmann, J., Reckmann, I., Brügger, B., Wieland, F., 2006b. Coatomer, the coat protein of COPI transport vesicles, discriminates endoplasmic reticulum residents from p24 proteins. Mol. Cell. Biol. 26, 8011–21. doi:10.1128/MCB.01055-06

Bettayeb, K., Chang, J.C., Luo, W., Aryal, S., Varotsis, D., Randolph, L., Netzer, W.J.,

Greengard, P., Flajolet, M., 2016a. δ-COP modulates Aβ peptide formation via retrograde trafficking of APP. Proc. Natl. Acad. Sci. 113, 5412–5417. doi:10.1073/pnas.1604156113

Bettayeb, K., Hooli, B. V., Parrado, A.R., Randolph, L., Varotsis, D., Aryal, S., Gresack, J., Tanzi, R.E., Greengard, P., Flajolet, M., 2016b. Relevance of the COPI complex for Alzheimer's disease progression in vivo. Proc. Natl. Acad. Sci. 113, 5418–5423. doi:10.1073/pnas.1604176113

Bhattacharya, N., O'Donnell, J., Stagg, S.M., 2012. The structure of the Sec13/31 COPII cage bound to Sec23. J. Mol. Biol. 420, 324–334. doi:10.1016/j.jmb.2012.04.024

Bi, X., Corpina, R. a, Goldberg, J., 2002. Structure of the Sec23/24-Sar1 pre-budding complex of the COPII vesicle coat. Nature 419, 271–277. doi:10.1038/nature01040

Bi, X., Mancias, J.D., Goldberg, J., 2007. Insights into COPII Coat Nucleation from the Structure of Sec23???Sar1 Complexed with the Active Fragment of Sec31. Dev. Cell 13, 635–645. doi:10.1016/j.devcel.2007.10.006

Bianchi, P., Fermo, E., Vercellati, C., Boschetti, C., Barcellini, W., Iurlo, A., Marcello, A.P., Righetti, P.G., Zanella, A., 2009. Congenital Dyserythropoietic Anemia type II (CDAII) is caused by mutations in the SEC23B gene. Hum. Mutat. 30, 1292–1298. doi:10.1002/humu.21077

Bielli, A., Haney, C.J., Gabreski, G., Watkins, S.C., Bannykh, S.I., Aridor, M., 2005. Regulation of Sar1 NH2 terminus by GTP binding and hydrolysis promotes membrane deformation to control COPII vesicle fission. J. Cell Biol. 171, 919–924. doi:10.1083/jcb.200509095

Blum, R., Feick, P., Puype, M., Vandekerckhove, J., Klengel, R., Nastainczykf, W., Schulz, I., 1996. Tmp21 and p24A, two type I proteins enriched in pancreatic microsomal membranes, are members of a protein family involved in vesicular trafficking. J. Biol. Chem. 271, 17183–17189. doi:10.1074/jbc.271.29.17183

Blum, R., Lepier, A., 2008. The luminal domain of p23 (Tmp21) plays a critical role in p23 cell surface trafficking. Traffic 9, 1530–1550. doi:10.1111/j.1600-0854.2008.00784.x

Blum, R., Pfeiffer, F., Feick, P., Nastainczyk, W., Kohler, B., Schäfer, K.H., Schulz, I., 1999. Intracellular localization and in vivo trafficking of p24A and p23. J. Cell Sci. 112 (Pt 4, 537–48.

Boehm, M., Aguilar, R.C., Bonifacino, J.S., 2001. Functional and physical interactions of the adaptor protein complex AP-4 with ADP-ribosylation factors (ARFs). EMBO J. 20, 6265–6276. doi:10.1093/emboj/20.22.6265

Boltz, K.A., Ellis, L.L., Carney, G.E., 2007. Drosophila melanogaster p24 genes have developmental, tissue-specific, and sex-specific expression patterns and functions. Dev. Dyn. 236, 544–555. doi:10.1002/dvdy.21032

Bonfanti, L., Mironov, A.A., Martínez-Menárguez, J.A., Martella, O., Fusella, A., Baldassarre, M., Buccione, R., Geuze, H.J., Mironov, A.A., Luini, A., 1998.

Procollagen traverses the Golgi stack without leaving the lumen of cisternae: Evidence for cisternal maturation. Cell 95, 993–1003. doi:10.1016/S0092-8674(00)81723-7

Bonnon, C., Wendeler, M.W., Paccaud, J.-P., Hauri, H.-P., 2010. Selective export of human GPI-anchored proteins from the endoplasmic reticulum. J. Cell Sci. 123, 1705–15. doi:10.1242/jcs.062950

Boyadjiev, S.A., Fromme, J.C., Ben, J., Chong, S.S., Nauta, C., Hur, D.J., Zhang, G., Hamamoto, S., Schekman, R., Ravazzola, M., Orci, L., Eyaid, W., 2006. Cranio-lenticulo-sutural dysplasia is caused by a SEC23A mutation leading to abnormal endoplasmic-reticulum-to-Golgi trafficking. Nat. Genet. 38, 1192–1197. doi:10.1038/ng1876

Brandizzi, F., Barlowe, C., 2013. Organization of the ER-Golgi interface for membrane traffic control. Nat. Rev. Mol. Cell Biol. 14, 382–92. doi:10.1038/nrm3588

Bremser, M., Nickel, W., Schweikert, M., Ravazzola, M., Amherdt, M., Hughes, C. a, Söllner, T.H., Rothman, J.E., Wieland, F.T., 1999. Coupling of Coat Assembly and Vesicle Budding to Packaging of Putative Cargo Receptors. Cell 96, 495–506. doi:10.1016/S0092-8674(00)80654-6

Brown, M.S., Goldstein, J.L., 1997. The SREBP pathway: Regulation of cholesterol metabolism by proteolysis of a membrane-bound transcription factor. Cell 89, 331–340. doi:10.1016/S0092-8674(00)80213-5

Bryant, C.E., Spring, D.R., Gangloff, M., Gay, N.J., 2010. The molecular basis of the host response to lipopolysaccharide. Nat Rev Micro 8, 8–14. doi:10.1038/nrmicro2266

Bue, C.A., Barlowe, C., 2009. Molecular dissection of Erv26p identifies separable cargo binding and coat protein sorting activities. J. Biol. Chem. 284, 24049–24060. doi:10.1074/jbc.M109.022590

Bue, C.A., Bentivoglio, C.M., Barlowe, C., 2006. Erv26p Directs Pro-Alkaline Phosphatase into Endoplasmic Reticulum–derived Coat Protein Complex II Transport Vesicles. Mol. Biol. Cell 17, 4780–4789. doi:10.1091/mbc.E06

Buechling, T., Chaudhary, V., Spirohn, K., Weiss, M., Boutros, M., 2011. p24 proteins are required for secretion of Wnt ligands. EMBO Rep. 12, 1265–1272. doi:10.1038/embor.2011.212

Bugianesi, E., 2005. Review article: steatosis, the metabolic syndrome and cancer. Aliment. Pharmacol. Ther. 22 Suppl 2, 40–43. doi:10.1111/j.1365-2036.2005.02594.x

Bugianesi, E., Gentilcore, E., Manini, R., Natale, S., Vanni, E., Villanova, N., David, E., Rizzetto, M., Marchesini, G., 2005. A randomized controlled trial of metformin versus vitamin E or prescriptive diet in nonalcoholic fatty liver disease. Am. J. Gastroenterol. 100, 1082–1090. doi:10.1111/j.1572-0241.2005.41583.x

Caillot, F., Derambure, C., Bioulac-Sage, P., François, A., Scotte, M., Goria, O., Hiron,

M., Daveau, M., Salier, J.P., 2009. Transient and etiology-related transcription regulation in cirrhosis prior to hepatocellular carcinoma occurrence. World J. Gastroenterol. 15, 300–309. doi:10.3748/wjg.15.300

Calfon, M., Zeng, H., Urano, F., Till, J.H., Hubbard, S.R., Harding, H.P., Clark, S.G., Ron, D., 2002. IRE1 couples endoplasmic reticulum load to secretory capacity by processing the XBP-1 mRNA. Nature 415, 92–96. doi:10.1038/nature01193

Cani, P.D., Amar, J., Iglesias, M.A., Poggi, M., Knauf, C., Bastelica, D., Neyrinck, A.M., Fava, F., Tuohy, K.M., Chabo, C., Ferrie, J., Gibson, G.R., Casteilla, L., Delzenne, N.M., Alessi, M.C., 2007. Original Article. Diabetes 56, 1761–1772. doi:10.2337/db06-1491.P.D.C.

Cardiff, R.D., Miller, C.H., Munn, R.J., 2014. Manual hematoxylin and eosin staining of mouse tissue sections. Cold Spring Harb. Protoc. 2014, pdb.prot073411. doi:10.1101/pdb.prot073411

Carney, E.W., Prideaux, V., Lye, S.J., Rossant, J., 1993. Progressive expression of trophoblast-specific genes during formation of mouse trophoblast giant cells in vitro. Mol. Reprod. Dev. 34, 357–368. doi:10.1002/mrd.1080340403

Carvalho, P., Goder, V., Rapoport, T.A., 2006. Distinct Ubiquitin-Ligase Complexes Define Convergent Pathways for the Degradation of ER Proteins. Cell 126, 361–373. doi:10.1016/j.cell.2006.05.043

Castillon, G.A., Aguilera-Romero, A., Manzano-Lopez, J., Epstein, S., Kajiwara, K., Funato, K., Watanabe, R., Riezman, H., Muñiz, M., 2011. The yeast p24 complex regulates GPI-anchored protein transport and quality control by monitoring anchor remodeling. Mol. Biol. Cell 22, 2924–36. doi:10.1091/mbc.E11-04-0294

Cazanave, S.C., Elmi, N.A., Akazawa, Y., Bronk, S.F., Mott, J.L., Gores, G.J., 2010. CHOP and AP-1 cooperatively mediate PUMA expression during lipoapoptosis. Am J Physiol Gastrointest Liver Physiol. 299, G236-243. doi:10.1152/ajpgi.00091.2010

Chen, F., Hasegawa, H., Schmitt-Ulms, G., Kawarai, T., Bohm, C., Katayama, T., Gu, Y., Sanjo, N., Glista, M., Rogaeva, E., Wakutani, Y., Pardossi-Piquard, R., Ruan, X., Tandon, A., Checler, F., Marambaud, P., Hansen, K., Westaway, D., St George-Hyslop, P., Fraser, P., 2006. TMP21 is a presenilin complex component that modulates gamma-secretase but not epsilon-secretase activity. Nature 440, 1208–12. doi:10.1038/nature04667

Chen, X.W., Wang, H., Bajaj, K., Zhang, P., Meng, Z.X., Ma, D., Bai, Y., Liu, H.H., Adams, E., Baines, A., Yu, G., Sartor, M.A., Zhang, B., Yi, Z., Lin, J., Young, S.G., Schekman, R., Ginsburg, D., 2013. SEC24A deficiency lowers plasma cholesterol through reduced PCSK9 secretion. Elife 2013, 1–23. doi:10.7554/eLife.00444

Christensen, K.E., Wu, Q., Wang, X., Deng, L., Caudill, M. a, Rozen, R., 2010. Steatosis in mice is associated with gender, folate intake, and expression of genes of one-carbon metabolism. J. Nutr. 140, 1736–1741. doi:10.3945/jn.110.124917

Christian Appenzeller-Herzog, Hauri, H.-P., 2005. Carbohydrate- and Conformation-

dependent Cargo Capture for ER-Exit□. Mol. Biol. Cell 16, 1–13. doi:10.1091/mbc.E04

Ciufo, L.F., Boyd, A., 2000. Identification of a lumenal sequence specifying the assembly of Emp24p into p24 complexes in the yeast secretory pathway. J. Biol. Chem. 275, 8382–8388. doi:10.1074/jbc.275.12.8382

Contreras, F.-X., Ernst, A.M., Haberkant, P., Björkholm, P., Lindahl, E., Gönen, B., Tischer, C., Elofsson, A., von Heijne, G., Thiele, C., Pepperkok, R., Wieland, F., Brügger, B., 2012. Molecular recognition of a single sphingolipid species by a protein's transmembrane domain. Nature 481, 525–9. doi:10.1038/nature10742

Contreras, I., Ortiz-Zapater, E., Aniento, F., 2004. Sorting signals in the cytosolic tail of membrane proteins involved in the interaction with plant ARF1 and coatomer. Plant J. 38, 685–698. doi:10.1111/j.1365-313X.2004.02075.x

Copic, A., Latham, C.F., Horlbeck, M.A., D'Arcangelo, J.G., Miller, E.A., 2012. ER Cargo Properties Specify a Requirement for COPII Coat Rigidity Mediated by Sec13p. Science (80-.). 335, 1359–1362. doi:10.1126/science.1215909

Čopič, A., Miller, E.A., 2012. ER Cargo Properties Specify A Requirement For COPII Coat Rigidity Mediated By Sec13p. Science (80-.). 76, 211–220. doi:10.1007/s11103-011-9767-z.Plastid

Cortez-Pinto, H., De Moura, M.C., Day, C.P., 2006. Non-alcoholic steatohepatitis: From cell biology to clinical practice. J. Hepatol. 44, 197–208. doi:10.1016/j.jhep.2005.09.002

Cross, J.C., 2000. Genetic insights into trophoblast differentiation and placental morphogenesis. Semin. Cell Dev. Biol. 11, 105–13. doi:10.1006/scdb.2000.0156

Cross, J.C., Hemberger, M., Lu, Y., Nozaki, T., Whiteley, K., Masutani, M., Adamson, S.L., 2002. Trophoblast functions, angiogenesis and remodeling of the maternal vasculature in the placenta. Mol. Cell. Endocrinol. 187, 207–12.

Cross, J.C., Nakano, H., Natale, D.R.C., Simmons, D.G., Watson, E.D., 2006. Branching morphogenesis during development of placental villi. Differentiation. 74, 393–401. doi:10.1111/j.1432-0436.2006.00103.x

Cross, J.C., Simmons, D.G., Watson, E.D., 2003. Chorioallantoic Morphogenesis and Formation of the Placental Villous Tree. ann.n.y.acad.sci 0.

Cuadrado, A., Orive, A., García-Suárez, C., Domínguez, A., Fernández-Escalante, J.C., Crespo, J., Pons-Romero, F., 2005. Non-alcoholic steatohepatitis (NASH) and hepatocellular carcinoma. Obes. Surg. 15, 442–6. doi:10.1381/0960892053576596

Cusi, K., 2012. Role of obesity and lipotoxicity in the development of nonalcoholic steatohepatitis: pathophysiology and clinical implications. Gastroenterology 142, 711–725.e6. doi:10.1053/j.gastro.2012.02.003

Cusi, K., Orsak, B., Bril, F., Lomonaco, R., Hecht, J., Ortiz-Lopez, C., Tio, F., Hardies, J., Darland, C., Musi, N., Webb, A., Portillo-Sanchez, P., 2016. Long-term

pioglitazone treatment for patients with nonalcoholic steatohepatitis and prediabetes or type 2 diabetes mellitus a randomized trial. Ann. Intern. Med. 165, 305–315. doi:10.7326/M15-1774

D'Souza-Schorey, C., Chavrier, P., 2006. ARF proteins: roles in membrane traffic and beyond. Nat. Rev. Mol. Cell Biol. 7, 347–358. doi:10.1038/nrm1910

Dancourt, J., Barlowe, C., 2010. Protein sorting receptors in the early secretory pathway. Annu. Rev. Biochem. 79, 777–802. doi:10.1146/annurev-biochem-061608-091319

Daniell, H., 2012. NIH Public Access 76, 211–220. doi:10.1007/s11103-011-9767-z.Plastid

Day, C.P., James, O.F.W., 1998. Steatohepatitis: A tale of two "Hits"? Gastroenterology 114, 842–845. doi:10.1016/S0016-5085(98)70599-2

Day, C.P., Saksena, S., 2002. Non-alcoholic steatohepatitis: definitions and pathogenesis. J. Gastroenterol. Hepatol. 17 Suppl 3, S377-84.

de Lédinghen, V., Combes, M., Trouette, H., Winnock, M., Amouretti, M., de Mascarel, A., Couzigou, P., 2004. Should a liver biopsy be done in patients with subclinical chronically elevated transaminases? Eur. J. Gastroenterol. Hepatol. 16, 879–83. doi:10.1097/00042737-200409000-00011

Delhaye, M., Louis, H., Degraef, C., Le Moine, O., Devière, J., Gulbis, B., Jacobovitz, D., Adler, M., Galand, P., 1996. Relationship between hepatocyte proliferative activity and liver functional reserve in human cirrhosis. Hepatology 23, 1003–1011. doi:10.1053/jhep.1996.v23.pm0008621125

Demi, R., Kaufmann, P., Kotowski, A., 1989. Fetal vasculogensis and angiogensis in human placental villi I, 1989.

Dempsey, E.W., 1972. The development of capillaries in the villi of early human placentas. Am. J. Anat. 134, 221–237. doi:10.1002/aja.1001340207

Denzel, a, Otto, F., Girod, a, Pepperkok, R., Watson, R., Rosewell, I., Bergeron, J.J., Solari, R.C., Owen, M.J., 2000. The p24 family member p23 is required for early embryonic development. Curr. Biol. 10, 55–8.

Diehl, A.M., 2004. Obesity and alcoholic liver disease. Alcohol 34, 81–87. doi:10.1016/j.alcohol.2004.07.010

Diehl, a M., Li, Z.P., Lin, H.Z., Yang, S.Q., 2005. Cytokines and the pathogenesis of non-alcoholic steatohepatitis. Gut 54, 303–306. doi:10.1136/gut.2003.024935

Dominguez, M., Dejgaard, K., Füllekrug, J., Dahan, S., Fazel, A., Paccaud, J.P., Thomas, D.Y., Bergeron, J.J.M., Nilsson, T., 1998. gp25L/emp24/p24 protein family members of the cis-Golgi network bind both COP I and II coatomer. J. Cell Biol. 140, 751–765. doi:10.1083/jcb.140.4.751

Downs, K., Enders, A., 2009. NIH Public Access. Dev dyn 238, 532–553. doi:10.1016/j.immuni.2010.12.017.Two-stage

Downs, K.M., 2006. In vitro methods for studying vascularization of the murine allantois and allantoic union with the chorion. Methods Mol. Med. 121, 241–272. doi:10.1385/1-59259-983-4:239

Downs, K.M., Bertler, C., 2000. Growth in the pre-fusion murine allantois. Anat. Embryol. (Berl). 202, 323–331. doi:10.1007/s004290000118

Downs, K.M., Gardner, R.L., 1995. An investigation into early placental ontogeny: allantoic attachment to the chorion is selective and developmentally regulated. Development 121, 407–16.

Downs, K.M., Temkin, R., Gifford, S., McHugh, J., 2001. Study of the murine allantois by allantoic explants. Dev. Biol. 233, 347–364. doi:10.1006/dbio.2001.0227

Drake, C.J., Fleming, P. a, 2000. Vasculogenesis in the day 6.5 to 9.5 mouse embryo. Blood 95, 1671–1679.

Du, X., Dong, Y., Shi, H., Li, J., Kong, S., Shi, D., Sun, L. V., Xu, T., Deng, K., Tao, W., 2014. Mst1 and Mst2 are essential regulators of trophoblast differentiation and placenta morphogenesis. PLoS One 9, 1–11. doi:10.1371/journal.pone.0090701

Duden, R., 2003. ER-to-Golgi transport: COP I and COP II function (Review). Mol. Membr. Biol. 20, 197–207. doi:10.1080/0968768031000122548

Dupressoir, A., Vernochet, C., Bawa, O., Harper, F., Pierron, G., Opolon, P., Heidmann, T., 2009. Syncytin-A knockout mice demonstrate the critical role in placentation of a fusogenic, endogenous retrovirus-derived, envelope gene. Proc Natl Acad Sci U S A 106, 12127–12132. doi:10.1073/pnas.0902925106

Dupressoir, A., Vernochet, C., Harper, F., Guegan, J., Dessen, P., Pierron, G., Heidmann, T., 2011. A pair of co-opted retroviral envelope syncytin genes is required for formation of the two-layered murine placental syncytiotrophoblast. Proc Natl Acad Sci U S A 108, E1164-73. doi:10.1073/pnas.1112304108

Duquet, A., Melotti, A., Mishra, S., Malerba, M., Seth, C., Conod, A., Ruiz i Altaba, A., 2014a. A novel genome-wide in vivo screen for metastatic suppressors in human colon cancer identifies the positive WNT-TCF pathway modulators TMED3 and SOX12. EMBO Mol. Med. 6, 882–901. doi:10.15252/emmm.201303799

Duquet, A., Melotti, A., Mishra, S., Malerba, M., Seth, C., Conod, A., Ruiz I Altaba, A., 2014b. A novel genome-wide in vivo screen for metastatic suppressors in human colon cancer identifies the positive WNT-TCF pathway modulators TMED3 and SOX12. EMBO Mol. Med. 6, 882–901. doi:10.15252/emmm.201303799

Eberlé, D., Hegarty, B., Bossard, P., Ferré, P., Foufelle, F., 2004. SREBP transcription factors: Master regulators of lipid homeostasis. Biochimie 86, 839–848. doi:10.1016/j.biochi.2004.09.018

Eckel, R.H., Grundy, S.M., Zimmet, P.Z., 2005. The metabolic syndrome. Lancet 365, 1415–1428. doi:10.1016/S0140-6736(05)66378-7

Editor, S., Robinson, D.G., 2007. Series Editor : David G . Robinson.

El-Serag, H.B., Rudolph, K.L., 2007. Hepatocellular Carcinoma: Epidemiology and Molecular Carcinogenesis. Gastroenterology 132, 2557–2576. doi:10.1053/j.gastro.2007.04.061

Emery, G., Rojo, M., Gruenberg, J., 2000. Introduction 2516, 2507–2516.

Espenshade, P., Gimeno, R.E., Holzmacher, E., Teung, P., Kaiser, C.A., 1995. Yeast SEC16 gene encodes a multidomain vesicle coat protein that interacts with Sec23p. J. Cell Biol. 131, 311–324. doi:10.1083/jcb.131.2.311

Eugster, A., Frigerio, G., Dale, M., Duden, R., 2000. COP I domains required for coatomer integrity, and novel interactions with ARF and ARF-GAP. EMBO J. 19, 3905–3917. doi:10.1093/emboj/19.15.3905

Ferré, P., Foufelle, F., 2010. Hepatic steatosis: A role for de novo lipogenesis and the transcription factor SREBP-1c. Diabetes, Obes. Metab. 12, 83–92. doi:10.1111/j.1463-1326.2010.01275.x

Fiedler, K., Veit, M., Stamnes, M. a, Rothman, J.E., 1996. Bimodal interaction of coatomer with the p24 family of putative cargo receptors. Science 273, 1396–9. doi:10.1126/science.273.5280.1396

Foley, N.H., Bray, I., Watters, K.M., Das, S., Bernas, T., Prehn, J.H.M., Stallings, R.L., 2012. NIH Public Access. Cell 18, 1089–1098. doi:10.1038/cdd.2010.172.MicroRNAs

Fromme, J.C., Ravazzola, M., Hamamoto, S., Al-balwi, M., Eyaid, W., Boyadjiev, S. a, Cosson, P., Schekman, R., 2008. NIH Public Access 13, 623–634. doi:10.1016/j.devcel.2007.10.005.The

Fujiwara, T., Dehart, D.B., Sulik, K.K., Hogan, B.L.M., 2002. Distinct requirements for extra-embryonic and embryonic bone morphogenetic protein 4 in the formation of the node and primitive streak and coordination of left-right asymmetry in the mouse. Development 129, 4685–4696.

Füllekrug, J., Suganuma, T., Tang, B.L., Hong, W., Storrie, B., Nilsson, T., 1999. Localization and recycling of gp27 (hp24gamma3): complex formation with other p24 family members. Mol. Biol. Cell 10, 1939–1955.

Galceran, J., Farin, I., Depew, M.J., Clevers, H., Grosschedl, R., 1999. deficiency in Lef1 − / − Tcf1 − / − mice 709–717.

Galceran, J., Hsu, S.C., Grosschedl, R., 2001. Rescue of a Wnt mutation by an activated form of LEF-1: regulation of maintenance but not initiation of Brachyury expression. Proc. Natl. Acad. Sci. U. S. A. 98, 8668–73. doi:10.1073/pnas.151258098

Garbes, L., Kim, K., Rieß, A., Hoyer-Kuhn, H., Beleggia, F., Bevot, A., Kim, M.J., Huh, Y.H., Kweon, H.S., Savarirayan, R., Amor, D., Kakadia, P.M., Lindig, T., Kagan, K.O., Becker, J., Boyadjiev, S.A., Wollnik, B., Semler, O., Bohlander, S.K., Kim, J., Netzer, C., 2015. Mutations in SEC24D, encoding a component of the COPII machinery, cause a syndromic form of osteogenesis imperfecta. Am. J. Hum. Genet.

96, 432–439. doi:10.1016/j.ajhg.2015.01.002

Gardner, B.M., Walter, P., 2011. Unfolded Proteins Are Ire1-Activating Ligands That Directly Induce the Unfolded Protein Response. Science (80-.). 333, 1891–1894. doi:10.1126/science.1209126

Gariboldi, M., Manenti, G., Canzian, F., Falvella, F.S., Pierotti, M.A., Porta, G. Della, Binelli, G., Dragani, T.A., 1993. Advances in Brief Chromosome Mapping of Murine Susceptibility Loci to Liver Carcinogenesis 1. Cancer 209–211.

George, E.L., Georges-Labouesse, E.N., Patel-King, R.S., Rayburn, H., Hynes, R.O., 1993. Defects in mesoderm, neural tube and vascular development in mouse embryos lacking fibronectin. Development 119, 1079–91.

Gething, M.J., Sambrook, J., 1992. Protein folding in the cell. Nature 355, 33–45. doi:10.1038/355033a0

Gimeno, R.E., Espenshade, P., Kaiser, C. a, 1996. COPII Coat Subunit Interactions: Sec24p and Sec23p Bind to Adjacent Regions of Secl6p. Mol Biol Cell 7, 1815–1823.

Go, G., Srivastava, R., Mani, A., 2014. NIH Public Access. cell metab 37, 651–663. doi:10.1080/15374410802148095.The

Goepfert, P.A., Shaw, K.L., Ritter, G.D., Mulligan, M.J., 1997. A sorting motif localizes the foamy virus glycoprotein to the endoplasmic reticulum. J Virol 71, 778–84.

Goldberg, J., 2000. Decoding of Sorting Signals by Coatomer through a GTPase Switch in the COPI Coat Complex 100, 671–679.

Gommel, D., Orci, L., Emig, E.M., Hannah, M.J., Ravazzola, M., Nickel, W., Helms, J.B., Wieland, F.T., Sohn, K., 1999. p24 and p23, the major transmembrane proteins of COPI-coated transport vesicles, form hetero-oligomeric complexes and cycle between the organelles of the early secretory pathway. FEBS Lett. 447, 179–185. doi:10.1016/S0014-5793(99)00246-X

Goopaster, B.H., DeLany, J.P., Otto, A.D., Kuller, L., Vockley, J., South-Paul, J.E., Thomas, S.B., Brown, J., McTigue, K., Hames, K.C., Lang, W., Jakicic, J.M., 2010. Effects of Diet and Physical Activity Interventions on Weight Loss and Cardiometabolic Risk Factors in Severely Obese Adults: A Randomized Trial 304, 1795–1802. doi:10.1001/jama.2010.1505.Effects

Greco, M., Chiappetta, A., Bruno, L., Bitonti, M.B., 2012. In Posidonia oceanica cadmium induces changes in DNA methylation and chromatin patterning. J. Exp. Bot. 63, 695–709. doi:10.1093/jxb/err313

Grigsby, P.L., 2016. Animal Models to Study Placental Development and Function throughout Normal and Dysfunctional Human Pregnancy. Semin. Reprod. Med. 34, 11–16. doi:10.1055/s-0035-1570031

Grootjans, J., Kaser, A., Kaufman, R.J., Blumberg, R.S., 2016. The unfolded protein response in immunity and inflammation. Nat. Rev. Immunol. 16, 469–484.

doi:10.1038/nri.2016.62

Guillemot, F., Nagy, a, Auerbach, a, Rossant, J., Joyner, a L., 1994. Essential role of Mash-2 in extraembryonic development. Nature. doi:10.1038/371333a0

Gupta, I.R., Lapointe, M., Yu, O.H., 2003. Morphogenesis during mouse embryonic kidney explant culture. Kidney Int. 63, 365–76. doi:10.1046/j.1523-1755.2003.00715.x

Gupta, S., Fahiminiya, S., Wang, T., Dempsey Nunez, L., Rosenblatt, D.S., Gibson, W.T., Gilfix, B., Bergeron, J.J.M., Jerome-Majewska, L.A., 2016. Somatic overgrowth associated with homozygous mutations in both *MAN1B1* and *SEC23A*. Mol. Case Stud. 2, a000737. doi:10.1101/mcs.a000737

Gurtner, G.C., Davis, V., Li, H., McCoy, M.J., Sharpe, a, Cybulsky, M.I., 1995. Targeted disruption of the murine VCAM1 gene: essential role of VCAM-1 in chorioallantoic fusion and placentation. Genes Dev. 9, 1–14. doi:10.1101/gad.9.1.1

Hadjantonakis, A.-K., Papaioannou, V.E., 2004. Dynamic in vivo imaging and cell tracking using a histone fluorescent protein fusion in mice. BMC Biotechnol. 4, 33. doi:10.1186/1472-6750-4-33

Harding, H.P., Zhang, Y., Ron, D., 1999. Protein translation and folding are coupled by an endoplasmic-reticulum-resident kinase. Nature 397, 271–274. doi:10.1038/16729

Harding, H.P., Zhang, Y., Zeng, H., Novoa, I., Lu, P.D., Calfon, M., Sadri, N., Yun, C., Popko, B., Paules, R., Stojdl, D.F., Bell, J.C., Hettmann, T., Leiden, J.M., Ron, D., 2003. An integrated stress response regulates amino acid metabolism and resistance to oxidative stress. Mol. Cell 11, 619–633. doi:10.1016/S1097-2765(03)00105-9

Hasegawa, H., Liu, L., Nishimura, M., 2010. Dilysine retrieval signal-containing p24 proteins collaborate in inhibiting ??-cleavage of amyloid precursor protein. J. Neurochem. 115, 771–781. doi:10.1111/j.1471-4159.2010.06977.x

Haze, K., Okada, T., Yoshida, H., Yanagi, H., Yura, T., Negishi, M., Mori, K., 2001. Identification of the G13 (cAMP-response-element-binding protein-related protein) gene product related to activating transcription factor 6 as a transcriptional activator of the mammalian unfolded protein response. Biochem. J. 355, 19–28. doi:10.1042/0264-6021:3550019

Heidelbaugh, J.J., Bruderly, M., 2006. Cirrhosis and chronic liver failure: Part I. Diagnosis and evaluation. Am. Fam. Physician 74.

Henkel, A., Green, R.M., 2013. The unfolded protein response in fatty liver disease. Semin. Liver Dis. 33, 321–329. doi:10.1055/s-0033-1358522

Hernandez-Verdun, D., Legrand, C., 1975. In vitro study of chorionic and ectoplacental trophoblast differentiation in the mouse. J. Embryol. Exp. Morphol. 34, 633–644.

Hetz, C., Glimcher, L.H., 2009. Fine-tuning of the unfolded protein response: Assembling the IRE1alpha interactome. Mol. Cell 35, 551–61. doi:10.1016/j.molcel.2009.08.021

Hitz, C., Vogt-Weisenhorn, D., Ruiz, P., Wurst, W., Floss, T., 2005. Progressive loss of the spongiotrophoblast layer of Birc6/Bruce mutants results in embryonic lethality. Genesis 42, 91–103. doi:10.1002/gene.20128

Horton, A.C., Ehlers, M.D., 2003. Dual modes of endoplasmic reticulum-to-Golgi transport in dendrites revealed by live-cell imaging. J. Neurosci. 23, 6188–6199. doi:23/15/6188 [pii]

Hosaka, M., Watanabe, T., Yamauchi, Y., Sakai, Y., Suda, M., Mizutani, S., Takeuchi, T., Isobe, T., Izumi, T., 2007. A subset of p23 localized on secretory granules in pancreatic beta-cells. J. Histochem. Cytochem. 55, 235–45. doi:10.1369/jhc.6A7093.2006

Hou, W., Sarikaya, D.P., Jerome-Majewska, L.A., 2016. Ex vivo culture of pre-placental tissues reveals that the allantois is required for maintained expression of Gcm1 and Tpbpα. Placenta 47, 12–23. doi:10.1016/j.placenta.2016.08.091

Hritz, I., Mandrekar, P., Velayudham, A., Catalano, D., Dolganiuc, A., Kodys, K., Kurt-Jones, E., Szabo, G., 2008. The critical role of toll-like receptor (TLR) 4 in alcoholic liver disease is independent of the common TLR adapter MyD88. Hepatology 48, 1224–1231. doi:10.1002/hep.22470

Hsia, K.-C., Hoelz, A., 2010. Crystal structure of alpha-COP in complex with epsilon-COP provides insight into the architecture of the COPI vesicular coat. Proc. Natl. Acad. Sci. U. S. A. 107, 11271–6. doi:10.1073/pnas.1006297107

Hu, D., Cross, J.C., 2010. Development and function of trophoblast giant cells in the rodent placenta. Int. J. Dev. Biol. 54, 341–354. doi:10.1387/ijdb.082768dh

Huang, M., Weissman, J.T., Béraud-Dufour, S., Luan, P., Wang, C., Chen, W., Aridor, M., Wilson, I.A., Balch, W.E., 2001. Crystal structure of Sar1-GDP at 1.7 ?? resolution and the role of the NH2 terminus in ER export. J. Cell Biol. 155, 937–948. doi:10.1083/jcb.200106039

Hübscher, S.G., 2006. Histological assessment of non-alcoholic fatty liver disease. Histopathology 49, 450–65. doi:10.1111/j.1365-2559.2006.02416.x

Hunter, P.J., Swanson, B.J., Haendel, M. a, Lyons, G.E., Cross, J.C., 1999. Mrj encodes a DnaJ-related co-chaperone that is essential for murine placental development. Development 126, 1247–58.

Inman, K.E., Downs, K.M., 2006. Brachyury is required for elongation and vasculogenesis in the murine allantois. Development 133, 2947–2959. doi:10.1242/dev.02454

Ishikawa, T., Okada, T., Ishikawa-Fujiwara, T., Todo, T., Kamei, Y., Shigenobu, S., Tanaka, M., Saito, T.L., Yoshimura, J., Morishita, S., Toyoda, A., Sakaki, Y., Taniguchi, Y., Takeda, S., Mori, K., 2013. ATF6α/β-mediated adjustment of ER chaperone levels is essential for development of the notochord in medaka fish. Mol. Biol. Cell 24, 1387–95. doi:10.1091/mbc.E12-11-0830

Itin, C., Roche, A.-C.C., Monsigny, M., Hauri, H.-P.P., 1996. ERGIC-53 Is a Functional

Mannose-selective and Calcium-dependent Human Homologue of Leguminous Lectins. Mol. Biol. Cell 7, 483–493.

Itin, C., Schindler, R., Hauri, H., 1995. Targeting of Protein ERGIC-53 to the ER / ERGIC / cis-Golffl Recycling Pathway. J. Cell Biol. 131, 57–67.

Iwawaki, T., Akai, R., Yamanaka, S., Kohno, K., 2009. Function of IRE1 alpha in the placenta is essential for placental development and embryonic viability. Proc. Natl. Acad. Sci. 106, 16657–16662. doi:10.1073/pnas.0903775106

Izumi, K., Brett, M., Nishi, E., Drunat, S., Tan, E.S., Fujiki, K., Lebon, S., Cham, B., Masuda, K., Arakawa, M., Jacquinet, A., Yamazumi, Y., Chen, S.T., Verloes, A., Okada, Y., Katou, Y., Nakamura, T., Akiyama, T., Gressens, P., Foo, R., Passemard, S., Tan, E.C., El Ghouzzi, V., Shirahige, K., 2016. ARCN1 Mutations Cause a Recognizable Craniofacial Syndrome Due to COPI-Mediated Transport Defects. Am. J. Hum. Genet. 99, 451–459. doi:10.1016/j.ajhg.2016.06.011

Jackson, L.P., 2014. Structure and mechanism of COPI vesicle biogenesis. Curr. Opin. Cell Biol. 29, 67–73. doi:10.1016/j.ceb.2014.04.009

Jenkins, C.M., Mancuso, D.J., Yan, W., Sims, H.F., Gibson, B., Gross, R.W., 2004. Identification, cloning, expression, and purification of three novel human calcium-independent phospholipase A2 family members possessing triacylglycerol lipase and acylglycerol transacylase activities. J. Biol. Chem. 279, 48968–48975. doi:10.1074/jbc.M407841200

Jenne, N., Frey, K., Br??gger, B., Wieland, F.T., 2002. Oligomeric state and stoichiometry of p24 proteins in the early secretory pathway. J. Biol. Chem. 277, 46504–46511. doi:10.1074/jbc.M206989200

Jerome-Majewska, L. a, Achkar, T., Luo, L., Lupu, F., Lacy, E., 2010. The trafficking protein Tmed2/p24beta(1) is required for morphogenesis of the mouse embryo and placenta. Dev. Biol. 341, 154–66. doi:10.1016/j.ydbio.2010.02.019

Ji, C., Kaplowitz, N., 2004. Hyperhomocysteinemia, endoplasmic reticulum stress, and alcoholic liver injury. World J. Gastroenterol. 10, 1699–1708. doi:10.3748/wjg.v10.i12.1699

Jones, B., Jones, E.L., Bonney, S.A., Patel, H.N., Mensenkamp, A.R., Eichenbaum-Voline, S., Rudling, M., Myrdal, U., Annesi, G., Naik, S., Meadows, N., Quattrone, A., Islam, S.A., Naoumova, R.P., Angelin, B., Infante, R., Levy, E., Roy, C.C., Freemont, P.S., Scott, J., Shoulders, C.C., 2003. Mutations in a Sar1 GTPase of COPII vesicles are associated with lipid absorption disorders. Nat. Genet. 34, 29–31. doi:10.1038/ng1145

Kadowaki, H., Nishitoh, H., 2013. Signaling pathways from the endoplasmic reticulum and their roles in disease. Genes (Basel). 4, 306–333. doi:10.3390/genes4030306

Kaiser, C.A., Schekman, R., 1990. Distinct sets of SEC genes govern transport vesicle formation and fusion early in the secretory pathway. Cell 61, 723–733. doi:10.1016/0092-8674(90)90483-U

Kappeler, F., Klopfenstein, D.R.C., Foguet, M., Paccaud, J.-P., Hauri, H.-P., 1997. The Recycling of ERGIC-53 in the Early Secretory Pathway. J. Biol. Chem. 272, 31801–31808. doi:10.1074/jbc.272.50.31801

Kaser, S., Moschen, A., Cayon, A., Kaser, A., Crespo, J., Pons-Romero, F., Ebenbichler, C.F., Patsch, J.R., Tilg, H., 2005. Adiponectin and its receptors in non-alcoholic steatohepatitis. Gut 54, 117–21. doi:10.1136/gut.2003.037010

Katsanou, V., Milatos, S., Yiakouvaki, A., Sgantzis, N., Kotsoni, A., Alexiou, M., Harokopos, V., Aidinis, V., Hemberger, M., Kontoyiannis, D.L., 2009. The RNA-binding protein Elavl1/HuR is essential for placental branching morphogenesis and embryonic development. Mol. Cell. Biol. 29, 2762–2776. doi:10.1128/MCB.01393-08

Kelly, B.T., Owen, D.J., 2011. Endocytic sorting of transmembrane protein cargo. Curr. Opin. Cell Biol. 23, 404–412. doi:10.1016/j.ceb.2011.03.004

Kim, D., Kim, W.R., 2017. Nonobese Fatty Liver Disease. Clin. Gastroenterol. Hepatol. 15, 474–485. doi:10.1016/j.cgh.2016.08.028

Kimberly, I., Downs, K.M., 2007. The Murine Allantois: Emerging Paradigms in Development of the Mammalian Umbilical Cord and Its Relation to the Fetus. Genesis 45, 418–426. doi:10.1002/dvg

Kleiner, D.E., Brunt, E.M., Van Natta, M., Behling, C., Contos, M.J., Cummings, O.W., Ferrell, L.D., Liu, Y.C., Torbenson, M.S., Unalp-Arida, A., Yeh, M., McCullough, A.J., Sanyal, A.J., 2005. Design and validation of a histological scoring system for nonalcoholic fatty liver disease. Hepatology 41, 1313–1321. doi:10.1002/hep.20701

Kumar, A.G., Dai, X.Y., Kozak, C.A., Mims, M.P., Gotto, A.M., Ballantyne, C.M., 1994. Murine VCAM-1. Molecular cloning, mapping, and analysis of a truncated form. J Immunol 153, 4088–4098.

Kung, L.F., Pagant, S., Futai, E., D'Arcangelo, J.G., Buchanan, R., Dittmar, J.C., Reid, R.J.D., Rothstein, R., Hamamoto, S., Snapp, E.L., Schekman, R., Miller, E.A., Antonny, B., Madden, D., Hamamoto, S., Orci, L., Schekman, R., Barlowe, C., Orci, L., Yeung, T., Hosobuchi, M., Hamamoto, S., Salama, N., Rexach, M., Ravazzola, M., Amherdt, M., Schekman, R., Beilharz, T., Egan, B., Silver, P., Hofmann, K., Lithgow, T., Bhattacharyya, D., Glick, B., Bi, X., Corpina, R., Goldberg, J., Bi, X., Mancias, J., Goldberg, J., Bielli, A., Haney, C., Gabreski, G., Watkins, S., Bannykh, S., Aridor, M., Bonifacino, J., Glick, B., Cai, H., Yu, S., Menon, S., Cai, Y., Lazarova, D., Fu, C., Reinisch, K., Hay, J., Ferro-Novick, S., Dittmar, J., Reid, R., Rothstein, R., Ellenberg, J., Siggia, E., Moreira, J., Smith, C., Presley, J., Worman, H., Lippincott-Schwartz, J., Espenshade, P., Gimeno, R., Holzmacher, E., Teung, P., Kaiser, C., Farhan, H., Reiterer, V., Korkhov, V., Schmid, J., Freissmuth, M., Sitte, H., Futai, E., Hamamoto, S., Orci, L., Schekman, R., Gimeno, R., Espenshade, P., Kaiser, C., Gimeno, R., Espenshade, P., Kaiser, C., Gyuris, J., Golemis, E., Chertkov, H., Brent, R., Hughes, H., Budnik, A., Schmidt, K., Palmer, K., Mantell, J., Noakes, C., Johnson, A., Carter, D., Verkade, P., Watson, P., Stephens, D., Iinuma, T., Shiga, A., Nakamoto, K., O′Brien, M., Aridor, M., Arimitsu, N., Tagaya,

M., Tani, K., Ivan, V., Voer, G. de, Xanthakis, D., Spoorendonk, K., Kondylis, V., Rabouille, C., Kaiser, C., Schekman, R., Kirchhausen, T., Kodera, C., Yorimitsu, T., Nakano, A., Sato, K., Kroll, E., Hyland, K., Hieter, P., Li, J., Kuehn, M., Herrmann, J., Schekman, R., Kurihara, T., Hamamoto, S., Gimeno, R., Kaiser, C., Schekman, R., Yoshihisa, T., Lai, C., Aronson, D., Snapp, E., Lee, M., Hamamoto, S., Schekman, R., Lee, M., Orci, L., Hamamoto, S., Futai, E., Ravazzola, M., Schekman, R., Long, K., Yamamoto, Y., Baker, A., Watkins, S., Coyne, C., Conway, J., Aridor, M., Lord, C., Bhandari, D., Menon, S., Ghassemian, M., Nycz, D., Hay, J., Ghosh, P., Ferro-Novick, S., Malhotra, V., Erlmann, P., Mancias, J., Goldberg, J., Matsuoka, K., Orci, L., Amherdt, M., Bednarek, S., Hamamoto, S., Schekman, R., Yeung, T., Miller, E., Antonny, B., Hamamoto, S., Schekman, R., Miller, E., Barlowe, C., Miller, E., Beilharz, T., Malkus, P., Lee, M., Hamamoto, S., Orci, L., Schekman, R., Miller, E., Liu, Y., Barlowe, C., Schekman, R., Mossessova, E., Bickford, L., Goldberg, J., Mumberg, D., Muller, R., Funk, M., Pagant, S., Kung, L., Dorrington, M., Lee, M., Miller, E., Parlati, F., McNew, J., Fukuda, R., Miller, R., Sollner, T., Rothman, J., Pucadyil, T., Schmid, S., Reid, R., Gonzalez-Barrera, S., Sunjevaric, I., Alvaro, D., Ciccone, S., Wagner, M., Rothstein, R., Rexach, M., Schekman, R., Saito, Y., Yamanushi, T., Oka, T., Nakano, A., Saito-Nakano, Y., Nakano, A., Sato, K., Nakano, A., Schuldiner, M., Collins, S., Thompson, N., Denic, V., Bhamidipati, A., Punna, T., Ihmels, J., Andrews, B., Boone, C., Greenblatt, J., Weissman, J., Krogan, N., Settles, E., Loftus, A., McKeown, A., Parthasarathy, R., Shaywitz, D., Espenshade, P., Gimeno, R., Kaiser, C., Sikorski, R., Hieter, P., Snapp, E., Hegde, R., Francolini, M., Lombardo, F., Colombo, S., Pedrazzini, E., Borgese, N., Lippincott-Schwartz, J., Springer, S., Schekman, R., Springer, S., Spang, A., Schekman, R., Stagg, S., LaPointe, P., Balch, W., Supek, F., Madden, D., Hamamoto, S., Orci, L., Schekman, R., Tabata, K., Sato, K., Ide, T., Nishizaka, T., Nakano, A., Noji, H., Watson, P., Townley, A., Koka, P., Palmer, K., Stephens, D., Whittle, J., Schwartz, T., Witte, K., Schuh, A., Hegermann, J., Sarkeshik, A., Mayers, J., Schwarze, K., Yates, J., Eimer, S., Audhya, A., Yoshihisa, T., Barlowe, C., Schekman, R., Zacharogianni, M., Kondylis, V., Tang, Y., Farhan, H., Xanthakis, D., Fuchs, F., Boutros, M., Rabouille, C., 2012. Sec24p and Sec16p cooperate to regulate the GTP cycle of the COPII coat. EMBO J. 31, 1014–1027. doi:10.1038/emboj.2011.444

Kwee, L., Baldwin, H.S., Shen, H.M., Stewart, C.L., Buck, C., Buck, C. a, Labow, M. a, 1995. Defective development of the embryonic and extraembryonic circulatory systems in vascular cell adhesion molecule (VCAM-1) deficient mice. Development 121, 489–503.

Lang, M.R., Lapierre, L. a, Frotscher, M., Goldenring, J.R., Knapik, E.W., 2006. Secretory COPII coat component Sec23a is essential for craniofacial chondrocyte maturation. Nat. Genet. 38, 1198–1203. doi:10.1038/ng1880

Lange, P.S., Chavez, J.C., Pinto, J.T., Coppola, G., Sun, C., Townes, T.M., Geschwind, D.H., Ratan, R.R., 2008. ATF4 is an oxidative stress-inducible, prodeath transcription factor in neurons in vitro and in vivo. J. Exp. Med. 205, 1227–1242. doi:10.1084/jem.20071460

Langer, J.D., Roth, C.M., Béthune, J., Stoops, E.H., Brügger, B., Herten, D.P., Wieland, F.T., 2008. A conformational change in the α-subunit of coatomer induced by ligand binding to γ-COP revealed by single-pair FRET. Traffic 9, 597–607. doi:10.1111/j.1600-0854.2007.00697.x

Langhans, M., Marcote, M.J., Pimpl, P., Virgili-López, G., Robinson, D.G., Aniento, F., 2008. In vivo trafficking and localization of p24 proteins in plant cells. Traffic 9, 770–785. doi:10.1111/j.1600-0854.2008.00719.x

Lanoix, J., Ouwendijk, J., Stark, A., Szafer, E., Cassel, D., Dejgaard, K., Weiss, M., Nilsson, T., 2001. Sorting of Golgi resident proteins into different subpopulations of COPI vesicles: A role for ArfGAP1. J. Cell Biol. 155, 1199–1212. doi:10.1083/jcb.200108017

Lauressergues, E., Bert, E., Duriez, P., Hum, D., Majd, Z., Staels, B., Cussac, D., 2012. Does endoplasmic reticulum stress participate in APD-induced hepatic metabolic dysregulation? Neuropharmacology 62, 784–796. doi:10.1016/j.neuropharm.2011.08.048

Lavoie, C., Paiement, J., Dominguez, M., Roy, L., Dahan, S., Gushue, J.N., Bergeron, J.J.M., 1999. Roles for ??2p24 and COPI in endoplasmic reticulum cargo exit site formation. J. Cell Biol. 146, 285–299. doi:10.1083/jcb.146.2.285

Le, T.H., Caldwell, S.H., Redick, J.A., Sheppard, B.L., Davis, C.A., Arseneau, K.O., Iezzoni, J.C., Hespenheide, E.E., Al-Osaimi, A., Peterson, T.C., 2004. The Zonal Distribution of Megamitochondria with Crystalline Inclusions in Nonalcoholic Steatohepatitis. Hepatology 39, 1423–1429. doi:10.1002/hep.20202

Leamy, A.K., Egnatchik, R.A., Young, J.D., 2013. Molecular mechanisms and the role of saturated fatty acids in the progression of non-alcoholic fatty liver disease. Prog. Lipid Res. 52, 165–174. doi:10.1016/j.plipres.2012.10.004

Lechleider, R.J., Ryan, J.L., Garrett, L., Eng, C., Deng, C., Wynshaw-Boris, A., Roberts, A.B., 2001. Targeted Mutagenesis of Smad1 Reveals an Essential Role in Chorioallantoic Fusion. Dev. Biol. 240, 157–167. doi:10.1006/dbio.2001.0469

Lee, A., Scapa, E., Cohen, D., Glimcher, L., 2008. Regulation of hepatic lipogenesis by the transcription factor XBP1. Science (80-.). 320, 1492–1496. doi:10.1126/science.1158042.Regulation

Lee, J.S., Mendez, R., Heng, H.H., Yang, Z.Q., Zhang, K., 2012. Pharmacological ER stress promotes hepatic lipogenesis and lipid droplet formation. Am. J. Transl. Res. 4, 102–113.

Lee, M.C.S., Miller, E.A., Goldberg, J., Orci, L., Schekman, R., 2004. Bi-Directional Protein Transport Between the Er and Golgi. Annu. Rev. Cell Dev. Biol. 20, 87–123. doi:10.1146/annurev.cellbio.20.010403.105307

Lee, M.C.S., Orci, L., Hamamoto, S., Futai, E., Ravazzola, M., Schekman, R., 2005. Sar1p N-terminal helix initiates membrane curvature and completes the fission of a COPII vesicle. Cell 122, 605–617. doi:10.1016/j.cell.2005.07.025

Letourneur, F., Gaynor, E.C., Hennecke, S., Démollière, C., Duden, R., Emr, S.D., Riezman, H., Cosson, P., 1994. Coatomer is essential for retrieval of dilysine-tagged proteins to the endoplasmic reticulum. Cell 79, 1199–1207. doi:10.1016/0092-8674(94)90011-6

Lewis, M.J., Pelham, H.R., 1990. A human homologue of the yeast HDEL receptor. Nature 348, 162–163. doi:10.1038/348162a0

Li, H., Meng, Q., Xiao, F., Chen, S., Du, Y., Yu, J., Wang, C., Guo, F., 2011. ATF4 deficiency protects mice from high-carbohydrate-diet-induced liver steatosis. Biochem. J. 438, 283–9. doi:10.1042/BJ20110263

Li, X., Wu, Y., Shen, C., Belenkaya, T.Y., Ray, L., Lin, X., 2015. Drosophila p24 and Sec22 regulate Wingless trafficking in the early secretory pathway. Biochem. Biophys. Res. Commun. 463, 483–9. doi:10.1016/j.bbrc.2015.04.151

Liao, F., Xu, H., Torrey, N., Road, P., Jolla, L., 2015. HHS Public Access 2, 483–489. doi:10.1126/scisignal.274pe36.Insulin

Liaunardy-Jopeace, A., Bryant, C.E., Gay, N.J., 2014. The COP II adaptor protein TMED7 is required to initiate and mediate the delivery of TLR4 to the plasma membrane. Sci. Signal. 7, ra70-ra70. doi:10.1126/scisignal.2005275

Loftus, A.F., Hsieh, V.L., Parthasarathy, R., 2012. Modulation of membrane rigidity by the human vesicle trafficking proteins Sar1A and Sar1B. Biochem. Biophys. Res.

Long, K.R., Yamamoto, Y., Baker, A.L., Watkins, S.C., Coyne, C.B., Conway, J.F., Aridor, M., 2010. Sar1 assembly regulates membrane constriction and ER export. J. Cell Biol. 190, 115–128. doi:10.1083/jcb.201004132

Lontok, E., Corse, E., Machamer, C.E., 2004. Intracellular targeting signals contribute to localization of coronavirus spike proteins near the virus assembly site. J. Virol. 78, 5913–22. doi:10.1128/JVI.78.11.5913-5922.2004

Louis, S., Loomba, R., Jolla, L., Natta, M.L. Van, Abdelmalek, M.F., Dasarathy, S., 2016. HHS Public Access 385, 956–965. doi:10.1016/S0140-6736(14)61933-4.Farnesoid

Lowe, M., Kreis, T.E., 1995. In vitro assembly and disassembly of coatomer. J Biol Chem 270, 31364–71. doi:10.1074/jbc.270.52.31364

Lu, J., Zhang, S., Nakano, H., Simmons, D.G., Wang, S., Kong, S., Wang, Q., Shen, L., Tu, Z., Wang, W., Wang, B., Wang, H., Wang, Y., van Es, J.H., Clevers, H., Leone, G., Cross, J.C., Wang, H., 2013. A positive feedback loop involving gcm1 and fzd5 directs chorionic branching morphogenesis in the placenta. PLoS Biol. 11, e1001536. doi:10.1371/journal.pbio.1001536

Luo, J., Sladek, R., Bader, J.A., Matthyssen, A., Rossant, J., Giguere, V., 1997. Placental abnormalities in mouse embryos lacking the orphan nuclear receptor ERR-beta. Nature 388, 778–782. doi:10.1038/42022

Luo, W., Wang, Y., Reiser, G., 2007. p24A, a type I transmembrane protein, controls

ARF1-dependent resensitization of protease-activated receptor-2 by influence on receptor trafficking. J. Biol. Chem. 282, 30246–30255. doi:10.1074/jbc.M703205200

Luo, W., Wang, Y., Reiser, G., 2011. Proteinase-activated receptors, nucleotide P2Y receptors, and μ-opioid receptor-1B are under the control of the type I transmembrane proteins p23 and p24A in post-Golgi trafficking. J. Neurochem. 117, 71–81. doi:10.1111/j.1471-4159.2011.07173.x

Luyendyk, J.P., Sullivan, B.P., Guo, G.L., Wang, R., 2010. Tissue factor-deficiency and protease activated receptor-1-deficiency reduce inflammation elicited by diet-induced steatohepatitis in mice. Am J Pathol 176, 177–86. doi:10.2353/ajpath.2010.090672

Ma, W., Goldberg, J., 2013. Rules for the recognition of dilysine retrieval motifs by coatomer. EMBO J. 32, 926–37. doi:10.1038/emboj.2013.41

Ma, Y., Brewer, J.W., Alan Diehl, J., Hendershot, L.M., 2002. Two distinct stress signaling pathways converge upon the CHOP promoter during the mammalian unfolded protein response. J. Mol. Biol. 318, 1351–1365. doi:10.1016/S0022-2836(02)00234-6

Ma, Y., Hendershot, L.M., 2004. ER chaperone functions during normal and stress conditions. J. Chem. Neuroanat. 28, 51–65. doi:10.1016/j.jchemneu.2003.08.007

Madan, A.K., Weldon, C.B., Long, W.P., Johnson, D., Raafat, A., 2004. Solid and Papillary Epithelial Neoplasm of the Pancreas. J. Surg. Oncol. 85, 193–198. doi:10.1002/jso.20019

Mahlapuu, M., Ormestad, M., Enerback, S., Carlsson, P., 2001. The forkhead transcription factor Foxf1 is required for differentiation of extra-embryonic and lateral plate mesoderm. Development 128, 155–166.

Majoul, I., Straub, M., Hell, S.W., Duden, R., Söling, H.D., 2001. KDEL-Cargo Regulates Interactions between Proteins Involved in COPI Vesicle Traffic: Measurements in Living Cells Using FRET. Dev. Cell 1, 139–153. doi:10.1016/S1534-5807(01)00004-1

Malhi, H., Kaufman, R.J., 2011. NIH Public Access. J Hepatol. 54, 795–809. doi:10.1016/j.jhep.2010.11.005.Endoplasmic

Malhotra, J.D., Miao, H., Zhang, K., Wolfson, A., Pennathur, S., Pipe, S.W., Kaufman, R.J., 2008. Antioxidants reduce endoplasmic reticulum stress and improve protein secretion. Proc. Natl. Acad. Sci. 105, 18525–18530. doi:10.1073/pnas.0809677105

Marciniak, S.J., Yun, C.Y., Oyadomari, S., Novoa, I., Zhang, Y., Jungreis, R., Nagata, K., Harding, H.P., Ron, D., 2004. CHOP induces death by promoting protein synthesis and oxidation in the stressed endoplasmic reticulum. Genes Dev. 18, 3066–3077. doi:10.1101/gad.1250704

Marelli, M., Smith, J.J., Jung, S., Yi, E., Nesvizhskii, A.I., Christmas, R.H., Saleem, R.A., Tam, Y.Y.C., Fagarasanu, A., Goodlett, D.R., Aebersold, R., Rachubinski,

R.A., Aitchison, J.D., 2004. Quantitative mass spectrometry reveals a role for the GTPase Rho1p in actin organization on the peroxisome membrane. J. Cell Biol. 167, 1099–112. doi:10.1083/jcb.200404119

Marques, M., Beauchamp, M.-C., Fleury, H., Laskov, I., Qiang, S., Pelmus, M., Provencher, D., Mes-Masson, A.-M., Gotlieb, W.H., Witcher, M., 2015. Chemotherapy reduces PARP1 in cancers of the ovary: implications for future clinical trials involving PARP inhibitors. BMC Med. 13, 217. doi:10.1186/s12916-015-0454-9

Marzioch, M., Henthorn, D.C., Herrmann, J.M., Wilson, R., Thomas, D.Y., Bergeron, J.J.M., Solari, R.C., Rowley, A., 1999. Erp1p and Erp2p, partners for Emp24p and Erv25p in a yeast p24 complex. Mol. Biol. Cell 10, 1923–1938. doi:10.1091/mbc.10.6.1923

Masaki, T., Yoshida, M., Noguchi, S., 1999. Targeted Disruption of CRE-Binding Factor TREB5 Gene Leads to Cellular Necrosis in Cardiac Myocytes at the Embryonic Stage. Biochem. Biophys. Res. Commun. 261, 350–356. doi:10.1006/bbrc.1999.0972

Matsuoka, K., Orci, L., Amherdt, M., Bednarek, S.Y., Hamamoto, S., Schekman, R., Yeung, T., 1998. COPII-coated vesicle formation reconstituted with purified coat proteins and chemically defined liposomes. Cell 93, 263–275. doi:10.1016/S0092-8674(00)81577-9

Matsuoka, K., Schekman, R., Orci, L., Heuser, J.E., 2001. Surface structure of the COPII-coated vesicle. Proc. Natl. Acad. Sci. U. S. A. 98, 13705–9. doi:10.1073/pnas.241522198

Mazzaferro, V., 2007. Results of Liver Transplantation: With or Without Milan Criteria? Vincenzo. Liver Transplant. 13, 465–466. doi:10.1002/lt.

Mazzaferro, V., 2011. Milan Criteria in Liver Transplantation for Hepatocellular Carcinoma: An Evidence-Based Analysis of 15 Years of Experience. Liver Transplant. 13, 465–466. doi:10.1002/lt.

Mazzaferro, V., REGALIA, E., DOCI, R., ANDREOLA, S., PULVIRENTI, A., BOZZETTI, F., MONTALTO, F., AMMATUNA, M., MORABITO, A., GENNARI, L., 1996. Carcinomas in Patients With Cirrhosis. N. Engl. J. Med. 334, 693–699. doi:10.1056/NEJM199603143341104

Mendler, M.H., Kanel, G., Govindarajan, S., 2005. Proposal for a histological scoring and grading system for non-alcoholic fatty liver disease. Liver Int. 25, 294–304. doi:10.1111/j.1478-3231.2005.01052.x

Merte, J., Jensen, D., Wright, K., Sarsfield, S., Wang, Y., Schekman, R., Ginty, D.D., 2010. Sec24b selectively sorts Vangl2 to regulate planar cell polarity during neural tube closure. Nat. Cell Biol. 12, 41-6-8. doi:10.1038/ncb2002

Miller, E.A., Barlowe, C., 2010. Regulation of coat assembly-sorting things out at the ER. Curr. Opin. Cell Biol. 22, 447–453. doi:10.1016/j.ceb.2010.04.003

Miller, E., Antonny, B., Hamamoto, S., Schekman, R., 2002. Cargo selection into COPII vesicles is driven by the Sec24p subunit. EMBO J. 21, 6105–6113. doi:10.1093/emboj/cdf605

Monkley, S.J., Delaney, S.J., Pennisi, D.J., Christiansen, J.H., Wainwright, B.J., 1996. Targeted disruption of the Wnt2 gene results in placentation defects. Development 122, 3343–3353.

Moral, P., Warburton, D., 2010. Mouse Cell Culture 633, 71–79. doi:10.1007/978-1-59745-019-5

Mori, K., 2000. Tripartite Management Minireview of Unfolded Proteins in the Endoplasmic Reticulum Cell 452 Figure 2. Mechanism for ER Stress–Induced Transcriptional Induction in Mammalian Cells. Cell 101, 451–454. doi:10.1016/S0092-8674(00)80855-7

Mossessova, E., Bickford, L.C., Goldberg, J., 2003. SNARE selectivity of the COPII coat. Cell 114, 483–495. doi:10.1016/S0092-8674(03)00608-1

Mould, A., Morgan, M. a J., Li, L., Bikoff, E.K., Robertson, E.J., 2012. Blimp1/Prdm1 governs terminal differentiation of endovascular trophoblast giant cells and defines multipotent progenitors in the developing placenta. Genes Dev. 26, 2063–74. doi:10.1101/gad.199828.112

Moursi, A.M., Globus, R.K., Damsky, C.H., 1997. Interactions between integrin receptors and fibronectin are required for calvarial osteoblast differentiation in vitro. J. Cell Sci. 110, 2187–2196.

Musso, G., Gambino, R., Cassader, M., Pagano, G., 2010. A meta-analysis of randomized trials for the treatment of nonalcoholic fatty liver disease. Hepatology 52, 79–104. doi:10.1002/hep.23623

Nagae, M., Hirata, T., Morita-Matsumoto, K., Theiler, R., Fujita, M., Kinoshita, T., Yamaguchi, Y., 2016. 3D Structure and Interaction of p24?? and p24?? Golgi Dynamics Domains: Implication for p24 Complex Formation and Cargo Transport. J. Mol. Biol. 428, 4087–4099. doi:10.1016/j.jmb.2016.08.023

Naiche, L.A., Papaioannou, V.E., 2003. Loss of Tbx4 blocks hindlimb development and affects vascularization and fusion of the allantois. Development 130, 2681–2693. doi:10.1242/dev.00504

Nakano, A., Brada, D., Schekman, R., 1988. A membrane glycoprotein, Secl2p, required for protein transport from the endoplasmic reticulum to the Golgi apparatus in yeast. J. Cell Biol 107, 851–863.

Nakano, N., Tsuchiya, Y., Kako, K., Umezaki, K., Sano, K., Ikeno, S., Otsuka, E., Shigeta, M., Nakagawa, A., Sakata, N., Itoh, F., Nakano, Y., Iemura, S., van Dinther, M., Natsume, T., ten Dijke, P., Itoh, S., 2017. TMED10 Interferes with TGF-β Signaling by Disrupting TGF-β Receptor Complex Formation, Journal of Biological Chemistry. doi:10.1074/jbc.M116.769109

Nan, Y.-M., Wu, W.-J., Fu, N., Liang, B.-L., Wang, R.-Q., Li, L.-X., Zhao, S.-X., Zhao,

J.-M., Yu, J., 2009. Antioxidants vitamin E and 1-aminobenzotriazole prevent experimental non-alcoholic steatohepatitis in mice. Scand. J. Gastroenterol. 44, 1121–1131. doi:10.1080/00365520903114912

Nichols, W.C., Seligsohn, U., Zivelin, A., Terry, V.H., Hertel, C.E., Wheatley, M.A., Moussalli, M.J., Hauri, H.P., Ciavarella, N., Kaufman, R.J., Ginsburg, D., 1998. Mutations in the ER-Golgi intermediate compartment protein ERGIC-53 cause combined deficiency of coagulation factors V and VIII. Cell 93, 61–70. doi:10.1016/S0092-8674(00)81146-0

Nickel, W., Sohn, K., Bünning, C., Wieland, F.T., 1997. p23, a major COPI-vesicle membrane protein, constitutively cycles through the early secretory pathway. Proc. Natl. Acad. Sci. 94, 11393–11398. doi:10.1073/pnas.94.21.11393

Nishitoh, H., Matsuzawa, A., Tobiume, K., Saegusa, K., Takeda, K., Inoue, K., Hori, S., Kakizuka, A., Ichijo, H., 2002. ASK1 is essential for endoplasmic reticulum stress-induced neuronal cell death triggered by expanded polyglutamine repeats. Genes Dev. 16, 1345–1355. doi:10.1101/gad.992302

North, T.E., De Bruijn, M.F.T.R., Stacy, T., Talebian, L., Lind, E., Robin, C., Binder, M., Dzierzak, E., Speck, N.A., 2002. Runx1 expression marks long-term repopulating hematopoietic stem cells in the midgestation mouse embryo. Immunity 16, 661–672. doi:10.1016/S1074-7613(02)00296-0

Nyfeler, B., Reiterer, V., Wendeler, M.W., Stefan, E., Zhang, B., Michnick, S.W., Hauri, H.P., 2008. Identification of ERGIC-53 as an intracellular transport receptor of α1-antitrypsin. J. Cell Biol. 180, 705–712. doi:10.1083/jcb.200709100

Orci, L., Glick, B.S., Rothman, J.E., 1986. A new type of coated vesicular carrier that appears not to contain clathrin: Its possible role in protein transport within the Golgi stack. Cell 46, 171–184. doi:10.1016/0092-8674(86)90734-8

Orci, L., Ravazzola, M., Meda, P., Holcomb, C., Moore, H.P., Hicke, L., Schekman, R., 1991. Mammalian Sec23p homologue is restricted to the endoplasmic reticulum transitional cytoplasm. Proc. Natl. Acad. Sci. U. S. A. 88, 8611–8615. doi:10.1073/pnas.88.19.8611

Oyadomari, S., Harding, H.P., Zhang, Y., Oyadomari, M., 2009. Mice. Cell 7, 520–532. doi:10.1016/j.cmet.2008.04.011.De-phosphorylation

Ozcan, L., Ergin, A.S., Lu, A., Chung, J., Sarkar, S., Nie, D., Myers, M.G., Ozcan, U., 2009. Endoplasmic Reticulum Stress Plays a Central Role in Development of Leptin Resistance. Cell Metab. 9, 35–51. doi:10.1016/j.cmet.2008.12.004

Paccaud, J.P., Reith, W., Carpentier, J.L., Ravazzola, M., Amherdt, M., Schekman, R., Orci, L., 1996. Cloning and functional characterization of mammalian homologues of the COPII component Sec23. Mol. Biol. Cell 7, 1535–46.

Parr, B.A., Cornish, V.A., Cybulsky, M.I., McMahon, A.P., 2001. Wnt7b Regulates Placental Development in Mice. Dev. Biol. 237, 324–332. doi:10.1006/dbio.2001.0373

Pastor-Cantizano, N., Montesinos, J.C., Bernat-Silvestre, C., Marcote, M.J., Aniento, F., 2015. P24 Family Proteins: Key Players in the Regulation of Trafficking Along the Secretory Pathway. Protoplasma. doi:10.1007/s00709-015-0858-6

Piscione, T.D., Yager, T.D., Gupta, I.R., Grinfeld, B., Pei, Y., Attisano, L., Wrana, J.L., Rosenblum, N.D., 1997. BMP-2 and OP-1 exert direct and opposite effects on renal branching morphogenesis. Am. J. Physiol. 273, F961-75.

Popoff, V., Adolf, F., Brugger, B., Wieland, F., 2011. COPI Budding within the Gogli Stack. Cold Spring Harb. Perspect. Biol. 1–20. doi:10.1101/cshperspect.a005231

Port, F., Hausmann, G., Basler, K., 2011a. A genome-wide RNA interference screen uncovers two p24 proteins as regulators of Wingless secretion. EMBO Rep. 12, 1144–1152. doi:10.1038/embor.2011.165

Port, F., Hausmann, G., Basler, K., 2011b. A genome-wide RNA interference screen uncovers two p24 proteins as regulators of Wingless secretion. EMBO Rep. 1–9. doi:10.1038/embor.2011.165

Pöschl, E., Schlötzer-Schrehardt, U., Brachvogel, B., Saito, K., Ninomiya, Y., Mayer, U., 2004. Collagen IV is essential for basement membrane stability but dispensable for initiation of its assembly during early development. Development 131, 1619–1628. doi:10.1242/dev.01037

Powers, J., Barlowe, C., 2002. Erv14p Directs a Transmembrane Secretory Protein into COPII-coated Transport Vesicles. Mol. Biol. Cell 13, 2170–2179. doi:10.1091/mbc.01

Pradere, J.P., Troeger, J.S., Dapito, D.H., Mencin, A.A., Schwabe, R.F., 2010. Toll-like receptor 4 and hepatic fibrogenesis. Semin. Liver Dis. 30, 232–244. doi:10.1055/s-0030-1255353

Proctor, L.K., Dunk, C., Baczyk, D., Kingdom, J.C.P., Adamson, S.L., 2009. Early gene expression and morphogenesis of the murine chorioallantoic placenta in vivo and in vitro. Placenta 30, 96–104. doi:10.1016/j.placenta.2008.09.014

Promlek, T., Ishiwata-Kimata, Y., Shido, M., Sakuramoto, M., Kohno, K., Kimata, Y., 2011. Membrane aberrancy and unfolded proteins activate the endoplasmic reticulum stress sensor Ire1 in different ways. Mol. Biol. Cell 22, 3520–3532. doi:10.1091/mbc.E11-04-0295

Puri, P., Mirshahi, F., Cheung, O., Natarajan, R., Maher, J.W., Kellum, J.M., Sanyal, A.J., 2008. Activation and Dysregulation of the Unfolded Protein Response in Nonalcoholic Fatty Liver Disease. Gastroenterology 134, 568–576. doi:10.1053/j.gastro.2007.10.039

Rafiullah, R., Aslamkhan, M., Paramasivam, N., Thiel, C., Mustafa, G., Wiemann, S., Schlesner, M., Wade, R.C., Rappold, G.A., Berkel, S., 2015. Homozygous missense mutation in the LMAN2L gene segregates with intellectual disability in a large consanguineous Pakistani family. J. Med. Genet. jmedgenet-2015-103179-. doi:10.1136/jmedgenet-2015-103179

Rahman, S.M., Schroeder-Gloeckler, J.M., Janssen, R.C., Jiang, H., Qadri, I., Maclean, K.N., Friedman, J.E., 2007. CCAAT/enhancing binding protein ?? deletion in mice attenuates inflammation, endoplasmic reticulum stress, and lipid accumulation in diet-induced nonalcoholic steatohepatitis. Hepatology 45, 1108–1117. doi:10.1002/hep.21614

Rai, A., Cross, J.C., 2014. Development of the hemochorial maternal vascular spaces in the placenta through endothelial and vasculogenic mimicry. Dev. Biol. 387, 131–141. doi:10.1016/j.ydbio.2014.01.015

Ramesh, S., Sanyal, A.J., 2005. Evaluation and management of non-alcoholic steatohepatitis. J. Hepatol. 42, 2–12. doi:10.1016/j.jhep.2004.11.022

Raza, A., Sood, G.K., 2014. Hepatocellular carcinoma review: Current treatment, and evidence-based medicine. World J. Gastroenterol. 20, 4115–4127. doi:10.3748/wjg.v20.i15.4115

Reinhard, C., Harter, C., Bremser, M., Brügger, B., Sohn, K., Helms, J.B., Wieland, F., 1999. Receptor-induced polymerization of coatomer. Proc. Natl. Acad. Sci. U. S. A. 96, 1224–1228. doi:10.1073/pnas.96.4.1224

Review T, LaBrecque DR, Abbas Z, Anania F, Ferenci P, Khan AG, Goh KL, Hamid SS, Isakov V, Lizarzabal M, Penaranda MM, Ramos JF, Sarin S, Stimac D, Thomson AB, UmarM, Krabshuis J, L.A., 2014. World Gastroenterology Organisation Global Guidelines: Nonalcoholic Fatty Liver Disease and Nonalcoholic Steatohepatitis. J. Clin. Gastroenterol. 48, 467–473. doi:10.1097/MCG.0000000000000116

Rodenhiser, D.I., Andrews, J., Kennette, W., Sadikovic, B., Mendlowitz, A., Tuck, A.B., Chambers, A.F., 2008. Epigenetic mapping and functional analysis in a breast cancer metastasis model using whole-genome promoter tiling microarrays. Breast Cancer Res. 10, R62. doi:10.1186/bcr2121

Rojo, M., Emery, G., Marjomäki, V., McDowall, a W., Parton, R.G., Gruenberg, J., 2000. The transmembrane protein p23 contributes to the organization of the Golgi apparatus. J. Cell Sci. 113 (Pt 6, 1043–1057.

Rojo, M., Pepperkok, R., Emery, G., Kellner, R., Stang, E., Parton, R.G., Gruenberg, J., 1997. Involvement of the transmembrane protein p23 in biosynthetic protein transport. J. Cell Biol. 139, 1119–1135. doi:10.1083/jcb.139.5.1119

Romero-Gómez, M., Zelber-Sagi, S., Trenell, M., 2017. Treatment of NAFLD with diet, physical activity and exercise. J. Hepatol. xxx. doi:10.1016/j.jhep.2017.05.016

Rossanese, O.W., Soderholm, J., Bevis, B.J., Sears, I.B., O'Connor, J., Williamson, E.K., Glick, B.S., 1999. Golgi structure correlates with transitional endoplasmic reticulum organization in Pichia pastoris and Saccharomyces cerevisiae. J. Cell Biol. 145, 69–81. doi:10.1083/jcb.145.1.69

Rossant, J., Cross, J.C., 2001. Placental development: lessons from mouse mutants. Nat. Rev. Genet. 2, 538–48. doi:10.1038/35080570

Rossant, J., W.Tamura-lis, w., 1981. Effect of culture conditions on diploid to giant-cell

transformation in postimplantation mouse trophoblast. J. Embryol. exp. Morph 62, 217–227.

S.Nahum, N.C.C.M.U., 2004. An update on non-alcoholic fatty liver disease. Invest Clín 56, 72–82. doi:10.1097/01.JAA.0000450801.19545.93

Sanyal, A.J., Campbell-Sargent, C., Mirshahi, F., Rizzo, W.B., Contos, M.J., Sterling, R.K., Luketic, V.A., Shiffman, M.L., Clore, J.N., 2001. Nonalcoholic steatohepatitis: Association of insulin resistance and mitochondrial abnormalities. Gastroenterology 120, 1183–1192. doi:10.1053/gast.2001.23256

Sanyal, A.J., Chalasani, N., Kowdley, K. V., McCullough, A., Diehl, A.M., Bass, N.M., Neuschwander-Tetri, B.A., Lavine, J.E., Tonascia, J., Unalp, A., Van Natta, M., Clark, J., Brunt, E.M., Kleiner, D.E., Hoofnagle, J.H., Robuck, P.R., 2010. Pioglitazone, vitamin E, or placebo for nonalcoholic steatohepatitis. N. Engl. J. Med. 362, 1675–85. doi:10.1056/NEJMoa0907929

Sanyal, A.J., Yoon, S.K., Lencioni, R., 2010. The etiology of hepatocellular carcinoma and consequences for treatment. Oncologist 15 Suppl 4, 14–22. doi:10.1634/theoncologist.2010-S4-14

Saran, S., Tran, D.D.H., Ewald, F., Koch, a, Hoffmann, a, Koch, M., Nashan, B., Tamura, T., 2015. Depletion of three combined THOC5 mRNA export protein target genes synergistically induces human hepatocellular carcinoma cell death. Oncogene 35, 1–8. doi:10.1038/onc.2015.433

Sarmah, S., Barrallo-Gimeno, A., Melville, D.B., Topczewski, J., Solnica-Krezel, L., Knapik, E.W., 2010. Sec24D-dependent transport of extracellular matrix proteins is required for zebrafish skeletal morphogenesis. PLoS One 5. doi:10.1371/journal.pone.0010367

Sato, K., 2004. Synthesis of Polypeptides Methionine by Using a Dicistroviral Entry Site Lacking Internal. J.Biochem 606, 601–606. doi:10.1093/jb/mvh

Sato, K., Nakano, A., 2005. Dissection of COPII subunit-cargo assembly and disassembly kinetics during Sar1p-GTP hydrolysis. Nat. Struct. Mol. Biol. 12, 167–174. doi:10.1038/nsmb893

Satpute-Krishnan, P., Ajinkya, M., Bhat, S., Itakura, E., Hegde, R.S., Lippincott-Schwartz, J., 2014. ER Stress-Induced Clearance of Misfolded GPI-Anchored Proteins via the Secretory Pathway. Cell 158, 522–533. doi:10.1016/j.cell.2014.06.026

Schattenberg, J.M., Singh, R., Wang, Y., Lefkowitch, J.H., Rigoli, R.M., Scherer, P.E., Czaja, M.J., 2006. JNK1 but not JNK2 promotes the development of steatohepatitis in mice. Hepatology 43, 163–172. doi:10.1002/hep.20999

Schekman, R., Rothman, J.E., 2002. Dissecting the membrane trafficking system. Lasker Basic Med. Res. Award. doi:10.1007/s004250050663

Schimmoller, F., Singer-kruger, B., Schroder, S., Kruger, U., Barlowe, C., Riezman, H., 1995. of selected proteins to the Golgi. EMBO J. 14, 1329–1339.

Schröder-Köhne, S., Letourneur, F., Riezman, H., 1998. Alpha-COP can discriminate between distinct, functional di-lysine signals in vitro and regulates access into retrograde transport. J. Cell Sci. 111 (Pt 2, 3459–70.

Schuiki, I., Volchuk, A., 2012. Diverse roles for the p24 family of proteins in eukaryotic cells. Biomol. Concepts 3, 561–570. doi:10.1515/bmc-2012-0028

Selwood, L., Johnson, M.H., 2006. Trophoblast and hypoblast in the monotreme, marsupial and eutherian mammal: Evolution and origins. BioEssays 28, 128–145. doi:10.1002/bies.20360

Seo, J., Fortuno, E.S., Jae, M.S., Stenesen, D., Tang, W., Parks, E.J., Adams, C.M., Townes, T., Graff, J.M., 2009. Atf4 regulates obesity, glucose homeostasis, and energy expenditure. Diabetes 58, 2565–2573. doi:10.2337/db09-0335

Serafini, T., Orci, L., Amherdt, M., Brunner, M., Kahn, R.A., Rothman, J.E., 1991. ADP-ribosylation factor is a subunit of the coat of Golgi-derived COP-coated vesicles: A novel role for a GTP-binding protein. Cell 67, 239–253. doi:10.1016/0092-8674(91)90176-Y

Sha, H., Qi, L., 2009. NIH Public Access 76, 211–220. doi:10.1007/s11103-011-9767-z.Plastid

Shawlot, W., Behringer, R.R., 1995. Requirement for Lim1 in head-organizer function. Nature. doi:10.1038/374425a0

Shimano, H., Shimomura, I., Hammer, R.E., Herz, J., Goldstein, J.L., Brown, M.S., Horton, J.D., 1997. Elevated levels of SREBP-2 and cholesterol synthesis in livers of mice homozygous for a targeted disruption of the SREBP-1 gene. J. Clin. Invest. 100, 2115–2124. doi:10.1172/JCI119746

Simmons, D.G., Cross, J.C., 2005. Determinants of trophoblast lineage and cell subtype specification in the mouse placenta. Dev. Biol. 284, 12–24. doi:10.1016/j.ydbio.2005.05.010

Simmons, D.G., Fortier, A.L., Cross, J.C., 2007. Diverse subtypes and developmental origins of trophoblast giant cells in the mouse placenta. Dev. Biol. 304, 567–78. doi:10.1016/j.ydbio.2007.01.009

Simmons, D.G., Natale, D.R.C., Begay, V., Hughes, M., Leutz, A., Cross, J.C., 2008. Early patterning of the chorion leads to the trilaminar trophoblast cell structure in the placental labyrinth. Development 135, 2083–91. doi:10.1242/dev.020099

Skelly, M.M., James, P.D., Ryder, S.D., 2001. Findings on liver biopsy to investigate abnormal liver function tests in the absence of diagnostic serology. J. Hepatol. 35, 195–199. doi:10.1016/S0168-8278(01)00094-0

Smith, M.H., Ploegh, H.L., Weissman, J.S., 2011. Road to ruin: targeting proteins for degradation in the endoplasmic reticulum. Science 334, 1086–90. doi:10.1126/science.1209235

Sohn, K., Orci, L., Ravazzola, M., Amherdt, M., Bremser, M., Lottspeich, F., Fiedler, K.,

Helms, J.B., Wieland, F.T., 1996. A major transmembrane protein of Golgi-derived COPI-coated vesicles involved in coatomer binding. J. Cell Biol. 135, 1239–1248. doi:10.1083/jcb.135.5.1239

Solloway, M.J., Robertson, E.J., 1999. Early embryonic lethality in Bmp5;Bmp7 double mutant mice suggests functional redundancy within the 60A subgroup. Development 126, 1753–1768.

Song, B., Scheuner, D., Ron, D., Pennathur, S., Kaufman, R.J., 2008. Chop deletion reduces oxidative stress, improves beta cell function, and promotes cell survival in multiple mouse models of diabetes. J. Clin. Invest. 118, 3378–3389. doi:10.1172/JCI34587DS1

Sriburi, R., Bommiasamy, H., Buldak, G.L., Robbins, G.R., Frank, M., Jackowski, S., Brewer, J.W., 2007. Coordinate regulation of phospholipid biosynthesis and secretory pathway gene expression in XBP-1(S)-induced endoplasmic reticulum biogenesis. J. Biol. Chem. 282, 7024–7034. doi:10.1074/jbc.M609490200

Stagg, S.M., LaPointe, P., Razvi, A., Gürkan, C., Potter, C.S., Carragher, B., Balch, W.E., 2008. Structural Basis for Cargo Regulation of COPII Coat Assembly. Cell 134, 474–484. doi:10.1016/j.cell.2008.06.024

Stamnes, M.A., Craighead, M.W., Hoe, M.H., Lampen, N., Geromanos, S., Tempst, P., Rothman, J.E., 1995. An integral membrane component of coatomer-coated transport vesicles defines a family of proteins involved in budding. Proc. Natl. Acad. Sci. U. S. A. 92, 8011–5. doi:10.1073/pnas.92.23.10816

Stamnes, M.A., Craighead, M.W., Hoe, M.H., Lampen, N., Rothman, J.E., Stamnes, M.A., Craighead, M.W., Hoe, M.E.E.H., Lampen, N., Geromanost, S., Temps, P., 1995. An Integral Membrane Component of Coatomer-Coated Transport Vesicles Defines a Family of Proteins Involved in Budding Geromanos , Paul Tempst and James E . Rothman Source : Proceedings of the National Academy of Sciences of the United States of America ,.

Stamnes, M.A., Rothman, J.E., 1993. The binding of AP-1 clathrin adaptor particles to Golgi membranes requires ADP-ribosylation factor, a small GTP-binding protein. Cell 73, 999–1005. doi:10.1016/0092-8674(93)90277-W

Stecca, B., Nait-Oumesmar, B., Kelley, K. a, Voss, A.K., Thomas, T., Lazzarini, R. a, 2002. Gcm1 expression defines three stages of chorio-allantoic interaction during placental development. Mech. Dev.

Steingrimsson, E., Tessarollo, L., Reid, S.W., Jenkins, N.A., Copeland, N.G., 1998. The bHLH-Zip transcription factor Tfeb is essential for placental vascularization. Development 125, 4607–4616.

Strating, J.R.P.M., Hafmans, T.G.M., Martens, G.J.M., 2009a. Functional diversity among p24 subfamily members. Biol. Cell 101, 207–19. doi:10.1042/BC20080075

Strating, J.R.P.M., Martens, G.J.M., 2009a. The p24 family and selective transport processes at the ER-Golgi interface. Biol. Cell 101, 495–509.

doi:10.1042/BC20080233

Strating, J.R.P.M., Martens, G.J.M., 2009b. The p24 family and selective transport processes at the ER-Golgi interface. Biol. Cell 101, 495–509. doi:10.1042/BC20080233

Strating, J.R.P.M., van Bakel, N.H.M., Leunissen, J. a M., Martens, G.J.M., 2009b. A comprehensive overview of the vertebrate p24 family: identification of a novel tissue-specifically expressed member. Mol. Biol. Evol. 26, 1707–14. doi:10.1093/molbev/msp099

Stumpo, D.J., Byrd, N. a, Phillips, R.S., Ghosh, S., Maronpot, R.R., Castranio, T., Meyers, E.N., Mishina, Y., Blackshear, P.J., 2004. Chorioallantoic Fusion Defects and Embryonic Lethality Resulting from Disruption of. Society 24, 6445–6455. doi:10.1128/MCB.24.14.6445

Supek, F., Madden, D.T., Hamamoto, S., Orci, L., Schekman, R., 2002. Sec16p potentiates the action of COPII proteins to bud transport vesicles. J. Cell Biol. 158, 1029–1038. doi:10.1083/jcb.200207053

Tabata, K. V, Sato, K., Ide, T., Nishizaka, T., Nakano, A., Noji, H., 2009. Visualization of cargo concentration by {COPII} minimal machinery in a planar lipid membrane. {Embo} J. 28, 3279–3289. doi:10.1038/emboj.2009.269

Takaki, A., Kawai, D., Yamamoto, K., 2013. Multiple hits, including oxidative stress, as pathogenesis and treatment target in non-alcoholic steatohepatitis (NASH). Int. J. Mol. Sci. 14, 20704–20728. doi:10.3390/ijms141020704

Takida, S., Maeda, Y., Kinoshita, T., Ikezawa, H., Kinoshita, T., Inoue, N., Muniz, M., Nuoffer, C., Hauri, H.P., Riezman, H., Morsomme, P., Prescianotto-Baschong, C., Riezman, H., Morsomme, P., Riezman, H., Carney, G.E., Bowen, N.J., Belden, W.J., Barlowe, C., Dominguez, M., Dejgaard, K., Fullekrug, J., Dahan, S., Fazel, A., Paccaud, J.P., Thomas, D.Y., Bergeron, J.J., Nilsson, T., Fullekrug, J., Suganuma, T., Tang, B.L., Hong, W., Storrie, B., Nilsson, T., Marzioch, M., Henthorn, D.C., Herrmann, J.M., Wilson, R., Thomas, D.Y., Bergeron, J.J., Solari, R.C., Rowley, A., Springer, S., Chen, E., Duden, R., Marzioch, M., Rowley, A., Hamamoto, S., Merchant, S., Schekman, R., Schimmoller, F., Singer-Kruger, B., Schroder, S., Kruger, U., Barlowe, C., Riezman, H., Denzel, A., Otto, F., Girod, A., Pepperkok, R., Watson, R., Rosewell, I., Bergeron, J.J., Solari, R.C., Owen, M.J., Nakamura, N., Inoue, N., Watanabe, R., Takahashi, M., Takeda, J., Stevens, V.L., Kinoshita, T., Urlinger, S., Baron, U., Thellmann, M., Hasan, M.T., Bujard, H., Hillen, W., Tanaka, S., Maeda, Y., Tashima, Y., Kinoshita, T., Tashima, Y., Taguchi, R., Murata, C., Ashida, H., Kinoshita, T., Maeda, Y., Gallione, C.J., Rose, J.K., Low, M.G., Elrod-Erickson, M.J., Kaiser, C.A., Stephens, D.J., Pepperkok, R., Hua, W., Sheff, D., Toomre, D., Mellman, I., Paladino, S., Pocard, T., Catino, M.A., Zurzolo, C., Polishchuk, R., Di Pentima, A., Lippincott-Schwartz, J., 2008. Mammalian GPI-anchored proteins require p24 proteins for their efficient transport from the ER to the plasma membrane. Biochem. J. 409, 555–62. doi:10.1042/BJ20070234

Tam, P.P., 1998. Postimplantation mouse development: whole embryo culture and micro-

manipulation. Int. J. Dev. Biol. 42, 895–902.

Tanaka, M., Gertsenstein, M., Rossant, J., Nagy, A., 1997. Mash2 acts cell autonomously in mouse spongiotrophoblast development. Dev. Biol. 190, 55–65. doi:10.1006/dbio.1997.8685

Tandra, S., Chalasani, N., 2011. NIH Public Access. J. Hepatol. 55, 810–820. doi:10.1016/j.jhep.2010.11.021.Presence

Tanigawa, G., Orci, L., Amherdt, M., Ravazzola, M., Helms, J.B., Rothman, J.E., 1993. Hydrolysis of bound GTP by ARF protein triggers uncoating of golgi-derived COP-coated vesicles. J. Cell Biol. 123, 1365–1371. doi:10.1083/jcb.123.6.1365

Tao, J., Zhu, M., Wang, H., Afelik, S., Vasievich, M.P., Chen, X.-W., Zhu, G., Jensen, J., Ginsburg, D., Zhang, B., 2012. SEC23B is required for the maintenance of murine professional secretory tissues. Proc. Natl. Acad. Sci. 109, E2001–E2009. doi:10.1073/pnas.1209207109

Terry, R.W., Kwee, L., Levine, J.F., Labow, M.A., 1993. Cytokine induction of an alternatively spliced murine vascular cell adhesion molecule (VCAM) mRNA encoding a glycosylphosphatidylinositol-anchored VCAM protein. Proc. Natl. Acad. Sci. U. S. A. 90, 5919–23.

Theiler, R., Fujita, M., Nagae, M., Yamaguchi, Y., Maeda, Y., Kinoshita, T., 2014. The α-helical region in p24γ2 subunit of p24 protein cargo receptor is pivotal for the recognition and transport of glycosylphosphatidylinositol-anchored proteins. J. Biol. Chem. 289, 16835–16843. doi:10.1074/jbc.M114.568311

Thiery, J.P., Sleeman, J.P., 2006. Complex networks orchestrate epithelial–mesenchymal transitions. Nat. Rev. Mol. Cell Biol. 7, 131–142. doi:10.1038/nrm1835

Tian, C., Stokowski, R.P., Kershenobich, D., Ballinger, D.G., Hinds, D.A., 2010. Variant in PNPLA3 is associated with alcoholic liver disease. Nat.Genet. 42, 21–23. doi:10.1038/ng.488

Tilg, H., Moschen, A.R., 2010. Evolution of inflammation in nonalcoholic fatty liver disease: The multiple parallel hits hypothesis. Hepatology 52, 1836–1846. doi:10.1002/hep.24001

Tolman, K.G., Dalpiaz, A.S., 2007. Treatment of non-alcoholic fatty liver disease. Ther. Clin. Risk Manag. 3, 1153–1163. doi:18516264

Torezan-Filho, M.A., Ferreira Alves, V.A., Neto, C.A., Fernandes, H.S., Strauss, E., 2004. Clinical significance of elevated alanine aminotransferase in blood donors: A follow-up study. Liver Int. 24, 575–581. doi:10.1111/j.1478-3231.2004.0970.x

Traub, L.M., 2009. Tickets to ride: selecting cargo for clathrin-regulated internalization. Nat. Rev. Mol. Cell Biol. 10, 583–96. doi:10.1038/nrm2751

Trial, R.P., Zein, C.O., Yerian, L.M., Gogate, P., Lopez, R., Clinic, C., 2012. NIH Public Access 54, 1610–1619. doi:10.1002/hep.24544.Pentoxifylline

Tritarelli, A., Oricchio, E., Ciciarello, M., Mangiacasale, R., Palena, A., Lavia, P., Soddu, S., Cundari, E., 2004. p53 Localization at Centrosomes during Mitosis and Postmitotic Checkpoint Are ATM-dependent and Require Serine 15 Phosphorylation. Mol. Biol. Cell 15, 3751–3737. doi:10.1091/mbc.E03

Ulyanova, T., Scott, L.M., Priestley, G. V., Jiang, Y., Nakamoto, B., Koni, P.A., Papayannopoulou, T., 2005. VCAM-1 expression in adult hematopoietic and nonhematopoietic cells is controlled by tissue-inductive signals and reflects their developmental origin. Blood 106, 86–94. doi:10.1182/blood-2004-09-3417

Urano, F., Bertolotti, a, Ron, D., 2000. IRE1 and efferent signaling from the endoplasmic reticulum. J. Cell Sci. 113 Pt 21, 3697–3702.

Usui, M., Yamaguchi, S., Tanji, Y., Tominaga, R., Ishigaki, Y., Fukumoto, M., Katagiri, H., Mori, K., Oka, Y., Ishihara, H., 2012. Atf6α-null mice are glucose intolerant due to pancreatic β-cell failure on a high-fat diet but partially resistant to diet-induced insulin resistance. Metabolism. 61, 1118–1126. doi:10.1016/j.metabol.2012.01.004

Vainio, P., Mpindi, J.P., Kohonen, P., Fey, V., Mirtti, T., Alanen, K.A., Perälä, M., Kallioniemi, O., Iljin, K., 2012. High-throughput transcriptomic and RNAi analysis identifies AIM1, ERGIC1, TMED3 and TPX2 as potential drug targets in prostate cancer. PLoS One 7. doi:10.1371/journal.pone.0039801

Van Gijssel, H.E., Maassen, C.B.M., Mulder, G.J., Meerman, J.H.N., 1997. P53 Protein Expression By Hepatocarcinogens in the Rat Liver and Its Potential Role in Mitoinhibition of Normal Hepatocytes As a Mechanism of Hepatic Tumour Promotion. Carcinogenesis 18, 1027–1033. doi:10.1093/carcin/18.5.1027

Vandesompele, J., De Preter, K., Pattyn, ilip, Poppe, B., Van Roy, N., De Paepe, A., Speleman, rank, 2002. Accurate normalization of real-time quantitative RT-PCR data by geometric averaging of multiple internal control genes. Genome Biol. 3, 34–1. doi:10.1186/gb-2002-3-7-research0034

Vetrivel, K., Thinakaran, G., 2008. Localization and regional distribution of p23/TMP21 in the brain Kulandaivelu. Neurobiol Dis. 32, 37–49. doi:10.1007/s11103-011-9767-z.Plastid

Wang, C., Huang, Z., Du, Y., Cheng, Y., Chen, S., Guo, F., 2010. ATF4 regulates lipid metabolism and thermogenesis. Cell Res. 20, 174–84. doi:10.1038/cr.2010.4

Wang, X., Yang, R., Jadhao, S.B., Yu, D., Hu, H., Glynn-Cunningham, N., Sztalryd, C., Silver, K.D., Gong, D.-W., 2012. Transmembrane Emp24 Protein Transport Domain 6 is Selectively Expressed in Pancreatic Islets and Implicated in Insulin Secretion and Diabetes. Pancreas 29, 997–1003. doi:10.1016/j.biotechadv.2011.08.021.Secreted

Wansleeben, C., Feitsma, H., Montcouquiol, M., Kroon, C., Cuppen, E., Meijlink, F., 2010. Planar cell polarity defects and defective Vangl2 trafficking in mutants for the COPII gene Sec24b. Development 137, 1067–1073. doi:10.1242/dev.041434

Watkin, L.B., 2015. HHS Public Access. Nat. Genet. 47, 654–660.

doi:10.14440/jbm.2015.54.A

Watson, E.D., Cross, J.C., 2005. Development of structures and transport functions in the mouse placenta. Physiology (Bethesda). 20, 180–93. doi:10.1152/physiol.00001.2005

Weissman, J.T., Plutner, H., Balch, W.E., 2001. The mammalian guanine nucleotide exchange factor mSec12 is essential for activation of the Sar1 GTPase directing endoplasmic reticulum export. Traffic 2, 465–475. doi:10.1034/j.1600-0854.2001.20704.x

Wen, C., Greenwald, I., 1999. p24 proteins and quality control of LIN-12 and GLP-1 trafficking in Caenorhabditis elegans. J. Cell Biol. 145, 1165–1175. doi:10.1083/jcb.145.6.1165

Wendeler, M.W., Paccaud, J.-P., Hauri, H.-P., Appenzeller, C., Andersson, H., Kappeler, F., Hauri, H., Appenzeller-Herzog, C., Hauri, H., Barlowe, C., Barlowe, C., Orci, L., Yeung, T., Hosobuchi, M., Hamamoto, S., Salama, N., Rexach, M., Ravazzola, M., Amherdt, M., Schekman, R., Kappeler, F., Klopfenstein, D., Foguet, M., Paccaud, J., Hauri, H., Kim, J., Hamamoto, S., Ravazzola, M., Orci, L., Schekman, R., Kurihara, T., Hamamoto, S., Gimeno, R., Kaiser, C., Schekman, R., Yoshihisa, T., Lee, M., Miller, E., Goldberg, J., Orci, L., Schekman, R., Miller, E., Beilharz, T., Malkus, P., Lee, M., Hamamoto, S., Orci, L., Schekman, R., Mossessova, E., Bickford, L., Goldberg, J., Nichols, W., Nishimura, N., Balch, W., Nufer, O., Guldbrandsen, S., Degen, M., Kappeler, F., Paccaud, J., Tani, K., Hauri, H., Nufer, O., Kappeler, F., Guldbrandsen, S., Hauri, H., Pagano, A., Letourneur, F., Garcia-Estefania, D., Carpentier, J., Orci, L., Paccaud, J., Peng, R., Antoni, A. De, Gallwitz, D., Shimoni, Y., Kurihara, T., Ravazzola, M., Amherdt, M., Orci, L., Schekman, R., Tang, B., Kausalya, J., Low, D., Lock, M., Hong, W., Vollenweider, F., Kappeler, F., Itin, C., Hauri, H., 2007. Role of Sec24 isoforms in selective export of membrane proteins from the endoplasmic reticulum. EMBO Rep. 8, 258–64. doi:10.1038/sj.embor.7400893

Whittle, J.R.R., Schwartz, T.U., 2010. Structure of the Sec13-Sec16 edge element, a template for assembly of the COPII vesicle coat. J. Cell Biol. 190, 347–361. doi:10.1083/jcb.201003092

Wong, N.S., Anderson, B.O., Khoo, K.S., Ang, P.T., Yip, C.H., Lu, Y.S., Voravud, N., Shao, Z.M., Pritchard, K.I., 2009. Management of HER2-positive breast cancer in Asia: consensus statement from the Asian Oncology Summit 2009. Lancet Oncol. 10, 1077–1085. doi:10.1016/S1470-2045(09)70230-X

Xiao, G., Zhang, T., Yu, S., Lee, S., Calabuig-Navarro, V., Yamauchi, J., Ringquist, S., Dong, H.H., 2013. ATF4 protein deficiency protects against high fructose-induced hypertriglyceridemia in mice. J. Biol. Chem. 288, 25350–25361. doi:10.1074/jbc.M113.470526

Xu, X., Kedlaya, R., Higuchi, H., Ikeda, S., Justice, M.J., Setaluri, V., Ikeda, A., 2010. Mutation in archain 1, a subunit of COPI coatomer complex, causes diluted coat color and Purkinje cell degeneration. PLoS Genet. 6, 10.

doi:10.1371/journal.pgen.1000956

Xu, X., Weinstein, M., Li, C., Naski, M., Cohen, R.I., Ornitz, D.M., Leder, P., Deng, C., 1998. Fibroblast growth factor receptor 2 (FGFR2)-mediated reciprocal regulation loop between FGF8 and FGF10 is essential for limb induction. Development 125, 753–765.

Yamamoto, K., Mori, K., 2010. Induction of Liver Steatosis and Lipid Droplet Formation in ATF6a -Knockout Mice Burdened with Pharmacological Endoplasmic Reticulum Stress. Mol. Biol. Cell 21, 4042–4056. doi:10.1091/mbc.E09

Yamamoto, K., Sato, T., Matsui, T., Sato, M., Okada, T., Yoshida, H., Harada, A., Mori, K., 2007. Transcriptional Induction of Mammalian ER Quality Control Proteins Is Mediated by Single or Combined Action of ATF6?? and XBP1. Dev. Cell 13, 365–376. doi:10.1016/j.devcel.2007.07.018

Yamamoto, K., Takahara, K., Oyadomari, S., Okada, T., Sato, T., Harada, A., Mori, K., 2010. Induction of liver steatosis and lipid droplet formation in ATF6alpha-knockout mice burdened with pharmacological endoplasmic reticulum stress. Mol. Biol. Cell 21, 2975–86. doi:10.1091/mbc.E09-02-0133

Yang, J.T., Rayburn, H., Hynes, R.O., 1995. Cell adhesion events mediated by alpha 4 integrins are essential in placental and cardiac development. Development 121, 549–60.

Yang, L., Jhaveri, R., Huang, J., Qi, Y., Diehl, A.M., 2007. Endoplasmic reticulum stress, hepatocyte CD1d and NKT cell abnormalities in murine fatty livers. Lab. Invest. 87, 927–937. doi:10.1038/labinvest.3700603

Yang, X.Y., Zhou, X.Y., Wang, Q.Q., Li, H., Chen, Y., Lei, Y.P., Ma, X.H., Kong, P., Shi, Y., Jin, L., Zhang, T., Wang, H.Y., 2013. Mutations in the COPII vesicle component gene SEC24B are associated with human neural tube defects. Hum. Mutat. 34, 1094–1101. doi:10.1002/humu.22338

Ying, Y., Zhao, G.Q., 2001. Cooperation of endoderm-derived BMP2 and extraembryonic ectoderm-derived BMP4 in primordial germ cell generation in the mouse. Dev. Biol. 232, 484–492. doi:10.1006/dbio.2001.0173

Yu, X., Breitman, M., Goldberg, J., 2012. A Structure-based mechanism for Arf1-dependent recruitment of coatomer to membranes. Cell 148, 530–542. doi:10.1016/j.cell.2012.01.015

Zakariyah, a, Hou, W., Slim, R., Jerome-Majewska, L., 2011. TMED2/p24β1 is expressed in all gestational stages of human placentas and in choriocarcinoma cell lines. Placenta 1–6. doi:10.1016/j.placenta.2011.12.009

Zeigler, B.M., Sugiyama, D., Chen, M., Guo, Y., Downs, K.M., Speck, N. a, 2006. The allantois and chorion, when isolated before circulation or chorio-allantoic fusion, have hematopoietic potential. Development 133, 4183–4192. doi:10.1242/dev.02596

Zeng, L., Lu, M., Mori, K., Luo, S., Lee, A.S., Zhu, Y., Shyy, J.Y.-J., 2004. ATF6 modulates SREBP2-mediated lipogenesis. EMBO J. 23, 950–958.

doi:10.1038/sj.emboj.7600106

Zhang, B., Zheng, C., Zhu, M., Tao, J., Vasievich, M.P., Baines, A., Kim, J., Schekman, R., Kaufman, R.J., Ginsburg, D., 2011. Mice deficient in LMAN1 exhibit FV and FVIII deficiencies and liver accumulation of α1-antitrypsin. Blood 118, 3384–3391. doi:10.1182/blood-2011-05-352815

Zhang, K., Wang, S., Malhotra, J., Hassler, J.R., Back, S.H., Wang, G., Chang, L., Xu, W., Miao, H., Leonardi, R., Chen, Y.E., Jackowski, S., Kaufman, R., 2011. The unfolded protein response transducer IRE1alpha prevents ER stress-induced hepatic steatosis. Embo J 30, 1357–1375. doi:emboj201152 [pii]\r10.1038/emboj.2011.52

Zhang, L., Volchuk, A., 2010. P24 Family Type 1 Transmembrane Proteins Are Required for Insulin Biosynthesis and Secretion in Pancreatic Beta-Cells. FEBS Lett. 584, 2298–304. doi:10.1016/j.febslet.2010.03.041

Zhang, Y.C., Zhou, Y., Yang, C.Z., Xiong, D.S., 2009. A review of ERGIC-53: Its structure, functions, regulation and relations with diseases. Histol. Histopathol. 24, 1193–1204. doi:10.14670/HH-24.1193

Zhao, L., Helms, J.B., Brügger, B., Harter, C., Martoglio, B., Graf, R., Brunner, J., Wieland, F.T., 1997. Direct and GTP-dependent interaction of ADP ribosylation factor 1 with coatomer subunit beta. Proc. Natl. Acad. Sci. U. S. A. 94, 4418–23. doi:10.1073/pnas.94.9.4418

Zhao, L., Helms, J.B., Brunner, J., Wieland, F.T., 1999. GTP-dependent binding of ADP-ribosylation factor to coatomer in close proximity to the binding site for dilysine retrieval motifs and p23. J. Biol. Chem. 274, 14198–14203. doi:10.1074/jbc.274.20.14198

Zhao, P., Metcalf, M., Bunnett, N.W., 2014. Biased signaling of protease-activated receptors. Front. Endocrinol. (Lausanne). 5, 1–16. doi:10.3389/fendo.2014.00067

Zheng, H., Yang, Y., Han, J., Jiang, W., Chen, C., Wang, M., Gao, R., Li, S., Tian, T., Wang, J., Ma, L., Ren, H., Zhou, W., 2016. TMED3 promotes hepatocellular carcinoma progression via IL-11/STAT3 signaling. Sci. Rep. 6, 37070. doi:10.1038/srep37070

Appendix: Permission to reprint

Dear Dr. Hou,

sorry I did completely missed the purpose of your question,
Please find below some information which will answer your question:
As a journal author, you retain rights for a large number of author uses, including use by your employing institute or company. These rights are retained and permitted without the need to obtain specific permission from Elsevier. These include are listed in detail at our website:

- Elsevier Author Rights

All other uses by authors should be authorized by Elsevier through the Global Rights Department and authors are encouraged to let Elsevier know of any particular needs or requirements. E-mail the Permissions Helpdesk or telephone (+1) 800-523-4069 x 3808 for more information.

Please help us improve our service by taking this 30 second survey.**Claire Monnin**
Journal Manager
ELSEVIER Global Journals Production
Tel: +441392285896
ELSEVIER
For assistance, please visit our Customer Support site where you can search for solutions on a range of topics and find answers to frequently asked questions.

Gmail

Dominic Hou <wenyang.hou@gmail.com>

use of article for PhD thesis [ref:_00DU0lfis._5000BblyyQ:ref]

1 message

plosone <plosone@plos.org> Wed, Sep 27, 2017 at 12:44 AM
To: "wenyang.hou@mail.mcgill.ca" <wenyang.hou@mail.mcgill.ca>

Dear Dr. Hou,

Thank you for your message. PLOS ONE publishes all of the content in the articles under an open access license called "CC-BY." This license allows you to download, reuse, reprint, modify, distribute, and/or copy articles or images in PLOS journals, so long as the original creators are credited (e.g., including the article's citation and/or the image credit). Additional permissions are not required. You can read about our open access license here: http://journals.plos.org/plosone/s/licenses-and-copyright

There are many ways to access our content, including HTML, XML, and PDF versions of each article. Higher resolution versions of figures can be downloaded directly from the article.

Thank you for your interest in PLOS ONE and for your continued support of the Open Access model. Please do not hesitate to be in touch with any additional questions.

Kind regards,

Amy

Amy Sutherland
Staff EO
PLOS ONE

Case Number: 05438001

———— Original Message ————
From: Dominic Hou [wenyang.hou@mail.mcgill.ca]
Sent: 26/09/2017
To: plosone@plos.org
Subject: use of article for PhD thesis

Dear Plosone editors/colleagues,

My name is Wenyang Hou, first author of the following article published by Plosone:

Hou, W., Gupta, S., Beauchamp, M., & Yuan, L. Jerome-Majewska, L (2017). Non-alcoholic fatty liver disease in mice with heterozygous mutation in TMED2, 1-19.

I would like to acquire a permit to re-publish this article into my phD thesis.

please let me know if it is okay,

thanks

–
Wenyang (Dominic) Hou
PhD candidate,
Dept. of Human Genetics, McGill University
Dr. Loydie Majewska laboratory
Lab address: MUHC Glen site, 1001 Decarie Blvd, ES12371,
Montreal, QC, H4A 3J1
ref:_00DU0lfis._5000BblyyQ:ref